NREL/TP-257-4655 • UC Category: 261 • DE93000012

Combined Experiment Phase I

Final Report

NREL/TP--257-4655

DE93 000012

C.P. Butterfield
W.P. Musial
D.A. Simms

National Renewable Energy Laboratory
(formerly the Solar Energy Research Institute)
1617 Cole Boulevard
Golden, Colorado 80401-3393
A Division of Midwest Research Institute
Operated for the U.S. Department of Energy
under Contract No. DE-AC02-83CH10093

October 1992

NOTICE

Printed in the United States of America
Available from:
National Technical Information Service
U.S. Department of Commerce
5285 Port Royal Road
Springfield, VA 22161

Price: Microfiche A01
Printed Copy A10

Codes are used for pricing all publications. The code is determined by the number of pages in the publication. Information pertaining to the pricing codes can be found in the current issue of the following publications which are generally available in most libraries: *Energy Research Abstracts (ERA)*; *Government Reports Announcements* and Index (*GRA* and I); *Scientific and Technical Abstract Reports (STAR)*; and publication NTIS-PR-360 available from NTIS at the above address.

Acknowledgments

This work was sponsored by the United States Department of Energy Wind/Hydro/Oceans Technologies Division. The authors wish to acknowledge the electronics instrumentation and mechanical skills of Mike Jenks whose many hours of diligence and perseverance in working on the turbine under extremely adverse conditions enabled this project to happen. The authors also appreciate Rick Clyne's expertise in assimilating and editing the information presented in this report. The following people provided valuable encouragement and advice on test setup and data analysis techniques: Al Eggers, Craig Hansen, Bob Akins, Bob Thresher, Gerry Gregorek, Mike Hoffman, and Karl Danninger.

1.0 Table of Contents

1.0 Table of Contents (continued)

1.0 Table of Contents (concluded)

1.1 List of Figures

1.1 List of Figures (concluded)

1.2 List of Tables

2.0 Introduction

Wind turbine operating experience has shown that current analysis techniques are inadequate when used to predict peak power and loads on a fixed-pitch wind turbine. Viterna and Corrigan (1981) and Tangler (1983) show evidence of higher-than-predicted power levels on stall-controlled wind turbines. Because performance and loads are the most important design information needed to achieve more reliable and inexpensive wind turbines, it is important to understand the cause of the discrepancy. The primary question is: How does the wind tunnel airfoil data differ from the airfoil performance on an operating horizontal axis wind turbine (HAWT)? The National Renewable Energy Laboratory (NREL) has been conducting a comprehensive test program focused on answering this question and understanding the basic fluid mechanics of rotating HAWT stall aerodynamics.

The basic approach was to instrument a wind turbine rotor, using an airfoil that was well documented by wind tunnel tests, and measure operating pressure distributions on the rotating blade. Based on the integrated values of the pressure data, airfoil performance coefficients were obtained, and comparisons were made between the rotating data and the wind tunnel data. Care was taken to minimize the aerodynamic and geometric differences between the rotating and the wind tunnel models. Models were made in the same molds, and the same instruments were used for both the rotating and wind tunnel cases.

This is the first of two reports describing the Combined Experiment Program and its results. This Phase I report covers background information such as test setup and instrumentation. It also includes wind tunnel test results and roughness testing. The Phase II report concentrates on the aerodynamic pressure test results. Average and unsteady aerodynamic measurements are presented. These reports were written for two reasons: The first is to disseminate basic aerodynamic data that will be useful for code validation and wind turbine design information. The second is to provide a current orientation for researchers using the data or participating in the Combined Experiment Program. These reports provide a comprehensive description of results to date and a description of how the experiment operates.

3.0 Background

The Combined Experiment was planned and carried out over a period of four years. It was the most comprehensive wind turbine test program ever attempted, with more than 200 signals simultaneously measured and recorded. The test program was divided into two phases: Phase I planning began in spring 1987. Phase II began following the completion of the Phase I tests in spring 1989. Many configurations of instrumentation were considered during each phase of testing as lessons were learned and instruments were improved. Although the instruments were continually upgraded, the major configuration change between Phase I and Phase II was the extent of the pressure measurements. The instrumented blade for Phase I had only one span-wise radial station of pressure taps (32 taps) at 80% radius, but the Phase II blade had four radial stations of pressure taps at radial positions ranging from 30% radius to 80% as well as six intermediate radial stations of taps located between the primary stations. A new instrumented blade was fabricated for both Phases I and II. The major instrumentation configuration changes that were made between Phases I and II were as follows:

- A thermal drift problem in the Phase I strain gages was corrected with more careful matching of the gage and blade thermal expansion properties.

- A second root-mounted video camera was added to the instrumented blade for Phase II and was pointed toward the tip of the blade. This camera could view the entire blade from one position.

- The R. M. Young U-V-W fixed-axis anemometers on the vertical plane array (VPA), in Phase I, were replaced by prop-vane anemometers.

- Two bi-vane anemometers were added at hub height on the north and south sides of the VPA.

- The sonic anemometer and the hot-film anemometers on the local meteorological tower were not operating during Phase II.

- In Phase II, a Honeywell 16-channel tape recorder replaced a Sabre-80 14-channel tape recorder. The Honeywell recorder had a higher bandwidth than the Sabre and allowed the tape to be played slower; therefore, more data per tape were recorded.

Phase I testing was conducted between July 1988 and May 1989. Many of the fifty-five 30-min analog tapes that were recorded were not usable because of various instrumentation problems, but there were enough good-quality records to establish a baseline data set. The Phase I tests were necessary to refine the details of the instrumentation and data acquisition system to gain a preliminary understanding of how to interpret the pressure measurements and process the data. The Phase I report will cover the test setup, instrumentation, wind tunnel tests, and airfoil roughness testing. Much of the Phase II success can be attributed to the Phase I experience.

Most of the data presented came from the more comprehensive Phase II data sets and will be presented in the Phase II report. This report will cover the wind turbine test results, including:

- Bin averaged aerodynamic coefficients data integrated from pressure distributions

- Bin averaged blade load data

- Unsteady aerodynamic data.

4.0 Test Setup

4.1 Test Site

The test site where all the atmospheric testing was conducted is located at the NREL Wind Energy Test Center at the Rocky Flats Plant 10 miles north of Golden, Colorado. Winter winds are dominant at this site from a prevailing direction of 292 deg. The local terrain is flat, with grassy vegetation extending over 1/2 mile upwind. However, the site sits only a few miles from the opening of Eldorado Canyon at the base of the Rocky Mountains, which are located directly upwind. The wind turbine was unobstructed by other structures or wind turbines. A layout of the wind site and test turbine is given in Simms and Butterfield (1990).

4.2 Test Turbine

The Combined Experiment Test Turbine was a modified Grumman Wind Stream 33. It was a 10-m-diam., three-bladed, downwind, free-yaw turbine equipped with full span pitch capability that is manually controlled during the testing to provide fixed-pitch (stall-controlled) operation at any pitch angle desired. The rotational speed of the rotor was a constant 72 RPM. The turbine was supported on a guyed-pole tower. It was equipped with a hinged base and gin pole to allow it to be tilted down easily. An electric winch was used to lower and raise the system during installation. A base-controlled yaw lock was added to allow locked yaw operation at arbitrary yaw positions from the ground. This yaw retention system had a strain-gaged link to measure yaw moments. Also added was a mechanical caliper brake system that could be operated manually from the control shed. The specifications for this wind turbine are shown in Figure 4-1. A schematic of the turbine's nacelle is shown in Figure 4-2.

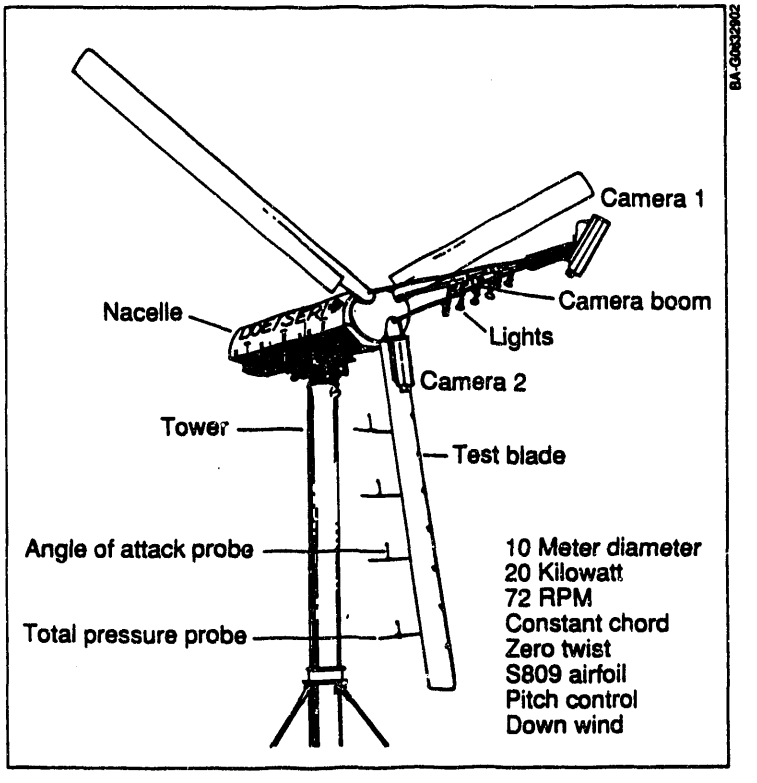

Figure 4-1. Test turbine description

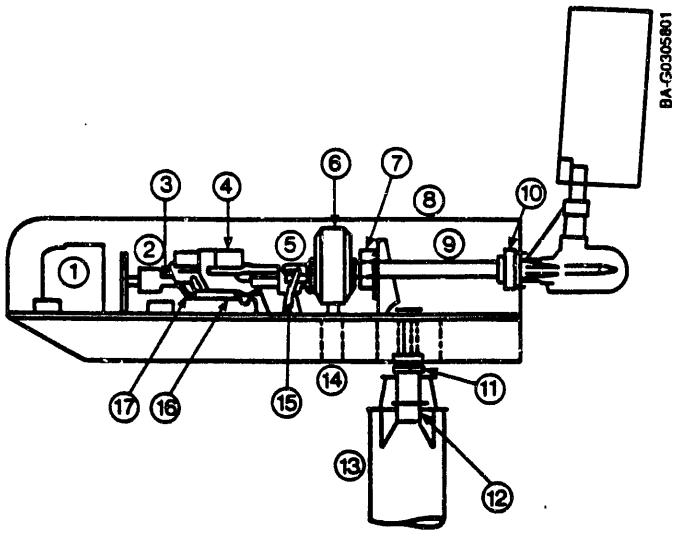

1 - Generator
2 - Disc brake
3 - H.S. shaft
4 - Pitch cont actuator
5 - Swivel
6 - Gear box
7 - Pillow block bearing
8 - Cowling
9 - Rotor shaft
10 - Flg block bearing
11 - Thrust bearing
12 - Vertical shaft
13 - Tower
14 - Strongback
15 - Torque link
16 - Redundant pitch cont actuator
17 - Redundant pitch actuator crank

Figure 4-2. Test turbine nacelle layout

The new blade was the most significant configuration change. The original blade platform was maintained, but the NREL S809 airfoil replaced the original Grumman airfoil. The S809 airfoil was developed by Airfoils, Inc., under contract to NREL (Simms and Butterfield, 1990). The primary reason this airfoil was chosen was that it had a well-documented wind tunnel data base that includes pressure distributions, separation boundary locations, drag data, and flow-visualization data.

The blades had a constant .45-m (18-in.) chord with zero twist. The blade material was a fiberglass/epoxy composite. The blades were designed to be stiff to limit aero-elastic blade deflections. The dynamic characteristics of the blade were tailored to avoid coalescence of rotor harmonics with flap-wise, edge-wise, and torsional natural frequencies. To minimize the possibility of aero-elastic instabilities, the mass and elastic axes were aligned with the aerodynamic axis. The instrumented blade was painted black to contrast with the white tufts that were used for flow visualization.

Some of the advantages of this turbine were:

- The rigid, three-bladed rotor reduced the amount of out-of-plane blade motion and minimized aero-elastic effects.

- The constant-chord, zero-twist blade reduced the effects of blade geometry on stalled flow.
- The downwind rotor configuration allowed a boom-mounted camera to view tufts on the low-pressure side of the blade without obstructions.
- The simplicity, small size, and high availability of parts made test modifications such as tower tilting, transducer mounting, and control system changes easy and inexpensive.
- The manual pitch control system allowed stall-controlled operation at any pitch angle.

4.3 MET Towers

The north MET tower or far-field MET tower was 50 m tall and was located 500 m upwind from the test turbine. Instruments mounted on this tower were used to measure the large-scale atmospheric conditions of the inflow.

For local inflow measurements, two Rohn 45-G guyed MET towers were erected directly upwind of the test machine in the prevailing wind direction. The two towers supported three cross-booms, where 13 anemometers in a VPA were mounted to measure the inflow in the near field. The VPA was positioned one rotor diameter (1D) upwind of the turbine.

A 55-ft local MET tower was located to the north of the VPA 1D upwind. Mounted on it were the high-frequency atmospheric instruments. Figure 4-3 shows the placement of the VPA and the local MET tower with respect to the turbine location. The specifics of the anemometry are discussed in Section 5.4.

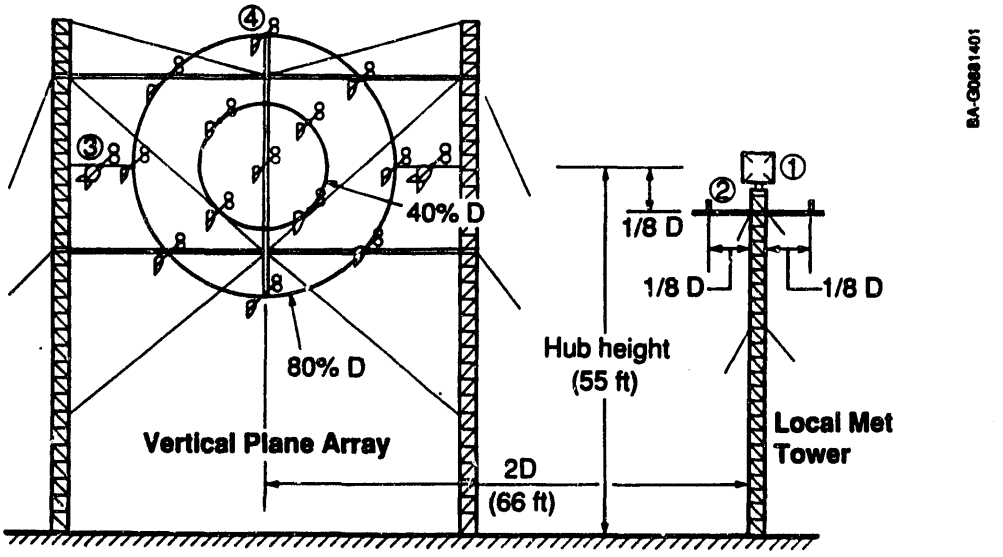

Item No.	Description	Quantity
1	U-V-W sonic anemometer	1
2	Ruggedized hot films	2
3	Bi vane anemometers	2
4	Prop vane anemometers	13

Figure 4-3. Vertical plane array layout

5.0 Instrumentation

5.1 Pressure Measurements

5.1.1 Pressure Taps

Blade surface pressures were the most important and the most difficult measurements to make. The accuracy of the aerodynamic performance coefficients was dependent on the individual pressure tap measurements because each coefficient is the integrated value of the measured pressure distribution at that radial station. The measurement approach was to install small pressure taps in the surface of the blade skin. Each opening was mounted flush to the airfoil surface and was 0.040 in. in diameter. The flush profile was necessary to prevent the taps themselves from disturbing the flow. Stainless steel tubes, each less than 0.5 m in length, were installed inside the blade's skin during manufacturing to carry surface pressures to the pressure transducer. For Phase I testing, 32 pressure taps were located at 80% of full blade span, where the Reynolds number is approximately 10^6. In Phase II, three more stations were added: one at 63%R, one at 47%R, and one at 30%R. The taps were aligned along the chord (instead of being staggered) so that span-wise variations in pressure distributions would not distort measured chord-wise distributions. The chord-wise spacing of the pressure taps is shown in Figure 5-1.

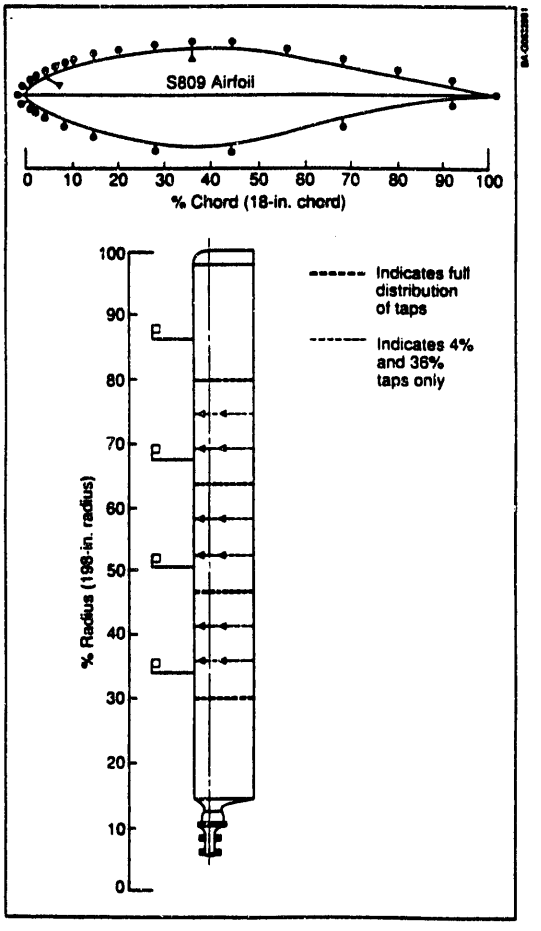

Figure 5-1. Blade layout

The tube lengths were minimized to avoid dynamic effects between the surface of the blade and the transducer. Pressure tap tube acoustical frequency response limits accurate pressure measurements to 20% of the first harmonic frequency. In the case of a 45-cm-long (18-in.) tube, the first harmonic is approximately 80 Hz according to Irwin, Cooper, and Hirard (1979). They describe how this can be corrected in software by measuring the acoustical transfer function of the tube and applying the measured transfer function to the data in the frequency domain. A recursive filter can also be used to apply the transfer function to the data in the time domain. This technique is used to get a full 100-Hz bandwidth from the pressure signals.

Transfer functions were measured between applied surface pressures and pressures measured by the transducer (Akins, 1987). Figure 5-2 shows that for a 10-in. stainless steel tube, only minimal distortion occurs below 50 Hz, but the most significant amplification occurs between 50 to 100 Hz. A typical spectral density plot for the 4% chord pressure tap at the 63% radial station is shown in Figure 5-3. The dynamic response of the pressure system shows the absence of significant spectral energy above 50 Hz, which indicates that the dynamic effects can be ignored. Based on these data, dynamic corrections were not made to the pressure measurements.

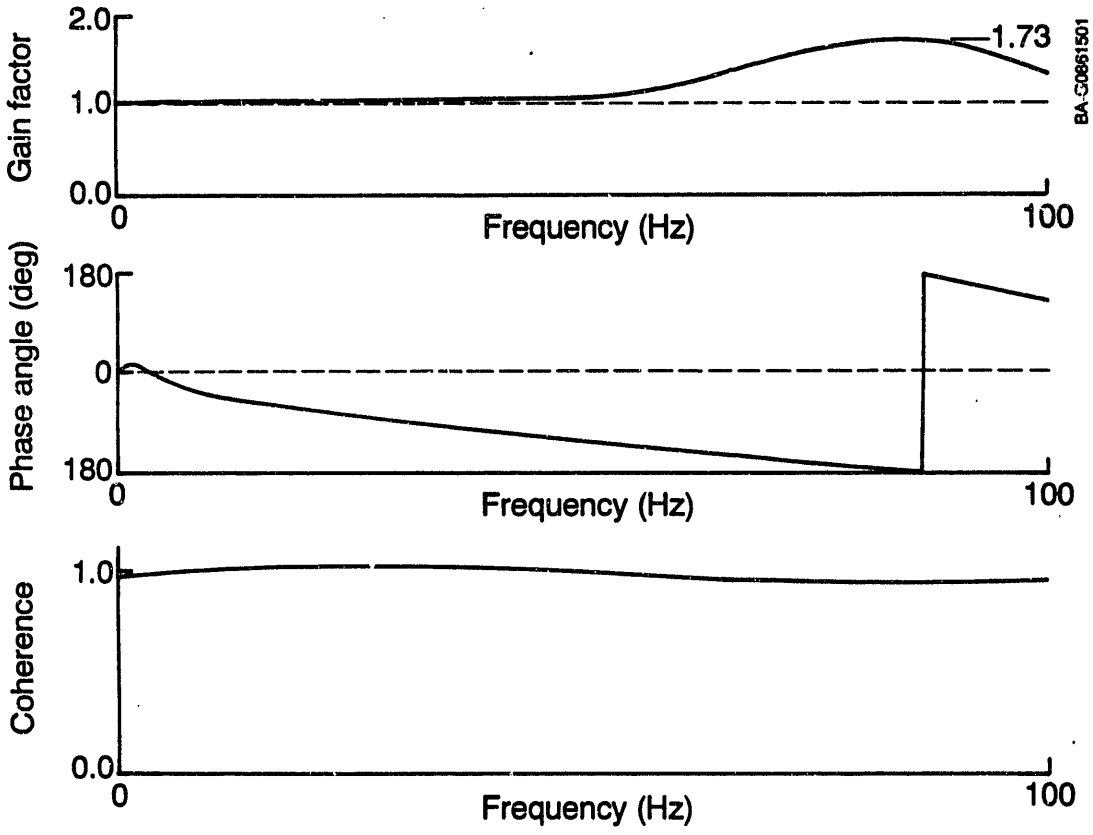

Figure 5-2. Typical pressure tap frequency response (.065" ID tube, 20" length)

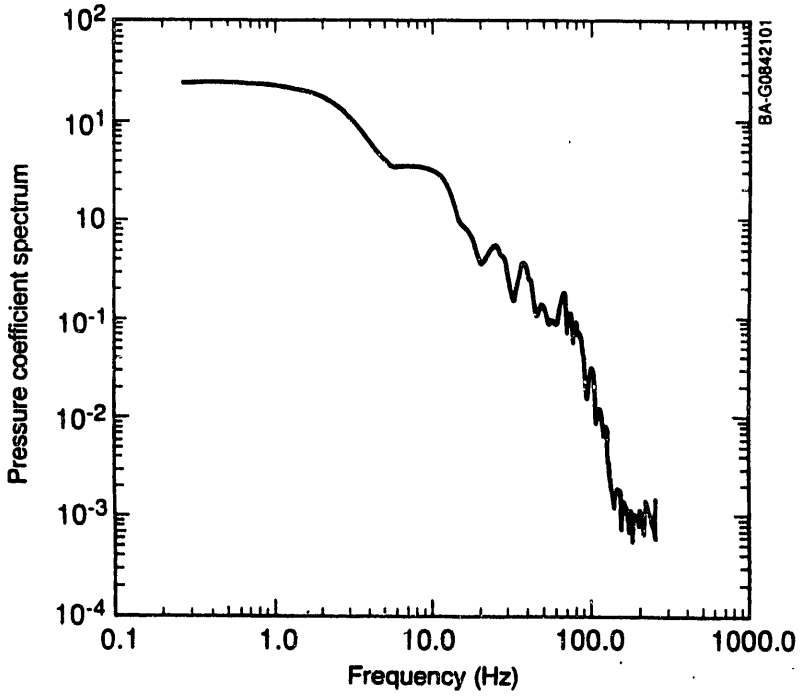

Figure 5-3. Typical pressure tap frequency content (4% chord, 63% span)

5.1.2 Pressure Transducer

The specifications of this test program required pressure measurements within 2% to 3% of the local dynamic pressure with a bandwidth of 100 Hz. This corresponded to an accuracy of 137 micro-bars (0.002 psi) at the 80% blade span and 11 micro-bars (0.0002 psi) at the inboard 30%R blade station. To obtain this accuracy, it was necessary to conduct frequent range and zero calibrations during the test. Pressure Systems International Model ESP-32 pressure transducers were used. They are electronic scanner-type transducers that provide remote calibration capability through a pneumatically operated valve. The transducers were installed inside the blade as close to the pressure taps as possible. One transducer was used at each 32-tap span-wise station. Figure 5-4 is a diagram showing the installation of the pressure transducers and pressure taps within the blade.

5.1.3 Pressure System Controller (PSC)

Remote control of calibration, scanner addressing, and demultiplexing of the analog multiplexed signal were performed by the PSC. The PSC was a hub-mounted microprocessor control unit. Figure 5-5 shows a block diagram of the PSC designed by NREL. The PSC was designed to control and process data from four ESP-32 transducers in parallel and is capable of processing as many as 128 pressure channels simultaneously without any loss in performance. A minimum frequency response of 100 Hz was required to study dynamic stall behavior on the rotating wind turbine blade. To accomplish this, the pressure port address was incremented from port-to-port at 16,646 Hz, resulting in complete scans of all pressure ports on each PCM stream at 520 Hz and a port-to-port settling time of 60 μsec. These samples were passed

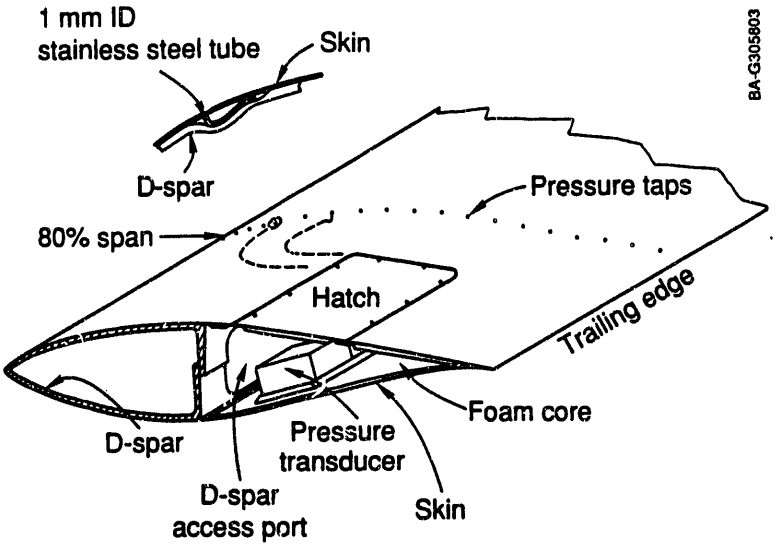

Figure 5-4. Transducer installation in blade

on to the PSC as analog multiplexed signals where they were digitized, distributed to 32 digital-to-analog (D/A) converters on a digital bus, and passed through individual reconstruction filters. The filters were 100-Hz precision, four-pole Butterworth filters. Each of the reconstructed analog output signals, one for each channel, was passed to the pulse code modulation (PCM) encoder. The output of the PCM system was passed over slip rings to the control building and was recorded on a wide-band tape recorder for later processing.

Although the processing from analog to digital and then back to digital was cumbersome, it provided flexibility and was very stable. When the system was designed, a frequency multiplexing system was to be used for data recording. This system would have required analog output.

A schematic of the pneumatic valve controls is shown in Figure 5-6. There are six independent pneumatic control valves in the PSC that are electronically controlled by the PSC. A 0.094-m^3 (1-ft^3) dry nitrogen control pressure reservoir supplies pneumatic control pressure at 80 psi to operate the pressure transducer functions.

A ramp calibration sequence is started by energizing a set of pneumatic valves in the controller. Control pressure is sent out the blade to the "purge valve" and shuttles a plate that connects all pressure input ports to a common calibration pressure line and connects all surface pressure tap tubes to a common purge pressure line. When the calibration command is given from the test shed, calibration pressure is simultaneously applied to all the taps in stepwise increments by a motorized syringe under microprocessor control. Calibration pressure is measured by a Setra 237 differential pressure transducer mounted in the PSC. The syringe provided a means of accurately applying small positive and negative pressures to the ESP-32 transducers.

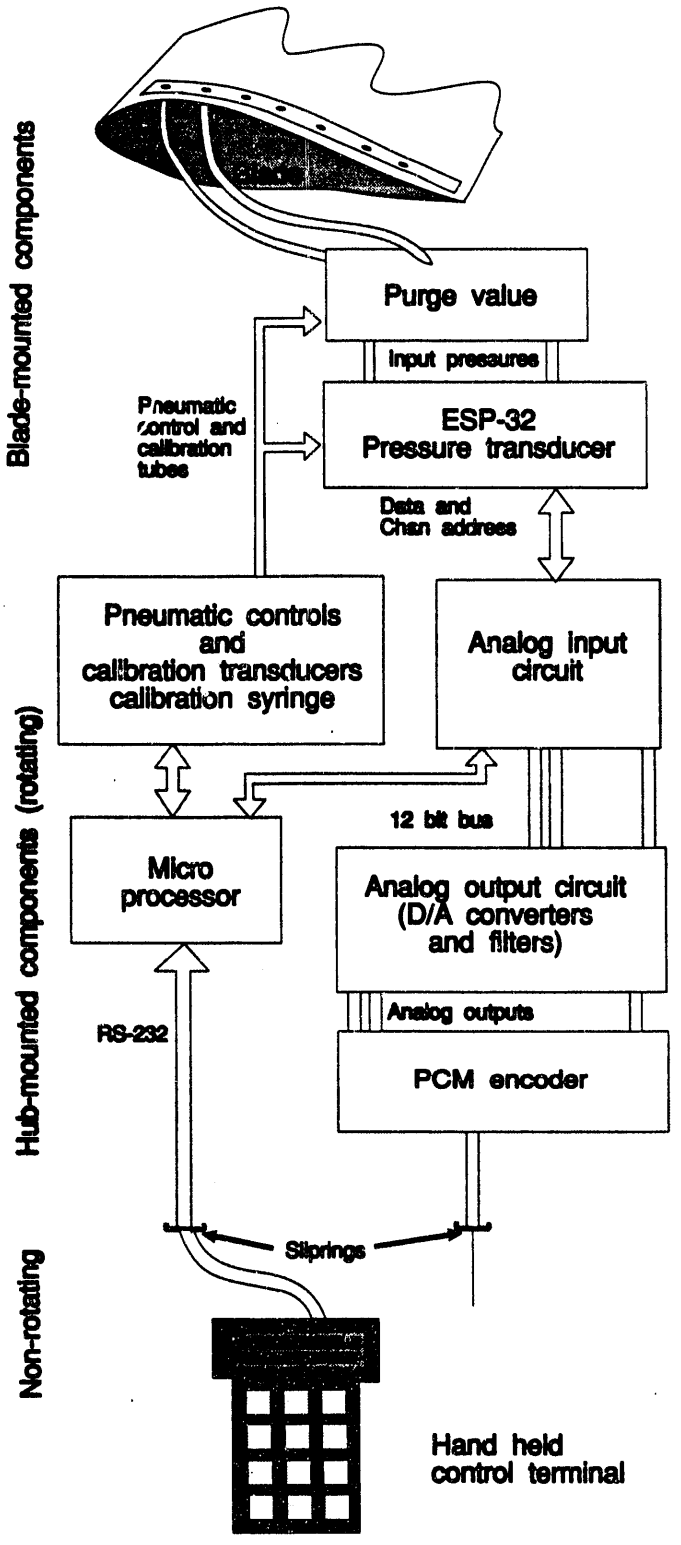

Figure 5-5. Pressure system controller block diagram

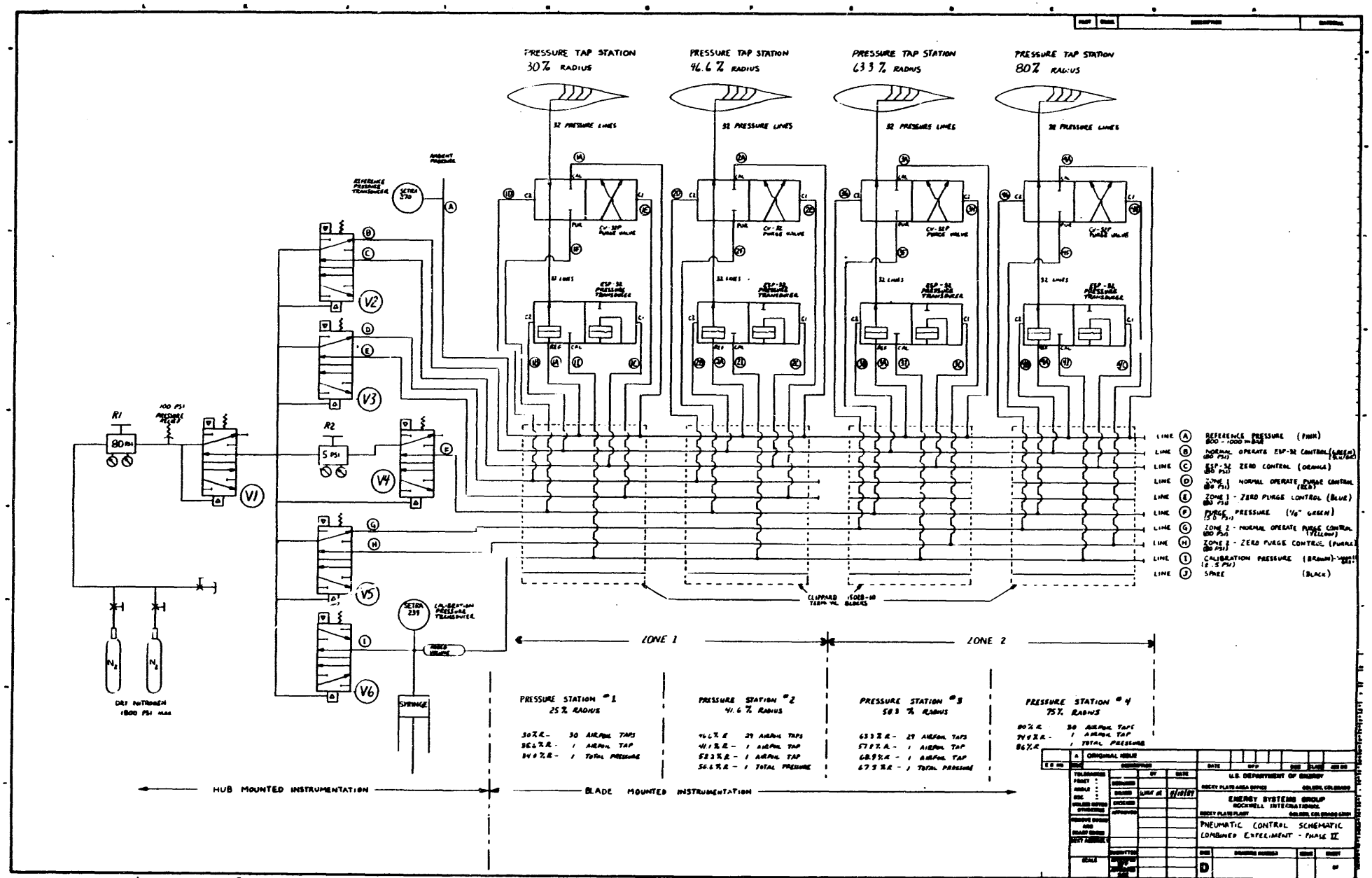

Figure 5-6. Pressure system controller—pneumatic controls schematic

If desired, a "purge" command could be given. For this option, a set of valves is energized that sends control pressure to a pneumatically controlled purge valve that is mounted next to the ESP-32. When the purge valve receives control pressure, all the pressure taps are connected to a regulated supply of dry nitrogen at 5 psi that is exhausted out all the pressure tap tubes to clear moisture or debris. This feature was exercised before each test to assure that no blockages were present.

Zero calibration was accomplished by energizing a different set of valves that send pneumatic control pressure out the blade to the ESP-32 transducer, which connects all input pressures to the reference pressure line. Zero calibrations were initiated every 5 min of testing to track zero drift on all channels.

5.1.4 Centrifugal Force Correction

Establishing a reference pressure for each transducer was non-trivial for transducers located in a rotating environment. The air pressures inside the rotating blade were unpredictable and rapidly fluctuating, so it was not possible to establish a reference pressure at the transducer. Instead, the reference tap of each ESP-32 transducer was connected to a single reference pressure line that was terminated at the hub-mounted PSC. This created another problem. Centrifugal forces acting on the column of air in the reference tube change the pressure along the radius of the wind turbine rotor. The actual reference pressure experienced by the transducers was calculated by using the following equation:

$$P_{atm} + P_{cf} = \tfrac{1}{2} \rho \, (r\Omega)^2 \, , \qquad (5\text{-}1)$$

where:

P_{atm} = atmospheric pressure
P_{cf} = pressure due to centrifugal force
r = radial distance to transducer
Ω = rotor speed
ρ = air density.

Tests were run to verify the accuracy of Eq. 5-1 and confirmed the predicted values to within the measurement accuracy of the transducer.

5.2 Angle-of-Attack (AOA) Transducer

The main objective of this test program was to compare wind tunnel data with rotating blade data. Before this could be done, an accurate means of measuring and comparing the AOA on a rotating blade was needed. Geometric AOA measurements are fairly easy to make in a wind tunnel where the air flow is precisely controlled, but on rotor they are much more difficult. To accomplish this, it was necessary to make measurements of the local inflow in front of the blade.

Figure 5-7 shows the flow angle sensor (FAS) that was developed by NREL for this test program. Lenschow (1971) describes early development and testing of a similar sensor that was used in atmospheric flight testing. The Combined Experiment FAS used a small, lightweight rigid flag that aligned itself with the local flow. The flag angle is measured with a commercial rotary position sensor mounted in a custom housing. The analog signals generated were sent to the hub, multiplexed, and recorded with the other signals by the data acquisition system. Flag angles were measured within 0.1-deg accuracy. The sensor was mounted 36 cm ahead of the leading edge on 5/8-in.-diam. carbon tubes. Transducers were positioned

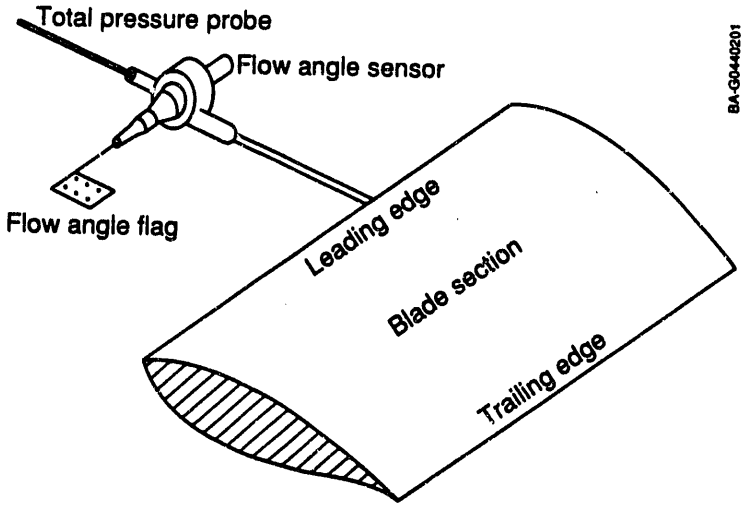

Figure 5-7. Local flow-angle transducer

6% outboard of each pressure station in order to limit flow disturbances on the blade near the pressure taps. A total pressure probe was mounted at the tip of each sensor to record the dynamic pressure, Q.

There were two areas of concern regarding the accuracy of this FAS. First, local upwash effects and induced velocities created by rotor wake expansions distort the flow around the airfoil. Figure 5-8 shows typical streamlines under the influence of circulation-induced upwash. This effect causes the FAS to measure a different flow angle than the geometric AOA, which is based on free stream flow. The second potential for error was the dynamic response characteristics of the sensor's flag. To investigate these issues, the sensor and probe were mounted on the wind tunnel model during tunnel testing. The effects of upwash, frequency response, and Reynolds number were determined. A steady-state and a dynamic correction were developed for the measured local flow angles (LFAs) using a combination of analytical and experimental techniques to accurately determine the true AOA.

Figure 5-9 shows the results of steady tests. The dashed line in represents a zero correction reference line or a condition where the FAS would measure the same angle as the geometric model angle during the wind tunnel testing. Triangles show data measured by the FAS with a solid line curve fit to these data. As can be seen, the upwash effect is important. At a geometric angle of 10 deg, the FAS indicates a 14-deg angle. The 4-deg discrepancy is due to the net effect of bound circulation and wake-induced flow. The solid line shows a prediction of the upwash effect. The Kutta-Joukowski Theorem was used to estimate the bound circulation, and the Biot-Savart Law was used to determine the local induced velocity. The vector sum of induced velocity—the resultant inflow velocity—was taken to determine the corrected flow angle. The agreement is reasonable at low angles where the flow is attached to the airfoil, but as the angle increases and the flow separates the agreement gets worse. Reynolds number effects were estimated to be insignificant for the steady-state wind tunnel tests. The measured wind tunnel data correction was used as the steady correction for the field test data analysis in this report. The details of this correction are presented by Gregorek, Hoffmann, and Mulh (1991).

To determine the dynamic response of the FAS, the flag was deflected and released in the wind tunnel at various Reynolds numbers. By recording the decay of the oscillations, a second-order system natural frequency and logarithmic damping ratio were determined. Figure 5-10 shows the angular displacement of the flag as the oscillations decay. Also shown are the analytical approximations for each case. From the comparisons, it is clear that the FAS is well damped but not critically damped, and the second-order differential equations model the response well.

There is at least one caution that should be recognized pertaining to the above discussion. It is possible that dynamic bound circulation changes could cause local flow field modifications that would alter the steady correction shown in Figure 5-9. These effects are unknown at this time. Future dynamic stall wind tunnel tests will attempt to address this issue. To investigate this, the FAS will be mounted on a wind tunnel model in the tunnel while the model AOA is oscillated at representative frequencies. The effect of the dynamic flow field on upwash will be reflected in a comparison between geometric AOA and measured LFA.

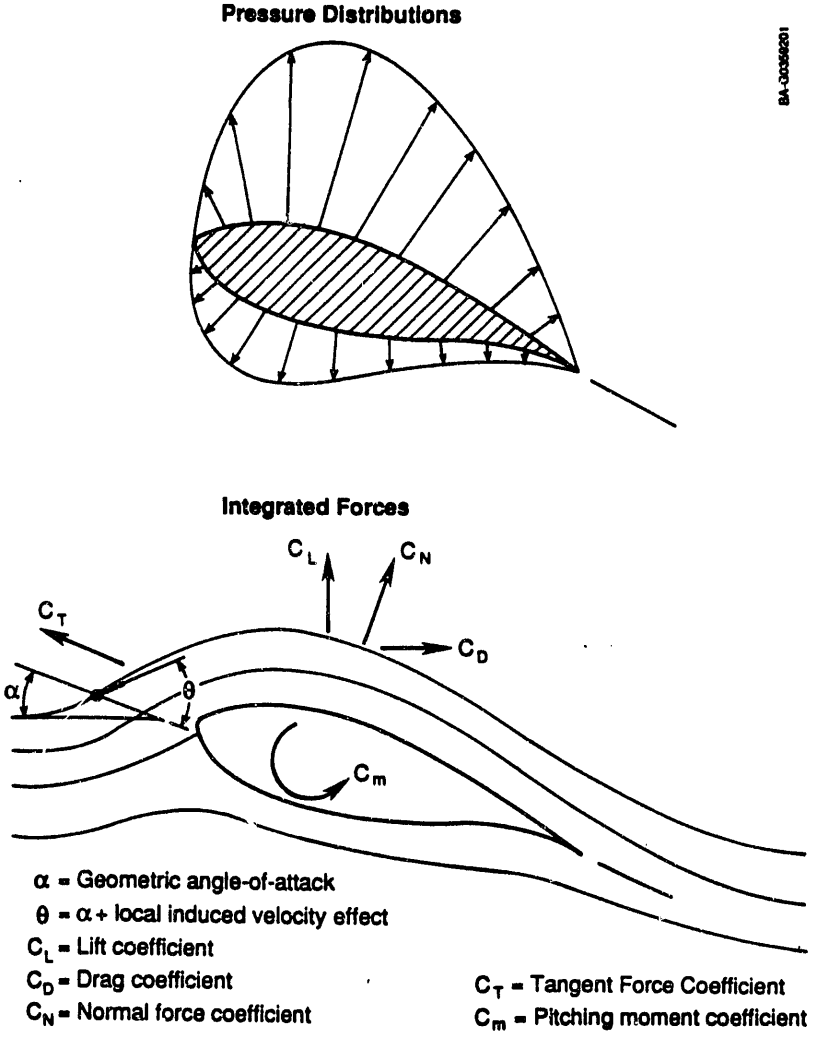

Figure 5-8. Upwash effect and terminology

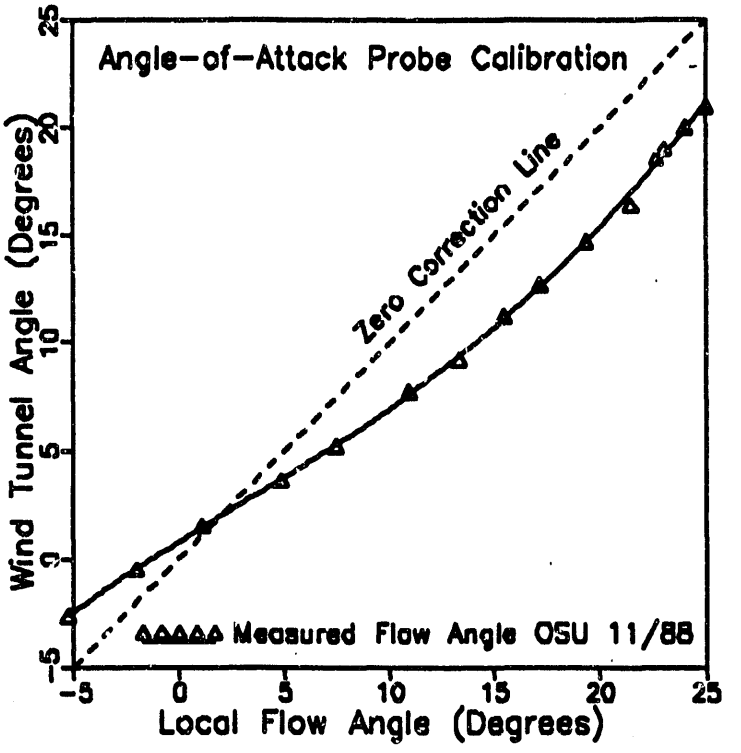

Figure 5-9. Wind tunnel calibration of the local flow-angle sensor

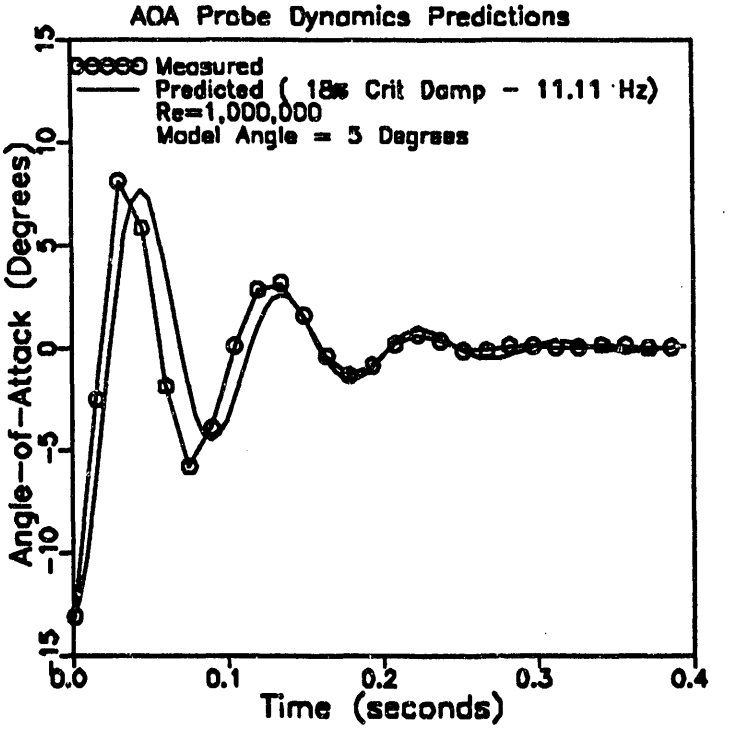

Figure 5-10. Dynamic response test of the flow-angle sensor (Reynolds number = 10^6)

The reader should note that LFA data are not corrected for either FAS dynamic characteristics or dynamic flow field effects. However, the FAS dynamic effects are estimated to be minimal for AOA variations less than 2 Hz because the sensor's natural frequency is approximately 10 Hz, or 8.3 times the rotational frequency. Also, the data are block averaged from 522 Hz to 10 Hz. This averaging should reduce the scatter because of FAS dynamics. Another observation that supports the assumption that dynamically induced errors in AOA measurements are small is shown in Figure 5-11. This shows that data scatter is relatively small for low to moderate LFAs. If the dynamic effects mentioned above were playing a large role, significant scatter would be expected throughout the entire range of LFA, but scatter is large only at high LFAs where stall is present. These results are discussed in more detail later in this report and also by Butterfield (1989). The data shown in Figure 5-11 were block averaged from 522 Hz to 10 Hz. This figure represents five minutes of time during yawed operation.

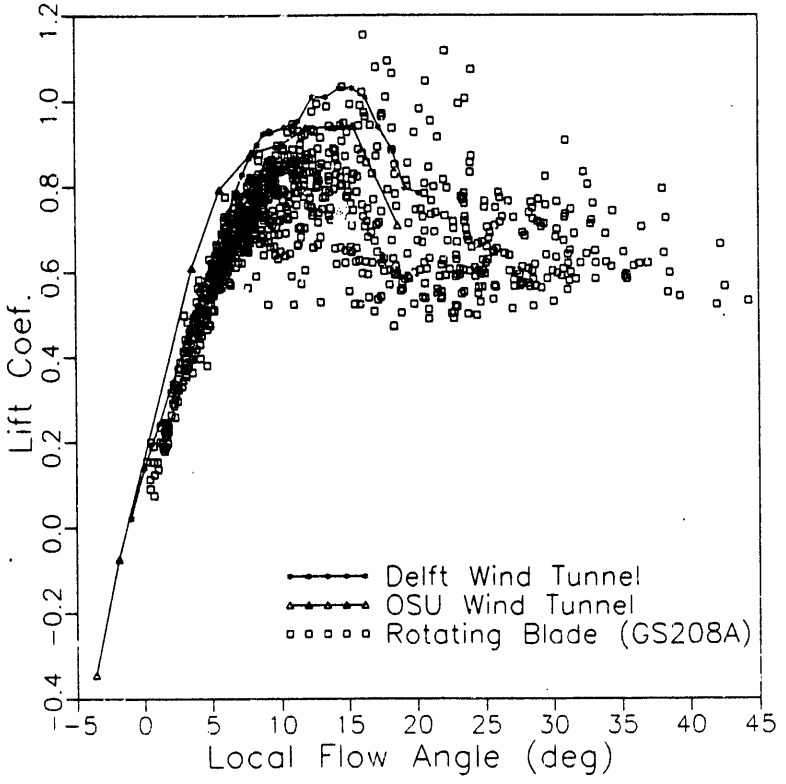

Figure 5-11. Lift characteristics at deep stall

5.3 Strain Gages

Strain gages were used to measure blade, tower, rotor, and yaw loads. Blade flap-wise and edge-wise loads were monitored at eight span-wise locations along the instrumented blade. Pitching moment (i.e., blade torsion) was monitored at three span-wise locations. Figure 5-12 shows the locations of all the blade strain gages. Load measurements were taken to help establish reliable blade load distributions to help us validate the measured aerodynamic pressure measurements.

Each strain gage bridge was made up of four active gage elements mounted inside the fiberglass blade skin. The gages were installed inside the skin during the blade manufacturing process to preserve the exterior airfoil shape and surface smoothness. The strain gages were positioned carefully to minimize flap-wise and edge-wise cross-talk. A maximum of 4% cross-talk was measured during the blade pull

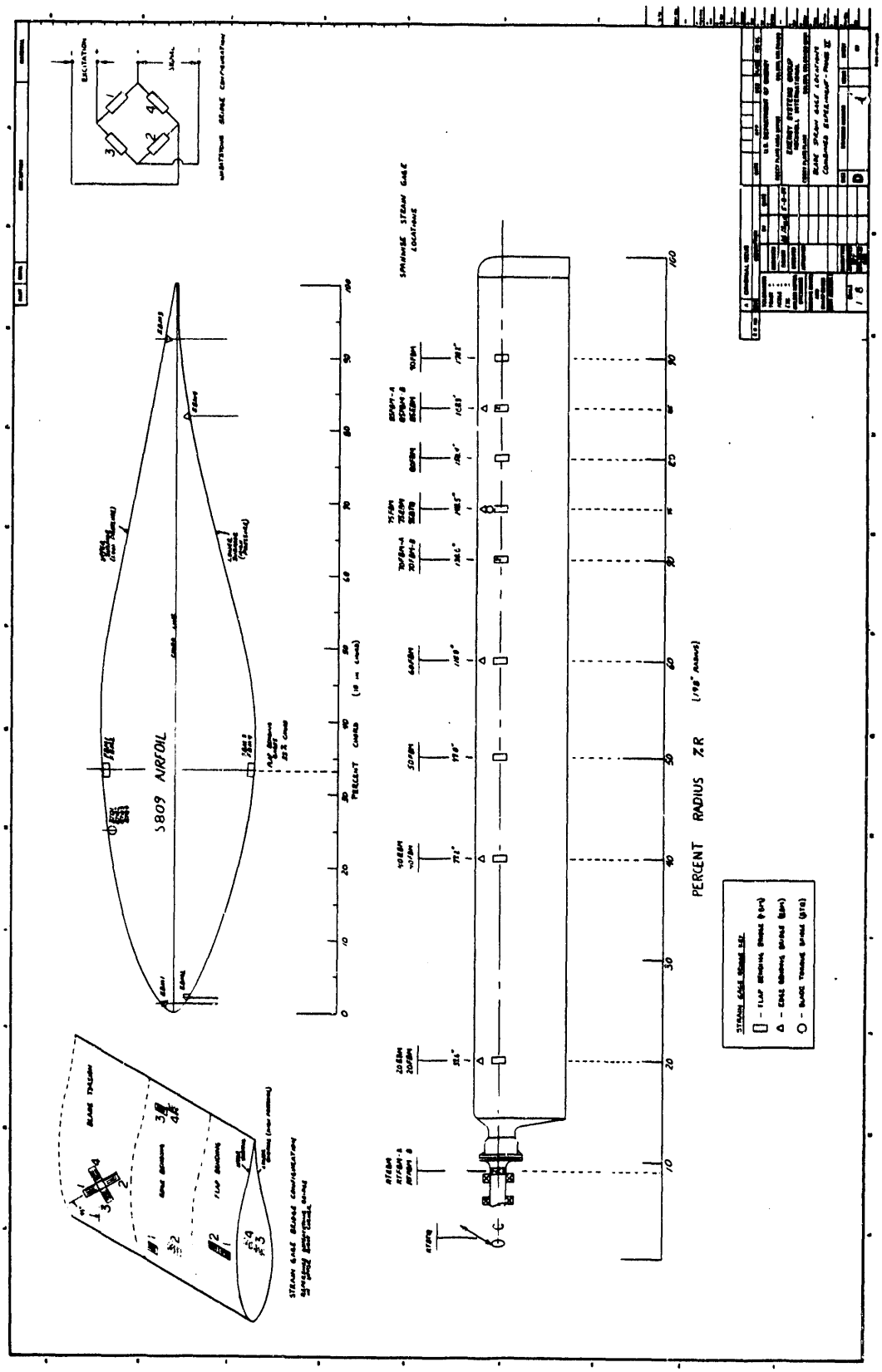

Figure 5-12. Instrumented blade strain gage - locations and bridge configurations

and strain gage calibration tests. These cross-channel interference effects were not considered significant, and corrections were not applied to the data.

5.4 Anemometers

A variety of anemometers was used during this testing. The primary near-field data were obtained from anemometers mounted on the VPA and the near-field MET tower. Far-field atmospheric stability data were provided at the test site's 50-m north MET tower.

A .8D ring of eight R. M. Young prop-vane anemometers was mounted on the VPA; they were the primary measure of local wind speed and direction. The anemometers were evenly spaced around the ring, which was centered 1D directly upwind at hub height. A .4D inner ring of R. M. Young three-axis prop anemometers provided low-frequency (0-1 Hz) wind-shear data, azimuthally varying wind data, and low-frequency inflow statistics during Phase I testing. The inner ring was concentric with the outer ring. A single R. M. Young prop vane was positioned at hub height in the center of the two rings. For Phase II testing, the inner ring of U-V-W prop vane anemometers was replaced by four prop vanes to make the wind-speed measurements more comparable. Two bi-vanes were also added for Phase II to provide a measurement of the vertical component of the wind. These were spaced 1D apart and centered on the VPA at hub height.

High-frequency (0-10 Hz) data were provided by a Kajieo Denki three-axis sonic anemometer mounted at hub height on the near-field MET tower and two TSI X-type dual-axis hot-wire anemometers mounted 1.2 m below hub height. The X-films provide measurements of horizontal and vertical wind velocity components at relatively high frequencies. An elevation view of the near-field anemometry is shown in Figure 5-13.

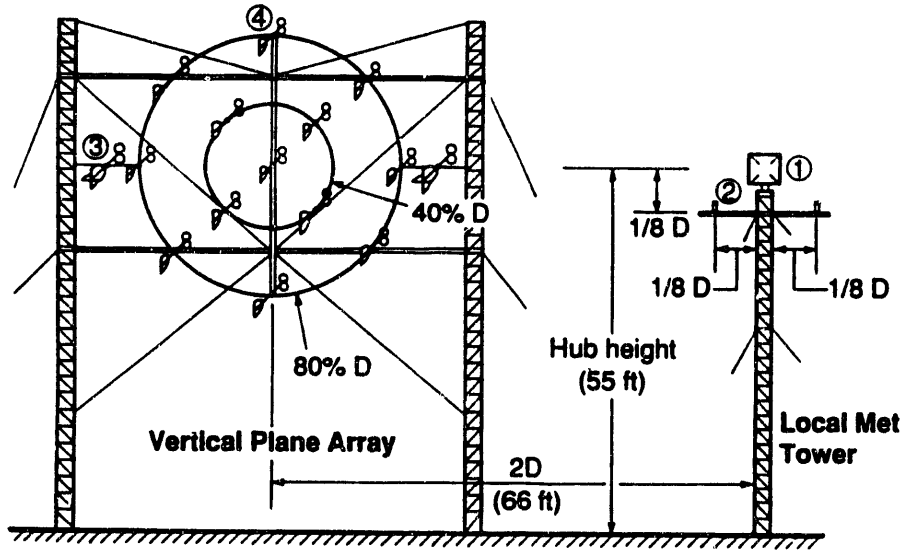

Item No.	Description	Quantity
1	U-V-W sonic anemometer	1
2	Ruggedized hot films	2
3	Bi vane anemometers	2
4	Prop vane anemometers	13

Figure 5-13. Vertical plane array layout

Far-field atmospheric data were recorded from the north MET tower. These data included temperature gradient, wind shear up to 50 m, relative humidity, and wind directions at four different altitudes. These data combined allowed measurements of atmospheric stability (Richardson number) to be made. These data were multiplexed near the tower base and telemetered to the Combined Experiment test shed where they were recorded.

5.5 Video Equipment

5.5.1 Cameras

A lightweight 10-ft boom was designed and mounted to the hub to hold the 10-lb, high-shutter-speed video camera. The boom and camera arrangement was designed to be stiff with a system fundamental frequency of 10 cycles per revolution (10P), and the axes of the boom and camera were mass balanced about the axis of rotation. The 10-ft boom length allowed a view angle of 30 deg at the tip of the blade and 45 deg at the 66% span. Additional equipment, such as the data acquisition system, the PSC, and lighting for night testing were also mounted on the boom.

For Phase I testing, a NISUS N-2000 video camera was used. A video monitor and recorder in the test shed were used to observe tufts on the low-pressure side of the blade. The camera used a mechanical shutter to freeze video frames in 1/625 of a second. Thirty video frames were recorded every second to allow one frame to be recorded for every 11 deg of rotor azimuth position. The horizontal resolution of this system is limited to approximately 250 lines. One problem with this system was that good angular measurements of the tufts were difficult to interpret from the video images. For Phase II, the entire video system was upgraded to improve the images of the tufts. The boom-mounted NISUS camera was replaced by a color Panasonic model WV-CL300. A second camera, a Panasonic WV-BD400 with a 15 to 160 mm Rainbow G10X16ME zoom lens, was also added to provide another independent view angle along the blade span. This camera was mounted on the blade itself and was allowed to pitch with the blade. This view provided a full span picture of all the tufts at one time and was instrumental in helping to identify and match flow patterns with the aerodynamic phenomena observed in the data.

5.5.2 Tufts

Tufts were attached to the surface of the instrumented blade to allow the air flow over the blade to be visualized. The tufts were made of thin, white, polyester thread measuring approximately 0.25 mm in diameter and 45 mm in length. They were attached to the downwind side of the blade with a small drop of fast drying glue. Tufts were placed in rows spaced 76 mm (3 in.) apart in the blade span-wise direction. In each row, the tufts were spaced one every 10% of the chord. The tufts on the leading edge and at 10% chord were intentionally omitted to avoid blade roughness effects that might have been created by the tufts themselves. The diameter of the tufts was chosen to minimize the effects on the boundary layer yet maintain good visibility for the video camera. If the tufts were large relative to the boundary layer thickness, they could cause transition or premature separation. This effect is discussed in more detail by Rae and Pope (1984).

5.5.3 Lighting

Night testing was generally preferred over daytime tests. The black coloring of the blade that was chosen to enhance the contrast of the tufts caused differential heating of the blade surfaces during the day. This led to a thermal drift problem with the blade strain gages. Also, daylight tended to produce a large amount of glare and reflections that interfered with the video images. Night testing required lighting to be added to illuminate the white tufts. Eleven tungsten-halogen 120-V spotlights were placed along the camera boom and directed at the blade. With this configuration, the video pixel intensity of a tuft was

35 on a gray scale of 0 to 256, and the black background was 10 to 15; the contrast was great enough so that the tufts could be seen easily. Unfortunately, there was still not enough light to operate the camera shutter, and moving images were blurred on the video display. In Phase II, the camera resolution was greatly improved, and remote control of the iris and focus adjustments were added.

5.6 Miscellaneous Transducers

In addition to the extensive hub-mounted instrumentation, several other measurements were required to complete the investigation of this turbine. Strain gages were mounted on the main shaft of the turbine to measure rotor torque and main shaft bending on two axes. Tower bending gages were mounted on two tower bending axes at the point just above the guy wire attachment. These gages were oriented to measure bending in the direction of the prevailing wind and orthogonal to the prevailing wind. Gages were mounted on the arm of the yaw brake to allow the measurement of yaw moment when the yaw brake was engaged. Special sensors were developed to measure yaw position (gear-driven potentiometer), pitch angle (gear-driven potentiometer), and rotor azimuth position (Trump Ross 512 pulse/revolution incremental encoder). Generator power was monitored using an Ohio Semitronics, Inc. (OSI) transducer in the test shed.

6.0 Data Acquisition and Reduction Systems

To accomplish the objectives of the Combined Experiment requires collecting data from three major areas: turbine rotating, turbine non-rotating, and meteorological. In the rotating turbine frame, measurements are made on the turbine blades, blade attachments, and hub. Typical parameters include strain gage bending moments and torsion, airfoil surface pressure distributions, total dynamic pressure, and blade pitch angle. These measurements provide data to determine blade aerodynamic and structural loads. In the non-rotating turbine frame, measurements characterize machine performance and determine turbine loads. This requires data from the turbine nacelle and tower, such as generator power production, tower bending, azimuth and yaw angles, and rotation speed.

To determine characteristics of the wind at the turbine, meteorological conditions are measured. Anemometers are used to measure near-field horizontal and vertical wind shear. This requires many channels of wind-speed and wind-direction data from local upwind anemometer arrays. Atmospheric stability measurements are also important in evaluating inflow characteristics. This requires far-field atmospheric boundary layer measurements, including anemometry, temperature, barometric pressure, and dew point.

In an effort to increase accuracy, simplify instrumentation, and reduce noise, analog data signals are sampled and encoded into digital PCM streams as close to the measurement source as possible. The streams are then telemetered to a convenient central receiving location and recorded on multi-track tape. Streams are conducted through slip rings and cables or transmitted over a radio frequency (RF) link. PCM stream layouts for the Combined Experiment are shown in Figure 6-1 and described in Section 6.1.

The Combined Experiment uses a customized digital PCM-based hardware system for data acquisition. The system was developed and is used for the following reasons:

- To provide required measurement bandwidth and accuracy, especially from pressure measurements on the rotating blade, and to minimize induced noise and electronic drift in rugged and harsh environments

- To perform automated multi-channel calibrations that enable essential rapid data verification in the field

- To generate all required ancillary parameters, provide uncertainty analyses, and allow complete comprehensive data postprocessing.

The system accomplishes these objectives by incorporating military-spec PCM encoders that digitize analog signals close to the measurement source and transmit information in digital format to the ground. The system also has built-in microprocessor-controlled calibration capabilities and prescribed calibration techniques that were designed to ensure data accuracy.

NREL developed a low-cost PC-based PCM decoding system specifically for use in the Combined Experiment to facilitate quick PCM data analysis. We were severely limited in our ability to decode multiple PCM streams for quick-look data processing and display in the field. There were no cost-effective commercial systems available that provided the required capabilities. We needed multiple-stream decoding, derivation of parameters from multiple channels (across PCM streams), graphic display, data storage, and a means to rapidly update calibration coefficients. We also needed the ability to monitor long-term meteorological conditions for evaluating current test status. These field capabilities are essential

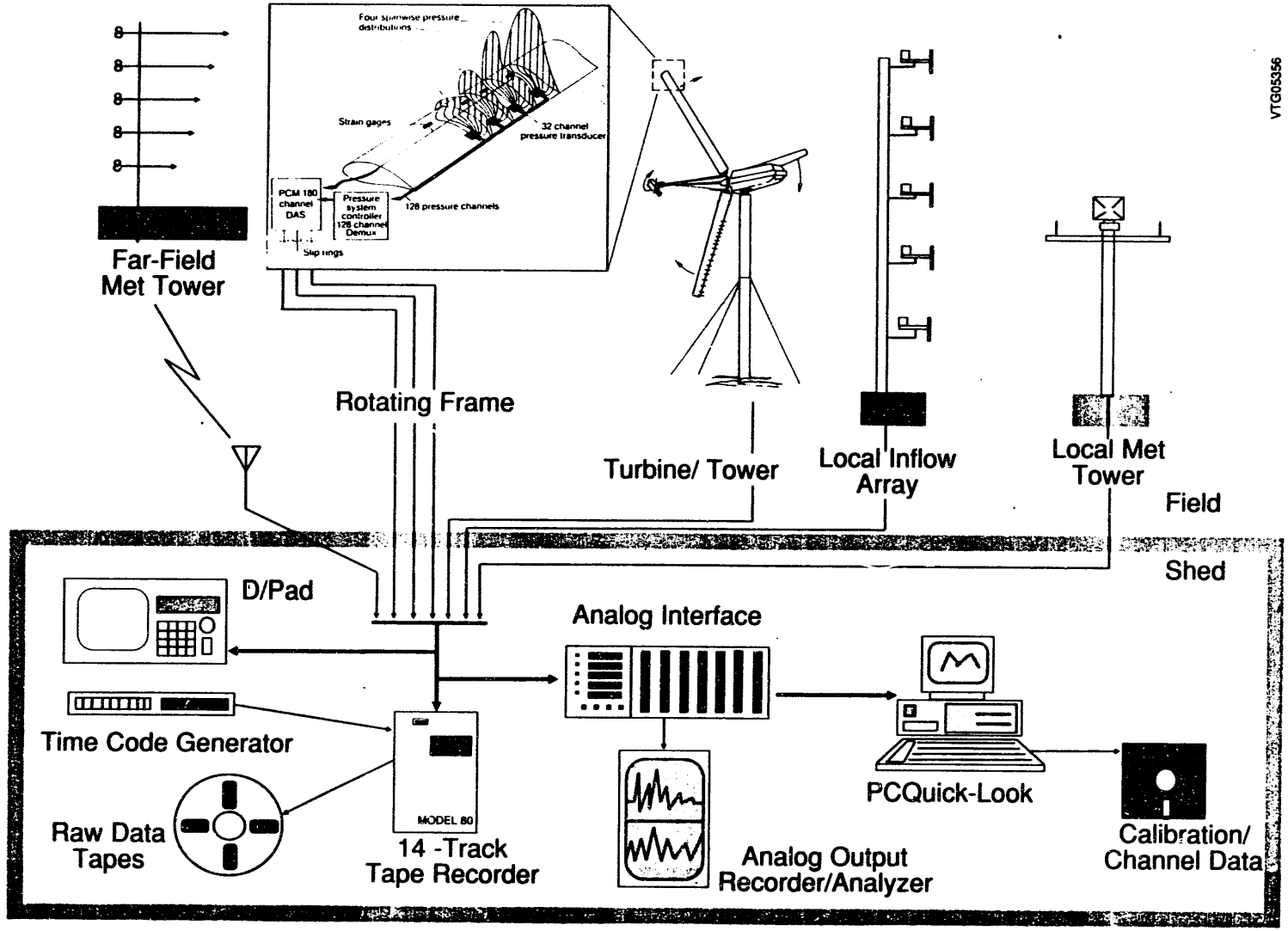

Figure 6-1. Combined experiment PCM streams

because debugging using laboratory-based postprocessing is inefficient and impractical. We therefore developed PC-based PCM decoding hardware (Simms and Butterfield, 1990) and wrote a custom "Quick-Look" PCM data management software program (Simms, 1990). These are described in Sections 6.2 and 6.3.

After initial field-based verification, PCM data streams from the Combined Experiment recorded on wide-band tape are extensively postprocessed in the laboratory. Many phases of comprehensive number crunching are necessary to produce the final required data sets to prescribed accuracy limits. These are described in Section 6.4. The basic processes involved are as follows:

- Use the PC-based Quick-Look system to produce valid calibration coefficients for all measured channels.

- Use a custom laboratory-based telemetry data reduction system called the EXPRT PCM Decommutation System (Fairchild Weston, 1985) to merge the PCM stream into a continuous time series.

- Use various UNIX-based computer systems and custom software to perform engineering unit conversions, derive ancillary parameters, generate spectra, provide digital filtering, generate statistics, and maintain a data base of all data records.

The data postprocessing path is shown in Figure 6-2. Along the way, there are also many data integrity checks. Final data records contain 239 channels at 520 samples per second. They are stored in 5-min-long engineering unit records, each requiring 150 Mbytes of disk storage space. We use an erasable optical disk system and a PC-based data base program to manage the current 5-h, 18-Gbyte data set. We have also developed a digital data processing system to filter data sets from 100-Hz to 40-, 10-, and 1-Hz bandwidth and generate power spectra in various frequency ranges. These are used to ensure data quality and facilitate subsequent data analyses.

6.1 Combined Experiment PCM Systems

PCM-encoded telemetry data systems provide highly accurate measurements over a wide dynamic range with low noise (Strock, 1983). These systems are ideal for collecting data related to the study of wind turbines, especially in the Combined Experiment, which requires accurate multiple-channel measurements taken from a variety of different locations. PCM systems consist of two basic components:

- Encoders to convert incoming analog signals into digital PCM values

- Decoders to decommutate the PCM values into data that can be computer processed.

Six PCM streams are used for data collection. Three streams are recorded in the rotating frame, two from local inflow and the turbine/tower, and one from far-field meteorology. Characteristics of the streams are summarized in Table 6-1.

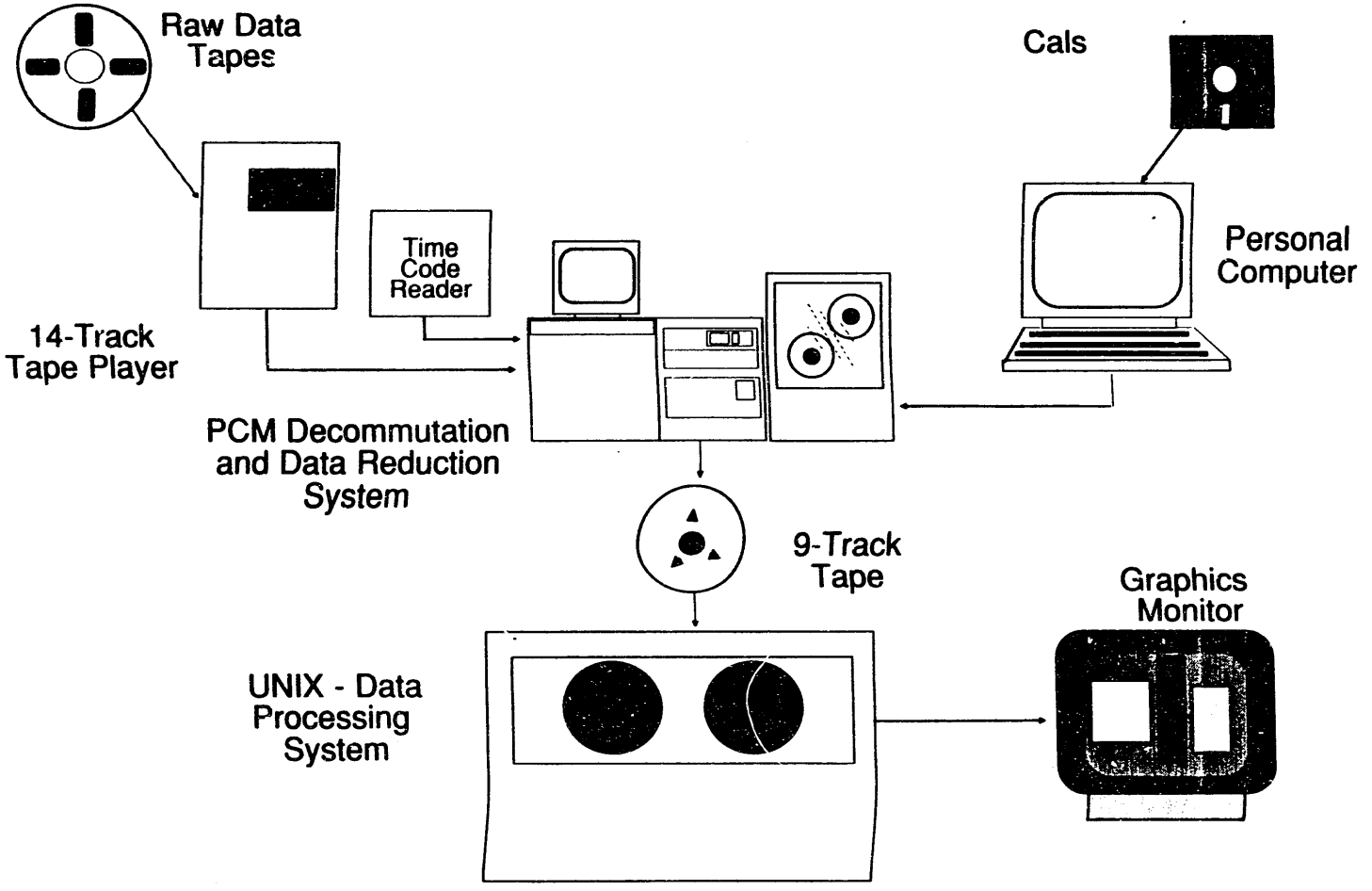

Figure 6-2. Full PCM data reduction and processing

Table 6-1. Combined Experiment PCM Systems

PCM #	Bit rate (Kbit/s)	Sample rate (Hz)	Number of channels	Sample interval (msec)	PCM source location
1	7.5	34.72	16	28.8	Far MET
2	15	69.44	16	14.4	Inflow
3	60	277.78	16	3.6	Inflow/Turbine
4	400	520.83	62	1.92	Rotor
8	400	520.83	62	1.92	Rotor
9	400	520.83	62	1.92	Rotor

The six PCM streams bring data from multiple sources in the field to a central location where they are collected, verified to ensure accuracy, and recorded to provide for subsequent laboratory-based processing and analysis. The system layout is shown in Figure 5-1 and is described in detail in Butterfield and Nelson (1990) and Butterfield, Jenks, Simms, and Musial (1990). All measurement transducers provide linear output voltages that are conditioned as specified in Appendix A and then input directly to PCM encoders. The signal conditioning/PCM encoding for streams 1, 2, and 3 each use a Fairchild-Weston 16-channel EMR 600 PCM Data Acquisition System that operates at various bit rates depending on data bandwidth requirements. The EMR 600 systems have a specified accuracy of 0.2% of full scale over the operating temperature range -50° to 120 °F. For PCM 1, the EMR 600 system is located in the data shed at site 1.1. Its PCM stream is telemetered to site 3.3 over an RF link. The EMR 600 systems for PCM streams 2 and 3 are located in the data shed at site 3.3. Analog signals for these two systems are conducted over cables from local transducers on the VPA and from the tower and nacelle. All the EMR 600 systems are in locations that offer a conditioned environment to minimize temperature-induced drift effects.

Streams 4, 8, and 9 each use a customized signal conditioning system coupled with three Loral 610 62-channel PCM encoders. The Loral 610s are specified as having full-scale accuracy of 0.4% over the operating temperature range of -40° to 185 °F. This is for digitizing and PCM encoding only. Signal conditioning accuracy varies depending on measurement type, as described below. These systems are all located on the wind turbine in the hub-mounted rotor package. The three PCM signals from the rotating frame are conducted through slip rings and run down the tower to the data shed. All operate at 400 Kbit/sec, which provides a data sample rate of 520.83 Hz on all 186 channels. The six PCM encoders provide the capability to measure 234 channels. Of these, 185 are currently considered active and necessary for the Unsteady Aero Experiment. Deactivated channels are for spare or redundant measurements, or they were used in previous phases of experimentation. In addition to the 185 direct measurements, there are five channels allocated for time and 45 subsequently derived ancillary parameters (i.e., integrated pressure distributions, disk-averaged wind speed, induced aerodynamic forces, etc.).

PCM encoders convert conditioned analog input voltages into digital counts. Overall accuracy is limited by the number of bits used in the digital code. All channels are sampled with 12-bit resolution that produces count values in the range from 0 to 4,095. This limits quantizing errors to .024% of full scale, provides a peak signal-to-noise ratio (S/N) of 83 dB, and defines maximum possible data accuracy. All channels in the Combined Experiment have been set up so that the required data range occupies as much of the available quantizing range as possible. Resulting quantizing errors are insignificant when compared to other sources of error in the data acquisition and processing procedures.

6.2 NREL PC-Based PCM Data Reduction System Hardware

In a single PC, the PCM decoding system provides continuous data acquisition to memory or disk from up to four streams simultaneously. A variety of software packages can subsequently be used to read and process the data. Single-stream real-time data monitoring is accomplished from a graphic bar chart display program.

The full complement of boards in a PC permits data handling from a maximum of 16 PCM streams containing up to 62 channels each. The boards are Inter-Range Instrumentation Group (IRIG) compatible and are designed for use with standard PCM encoders. The data streams can be accessed by cyclic sampling or simultaneous acquisition or both. Maximum acquisition rates and data storage capacity depend on PC hardware.

Optional analog interface modules can be used in conjunction with the PC-PCM decoder boards. These provide digital-to-analog conversion of up to 8 user-selectable channels per PCM stream, or 32 channels total. Incorporating the PC-PCM system into small portable computers simplifies remote test monitoring of PCM data. The complete system provides test engineers with the ability to decode PCM data and perform quick-look data analysis in the field.

6.2.1 Objectives of PC-PCM System Development

The NREL PC-PCM system consists of AT-compatible hardware boards for decoding and combining PCM data streams and DOS software for control and management of data acquisition. Up to four boards can be installed in a single PC, providing the capability to combine data from four PCM streams direct to disk or memory.

Our main objective was to provide a cost-effective PCM decoding system that could be duplicated at our many test sites to maintain consistency among systems. Future plans include development of an inexpensive turn-key data acquisition system that could be used by the wind industry. For many reasons described below, we decided that a PC-based system was most practical.

We contracted with a local electronics development company (Apex Systems, 1988) to develop the PC-based PCM decoding capability. We wanted a system built on printed circuit boards that could be installed in the expansion slots of a PC/AT or compatible computer. The system should include basic control software to initialize and operate the boards. It should also provide a simple user interface to allow easy acquisition and examination of data from different PCM streams.

We specified four PCM input channels for each board, from which one could be software selected to read data. A maximum of four boards could be installed, which would allow access to 16 PCM streams from a single computer. Multiple boards would permit acquisition from up to four streams simultaneously, and would tag and interleave multiple incoming data into a contiguous digital time series.

We also specified that data be written directly to PC memory or disk files. This would enable subsequent data processing and analysis to take advantage of the huge resource of software packages available for PCs, according to user preference. It also would enable easy development of custom packages in the many available software languages. The widespread use of PCs also would permit easy distribution of a developed data acquisition and processing package to interested users.

6.2.2 PC-PCM Decoding System Hardware

The PC-PCM hardware boards support a subset of the IRIG PCM standard, designed to synchronize and decommutate NRZ or Bi-Phase L PCM streams in the range of 1 to 800 Kbits/sec at 8 to 12 bits/word and 2 to 64 words/frame. Multiple PCM streams (at various rates) can be combined and interleaved into a contiguous digital time series. Maximum data throughput depends on characteristics of the PC hardware, such as central processing unit (CPU) rate and disk access speed. We typically do not super-multiplex or subcommutate channels in the PCM frames. All channels on a given PCM encoder are sampled at the same rate as that required for the highest rate channel. Those channels that do not require the fast rate are anti-alias filtered to a lower bandwidth and can subsequently be decimated in software. The PC-PCM decoder board specifications are summarized in Table 6-2.

Table 6-2. Specifications for PC-PCM Decoder Board

Bit rate	1-800 Kbits/sec
Input streams	4 (only one processed at a time)
Input polarity	Negative or positive
Input resistance	> 10 Kohms
Codes	Bi-phase L, NRZ
Bit sync type	Phase-locked loop (PLL)
Input data format	8-12 bits/word, most significant bit (MSB) first
Words per frame	2-64 (including sync)
Sync words per frame	1-3 (maximum 32 bits)

In conjunction with the PCM decoder boards, we developed an analog interface module that reconstructs analog output from up to eight channels per stream. The basic intent was to provide the ability to use real-time analog test instruments such as a spectrum analyzer or a chart recorder. The analog module is an optional part of the system. Specifications are shown in Table 6-3.

Table 6-3. Specifications for Analog Interface Module

Analog output	8 channels (user selectable via thumb wheels)
Output polarity	Unipolar or bipolar
Output range	0 to 10 V, 0 to 20 V, -5 to +5 V, -10 to +10 V
PCM input	4 (only one processed at a time)
Status lights	PLL lock, frame sync, first-in, first-out (FIFO), disabled

6.2.3 PC-PCM Decoding System Software

The PC-PCM hardware boards are controlled by DOS software written in C. Three programs and three ASCII configuration files provide basic capabilities. The first program, PCMTEST, initializes boards and captures data. The second program, PCMDUMP, reads captured binary data files. The third program, PCMBAR, generates a real-time bar chart graphics display. These programs input PCM system descriptions from DOS ASCII format data files that are easily accessed and modified by the user. A configuration file (.CFG) contains information describing how PCM hardware boards are configured in the PC. A stream file (.STM) defines characteristics of each PCM stream. The capture file (.CAP)

contains a list of instructions for a capture operation. These parameters and the range of options are summarized in Table 6-4.

Table 6-4. User-Definable Options for the PC-PCM System

Configuration File:	
Base I/O address	I/O address of the first PCM board (Board 0) (2-3 hex digits)
Number of cards	Number of PCM cards installed in the PC (1-4)
Signals per card	Number of input streams attached to card (4)
Direct memory access (DMA)	DMA channel that PCM board 0 is configured for (5-7)
channel	Interrupt channel that PCM board 0 is configured for (0-15)
Interrupt channel	Size of memory buffers in bytes (512-65, 024)
Buffer size	Number of memory buffers (2-64)
Buffers	
Stream File:	
Bit rate	Rate of transmission in bits/second (1000-800,000)
Data format	PCM format (NRZ or Bi-phase L)
Signal polarity	Whether signal is inverted (positive or negative)
Bits per word	Bits in each word (2-13)
Words per frame	Length of frame, including sync words (2-64)
Synchronization	Binary of hex sync pattern
Capture File:	
Card n	Specifications for board n (0-3)
Signal = stream	Links PCM stream to input signal (0-3)
Use	Which signal to read data from (0-3)
Capture channels	List of channels to capture (1-62)
Max frame count	Total number of frames to capture (optional)

The PCMTEST program can capture any amount of data up to the available space limit. If data are captured to disk, the maximum amount is determined by the space remaining on the hard disk drive. If data are captured to memory, the maximum amount is determined by available remaining system memory. Larger memory captures are possible by using extended memory configured as a random-access memory (RAM) disk. The amount of data to capture is specified in time (seconds), file size (kilobytes), or frame count.

PCMDUMP is a postprocess program used to generate time series data files from the raw binary capture files. This facilitates examining PCM data and interfacing with data analysis software. The PCMDUMP program can generate either ASCII or binary data files and can separate an individual stream from a multiple-stream data set.

The resulting delivered system had one benefit that we did not anticipate. Invoked from a batch file, the software can reinitialize a board fast enough to enable quick sampling from each input PCM stream. Therefore, a single board can cycle through, sample, and store data from four streams rapidly enough to update a real-time display run from other application software. Many factors affect the scan rate, including number of channels, number of samples per channel, and interim calculation requirements. Typical update rates for a 15-channel display from four PCM streams (including first-order engineering unit conversion and derived parameter calculations) occur in less than a second. The usefulness of PCM stream scanning depends on the nature of the data because intermittent sampling may cause aliasing, or

transients may be missed. However, for many of our averaged data applications, the monitoring of many channels by scanning across multiple streams is very useful.

6.2.4 Data Flow in the Computer

A clear understanding of the data flow inside the computer is helpful in understanding the capabilities and limitations of the PCM decoder board. Figure 6-3 shows the data flow inside the PC, described below. PCM data streams can be input directly to the PC-PCM decoder board or interfaced through an analog module. The analog module allows the user to select up to eight desired channels (via thumb-wheel dials) for analog output. The analog voltage output can be selected in the 10- or 20-V span range, bipolar or unipolar. The analog module also interfaces the PC-PCM boards to panel-mounted liquid-emitting diodes (LEDs) to inform the user of system status. (The status LED panel could also be built independently of the D/A system.) Status lights indicate capture activity, PLL status, frame sync status, PC memory status, and error state.

The PCM decoder boards are under the control of the capture software running in PC system memory. This program can be run on its own or via user application software. The capture program writes binary-format tagged PCM data. Each data word is tagged with its corresponding PCM board number. Captured data can be accessed by the application program through memory or disk files.

The capture software reads user-defined parameters from the capture control disk files, then initiates and terminates the capture operation. Before initiating capture, the direct memory access (DMA) controller is initialized to define the starting address and size of the first memory buffer. The DMA controller has a special address generator that allows it to move data from the PCM decoder card to the addresses in memory. When capture is initiated, the DMA controller moves data from the PCM board to the first memory buffer in 16-bit words. When the buffer is full, the DMA controller informs the PCM decoder card, which in turn generates an interrupt to the capture software.

Upon receiving the interrupt, the capture software reinitializes the DMA controller to transfer data to the next available buffer. This process is repeated until the capture is complete. While the buffers are being filled, application software could simultaneously access the data in the full buffers. Flags are provided for each buffer to define when they are full, empty, or in use.

This structure has many advantages. First, the DMA controller moves data from the PCM decoder board to memory more quickly than a software transfer does, and it is an independent process. The DMA controller actually takes over the PC/AT bus when data are transferred and does not burden the microprocessor. This makes the application software simpler and more efficient. Memory buffers provide another advantage. When data are being transferred to the hard disk, these buffers store data until the hard disk can rotate to the proper sector to write the data. Without these buffers, data would be lost.

6.2.5 Data Capture Performance Estimates

In single-stream mode, a typical PC/AT can capture PCM data to disk at rates up to 800 Kbits/sec. For multiple-stream disk capture, quantifying performance is difficult due to many possible combinations of PCM stream rates and PC capabilities. An algorithm for estimating disk data capture rate is

$$DCR = 16 * (BR / BPW) * (CWPF/WPF) \quad (6\text{-}1)$$

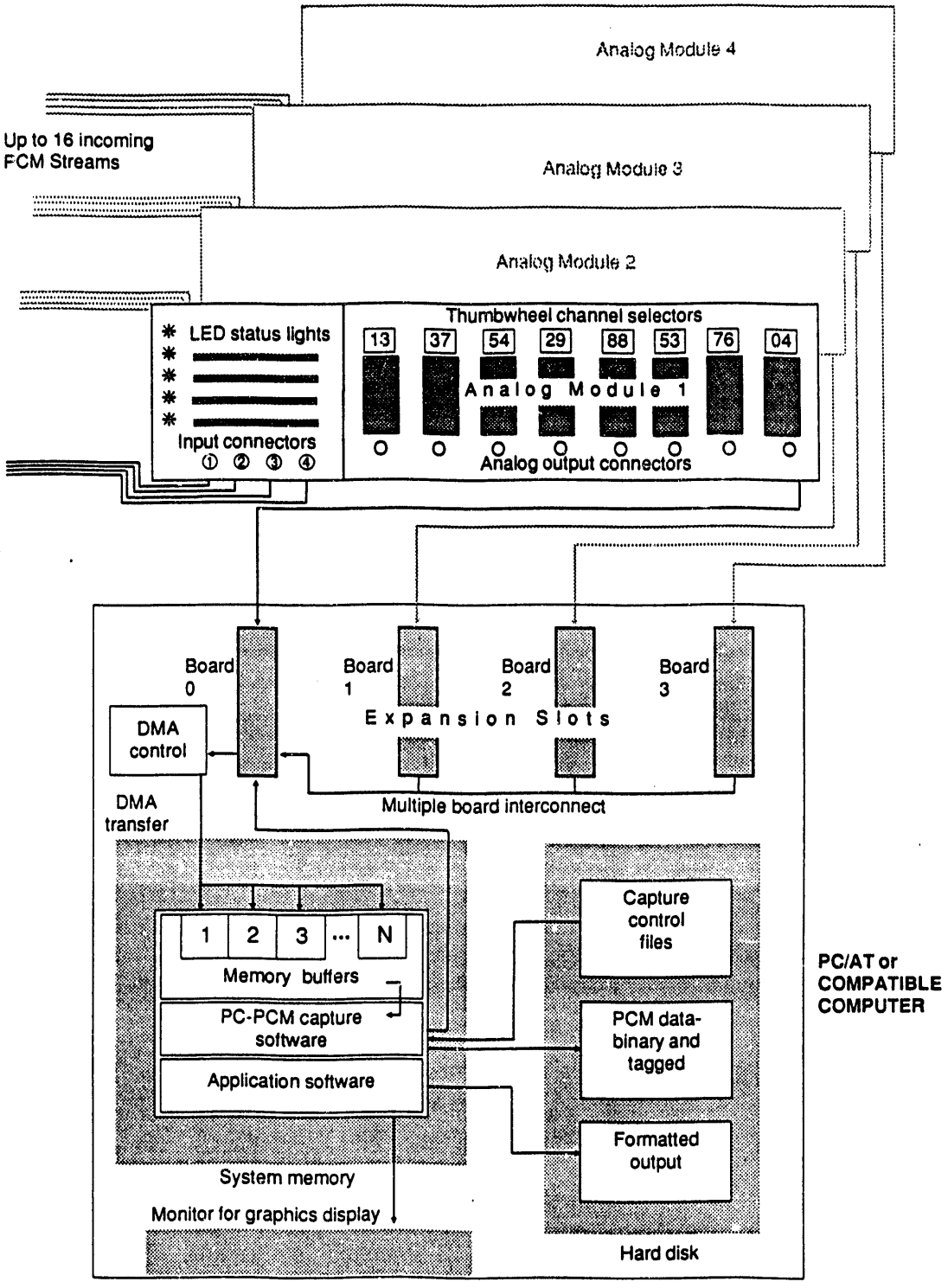

Figure 6-3. Data flow in the PC

where:

DCR = PC data disk capture rate in bits/second
BR = Incoming PCM bit rate in bits/second
BPW = Data bits per PCM word
CWPF = Words captured per PCM frame
WPF = Total words per PCM frame, including sync.

The data capture rate (DCR) for multiple cards is the sum of the DCRs for each individual card.

To provide some rough performance estimates, a test was run using four PC-PCM boards installed in a 25-MHz 80386-based PC. A PCM simulator was used to generate 62 channels of 12-bit words in Bi-Phase L format with 2 sync words per frame. Data were captured to contiguous blocks of disk storage space. The PC system could continuously capture to disk all channels of data from two 800-Kbit/sec streams. It could also capture all channels from four 400-Kbit/sec streams. The maximum occurred with three 800-Kbit/sec streams, each capturing 45 channels. At rates above this, the hard disk could not keep up with incoming data, and capture was terminated by a buffer overflow error condition.

Based on Eq. 6-1, the corresponding upper limit of disk data capture for this configuration is approximately 2.25 Mbits/sec. The PC's hard disk was rated at 10 Mbits/sec, indicating that the required PC disk speed should be 4 to 5 times the maximum data capture rate in order to ensure adequate performance. Many factors are likely to affect these values, including disk fragmentation, disk interface type, disk interleave, buffer size, CPU speed, and other installed PC options.

With the same system configuration, there were no performance limits when capturing data to memory. PCM data from four 64-channel, 800-Kbit/sec streams were successfully captured to an extended memory RAM disk. This is useful for providing higher-rate capture, but data quantities are limited because of memory restrictions. Large amounts of memory are less common and more expensive than comparable disk space.

6.2.6 Architecture of PCM Decoder Board

The PCM decoder board has a programmable bit detector for extracting the ones and zeros from the PCM signal. These are passed on to the frame and word processing section where the words are extracted and then interfaced to the PC. The following paragraphs discuss each of these in detail.

Bit Detector: Figure 6-4 shows the bit detection circuitry. A multiplexer controlled by the software selects between any one of four input signals. Following the multiplexer are buffer, filter, and comparator. These circuits convert the selected signal to digital levels. The data clock synchronizer extracts the bit clock rate from the incoming signal. The data bit detector circuit uses the bit clock and the signal from the comparator to generate a data bit stream of ones and zeros.

Frame and Word Processing: Figure 6-5 shows the decoder board frame synchronization circuitry. The bit clock clocks the data bits into both the frame synchronizer and the serial-to-parallel circuit. The frame synchronizer is programmed with the sync words. This information is used to detect and synchronize on

the data frame. The serial-to-parallel circuit is nothing more than a shift register with parallel output. When commanded by the frame synchronizer, the serial-to-parallel circuit strobes a complete word of information into the FIFO buffer. A FIFO buffer is necessary because the PCM stream is continuous with no gaps in the data, whereas the PC/AT bus cannot continuously accept data. The FIFO acts as a variable-sized buffer, holding the data until the PC/AT can pick it up. When a large amount of data is captured to the hard disk and the incoming bit rate is very high, it is possible for the FIFO to fill up faster than it can empty. When this happens, a FIFO full error is generated, a warning signal level is activated, and data capture stops. A frame termination counter option allows the user to specify the number of frames before the capture process is automatically terminated.

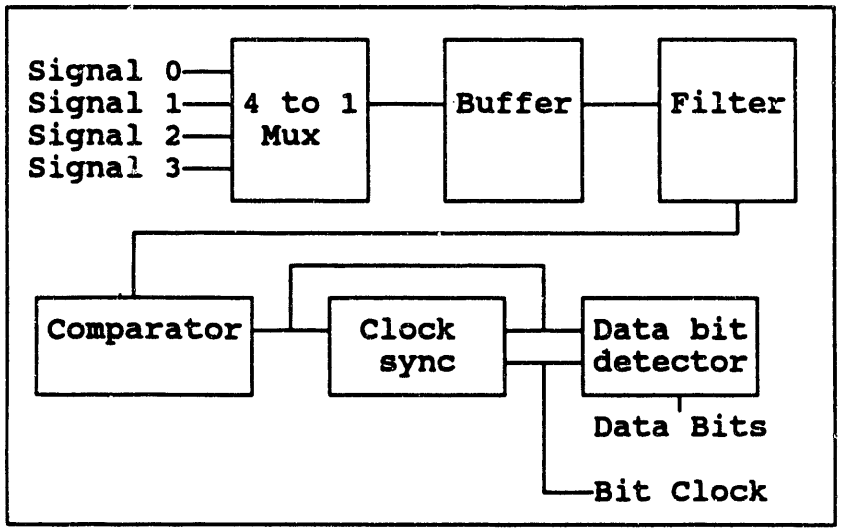

Figure 6-4. Decoder board bit detector

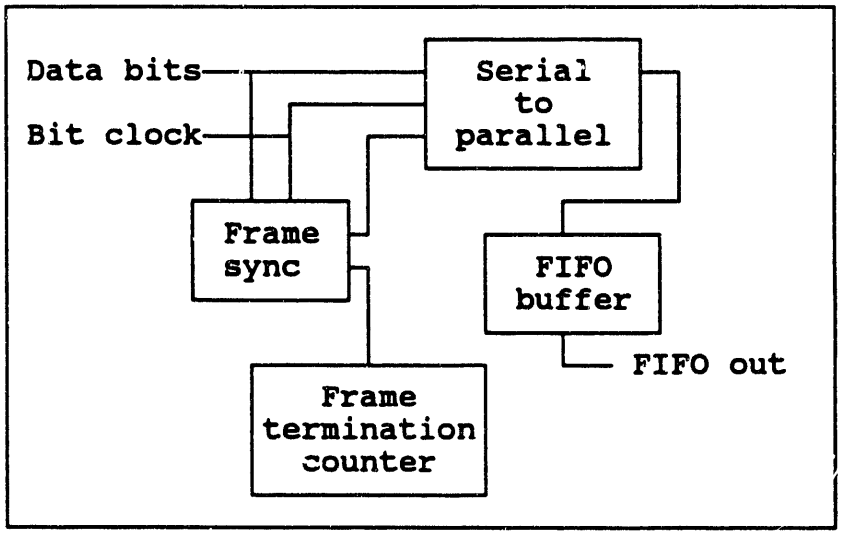

Figure 6-5. Decoder board frame synchronizer

PC Interface and Control: Figure 6-6 shows PC interface and control circuits that interface the PCM data decoder to the PC/AT bus. The FIFO output must be connected to the PC/AT data bus to transfer data. This process is controlled by the control block, which also controls programmable functions and interfaces to the multiple-board arbitration circuit. The multiple-board connector provides an independent data path between boards. The master board determines which boards have data ready to transfer to the PC/AT bus. If more than one board has data at the same time, the arbitration circuitry controls the order of data transfer.

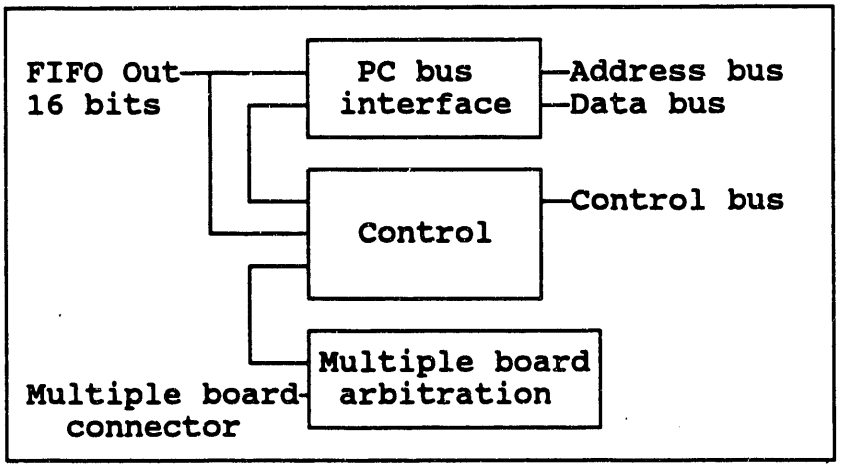

Figure 6-6. PC interface and control

6.3 NREL PC-PCM Data Reduction System "Quick-Look" Software

The Quick-Look program is a comprehensive software package designed to manage data from multiple incoming data sources. It provides a way to quickly examine field data in an experiment test environment. Program menus allow easy access to options that facilitate organization, acquisition, processing, and display of information from many PCM data streams.

The program presumes that a PC cannot process all incoming data in real time. It compensates for this by using techniques to reduce the quantity of incoming data to a manageable level. The data reduction techniques impose limitations that the user must be aware of, and they may not be appropriate in certain situations. However, for most of our quick-look requirements, the imposed limitations are not of concern.

In our typical field experiments, we have found the Quick-Look program to be extremely beneficial, especially for monitoring in real time and conducting multichannel calibrations. The ability to grab contiguous time series data blocks from multiple streams allows access to high-rate phenomena. Graphic review features provide the test engineer with a means to quickly interpret results. Data bases providing histories of channel configurations and calibration coefficients are essential for accurate postprocessing of recorded raw data sets.

6.3.1 Overview of the Quick-Look Program

The Quick-Look program is used on a DOS-based PC interfaced with peripheral PCM decoders in an experiment test environment. The major objective in developing the program was to provide a way to quickly examine data from PCM streams in the field. Other objectives include on-line channel data base management, hardware debugging capability, and automated calibration procedures.

Menus are presented to the user enabling quick selection of desired options. Each menu contains a title, followed by lines listing current available options. The user uses the arrow keys to move a highlighted bar up and down to select the desired operation. From there, another level of menu options may appear, or option execution may begin.

The main program menu presents the user with options that are summarized in Table 6-5. These options identify all the basic features of the Quick-Look program.

Table 6-5. Quick-Look Program Features

Hardware Setup	The definition of all parameters related to interfacing the PC with peripheral PCM decoding devices.
PCM Configuration Data Base	Data base in which to define and maintain the characteristics of all potential incoming PCM streams.
Channel Data Base	Data base in which to define and maintain information associated with all measured data channels.
Derived-Parameter Data Base	Data base in which to establish and organize ancillary derived channel equations.
Data Acquisition	The selection of channels, monitoring of current conditions, collecting of data, and storing of it in a disk file.
Recorded Data Display	Comprehensive graphic or alphanumeric display of previously recorded data sets.
Channel Calibration	Multiple-channel data processor using least-squares linear regression to generate calibration coefficient.
File Maintenance	System to organize and catalog experiment-associated data files and channel data bases.
Test Event Log	Record of the sequence of experiment events.

Typical components of PC-based data acquisition systems common to both the Quick-Look system and most commercial data acquisition systems are not described here. This report concentrates on the particular capabilities of the Quick-Look program related to quick handling of PCM data in the field and conducting of calibrations. Although this program was developed to allow the PC to be interfaced with PCM data, the capabilities for data management outlined here could be applied to other types of telemetry-based experiment data handling systems as well.

6.3.2 Limitations of PC-Based Data Processing

A basic premise of the Quick-Look program is that the PC cannot process all incoming data in real time. Because of DOS and CPU limitations, data collection and data processing are not done at the same time. These tasks could be combined if incoming data rates are sufficiently slow. However, for most of our applications, we have found that the typical PC cannot concurrently do both adequately. If the processes are independent, the CPU can be fully dedicated to each task separately. This allows access to higher-rate incoming data and provides greater data processing capability.

To compensate for the limitations imposed by the PC, two techniques can be used to effectively reduce the quantity of incoming data to a manageable level. First, the PCM data streams can be periodically sampled at a controllable rate. This allows the PC's CPU to selectively alternate between data acquisition and processing. Second, data can be recorded to disk or memory over a given duration of time and then postprocessed.

These data reduction techniques impose restrictions that the user must be aware of, and they may not be appropriate in certain situations. For example, transients may be missed, or aliasing could be introduced. To provide data values representative of existing conditions, the data segments should be stationary time history records (Bendat and Piersol, 1980). The Quick-Look program provides many features that allow evaluation of time series data. It is up to the user to ensure that the data segments are sufficiently long and statistically meaningful to produce adequate results.

For most of our quick-look requirements, the limits imposed by the PC-based system are not of concern. In our typical field experiments, we have found this system to be extremely useful, especially for monitoring current conditions and conducting channel calibrations. We do not, however, use this system as a substitute for full data processing. Usually, all PCM data streams are recorded independently of this system to provide complete data sets for comprehensive postprocessing, as shown in Figure 6-2.

6.3.3 Interfacing a PC to the PCM Data Streams

The main function of the Quick-Look program is to interface a PC with PCM data. This requires some type of PCM decoding hardware with the ability to transfer data into a PC. The data transfer can be done in a variety of ways, such as through a simple but slow serial communication port or complex but fast DMA buffers. The PCM decoding hardware can be outside or inside the PC. This report assumes that PCM data are provided to the Quick-Look program through a PC-based PCM-decoding hardware system developed by NREL (Simms and Butterfield, 1990). The Quick-Look program could support other PCM decoders if appropriate interface drivers were provided; however, some of the software features described here depend on unique capabilities provided by the NREL decoding system.

The NREL PC-PCM decoding system consists of printed circuit boards (APEX Systems, 1988) that fit directly inside the chassis of a PC/AT or compatible computer and basic control software. PCM data are decoded on the board and DMA transferred to PC memory or disk. One board can decode one PCM stream at a time. Up to four boards can be installed into a PC, permitting data from four streams to be simultaneously combined. The Quick-Look program builds all data files necessary for setting up PC-PCM boards and overlays control software to accomplish data acquisition.

The full complement of four boards in a PC allows the Quick-Look program to manage data from up to 16 PCM streams. Each board has four inputs and can be quickly reconfigured to cycle through the input to sample data from different PCM streams. Various combinations of cyclic or concurrent acquisition can be used. Maximum data collection rates vary, depending on hardware limitations and other variables that are discussed below. The boards support standard-format IRIG-compatible PCM streams with bit rates in the range of 1000 to 800,000 bits/sec and a maximum of 64 data words (including sync) per frame. Based on 12-bit data resolution, channel sample rates from 1.3 to 33,000 Hz are possible.

The Quick-Look program assumes that each channel of input data is a time history record and that each record has a constant sample rate. However, because data can originate from multiple PCM streams of varying rates, channels may have different sample rates. Data are transmitted to the program through arrays either in memory or on disk files. If multiple PC-PCM boards are used, data from up to four PCM streams can be collected simultaneously. All incoming data are meshed into a single file. After they are collected, they are decoded for display by the Quick-Look program. If a single PC-PCM board is used, it is still possible to cycle through and monitor up to four PCM streams, but simultaneous acquisition from multiple streams is not possible. Software decoding of subcommutated or super-multiplexed PCM data is not supported.

To keep track of up to 16 PCM input, the Quick-Look program provides a location matrix into which the user assigns incoming PCM streams to their respective input locations. When data are requested from a particular PCM stream, the program uses the matrix to determine how to set up acquisition so that the correct PCM streams are accessed.

During acquisition of PCM data, all values are based on raw counts, which are derived from binary data words that have been decoded from the PCM data streams. Data resolution is determined by the number of bits used to represent each measured data value. We typically use 12-bit resolution, which is 1 part in 2^{12}, corresponding to count values ranging from 0 to 4,095.
The Quick-Look program interprets the raw count values provided by the PCM decoding hardware and converts them to engineering units. As described above, because of the potentially large amount of incoming data and the limitations of the PC, the Quick-Look program does not acquire and process the data simultaneously. It uses techniques of contiguous or sampled acquisition to reduce the volume of incoming data to a manageable level. These techniques are described below.

6.3.4 Contiguous Data Acquisition

In contiguous data acquisition, data streams are recorded as time history record blocks with no gaps. Data from up to four streams can be acquired simultaneously to a disk file up to the limit of available disk space. The data blocks are then postprocessed using features of the Quick-Look program or other data analysis programs.

While contiguous data collection is occurring, no other process can run. After the block of data is acquired, summary statistics are presented on the monitor display. From these, the user can decide whether the data set meets the necessary criteria.

The required number of samples is specified by the user as a time duration. The total resulting number of data points depends on bit rate, number of streams, and channels per stream. Large quantities of data are not practical in this mode. Upward from 50,000 individual data values start to become difficult for two reasons:

1. ***Disk storage resources are quickly exhausted.*** Raw data are input to the program in an efficient binary integer format. However, to produce practical data sets, they are converted to engineering units and copied to an ASCII file in 80-column E12.3 format with corresponding time. This is very readable (and printable) but not storage efficient.

2. ***It takes a long time to process.*** It is CPU intensive to decode and sort the raw binary data, especially for multi-board acquisition. Data from the PCM streams are intermeshed in one binary file as they are acquired. Each data value is encoded with a tag that identifies the stream and channel it came from. The tag has to be removed from the data and used for sorting. The raw data values usually require conversion to engineering units. Slower-rate data are interpolated to the rate of the fastest stream. The final data file is chronologically organized as a time series, with each record consisting of a time value followed by data values from each requested channel for that time.

6.3.5 Real-Time Data Monitoring

Sampled data acquisition is used to provide a real-time data monitoring capability. The incoming PCM streams are periodically sampled to acquire small segments of contiguous data. The segments are quickly processed and displayed to show current conditions. The process is continuously repeated. Up to 135 channels from any combination of incoming PCM streams can be displayed. Each representative value

for each channel is determined by averaging 1 to 10,000 contiguous samples. The user selects channels for display and defines an appropriate averaging interval.

Data monitoring is a cyclic repetitive process that is controlled by the Quick-Look program. This is shown in Figure 6-7 and can be described in three basic steps:

1. PCM-stream data acquisition is initiated to obtain data segments from each requested channel. The Quick-Look program overlays an independent data capture program that initializes the PCM decoding boards, locks onto the PCM streams, and initiates data capture. All PCM streams containing requested channels are sampled to obtain enough contiguous data frames for the required averaging interval. Data are written to RAM disk, and control is returned to the Quick-Look program.

2. The Quick-Look program reads data from RAM disk and sorts by requested channel. Mean and standard deviations are calculated for each channel from the total number of samples in the sample period. PCM data in units of counts can be converted to engineering units using the slope and offset from the channel data base. If derived channels are requested, calculations are performed using equations from the derived-channel data base. Any combination of derive channels and measured channels can be displayed.

3. Resulting values are displayed on the screen in either raw PCM counts or engineering units. The main reason for displaying counts is to conduct calibrations. The screen display is an alphanumeric representation of the current conditions for the requested set of data channels. The program monitors in pages of 15 channels each. Only one page is displayed at a time. The user can easily select from among several pages by keying the desired page number. All pages are updated simultaneously after each set of data is processed. Each channel is displayed beginning with channel number, name, and units from the channel data base, followed by the current mean and standard deviation.

For example, selected channels would be displayed on the monitor in the following format:

```
201:Anemometer #1 (m/s) ..... 1.067E+01 (2.502E-01)
307:Power Supply (Volts) ..... 2.502E+00 (6.745E-02)
402:Bending Moment (N-m) ..... 5.678E+02 (3.456E+01)
        .                              .
        .                              .
        .                              .
```

The first digit of the channel number identifies the PCM stream, and the next two digits identify the data word. The mean and standard deviation values continuously change as data monitoring cycles. The monitor display may lag behind real time by a few seconds, depending on calculation overhead. For the Combined Experiment data streams of Table 6-1, practical data monitor update rates of 1 to 10 sec were easily achievable.

At any time during data monitoring, data collection can be initiated via a user-entered keystroke. This causes monitor-displayed mean and standard deviation values to be permanently recorded in an ASCII disk file. The data monitor will continue to update and will note that data collection is in progress. The collection can be suspended and restarted at any time. Upon termination of data monitoring, collection is stopped, and mean values for the entire period are calculated. These are inserted at the beginning of the data file, and the file is closed and saved. The user is notified of the file name, is shown the file for browsing, and has the option of printing a copy.

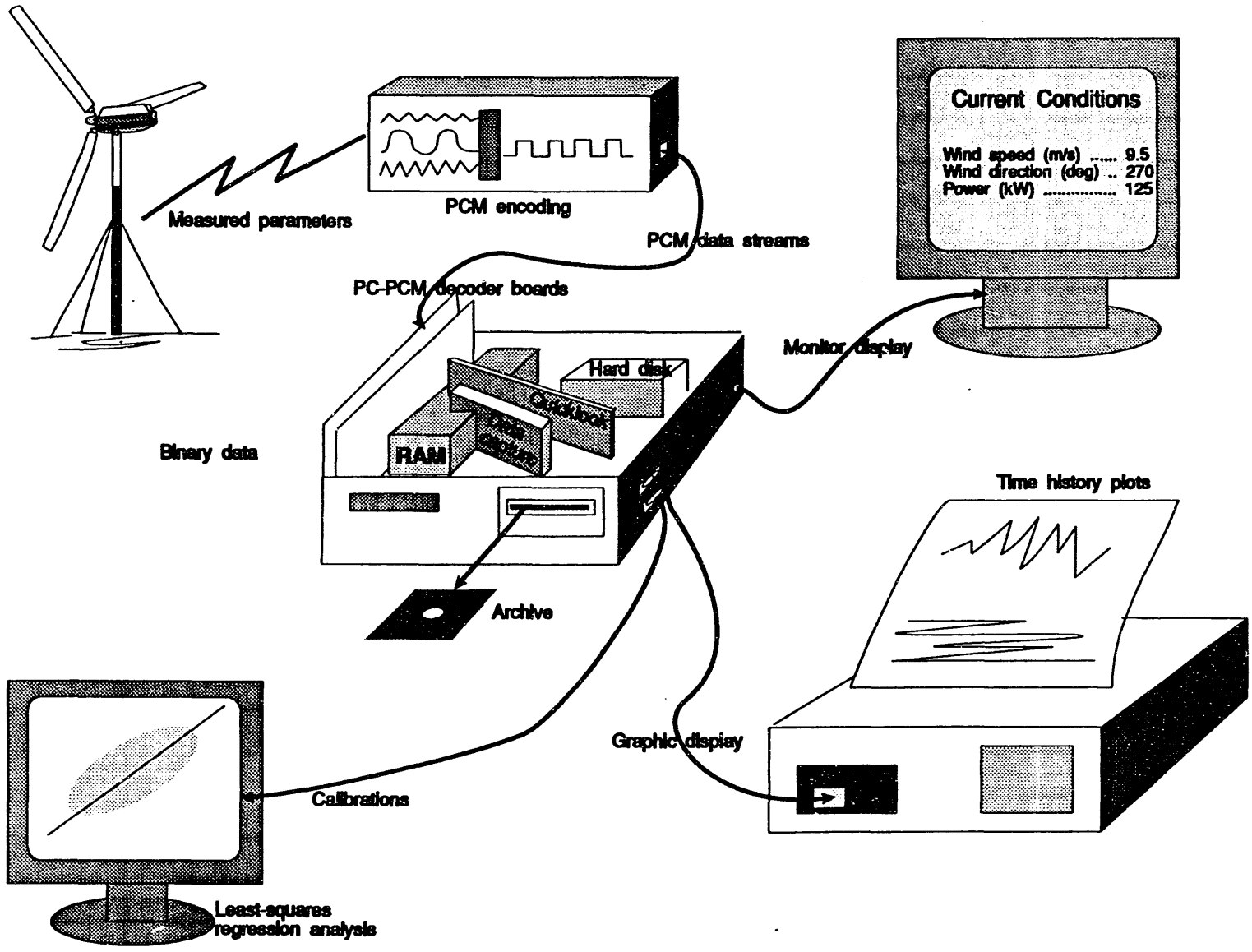

Figure 6-7. Quick-look program data flow

6.3.6 Data Monitoring Features

Typically, the monitor displays current rapidly changing conditions. The current values are calculated by averaging contiguous samples. Another level of averaging is also possible. A parallel monitor display is available to show long-term averaged values that are determined from the current condition values. Keystrokes are used to toggle between the long- and short-term displays. For long-term averaging, current display values are summed for each channel (measured and derived) over the averaging period. At the end of each period the sums are divided by the number of scans, and the average display is updated. The user defines an appropriate long-term averaging period (typically in minutes).

Because up to 135 data channels can be monitored, it would be impractical to expect the user to re-enter the list of desired channels each time he or she wants to monitor data. To overcome this, the program provides a means of defining and saving collections of display channels. A user-defined name is associated with each collection. The user assembles a collection of channels, and the Quick-Look program adds it to a list of available selections. When data acquisition is initiated from the main menu, the user is presented with a menu containing the list of all available collections of channels and selects the appropriate one using the arrow keys. It is also possible to modify an existing collection, delete obsolete ones, and define new ones.

For real-time data monitoring, a range-check feature exists that highlights the display when a value is out of range. The user enters the maximum and minimum allowable values for a particular channel in the channel data base. If a value is outside the range, it is displayed with a conspicuous red background.

Another type of real-time data monitor is provided in the form of a graphic bar chart display. This can be invoked at any time during alphanumeric data monitoring via a user-entered keystroke. Up to 62 measured channel values are graphically displayed as bar graphs on the screen. The Quick-Look program sets up the bar chart display with the desired PCM stream configuration and channels. The bar chart monitor shows data in units of counts and can be used on only one PCM stream at a time. Its display update rate is very fast, typically many times per second. It is useful for quickly checking a large number of channels at once because dead channels are readily detected and easily identified.

6.3.7 Factors Affecting Data Monitor Rates

The rate at which the data monitor display updates itself is affected by many factors. Some depend on which program options the user selects. Others are inherent in the hardware. Some of the factors are

1. CPU speed of the PC
2. Number of channels to display
3. Number of scans to average for each sample
4. Whether engineering unit conversion is done
5. Whether derived parameters are calculated
6. Overhead of the PC-PCM board capture software
7. Bit rate of the incoming PCM stream(s)
8. PCM stream consistency and quality
9. Whether data are captured to RAM or hard disk
10. Whether simultaneous or cyclic acquisition is used
11. Whether data collection is occurring.

6.3.8 Data Base of PCM Stream Configuration

The Quick-Look program provides a form into which a set of configuration parameters defining each PCM stream can be input. The parameters are then used to set up decoding hardware to access streams whose channels are requested. The configuration parameters are

1. PCM stream title
2. Number of data words per frame (data channels)
3. Number of sync words per frame
4. Binary sync bit pattern
5. Bit rate in bits/second
6. PCM data format (Bi-phase L or NRZ)
7. Signal polarity
8. Bits/word
9. Samples to average.

6.3.9 Data Base of Channel Parameters

A data base is kept for each channel of each PCM stream. A maximum of 70 channels per stream is allowed. The data base consists of a set of user-definable parameters and corresponding data. For the Combined Experiment, the following parameters fields are used:

1. Channel description
2. Sensor location
3. Sensor type
4. Sensor ID number
5. Anti-alias filter setting
6. Sample rate
7. Engineering data units
8. Slope (engineering units/count)
9. Offset (engineering units)
10. Range maximum
11. Range minimum
12. Reference channel for calibration
13. Low, zero (mid), and high calibration values
14. Flag to print mean values to a log file
15. Date and time of latest revision.

Parameters 2 to 6 are available for bookkeeping purposes, and other than for comprehensive printouts, they are not used elsewhere in the program. Values do not have to be entered in these fields. Parameters 1 and 7 to 14 are used in various other places in the software. Values may need to be entered in these fields depending on the program option selected.

The channel data base option of the Quick-Look program provides access to these parameters for any channel on any PCM stream. The user is presented with a form on the screen that displays current parameter values, which can easily be updated or modified. If any changes are made, a new version of the data base file is written and becomes the current version. Parameter 15 is updated automatically if any changes are made in any field.

Previous versions of the channel data base are retained so that a history of the channel, including calibration coefficients, is available. The program allows previous versions to easily be recovered. This is especially useful for postprocessing raw PCM data recorded on tape, allowing ready access to data values in correct engineering units.

6.3.10 Derived Channel Data Base

A data base of all derived channels is maintained by the Quick-Look program. A derived channel can be a function of many channels from multiple PCM streams. When the user selects the derived-channel data base option, a simple form is presented in which the channel description and derived equation are entered. The equation may contain constants, functions, or measured channel numbers. Upon completion, the derived-channel information is saved and made available for use either in monitoring or generating data files.

6.3.11 Rapid Multi-Channel Calibration Capability

Only linear engineering unit conversions are provided, one slope and offset pair for each channel. The slopes and offsets can be input manually into the channel data base, if known. They can also be generated based on measured data obtained during "calibration runs" and automatically inserted into the channel data base. It is possible to quickly generate and update calibration coefficients for many channels from many PCM streams simultaneously. There are four options for calibration runs:

1. 3-level high/mid/low calibration data
2. 2-level high/low calibration data
3. 1-level zero calibrations (determines offset only)
4. A function of another "reference" data channel.

For the first two options, PCM count data are collected at the constant calibration levels for a short duration of time and stored in a file. The channel data base contains a value in engineering units that should coincide with the measured count value at each level. The count data are read from a file and compared to the reference values. A least-squares regression line is generated from which a slope and offset are found, and correlation statistics are calculated.

For the third option, count values corresponding to the channel zero (or any known level) are stored to a file. The data base zero value is used as a reference, and a new offset is calculated.

For the fourth option, engineering unit data are concurrently measured from a reference channel used to generate coefficients for the channels to be calibrated. The relation between the reference channel and the channel to be calibrated is limited to a simple user-defined mathematical function entered in the channel data base. A least-squares regression line is generated to obtain the relation between the two variables. This allows a ramp calibration to be done, in which the data values are distributed over a wide range as opposed to discrete known levels.

Upon completion of a calibration run, the user is presented with a page of summary regression statistics, other information pertinent to the least-squares fit, and new calibration values. The user can opt to accept or decline the cal coefficients based on these statistics. He or she can also set up criteria that automate the acceptance process using defined tolerances. For example, the user can identify acceptable ranges of standard error and correlation coefficients. If the regression statistics are within the ranges, cal coefficients are automatically accepted and inserted in the data base. This provides a means of quickly

calibrating many channels. It has proven very useful in the Combined Experiment, in which calibrations of 128 pressure channels are required every 5 min of testing.

6.3.12 Event Log File

The Quick-Look program provides a means for maintaining a log of events that occur during an experiment. The user can set up a log file at any time. The log feature automatically notes when data acquisition occurred and summarizes channels used and mean data values during the interval. If any changes are made in the channel data base, it is noted in the log that a new version was generated. If any channels are recalibrated, their new calibration coefficients and regression statistics are included in the log. The user can easily enter comments, which will be time stamped.

6.3.13 Quick Review of Recorded Data

Upon completion of data collection to a file, the file is immediately available for review. It is presented to the user and can be scanned and printed. Channel values can also be displayed easily using included graphics programs. Two- (2D) or three-dimensional (3D) plot capability is available. Basically, all the user has to do is select a data file, plot type, and desired channels. Available plot types are as follows:

- *2D time series plots:* Channel data are plotted on the ordinate axis with time on the abscissa. Axes' maximum and minimum are automatically chosen based on data range. Channel data are plotted in appropriate units. A legend that uses the channel name to identify each curve is automatically included. Up to 10 channels of data can be displayed on one graph.

- *2D X-vs.-Y plots:* Channel data are plotted on both axes for comparison. A legend is generated from the name of each Y-axis channel to distinguish among multiple comparisons. Up to 10 comparisons can be displayed on one graph.

- *Custom 2D plots:* This option provides the user with some flexibility to generate custom-format plots.

- *3D plots of time-vs.-channel-vs.-data value:* This option provides a quick way to look at time series from many similar channels simultaneously. Time is plotted incrementally on the X axis. (It is assumed that the scans occur at even intervals of time.) Selected channels are plotted on the Y axis incrementally in the order in which they were selected. The data value magnitudes are plotted on the Z axis. The XYZ values are shown as a surface in three dimensions. Any deviation among channels is readily noticeable on the plot surface. Appropriate surface display depends on the particular data set, and display options are available to improve the view.

6.4 Combined Experiment Data Processing

Data processing requirements depend on what the data are to be used for. Data from the Combined and Unsteady Aero Experiments are destined for a wide variety of different potential uses, and it is difficult to specify generic requirements. There are certain in-house projects and applications that dictate initial necessities. Some of the subcontractors have also specified their needs. A channel measurement may require greater accuracy for some applications than for others. We have attempted to incorporate the measurement needs from all potential sources and, in addition, anticipate what future data analyses might require. These measurement requirements are summarized in Appendix B.

The main objective is to provide channel data measurements within the defined tolerance ranges to the specified levels of confidence. It would be impossible, however, to make all measurements to these levels.

With 239 total channels, there is always the potential for some to be out of commission, not working properly, or not in calibration. It is therefore the test engineer's job to determine the severity of out-of-tolerance data channels. This depends entirely on the objectives of the particular test. It is the duty of the test engineer to ascertain what channel measurements are critical for that test. If critical measurements are within required tolerances, the data set is considered valid, and those channels that are out of tolerance are listed and noted so that subsequent data users are aware of their status. For example, if a blade azimuth signal is out of tolerance, but the test requires non-rotating data, the azimuth signal accuracy is not critical to the validity of the data set. If, however, critical channel measurements are out of tolerance, the data set is considered invalid and is not used. It is important for the test engineer to be able to assess this in the field so that he knows that it is necessary to re-acquire the data set.

Most of the tests conducted under the Combined Experiment require that pressure channels be within specified tolerances to a confidence level of one standard deviation. This pressure measurement accuracy criteria is typically the determining factor for accepting or declining a data set because these measurements demand the least allowable error. There are also varying requirements that certain other important data channels be functioning properly. The test engineer weighs the results of the calibrations of the critical channels while considering the objectives of the particular test to determine if the data set is worth further postprocessing. The test engineer has many tools at his disposal in the field for assessing data quality and can usually successfully identify valid data sets. Not only can he perform calibrations, but he can also monitor conditions in real time, cross-check redundant measurements, check acceptability of derived parameters, and scan channels for out-of-range data. This greatly reduces the amount of invalid data submitted for subsequent time-consuming postprocessing.

6.4.1 Measurement Accuracy

Under no circumstances do we use the manufacturer-specified accuracy of any transducer, signal conditioner, or PCM encoder. We also do not rely on manufacturer calibrations or manufacturer-recommended calibration intervals; i.e., that transducers or equipment calibrated at recommended intervals will unconditionally provide accurate results. Rather, *accuracy is determined by conducting regular periodic pre- and post-calibrations on the full data path of all measured channels.* The results of the calibrations are then used to specify measurement accuracy.

Pre- and post-calibration sequences were designed and are utilized to provide a direct measurement of data accuracy. Pre- and post-calibrations are performed on the complete data path of each channel for each data set. Two criteria have to be met to ensure adequate calibrations. First, regression statistics resulting from calculated coefficients of each calibration are required to lie within specified error limits. Second, if the difference between the pre- and post-calibration coefficients exceeds the specified tolerance, data collected during the interval between calibrations are considered out of tolerance for that channel. Measurement tolerances and calibration procedures for all channels are shown in Appendix B. Calibrations for all channels are conducted at time intervals sufficient to ensure the accuracy of intermediate data and were determined from test experience. These time intervals vary from minutes to months, depending on the transducer or system component being calibrated and the required channel accuracy. They are categorized according to calibration procedure and are listed in Section 6.4.3.

The objective in calibrating the full data path is to measure the accuracy of all components of the data acquisition system that affect data measurement. This includes the transducer itself, connecting cables, signal conditioner, and A/D converter. Full data path calibrations are conducted on all channels. For the Combined Experiment, they are performed in two basic ways:

1. ***Single-part or "end-to-end" calibrations:*** The most preferable way to calibrate a channel is to directly measure the full-channel response using an external reference that produces a known result. That way, all the components along the data path are calibrated together, and the accuracy of the full system can be calculated (i.e., blade pulls or reference pressure transducer).

2. ***Two-part calibrations:*** For some channels, it is not possible to calibrate the transducer in situ. For these, full-channel accuracy is determined from two calibrations, an electronics calibration and a transducer calibration. The electronics calibration is performed by replacing the transducer input signal with a known precision reference voltage. This measures the response of the electronic portion of the signal path (mainly the signal conditioning and A/D conversion systems), which is usually most prone to drift. The accuracy of the transducer is determined by external pre- and post-calibration to ensure that it remained within tolerance during use. A good example of this is the wind speed channels, where the electronics are drift calibrated with each data set, but the anemometers themselves are calibrated seasonally in the wind tunnel. In these cases, the root-mean-square (RMS) sum of the accuracy values from various component calibrations determined the overall channel accuracy.

Procedures for performing calibrations to produce measurement accuracy within required statistical significance levels are detailed in the calibration procedure column of Appendix B. Those channels in which the transducer requires an external calibration (calibration procedure prefixed by an E) are two-part calibrations. All other channels are calibrated with an end-to-end calibration. Some channels (such as pressures and strain gages) require two end-to-end calibrations, one to calculate slope and another to calculate offset.

The pre- and post-calibration strategy assumes that the channel measurement stayed within calibration during the intervening period. Obviously, this may not be the case, but because it is impossible to continuously calibrate channels, some assumptions have to be made. We have conducted many calibration studies to define appropriate calibration intervals necessary to ensure data accuracy. We have also devised many built-in "sanity checks," which are used to periodically check the data validity of important channels.

6.4.2 Features of the Custom Data Calibration System

It is the objective of the test engineer in the field to produce measurements that are within the tolerance limits specified in Appendix B. It is very difficult, however, to completely ensure the accuracy of all channels, considering the limited facilities and time available in the field. To guarantee that all channel measurements are within the required error tolerance limits is no small task, especially when each 10 min of operation requires re-calibration of at least 200 channels, some of them to extremely tight tolerance limits (to calibrate pressure channels to .2% full-scale allowable error requires least-squares linear regression calculations on hundreds of data points for each channel). For that reason, a custom data calibration system was developed with the specific objective of assisting the test engineer in the field. It provides a variety of tools to initially assess the accuracy of the data by performing calibrations and examining important or critical channel measurements. This strategy has proven to be very useful because the test engineer can quickly identify and eliminate out-of-tolerance data. It saves having to spend a lot of time and effort postprocessing data sets only to find that they contain worthless information. It also lets the test engineer immediately know the status of the test matrix. Subsequent rigorous postprocessing analyses are performed to provide final data accuracy values.

The custom data calibration system consists of 3 components:

1. ***Microprocessor-controlled, rotor-mounted PSC:*** As seen in Appendix B, pressure measurements are those that require the most stringent calibration tolerances. The PSC was designed and built to provide

in-flight National Institute of Science and Technology-traceable reference calibration pressures to all pressure ports. While the machine is operating, the test engineer can initiate a command from the ground that causes the pressure transducers to replace the measured tap pressures with reference calibration pressure on all 128 ports simultaneously. The reference pressure ramps up and down across the measurement range to allow acquisition and calibration of each channel to the required level of statistical significance. The PSC also provides necessary anti-alias filtering and high-quality signal conditioning on all incoming analog pressure measurements to minimize drift and ensure data accuracy.

2. ***High- and low-calibration shunt system:*** For some channels, it is impossible or unnecessary to perform a complete end-to-end calibration in the field. A good example is wind speed. The anemometers only require annual calibration in the wind tunnel. The electronics, however, from the output of the transducers through the signal conditioning and data acquisition system, require more frequent calibration to compensate for drift. This is done by periodically replacing incoming transducer voltages with a known precision reference voltage. A single-point calibration is used to compensate for electronics drift by providing a reference for re-calculating the channel offset in engineering units. A two-point calibration can be used to provide a slope check.

3. ***PC-based Quick-Look automated calibration system:*** The experiment test environment rules out the use of significant resources in the field to verify calibration results. We therefore developed the Quick-Look system, which is a PC-based PCM data processing package. It simplifies the process of acquiring selected sets of channel data during calibration intervals and then automates generating engineering unit calibration coefficients and maintaining data bases of calibration histories. It also allows easy examination and channel cross-checking in real time. The Quick-Look system combines custom-developed PCM-decoding hardware boards with a custom-written software analysis package. The hardware boards are inserted into a PC to convert incoming PCM stream data to disk files. This capability is described in detail in Simms (1990). The software was developed to provide the test engineer with a quick way to conduct multi-channel calibrations in the field. It is described in Simms and Butterfield (1990).

It would have been impossible to conduct the frequent calibrations required by the Combined Experiment and manage all the resulting information without custom data calibration system capabilities. In previous experiments, we had to rely on laboratory-based postprocessing analyses to provide calibration results. Often, by that time, it was too late to go back into the field if subtle or overlooked problems surfaced when analyzing data. At the time of planning for the Combined Experiment, we only had a basic field system that could display a limited number of channel data values. Cost-effective commercial systems that could provide more comprehensive field analysis were not available. We therefore had no choice but to develop our own system to satisfy specific field data verification requirements For that reason, the Quick-Look system, in conjunction with PC-PCM decoding boards, was developed. Recently, low-cost commercial PC-based systems have become available that provide expanded field display capability; these might be useful in future tests.

6.4.3 Combined Experiment Calibration Sequences

The calibration sequences can be classified into three categories: automatic, manual, and external. The sequences are performed at various time intervals to provide information necessary to compute measurement accuracy. Specific procedures are defined that the test engineer must undertake in order to perform the calibration sequences.

1. ***Automatic calibrations*** are those initiated by the test engineer in the test shed to automatically invoke the calibration sequence and cause data channels to measure calibration data. Automatic calibrations are used to calibrate the most sensitive channels (those that require the highest measurement tolerances). They

are usually conducted immediately before and after a data event and are directly recorded to the 14-track data tape. There is not enough time to process the results of these calibrations during data acquisition because the objective is to get the calibration sequences as close as possible in time to the actual data event. The four types of automatic calibrations performed in the Combined/Unsteady Aero Experiments are shown in Table 6-6.

Table 6-6. Automatic Calibration Procedures

Procedure	Description	Calibrate
A1	PCM 2&3 high and low shunt calibration	Offset
A2	Strain gage slow rotations	Offset
A3	Pressure system ramp calibration	Slope
A4	Pressure system short-line zero calibration	Offset

2. ***Manual calibration*** requires the test engineer to set up and conduct the calibration in the field on the transducers in situ. These calibrations should be performed within the specified time intervals. These are done using the Quick-Look system, and all data are saved as PC data sets in units of raw counts. Two sets, a pre- and a post-calibration, need to be done for each affected channel before final accuracy values can be specified. The manual calibration procedures and recommended time intervals are shown in Table 6-7.

3. ***External calibration*** requires the transducer to be removed and calibrated in the calibration lab or in the wind tunnel. These calibrations require more effort and are typically done on channels that are very stable or require less measurement tolerance and do not need frequent calibration. The calibration results are worked up to ensure that all measurements are within the required accuracy. Two sets, a pre- and post-calibration, need to be done for each transducer before final accuracy values can be specified. External calibration procedures are shown in Table 6-8.

Table 6-7. Manual Calibration Procedures

Procedure	Description	Frequency	Calibrate
M1	PCM 1 north MET electronics	< 1 week	Offset
M2	AOA transducers	< 1 week	Slope & Offset
M3	Blade pitch angle	< 1 week	Slope & Offset
M4	Machine yaw angle potentiometer	< 1 month	Slope & Offset
M5	Blade azimuth angle potentiometer	< 1 month	Slope & Offset
M6	VPA wind directions	< 1 month	Slope & Offset
M7	VPA wind elevations	< 1 month	Slope & Offset
M8	Blade pulls for blade strain gages	< 1 month	Slope
M9	Tower pull for tower strain gates	< 1 year	Slope & Offset
M10	Yaw pull for yaw moment	< 1 year	Slope & Offset

Table 6-8. External Calibration Procedures

Procedure	Description	Frequency	Calibrate
E1	Anemometer calibrations in wind tunnel	< 1 year	Slope
E2	Differential pressure sensor in calibration lab	< 1 year	Slope
E3	Absolute pressure sensor in calibration lab	< 1 year	Slope
E4	Differential temperature sensor in calibration lab	< 1 year	Slope
E5	Absolute temperature sensor in calibration lab	< 1 year	Slope
E6	Power transducers in calibration lab	< 1 year	Slope

The recommended frequency of calibration intervals is to be used only as a guide. The stated intervals are based on test experience to provide required accuracy values. Exact timing is not critical because calibrating at these intervals does not guarantee data accuracy. What is important is to perform pre- and post-calibrations. It should be the objective of the test engineer to see that all channels are pre- and post-calibrated at appropriate times as close as possible to when experiment data events are recorded.

6.4.4 Field Data Recording and Processing Requirements

A data event consists of 10 min of recorded data, during which all required parameters are measured. It is bounded by calibration sequences designed to ensure data validity. All information necessary to conduct required calibrations is recorded so that calibration sequences can be reproduced. It is most preferable to directly record raw PCM count data coming from channels during calibration sequences. From these, count to engineering unit conversions are derived. Each 14-track tape should contain two data events, preceded and followed by the appropriate automatic calibration sequences as defined in Table 6-9.

Calibrations 8 through 11 are optional if events 1 and 2 are done within an hour. The overall objective is for all channels of each data event to have a pre- and a post-calibration sequence recorded on tape. Over a longer term, manual and external calibrations should be performed in a timely fashion to maintain data base calibration coefficients up to date and to guarantee data accuracy. A hypothetical schedule is shown in Table 6-10 that assumes an experiment conducted over a 6-month period in which various sets of data events are collected. The pre- and post-calibrations should be performed as close to the data events as practical. All data are recorded on the Quick-Look system and calibration coefficients generated according to prescribed methods. Some of the intermediate calibrations could be omitted if data sets are recorded close enough together in time.

All information necessary to generate calibration coefficients for all measured channels is available to the test engineer in the field. The calibration procedures are performed by the test engineer at required time intervals to provide the information necessary to assess data accuracy and to determine if the data sets are valid or need to be re-acquired. The test engineer can work up the data at any convenient time after a data event or tape has been collected.

In addition to conducting calibration, other methods have been devised to ensure that critical data measurements are valid. These methods depend entirely on the channels being measured and the availability of built-in redundancy or cross-checking measurements. For example, to ensure that the VPA anemometers are functioning correctly, we have found that long-term averages to check horizontal wind stratification will readily pinpoint out-of-calibration anemometers. For verifying pressure measurements, we have wind tunnel data from three independent sources in which pressure distributions as an AOA

Table 6-9. Event Acquisition Procedure

#	Type	Description	Time
1.	A1	Pre-PCM 2&3 high and low calibrations	< 1 hour prior to event 1
2.	A2	Pre-slow rotations	< 1 hour prior to event 1
3.	A3	Pre-pressure systems ramp calibration	Immediately prior to event 1
4.	A4	Pre-pressure system zero calibration	Immediately prior to event 1
5.		**Event 1:10 min of run data**	
6.	A4	Post-pressure system zero calibration	Immediately following event 1
7.	A3	Post-pressure system ramp calibration	Immediately following event 1
8.	A2	Post-slow rotations	< 1 hour after event 1 (can sub 10 or 17)
9.	A1	Post-PCM 2&3 high and low calibrations	< 1 hour after event 1 (can sub 9 or 18)
10.	A1	Pre-PCM 2&3 high and low calibrations	< 1 hour prior to event 2 (can sub 1 or 9)
11.	A2	Pre-slow rotations	< 1 hour prior to event 2 (can sub 2 or 8)
12.	A3	Pre-pressure system ramp calibration	Immediately prior to event 2
13.	A4	Pre-pressure system zero calibration	Immediately prior to event 2
14.		**Event 2:10 min of run data**	
15.	A4	Post-pressure system zero calibration	Immediately following event 2
16.	A3	Post-pressure system ramp calibration	Immediately following event 2
17.	A2	Post-slow rotations	< 1 hour after event 2
18.	A1	Post-PCM 2&3 high and low calibrations	< 1 hour after event 2

Table 6-10. Six-month Experiment Acquisition Procedure

#	Type	Description	Time
1.	E1	Pre-wind tunnel calibrations	Up to 2 months before experiment
2.	E2-E6	Pre-calibration lab transducer calibrations	Up to 2 months before experiment
3.	M9, M10	Pre-tower and yaw pull calibrations	Up to 2 months before experiment
4.	M4-M8	Pre-event set #1 in situ transducer calibrations	Up to 2 weeks before event set #1
5.	M1-M3	Pre-event set #1 critical calibrations	Up to 3 days before event set #1
6.		**1 week of Data Events Set #1 (See Table 6-9)**	
7.	M1-M3	Post-event set #1 critical calibrations	Up to 3 days after event set #1
8.	M4-M8	Post-event set #1 in situ transducer calibrations	Up to 2 weeks after event set #1
9.	M4-M8	Pre-event set #2 in situ transducer calibrations	Up to 2 weeks before event set #2
10.	M1-M3	Pre-event set #2 critical calibrations	Up to 3 days before event set #2
11.		**1 week of Data Events Set #2 (See Table 6-9)**	
12.	M1-M3	Post-event set #2 critical calibrations	Up to 3 days after event set #2
13.	M4-M8	Post-event set #2 in situ transducer calibrations	Up to 2 weeks after event set #1
	.		.
	.		.
	.		.
n-2	M9, M10	Post-tower and yaw pull calibrations	Up to 2 months after experiment
n-1	E2-E6	Post-calibration lab transducer calibrations	Up to 2 months after experiment
n	E1	Post-wind tunnel calibrations	Up to 2 months after equipment

function are documented. We have found that pressure distribution data binned according to the AOA is a good way to validate pressure measurements. These and other techniques are built into various processing routines that are used to check and verify critical measurements.

6.4.5 Comprehensive Data Postprocessing

As stated above, final channel accuracy values cannot be calculated until all post-event calibration procedures have been performed and processed. All post-calibrations should be performed as soon as possible after the experiment has been completed. For that reason, it is especially important to remove anemometers or other transducers so that they are not damaged if they cannot immediately be post-calibrated. After post-calibrations, resulting measurement accuracies for all channels should be calculated and incorporated into the channel data base for use in subsequent comprehensive postprocessing analysis.

Many subsequent processes are applied to the data sets during the postprocessing phase. All channel data are reduced to sample rates, shown in Appendix C, by decimation and filtering. This requires the use of various computer systems and software packages, as shown in Figure 6-8. These procedures are described further in other reports and are summarized below:

1. Record PCM streams and time code to 14-track analog tape.

2. Perform Quick-Look display and analysis in the field.

3. Generate calibration coefficients for all channels using Quick-Look system.

4. Associate and assemble appropriate calibration coefficients with each channel for each 10-min data set.

5. Make two passes through the NREL/Fairchild-Weston PCM Telemetry Data Reduction System to reduce and combine PCM streams into two groups of three streams each; output binary data sets to digital 9-track tape.

6. Load digital tape stream sets into UNIX system.

7. Use custom UNIX/C software to combine two groups of three streams each into one continuous time series that contains all six streams combined to 1-msec precision.

8. Use custom UNIX/C software to
   a. Convert counts to engineering units
   b. Convert multi-rate data to common rate of 1.92 msec (520.83 Hz)
   c. Generate secondary derived parameters
   d. Smooth azimuth angle signal for azimuth averaging
   e. Store data sets to optical media.

9. Use GENPRO to
   a. Low-pass filter all channels to 40-Hz bandwidth
   b. Low-pass filter all channels to 10-Hz bandwidth
   c. Low-pass filter all channels to 1-Hz bandwidth
   d. Interpolate and smooth low-rate data to higher rates
   e. Generate power spectra for selected channels
   f. Generate statistics for all data sets.

10. Use PC-based data base (File Express) on PC-NFS network to maintain summary statistics data base of selected channels from all processed data sets and provide on-line access for other users.

11. Provide data sets on optical media data base for analysis by other users.

6.4.6 Dynamic Effects

All calibrations and data postprocessing methods are designed to verify the accuracy of steady-state data measurements. Other considerations that result from the effects of the dynamic response of transducers also affect data accuracy. These are difficult to assess and cannot be measured directly from the above-described calibration procedures. Based on previous test experience, we have estimated that measurements may be susceptible to accuracy deficiencies because of dynamic effects and have identified them in various reports. One of the objectives of conducting these types of experiments is to discover and document such potential sources of error. Further postprocessing analyses may also reveal other areas that need to be considered. This information will be useful in designing future tests and providing field-based means for identifying problems and conducting calibrations.

Two major areas of concern associated with dynamic effects were originally identified and addressed during experiment planning. First was the dynamic frequency response of the pressure system. An "organ pipe" effect could exist in the tubing needed to connect pressure transducers to the surface tapes. This would cause gain amplifications and phase effects that occur as a function of frequency and tube length. Special test apparatus were developed to measure the actual dynamic response of the system. In addition, Akins (1987) used an independent system to measure and document the effects. Results showed that no significant phase or gain effects were evident given the configuration of the system up to frequencies of 80 Hz. Because all processed data sets show no appreciable pressure information above 40 Hz, we have concluded that the frequency response of pressure system measurements are valid.

The second source of potential dynamic effect error is aliasing. Aliasing is inherent in all digital data processing that is preceded by analog-to-digital conversion. Aliasing errors are a function of sample rate and filter set point. In the Combined/Unsteady Aero Experiment tests, data channels are sampled at various rates, depending on required bandwidth, and are anti-alias filtered with 4-pole low-pass Butterworth analog filters (see Appendix C). For all channels on a given PCM stream, the sample rate is dictated by the channel(s) with the maximum required bandwidth. All channels are over-sampled by at least a factor of 5 over the required bandwidth. Factor of 5 over-sampling, in conjunction with 4-pole Butterworth anti-alias filters, results in an RMS aliasing error of 2%. Lower-bandwidth channels, which are further over-sampled, have even smaller errors. For example, pressure measurements are anti-alias filtered with a 4-pole 100-Hz Butterworth filter and sampled at 520 Hz. This results in aliasing errors that are less than 2% in the range of 0- to 100-Hz bandwidth. In reality, there is very little pressure information above 40 Hz, and resulting aliasing errors in this range are less than .1% (Strock, 1983).

One additional source of dynamic error may exist in prop-vane measurements. Analyses conducted to study differences between prop-vane and sonic anemometers indicate that wind-speed measurements made in turbulent conditions in the wake of a wind farm may show significant dynamically induced errors. These effects are currently under study, and it is not known if the turbulence at site 3.3 would produce similar effects.

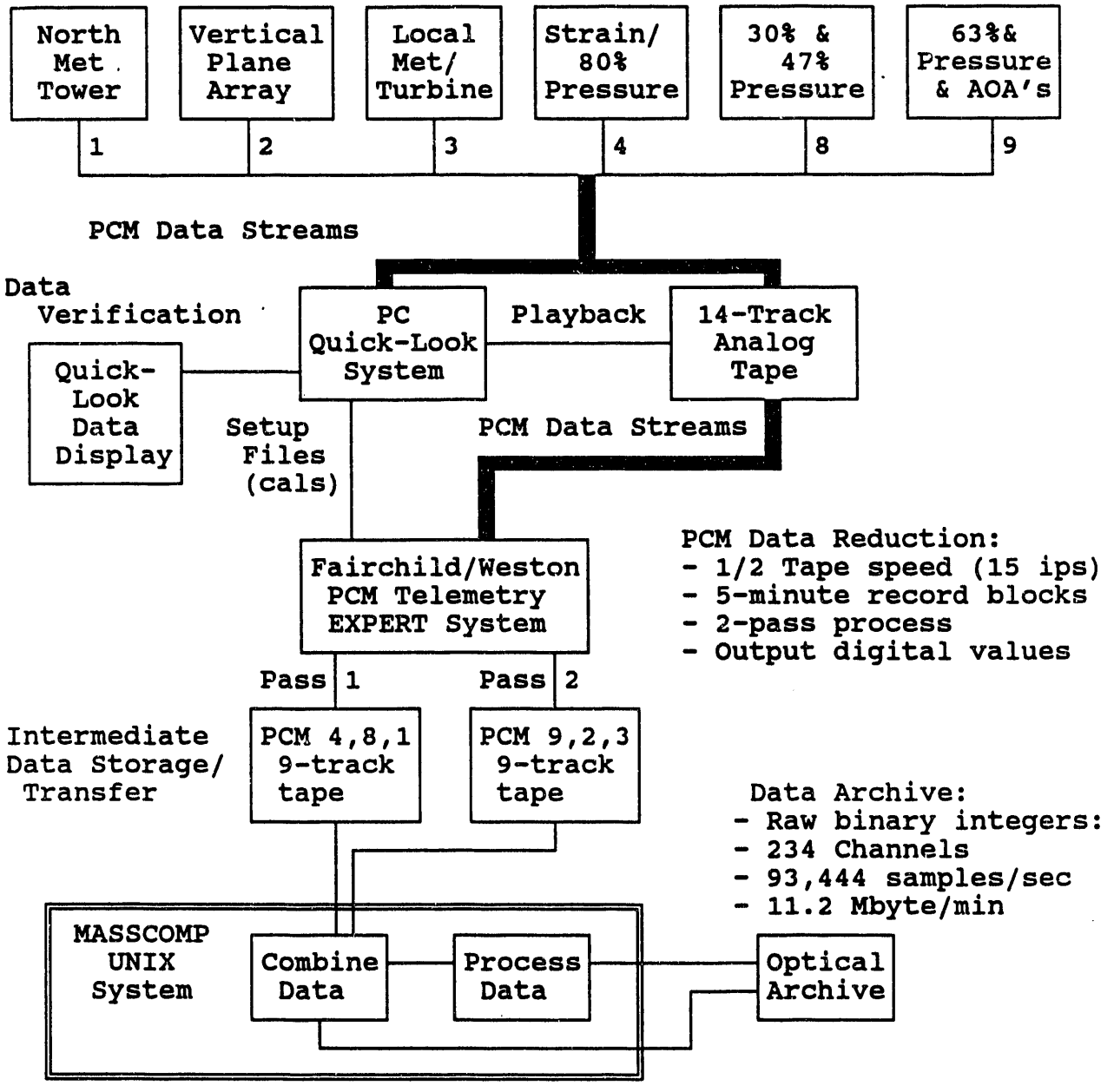

Figure 6-8. Combined experiment phase II data processing plan

7.0 Wind Tunnel Testing

Wind tunnel data were used as reference data sets to compare with wind turbine data because this is the type of data that is used by designers as input to performance and structural design codes. For this reason, it was important to have an extensive data base for all operating conditions tested in the field. It was also important that this data base correspond to the exact airfoil under test. The wind tunnel data should represent the same chord, Reynolds number range, AOA range, pressure tap locations, and surface imperfections. Unfortunately, meeting all these criteria with one data set measured from one wind tunnel was not possible. For this reason, several wind tunnel tests were run; each one satisfied a different aspect of the required reference data set. These different wind tunnel test programs are described in this section.

The airfoil chosen for the Combined Experiment was the S809, as mentioned earlier. This airfoil was chosen because it was developed specifically for wind turbine applications, there was a wind tunnel data base available from the Delft wind tunnel in The Netherlands, and NREL had extensive airfoil design analysis results from the Eppler design code (Somers, 1989).

7.1 DELFT Tunnel Tests

The objectives of the Delft wind tunnel tests were to confirm the analytical design of the airfoil and to calibrate the analysis code used to perform the design. To meet these objectives, an extremely accurate 600.0-mm (23.6-in.) chord model was fabricated from aluminum and buffed to a surface finish that was within 0.1 mm (0.004 in.) of the specified airfoil coordinates. Pressure taps were staggered on upper and lower surfaces at 108 locations. This level of model accuracy was necessary for model validation but was not practical for operating field tests on the Combined Experiment rotor. Butterfield (1989a) describes the differences between the accurate Delft model and the model used in field tests and in Ohio State University wind tunnel tests.

Appendix D contains a summary of Somers (1989). This summary includes a brief description of the test setup and a subset of the total results from these tests.

7.2 Ohio State University (OSU) Wind Tunnel Tests

Airfoil test data can be affected by surface irregularities, pressure tap locations, trailing edge accuracy, and many other test setup details. It was important that the reference data set represent the exact airfoil and instrumentation configuration, so that differences detected between the rotating blade data and the wind tunnel data could be attributed to rotating blade effects. It was also important to establish an unsteady (dynamic stall) reference data set.

For these reasons, a second series of wind tunnel tests was conducted. These tests used a 2D model that was fabricated using the same molds used to make the test blade. This assured that the same surface irregularities, trailing edge accuracy, chord length, and pressure tap locations would exist on the wind tunnel test model. The same pressure measurement instrumentation was used in the wind tunnel as on the test turbine. The same AOA probe was used during these tests to assure any effects of the probe would be included in the reference data sets.

The OSU wind tunnel was an open-circuit type with a .92 m × 1.5 m (3 ft × 5 ft) test section. The model had a 0.46-m (18-in.) chord length and spanned the 0.92-m dimension of the tunnel. The pressure tap locations and pressure measurement instrumentation used was the same as that used on the Combined

Experiment rotor that was described earlier. Appendix E contains a description of the test setup and results from this test program.

7.2.1 Steady Tests

Constant wind-speed tests were run for Reynolds numbers ranging from 1,000,000 to 2,000,000. During these tests, pressure measurements were recorded and integrated using the method described by Rae and Pope (1984). The AOA probe was calibrated at the same time by recording the airfoil geometric angle and the flag angle on the probe simultaneously. The discrepancy between the two angles was assumed to be due to upwash, as described in Section 5.2. Because of tunnel blockage effects, the AOA range was limited to 20 deg. A Pitot tube was used to measure the total drag using the wake momentum deficit approach described by Rae and Pope (1984).

The results of these tests agreed with the Delft data in general. Figure 7-1 shows a comparison of lift coefficient data from all three wind tunnels. The slope of the OSU data is 12% greater than the Delft data for AOAs less than 5 deg. The maximum lift coefficient ($C_{L(max)}$) is 8% less than the Delft data. Regardless of the small quantitative differences, the qualitative differences were judged to be reasonable for the purposes of this test program. These differences could be due to model differences and wind tunnel differences. The pressure distributions appeared to be quantitatively and qualitatively similar in terms of the stall progression and pressure profiles. Comparison pressure distributions shown in Appendices D and E demonstrate the similarity. For this reason it was felt that the OSU data represented the Combined Experiment airfoil better than the Delft data, but both would be used for comparisons with rotating blade data.

7.2.2 Unsteady Aerodynamics Tests

Because wind turbines operate in an unsteady aerodynamic environment, an unsteady aerodynamic reference data base was required. The OSU wind tunnel dynamic stall tester was used to oscillate the

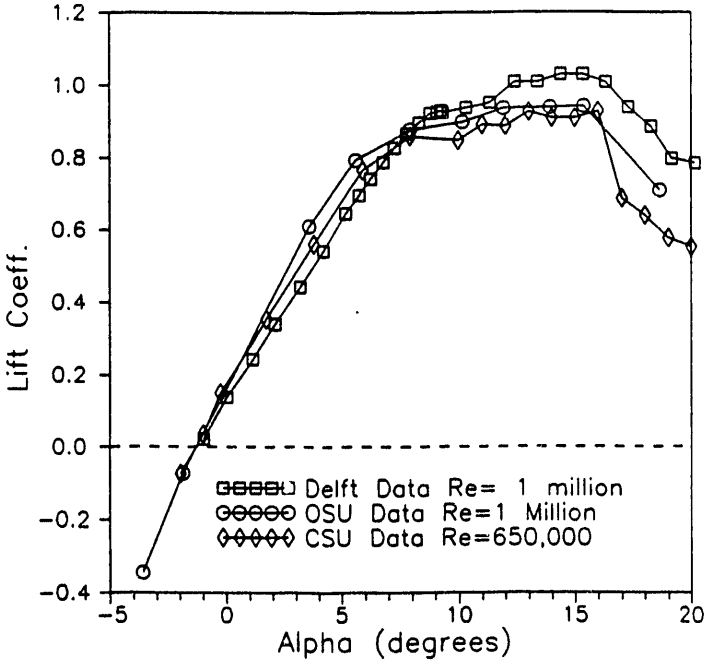

Figure 7-1. Wind tunnel data comparison

model AOA in a sinusoidal manner. Various amplitudes and frequencies of oscillation were tested, and the results are described in Appendix E.

7.2.3 Rough Airfoil Performance

Stall-controlled wind turbines suffer performance losses when the blade leading edges accumulate debris from insect impacts and airborne particulates. To document the sensitivity of the S809 to leading edge roughness, buildup tests were conducted at OSU. Appendix E describes steady and unsteady airfoil performance tests with roughness added to the leading edge of the model. The results of these tests provided a reference data set for the rough blade tests conducted on the Combined Experiment turbine. The results of these tests are discussed in section 8.0.

7.3 Colorado State University Wind Tunnel

The Delft and OSU test data were limited to AOAs less than 22 deg and 20, respectively. Blockage effects beyond these angles resulted in unacceptable errors. The Combined Experiment was focused on stall and deep stall airfoil performance that occurs at AOAs from 15 to 30 deg. For this reason, an additional wind tunnel test was conducted at the Colorado State University (CSU) Environmental Wind Tunnel. The large 3.66 m (12 ft) × 1 m (39 in.) test section available in this tunnel significantly reduced the blockage effects during high AOA testing.

7.3.1 Wind Tunnel Test Setup

The CSU Environmental Wind Tunnel was originally designed for studying flow over models of cities and buildings. The test section was reduced to 3.66 m (12 ft.) × 1 m (39 in.), which allowed a 1-m airfoil test section to be inserted across the narrow dimension. This resulted in a wide test section that would minimize the blockage effects. The solid blockage was 0.28% using Thom's method (Rae and Pope, 1984). Figure 7-2 shows the general layout of the tunnel and the modifications that were made for this test. The modified, open-circuit tunnel was capable of a maximum velocity of 27 m/sec (88 ft/sec), which resulted in a Reynolds number, based on the 0.46-m (1.5-ft) chord, of 650,000. This Reynolds number value is lower than the HAWT test conditions of 880,000 at the 80% blade span, but it was felt that previous wind tunnel data would accurately describe the airfoil performance for Reynolds number values from 750,000 to 3 million for AOA values less than 20 deg. Pressure distribution measurements were made on the model along with pitot tube measurements 2 chord lengths displaced from each side of the model and 1 chord length upwind of the model leading edge. Tunnel temperature, probe total pressure, local flow angle at 0.6 chord ahead of the leading edge, and model pitch angle relative to the tunnel axis were also measured.

Normally, airfoil drag is measured by measuring the velocity profile in the wake of the airfoil and then equating the momentum deficit in that wake to the total drag. This requires a movable Pitot tube or a wake rake positioned downwind of the airfoil. These measurements were not possible to make on the rotating wind turbine blade. There is also evidence that this technique is inaccurate when large-scale separation is present due to rotational flow in the wake. Because NREL's focus was stall behavior, where large-scale separation is always present, it was decided that only pressure drag (C_{Dp}) would be measured. Because C_{Dp} is determined from pressure distribution integrations (Rae and Pope, 1984), wind tunnel data could be compared with HAWT data directly.

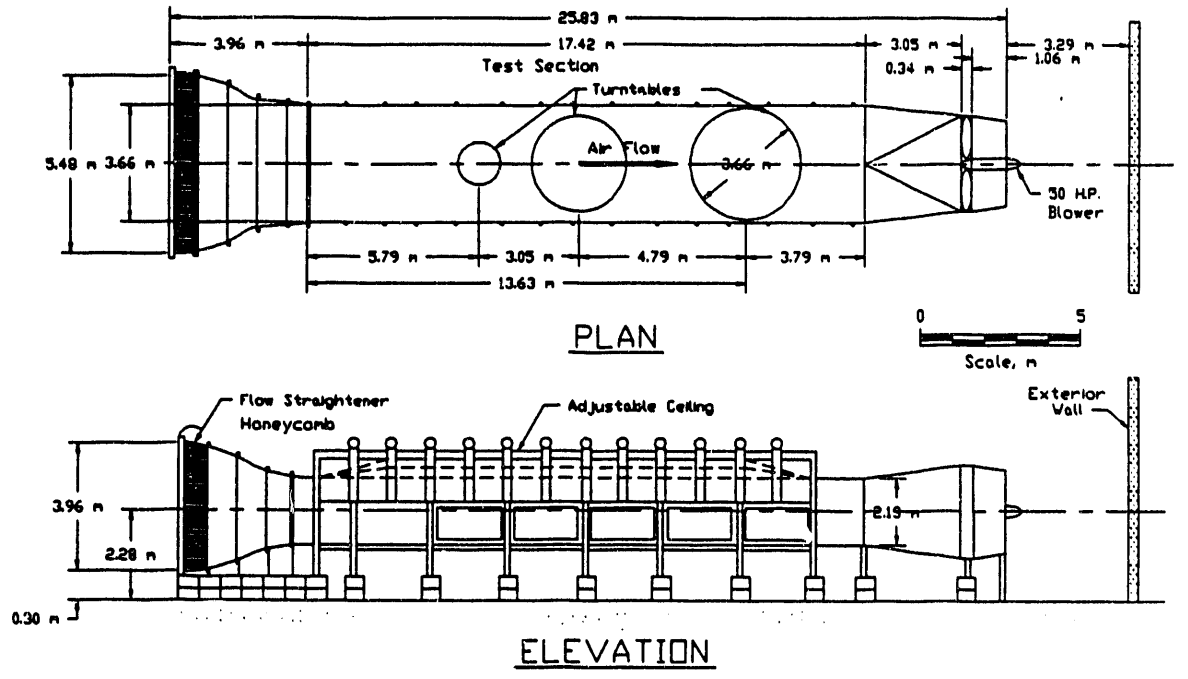

Figure 7-2. Colorado State University environmental wind tunnel

Tunnel turbulence level was a major concern. High-frequency turbulence can affect the airfoil boundary layer, which will affect the performance. To address this concern, a Pitot tube traverse test and a hot-wire traverse test were conducted. The traverses were performed across the test section mid-span in the same location as the model. The results of the first test, shown in Figure 7-3, describe a 6-cm (2.5-in.) boundary layer at the tunnel wall and an acceptable flat velocity distribution across the tunnel. The results of the second hot-wire traverse confirmed the location of the boundary layer. A value of 1% turbulence intensity was measured at the mid-span of the test section. This is a high value for airfoil testing, but the important consideration is the scale of the turbulence. If the scale is close to that of the airfoil boundary layer, it can trip laminar flow into turbulent flow and thus modify performance. If the scale is large, there should be little effect. Figure 7-4 shows a plot of the power spectral density (PSD) of the hot-wire data at the tunnel mid-span at a tunnel speed of 24.5 m/sec (80 ft/sec). The PSD has been multiplied by frequency and normalized by the standard deviation squared. The area under the curve is unity and represents the measured turbulent intensity of 1%. It is clear that the majority of the energy is below 1 Hz (24-m scale). This scale of turbulence is much larger than the boundary layer and therefore should have minimal effect on the performance of the airfoil. These fluctuations were due to small changes in average tunnel speed control.

The airfoil model was 99 cm (39 in.) long with a chord of 45.7 cm (18 in.). This model was the same one used in the OSU wind tunnel tests described in section 7.2. It was placed in the wind tunnel, bridging the narrow dimension (99 cm). This allowed the wake of the airfoil to expand across the 3.67-m dimension of the tunnel. A rubber seal was placed between the wall of the tunnel and the end of the model to prevent leaks. The model was fabricated from the blade molds used to build the blades. This was done to assure that the model would accurately represent the HAWT blade. Pressure taps were installed inside the model using 25- to 38-cm-long, 1-mm-inside-diam. stainless steel tubing. Each tube led from the airfoil surface to a pressure transducer mounted inside the model. The 31 pressure tap locations and installations were identical to the HAWT blade installation.

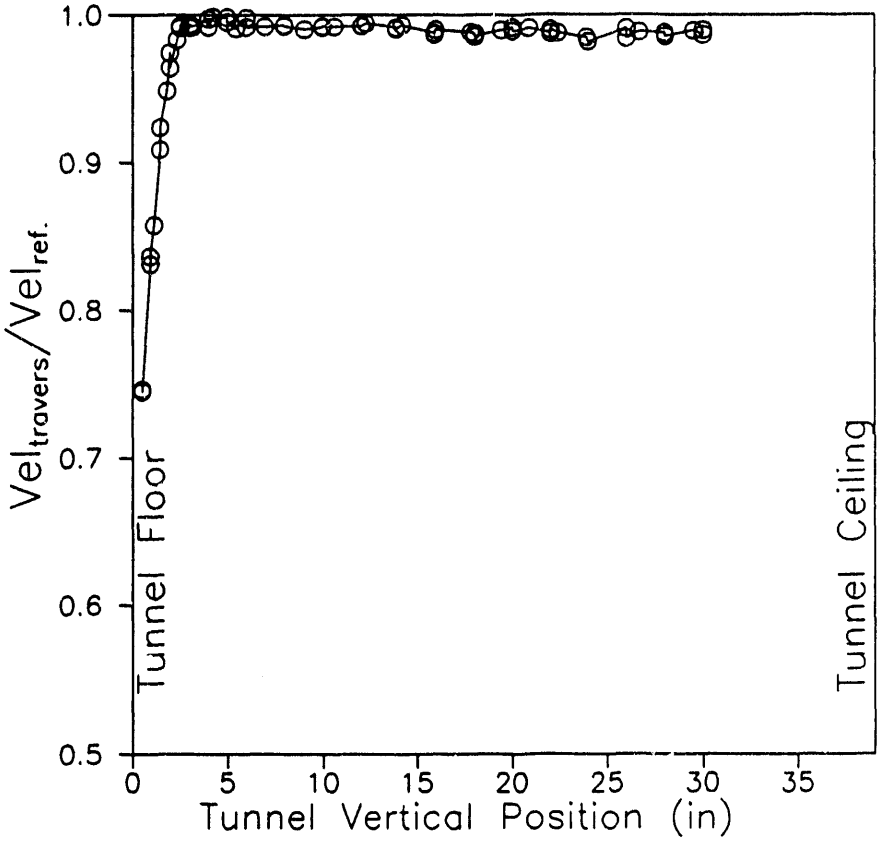

Figure 7-3. Velocity profile of test section for CSU wind tunnel

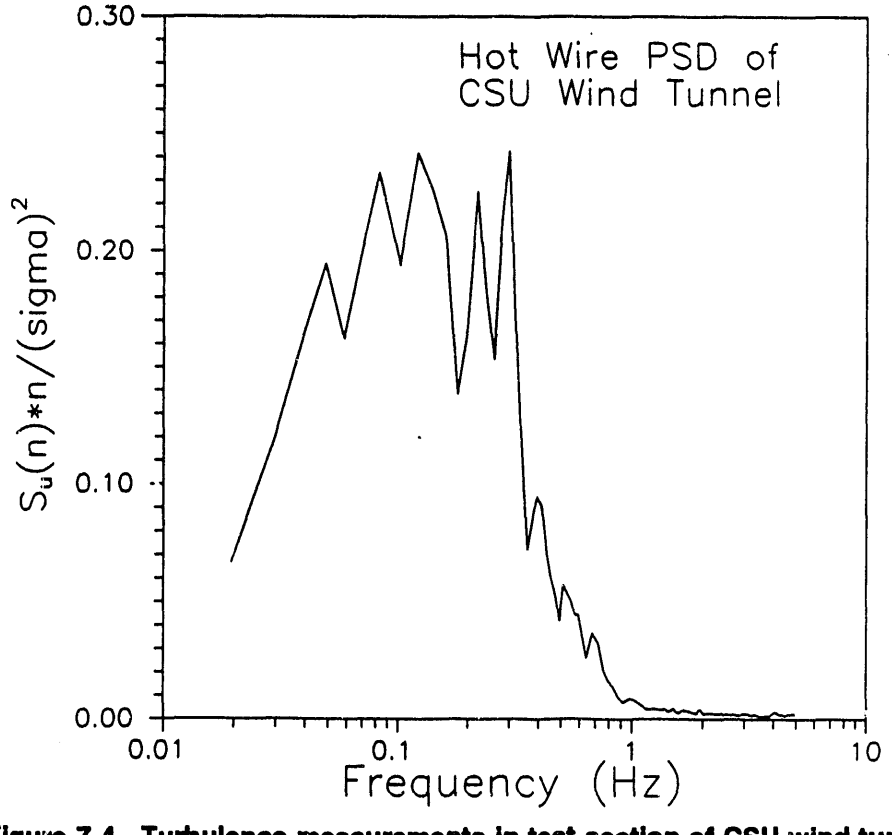

Figure 7-4. Turbulence measurements in test section of CSU wind tunnel

The model also included an LFA probe and a total pressure probe mounted on the leading edge (Section 5.2). A 5-cm-(2-in.)-long, lightweight fiberglass flag was used to sense local flow angles. The same probe was mounted on the HAWT blade. To accurately account for the induced upwash effect on this LFA probe, measurements were taken during the wind tunnel tests and compared with previous measurements made at a Reynolds number of 1 million. Section 5.2 describes the LFA probe and previous calibration measurements of this probe in the OSU wind tunnel.

Each data channel was filtered with a roll-off frequency of 100 Hz and then sampled at 520 Hz using a PCM encoder. The PCM stream was recorded on a Honeywell 101 tape recorder and later decoded and analyzed. The pressure system instrumentation and recording equipment is described in detail in Section 5.1.

7.3.2 Data Analysis

The wind tunnel data were steady and therefore needed no special processing. Pressure measurements were normalized by local tunnel dynamic pressure to get pressure coefficients (C_p). Pressure coefficient distributions were integrated around the airfoil to obtain values of normal force coefficient (C_n), tangent force coefficient (C_T), and pitching moment coefficient (C_m). These were used along with AOA measurements to calculate lift and pressure drag coefficients (C_L, C_{Dp}), using the method described by Rae and Pope (1984).

7.3.3 Wind Tunnel Results

A comparison of C_L data recorded from the three different wind tunnels was made first to establish a baseline validity check on the CSU wind tunnel data. As can be seen from Figure 7-1, the curves do not all look exactly alike. The Reynolds numbers for all three are not the same, which could be one of the explanations, but in general the comparison is reasonable. The slope of each curve is approximately the same, the zero lift angle is similar, and $C_{L(max)}$ is similar but decreasing with the Reynolds number. Figure 7-5 shows how $C_{L(max)}$ decreases with the Reynolds number and compares the general trend with the NACA 4412 and NACA 64-418 airfoils. This comparison shows that it is reasonable to expect a drop in $C_{L(max)}$ in the CSU data because of the Reynolds number. Additional data will be presented in Section 8.0.

From these comparisons, it was felt that the CSU data did not match previous wind tunnel data perfectly, but they were the best to use in HAWT comparisons because they represented the performance of an exact copy of the airfoil and instrumentation of the HAWT blade. Any differences between this set of data and the HAWT data would most likely be due to real differences occurring between 2D wind tunnel conditions and 3D wind turbine aerodynamics. The CSU data also contained values of AOA up to 90 deg. Previous wind tunnel test data only had values up to 20 deg. High values of AOA were needed to compare deep stall HAWT data to wind tunnel data. Figure 7-6 shows the results of the high AOA data for a tunnel speed of 26 m/sec (88 ft/sec) and a Reynolds number equal to 650,000.

Appendix F through Appendix L contain the complete results from the CSU wind tunnel test. The results include C, C_T, lift, pressure drag, C_L, C_{DP}, C_M, and pressure distributions. Three tunnel speeds were run corresponding to Reynolds numbers of 350,000, 500,000, and 650,000.

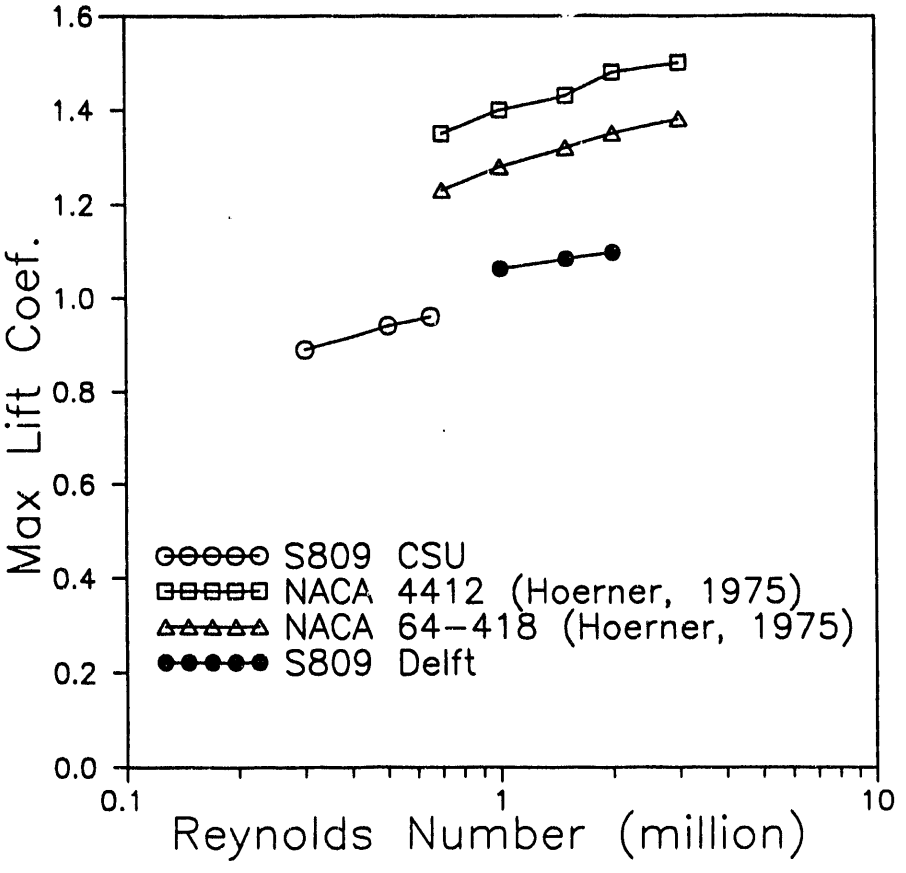

Figure 7-5. Reynolds number effects on S809 airfoil and comparison airfoils

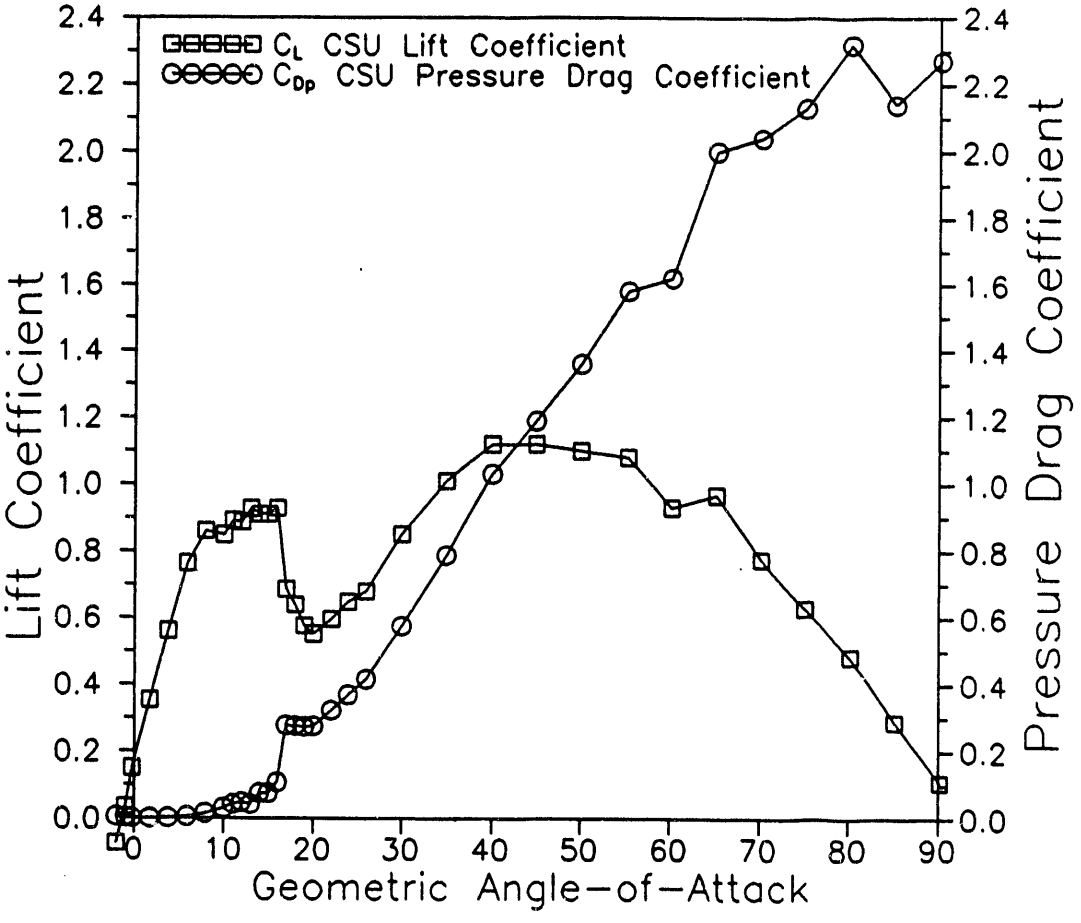

Figure 7-6. Lift and drag results for the S809 airfoil in the CSU wind tunnel

8.0 Rough Airfoil Performance Tests

8.1 Background

Blade surface roughness has been observed to decrease the efficiency of stall-controlled wind turbines by as much as 40% (Yekutieli and Clark, 1987). Most of the degradation can typically be attributed to premature stalling of the airfoil, which lowers the maximum lift coefficient. Figure 8-1 illustrates the effect this can have on stall-controlled rotors. It shows a dramatic difference in the peak power performance for an Enertech 60-kW wind turbine before and after a rain shower. A smaller decline in rotor performance caused by leading edge roughness is experienced at lower AOAs, which can be a significant factor in determining energy capture for pitch-controlled wind turbines (Holtz, 1988).

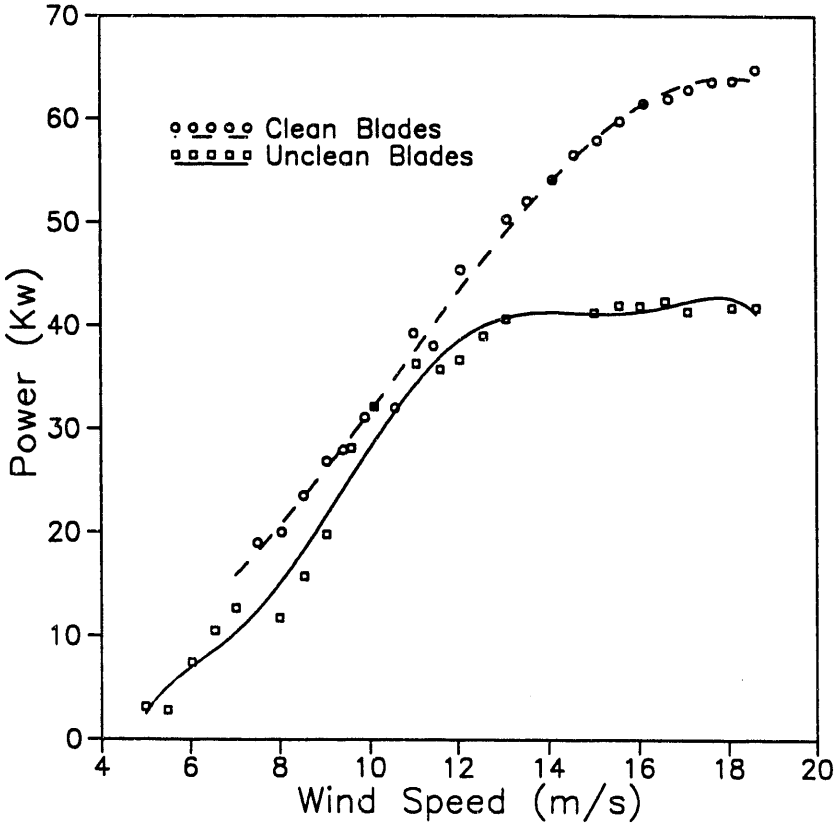

Figure 8-1. 60-kilowatt HAWT performance

Leading edge roughness on wind turbine blades is a universal problem that affects virtually every configuration of wind turbine. It has contributed significantly to producing lower energy, fouling wind turbine control algorithms, and making loads more difficult to predict. Traditional airfoils, such as the NACA 44XX or 23XXX, are being discarded by wind turbine blade designers as they become more aware of the high degree of roughness sensitivity that these airfoils have. Newer airfoil designs such as the NREL airfoil families and the LS-1 series from the National Aeronautics and Space Administration are becoming more popular largely because of their relative insensitivity to roughness.

The effects of roughness on airfoils are most commonly inferred by examining the influence on the rotor's power curve. This method is accurate and reliable for determining the impact on energy capture for a

specific HAWT configuration, but it does not provide much information about changes to the aerodynamic properties of the airfoil. Wind tunnel tests may be used to predict performance degradations caused by roughness in the sub-stall regions, but stalled airfoil behavior is radically different on a rotating blade. The problem is that the stalled airfoil performance on a rotating wing is modified by 3D flow effects (Madsen, Rasmussen, and Pedersen, 1988). It is common for wind turbine designers to underestimate peak performance and loads using wind tunnel airfoil data. Measurements taken directly off the rotating airfoil are the only accurate way to completely determine the effect of roughness on airfoil properties.

8.2 Roughness Description

Most airfoil roughness problems experienced by HAWTs have been caused primarily by insects accumulating on the surface near the leading edge of the blade. The distribution is generally non-uniform, with larger particle sizes and particle densities distributed near the leading edge, rapidly declining toward the trailing edge. In general, particle size usually increases and particle density decreases when progressing from the tip toward the root of the blade.

The NACA standard roughness was created to simulate the typical roughness distribution experienced by aircraft. This standard consists of a uniform distribution of particles between the leading edge and the 8% chord line on the upper and lower surfaces of the airfoil (Bragg and Gregorek, 1989). Particle size is defined by the non-dimensional ratio of the particle diameter (k) divided by the chord length (c). The k/c value for the NACA standard roughness is .00046, which corresponds to grit sizes of .21 mm (.0083 in.) for the Combined Experiment rotor.

Operating conditions for wind turbines are quite different than for aircraft, however. Wind turbines operate closer to the ground and at lower Reynolds numbers and are cleaned less frequently. Consequently, the NACA standard roughness is not severe enough to represent the actual accumulation of insects observed by the authors. In order to do a realistic test of rough airfoil performance on the S809, it was necessary to create a roughness pattern that was more appropriate for wind turbine applications.

A "simulated insect" roughness was developed and applied to all three blades over the outer 3.35 m (11 ft). Coarse grit particles ranging in size from 0.5 to 1.0 mm (.020 to .040 in.) were distributed onto a 20.3-cm-wide (8-in.) strip of 3M #444 double-coated tape, 0.05-mm thick, that was centered on the leading edges of each blade. The grit was scattered randomly by dropping it onto the leading edge tape from above while the blade was horizontal with the leading edge positioned upward. This created grit patterns of varying density that approximated the natural accumulation of insects and dirt on the blades. Grit densities were highest at the leading edge where 62 particles/cm^2 (400 particles/in^2.) were counted and dropped off to zero particles near the aft edge of the tape. A photograph of the roughness distribution used is shown in Figure 8-2. The resulting k/c values ranged from .0011 to .0022, or roughly 2 to 4 times the NACA standard roughness size. Although the grit densities tapered off toward the trailing edge, some grit particles were scattered back as far as 20% chord.

Particle size and placement on the low-pressure surface of the airfoil are the two leading factors in determining the severity of roughness (Bragg and Gregorek, 1989). When compared to NACA standard roughness, the NREL roughness distribution was more severe. This was an important factor in comparing the data from this test with other airfoil data.

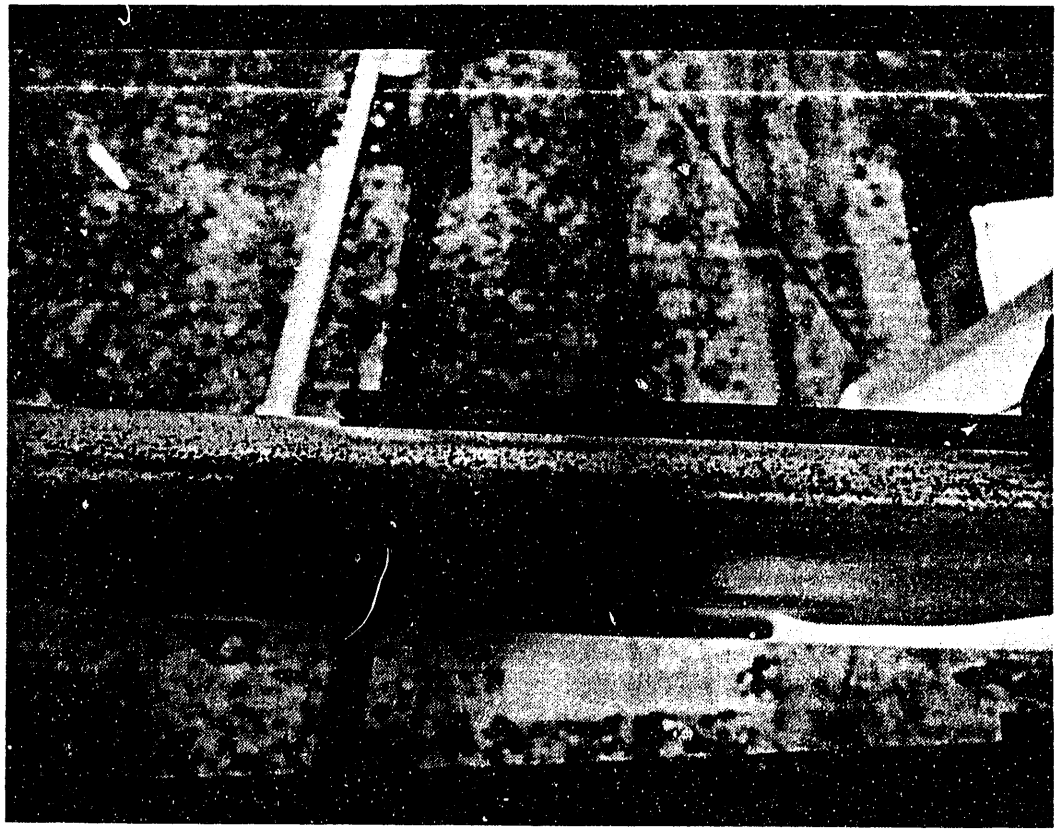

Figure 8-2. Roughness distribution on leading edges of test turbine blades

8.3 Roughness Testing

All the wind turbine roughness testing was conducted during Phase I of the Combined Experiment in May 1989. Wind tunnel roughness tests were conducted at CSU in September 1989. Wind turbine tests were conducted over wind speeds ranging from 5 m/sec (11.2 mph) to 30 m/sec (67.1 mph). Rough rotor data of 3.5 h were recorded. Electrical power, shaft torque, and nine prop-vane anemometer signals were the primary signals used for the performance comparisons; however, the active pressure, blade load, and inflow signals were used to determine the aerodynamic effects of roughness on the airfoil. Most of the analysis and data reduction techniques used follow the procedures described in the previous sections, but some small changes were introduced for simplicity. The interested reader is referred to Musial, Butterfield, and Jenks (1989) and Musial and Butterfield (1990).

8.4 Rough Performance Results

A fifth-order polynomial was fit through each data set of rough and smooth data to obtain an accurate evaluation of the rough rotor performance effects. These curves are compared in Figure 8-3 from 5 m/sec (11.2 mph) to 22 m/sec (49.2 mph). Both curves have approximately the same shape, but the rough data

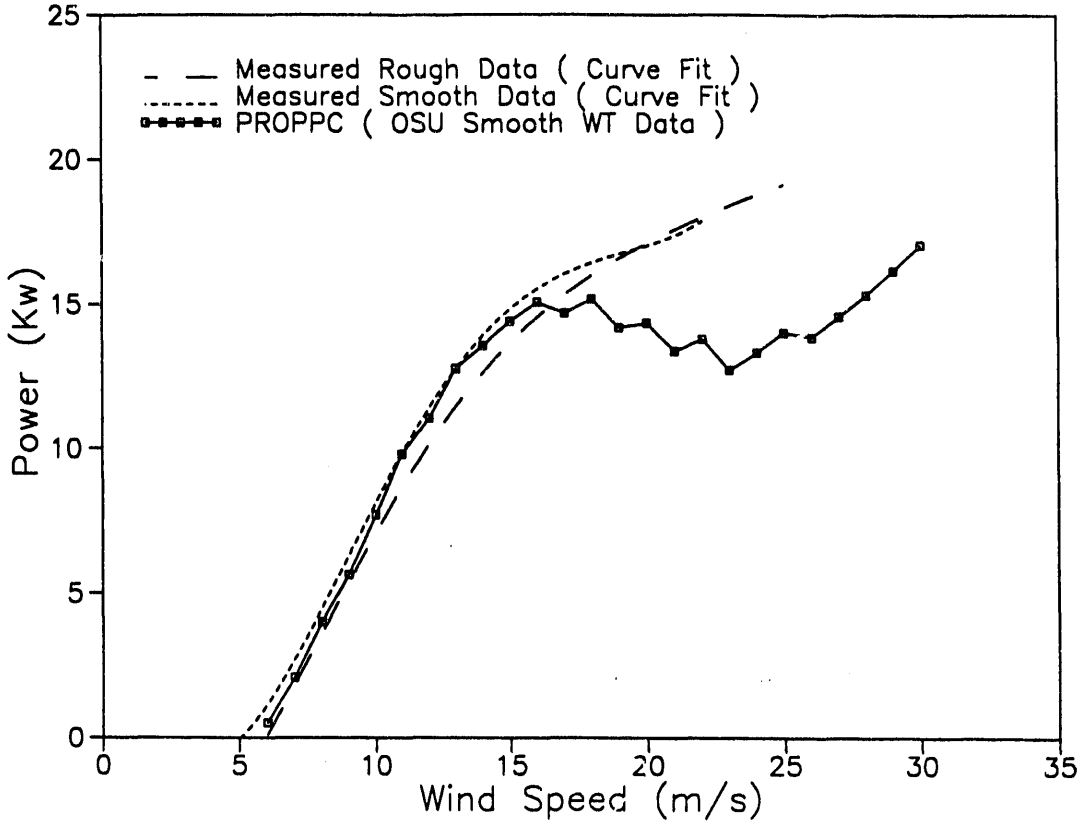

Figure 8-3. Combined experiment wind turbine performance

curve is about 10% lower than the smooth data curve for most of the low to moderate wind speeds. At about 15 m/sec (33.6 mph), the two curves converge, and at 19 m/sec (42.5 mph), they cross.

Another way to look at this degradation is shown in Figure 8-4, where two normalized power curves are plotted on the same graph. Both are plots of rough rotor performance normalized against smooth rotor performance for the range of wind speeds tested. A value of 1.0 on this curve would indicate no effective change caused by roughness. The percent of degradation caused by roughness is greatest at low wind speeds for these curves. As indicated, one curve is mechanical power, and one curve is electrical power. Because data for these two curves were measured using independent transducers, their agreement is presented here to validate the accuracy of the measurement.

In Figure 8-3, the measured rough and smooth mechanical power curves are also compared to a predicted power curve that was generated using PROPPC performance code with 2D lift and drag data. Lift coefficients from the OSU wind tunnel tests that were used to generate the predicted power curve are shown in Figure 8-5. The smooth measured data match the analytical predictions very closely until approximately 15 m/sec (33.6 mph), where the analytical power curves reach a maximum value at about 15 kW and begin to roll off. The measured smooth power curve continues to increase beyond 18 kW without leveling off. At low wind speeds below 15 m/sec (33.6 mph), the smooth, predicted curves exceed the rough data, as expected. As seen previously in Figure 8-4, the rotor experiences an average

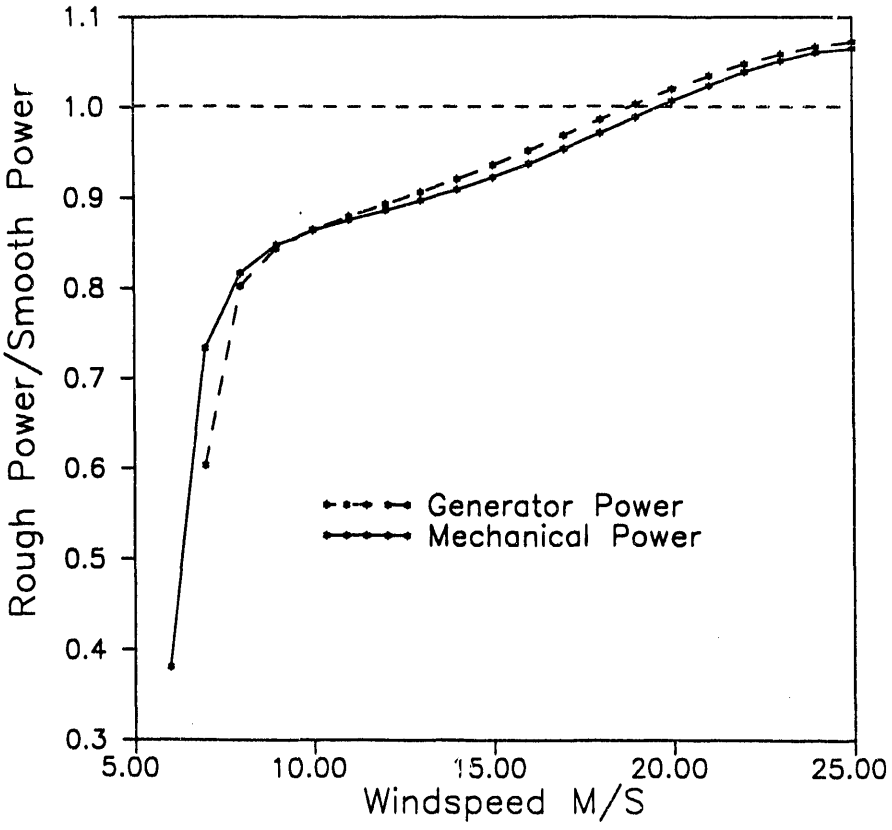

Figure 8-4. Normalized power output—combined experiment

decline of 10% in power production because of the leading edge roughness, but the rough and smooth measured power curves diverge from the predicted curve and continue to increase without reaching an upper limit. This is a familiar problem that relates to the stall characteristics of wind turbines rather than a roughness phenomenon.

The effects of roughness on the Combined Experiment wind turbine were examined above by comparing rough and smooth power curves. It is clear that roughness had a negative effect on performance over most of the operating range, but this rotor did not experience the drop-off in peak power that is usually seen on stall-controlled rotors. It was not clear what caused this effect.

This wind turbine differs from most commercial stall control wind turbines because of its constant chord, zero-twist rotor. Therefore, much of the inboard sections of the rotor operate in the stall region even at low to moderate wind speeds. Much of the peak power performance is dictated by the deep stall characteristics of the airfoil and not by the low AOA section properties (AOA = 0-10 deg). In order to understand what is happening on this rotor, it is necessary to look at the stalled airfoil properties.

8.5 Rough S809 Airfoil Characteristics

To study the effect of roughness on airfoil properties, aerodynamic pressure measurements taken at 80% span were used. Figure 8-6 shows the rough and smooth C_l versus AOA curves for the rotating (wind turbine) and non-rotating (wind tunnel) cases out to 25-deg AOA. All four curves are in good agreement for very low AOA (0-3 deg). At 3 deg the rough data for both the 2D and 3D cases begin to drop off

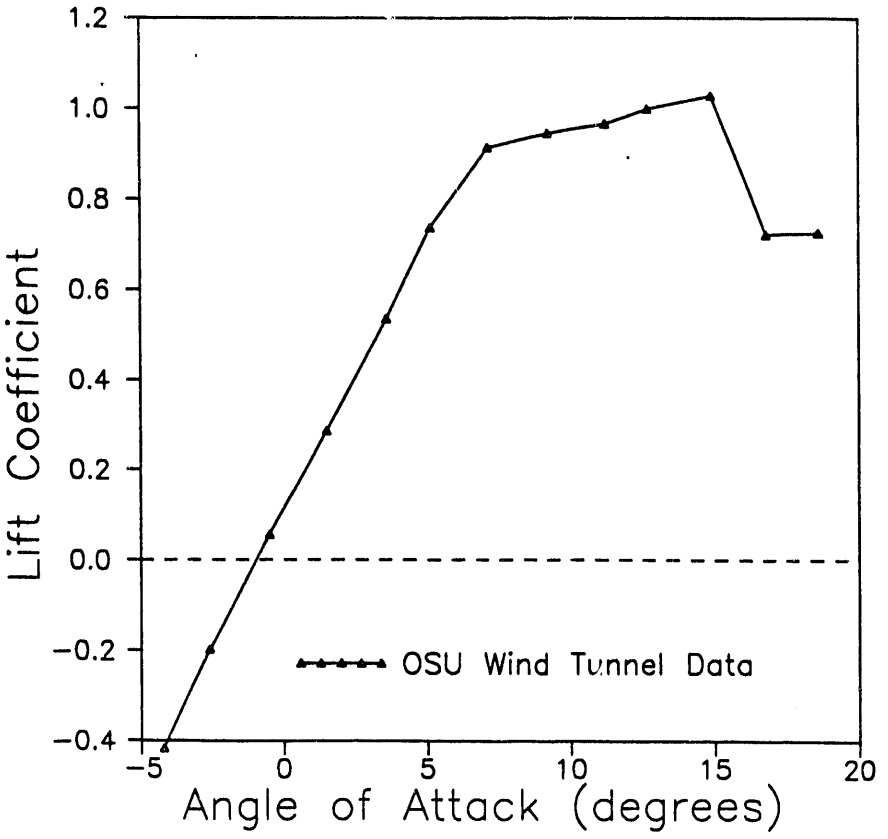

Figure 8-5. S809 OSU wind tunnel data

from the smooth airfoil curves. The two rough and the two smooth curves continue to maintain reasonable agreement, respectively, until 11 deg, where the rough 2D data reach a peak of .73 and drop to about .63, but the rotating data flatten out at about .75.

Meanwhile, both of the smooth data curves continuously increase monotonically through about 15 deg. The smooth wind tunnel data stalls abruptly at 17 deg after reaching a $C_{L(max)}$ of .96. This would be expected from previous static tests. The rotating smooth data reached its peak at about the same AOA but did not drop off, exhibiting delayed stall characteristics.

Although the smooth wind tunnel data stall sharply at 17 deg, the rough wind tunnel data recover unexpectedly from the drop-off measured between 11 and 16 deg and increase to a $C_{L(max)}$ of about .98 at an AOA of 18 deg. This secondary peak is sustained until 20-deg AOA where it decreases back to a value of $C_{L(max)}$ near 0.7. The secondary peak experienced by the rough wind tunnel data actually exceeded the smooth airfoil performance but at a higher AOA. One probable explanation is that the added boundary layer turbulence, induced by the leading edge roughness, caused energy from the outer flow to be introduced into the boundary layer. This added energy modified the boundary layer velocity distribution, resulting in a delayed separation. This would account for the higher C_L values measured. It should be noted that this secondary recovery peak in the rough wind tunnel data was only present at a Reynolds number of 650,000.

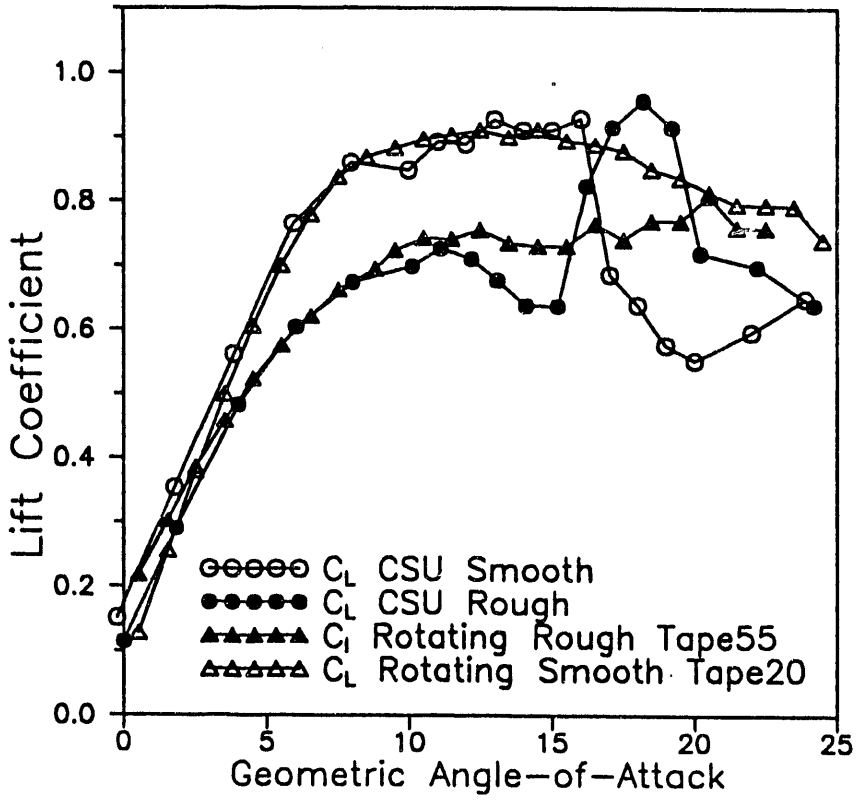

Figure 8-6. Comparison of rough and smooth C_L data from rotating and nonrotating airfoil tests

At higher AOAs, near 20 deg, the smooth rotating C_L values are sustained at levels about equal to the rough rotating airfoil data. However, note that it is even more significant than the effect of roughness for both the rough and smooth rotating data curves, where they exceed the smooth wind tunnel C_L data by 25% because of delayed stall.

The effects of roughness on maximum lift coefficient are seen in Figure 8-7. For both the rotating and non-rotating cases, roughness on the leading edge of this airfoil lowered $C_{L(max)}$ by 22%. This decrease in $C_{L(max)}$ was greater than expected; however, when compared to data from other airfoils, the S809 roughness sensitivity effects were actually smaller. Figure 8-7 (Bragg and Gregorek, 1989) shows the effect of standard NACA roughness on $C_{L(max)}$ as a function of the airfoil thickness for the NACA 44XX and the NACA 230XX airfoil families. The data point corresponding to the 22% change in $C_{L(max)}$ for the S809 airfoil used on the Combined Experiment rotor is included on this plot for comparison. It can be seen that the S809 is a significant improvement over both NACA airfoils. It should be pointed out that the roughness used to generate the data for the NACA airfoils was the standard NACA roughness. The roughness used to test the S809 was the simulated insect roughness. As discussed earlier, the simulated insects have k/c values 2 to 4 times greater than the standard NACA roughness. On the NACA 0012 airfoil, Hoerner (1975) shows that this higher degree of roughness would have doubled the reduction in $C_{L(max)}$. Unfortunately, the magnitude of $C_{L(max)}$ change because of increasing roughness size was not available for the airfoils in Figure 8-7, but the trend established by Hoerner (1975) would indicate that rough performance improvements experienced by the S809 over the 44XX and the 230XX airfoils are probably conservative.

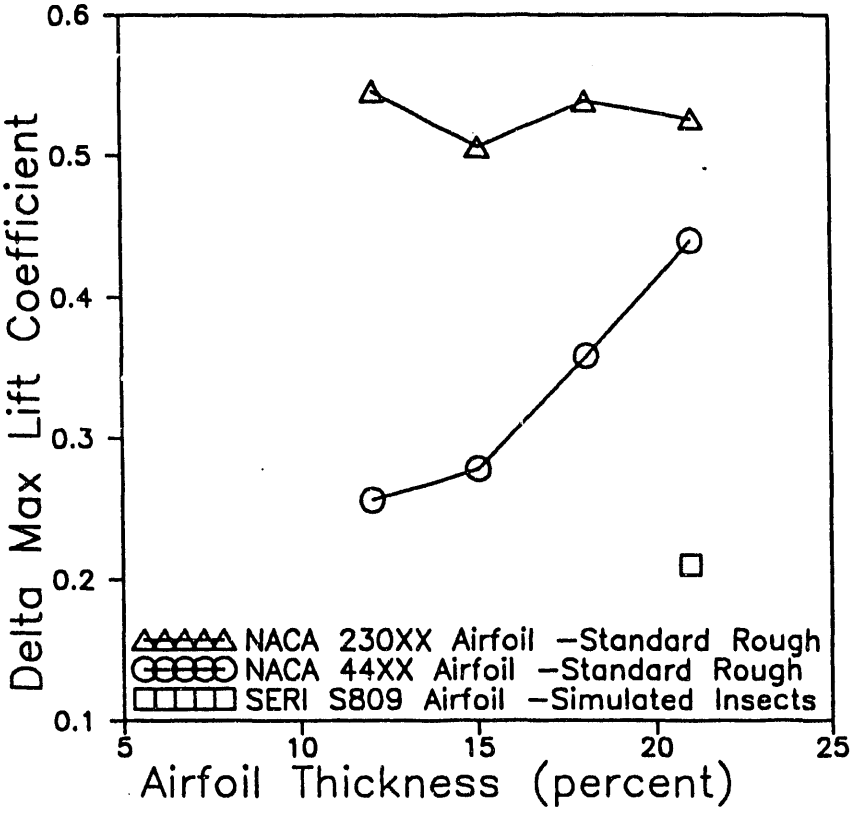

Figure 8-7. Change in $C_{L(max)}$ caused by NACA standard roughness and airfoil thickness for typical wind turbine airfoils

The rough and smooth CL versus AOA curves for the LS(1)-0413 airfoil (unmodified) from Bragg and Gregorek (1989) are shown in Figure 8-8. As with the NACA airfoils in Figure 8-7, these data show the effect of NACA standard roughness on the LS(1)-0413. From these data a 28% decrease in $C_{L(max)}$ can be seen.

This result is contradicted by other wind tunnel test data that have been presented for the LS(1) airfoils as well as for the NREL airfoils (Somers, 1991; Miley, 1982, McGhee and Beasley, 1981; McGhee, Beasley, and Somers, 1977). These reports indicate very small changes in airfoil performance for the LS(1) series and NREL airfoils when roughness was applied to the airfoil. However, all of these tests were performed using only a small local disturbance at about .075 x/c to fix boundary layer transition near the leading edge. This was much less severe than the wraparound roughness cases used at NREL and OSU (NACA standard) and caused the roughness sensitivity characteristics to appear mild.

When comparing the data from Bragg and Gregorek (1989) with the S809 curves in Figure 8-6, it can be seen that there is a slight improvement in roughness sensitivity for the S809 airfoil over the LS(1). However, several cautions should be noted when comparing these two data sets. First, the LS(1) data were taken at Reynolds number = 3,000,000, but the S809 data were taken at Reynolds number = 650,000. In Hoerner (1975), a lowering of the Reynolds number was shown to lower $C_{L(max)}$. However, when standard NACA roughness was applied to the NACA 4412 and NACA 64-418 airfoils, the reduction in $C_{L(max)}$ remained constant with a decreasing Reynolds number. It is probable that the LS(1) series will be affected in the same way. Second, NACA standard roughness was used on the LS(1) tests but larger-sized, simulated insect roughness was used on the S809 tests. The effect of roughness size was discussed earlier. Finally, the LS(1)-0413 has a t/c ratio of .13 compared to .21 for the S809. It is not known if this difference in the airfoil thicknesses is significant.

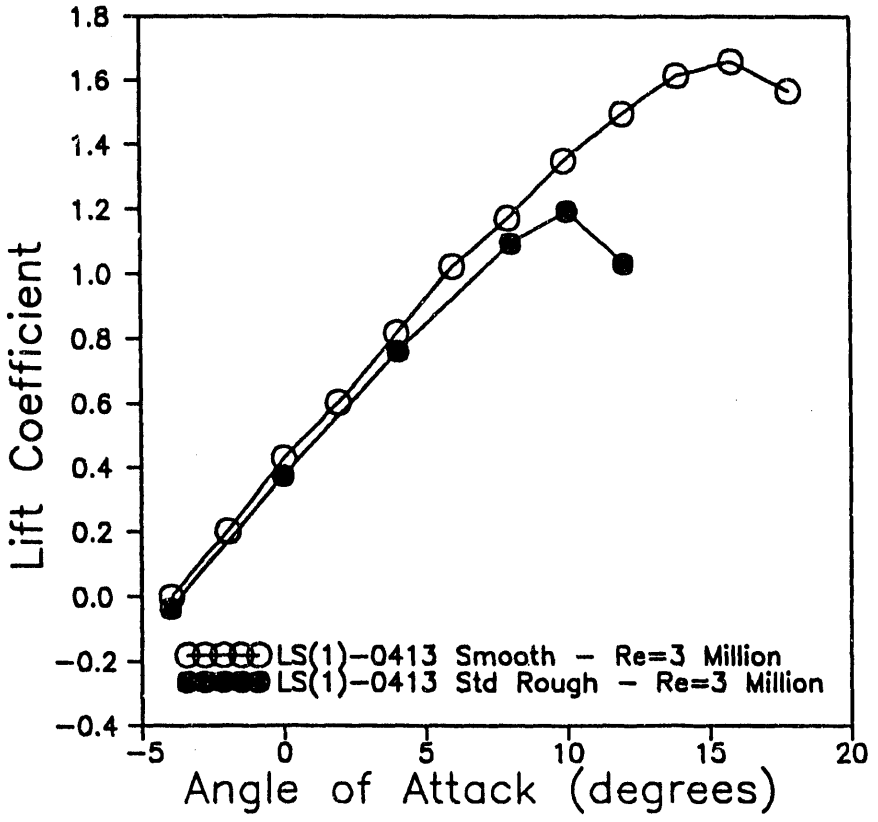

Figure 8-8. LS(1)0413 smooth and rough airfoil performance

No wind tunnel testing has been done on the modified LS(1) airfoils using realistic wind turbine roughness, so it is not known how those airfoils compare to the S809.

8.6 Wind Tunnel and Rotating Comparisons of Rough Airfoil Data

Studying section coefficients, such as CL in the above discussion, gives a more complete picture of how roughness changes the airfoil properties. In order to understand the specifics of what is happening on the airfoils, it is necessary to examine the pressure distributions across the airfoil section. A complete compilation of all the wind tunnel test pressure distributions is contained in Appendix H.

In Figure 8-6, there were at least three AOAs where distinctly different and interesting phenomena were identified on the C_L versus AOA curves. At 11 deg the two rough airfoil curves reach an initial maximum value; at 14 deg the rough curves have dropped off but the two smooth curves have reached a maximum; and at 18 deg the rough wind tunnel data have recovered but the smooth wind tunnel data have stalled. At each of these AOA cases, airfoil pressure distributions were plotted for each of the four curves in Figure 8-6. These three pressure distribution plots are shown in Figures 8-9 through 8-11.

In Figure 8-9, the pressure distributions are shown at about 11-deg AOA. At this angle, the rough wind tunnel (solid circles in Figure 8-9) and rough wind turbine (solid triangles) data agree along the high pressure or upwind side (lower curves in the figure). They also agree from the leading edge to .40 x/c on the low-pressure side (upper curves). From .40 x/c on the low-pressure side to the trailing edge, the pressure distribution is characterized by a flat region that is caused by separation of the flow from the

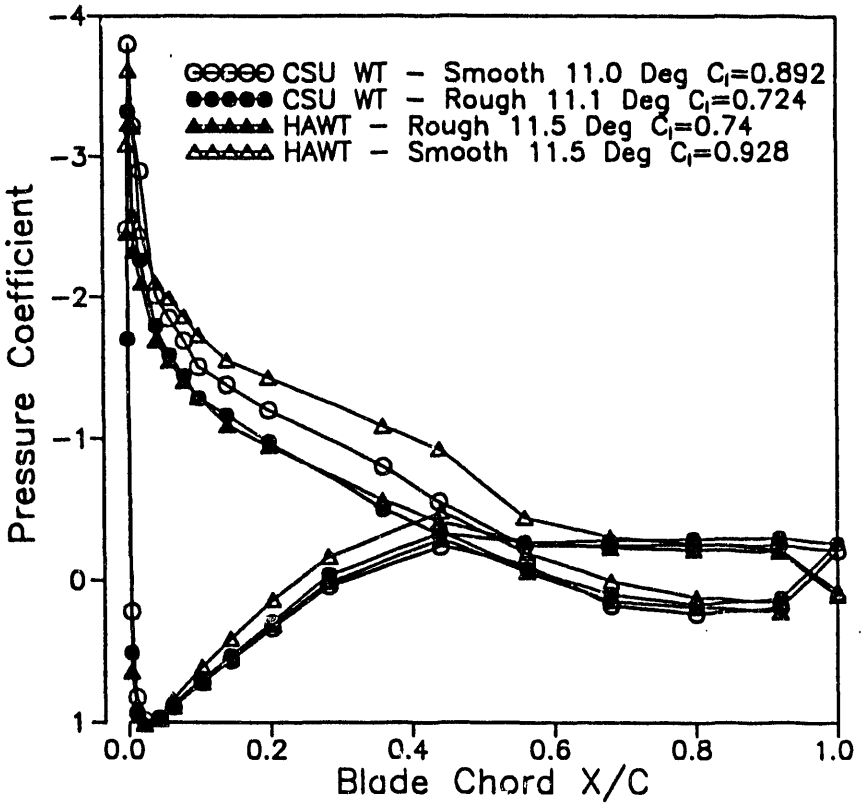

Figure 8-9. A comparison of pressure distributions for 11° angle of attack

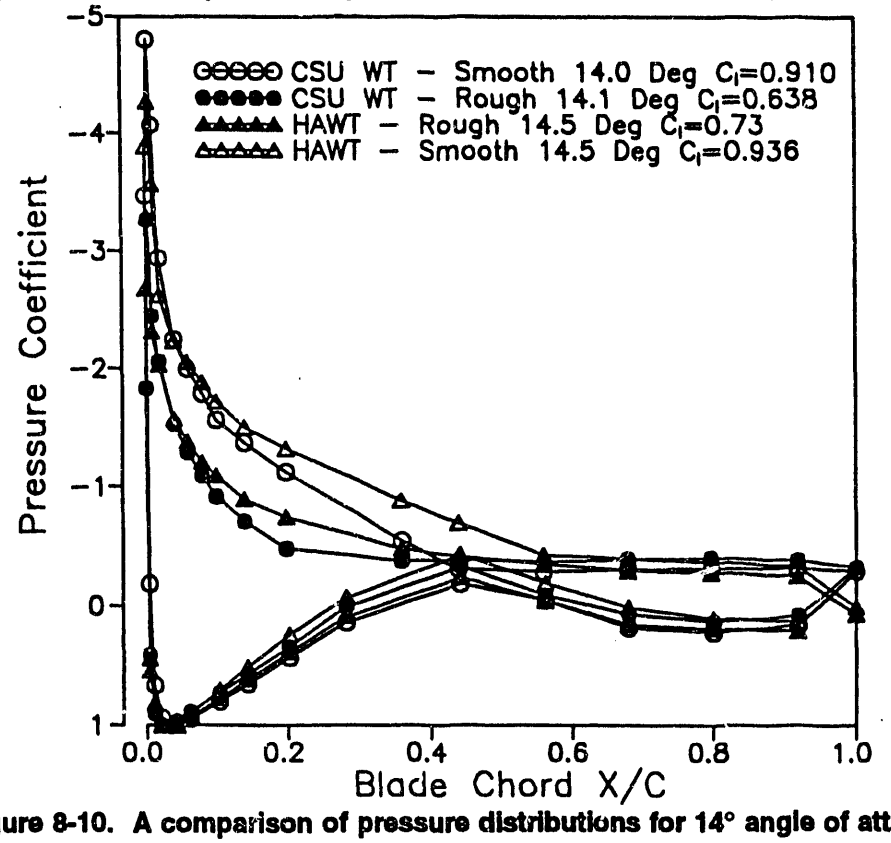

Figure 8-10. A comparison of pressure distributions for 14° angle of attack

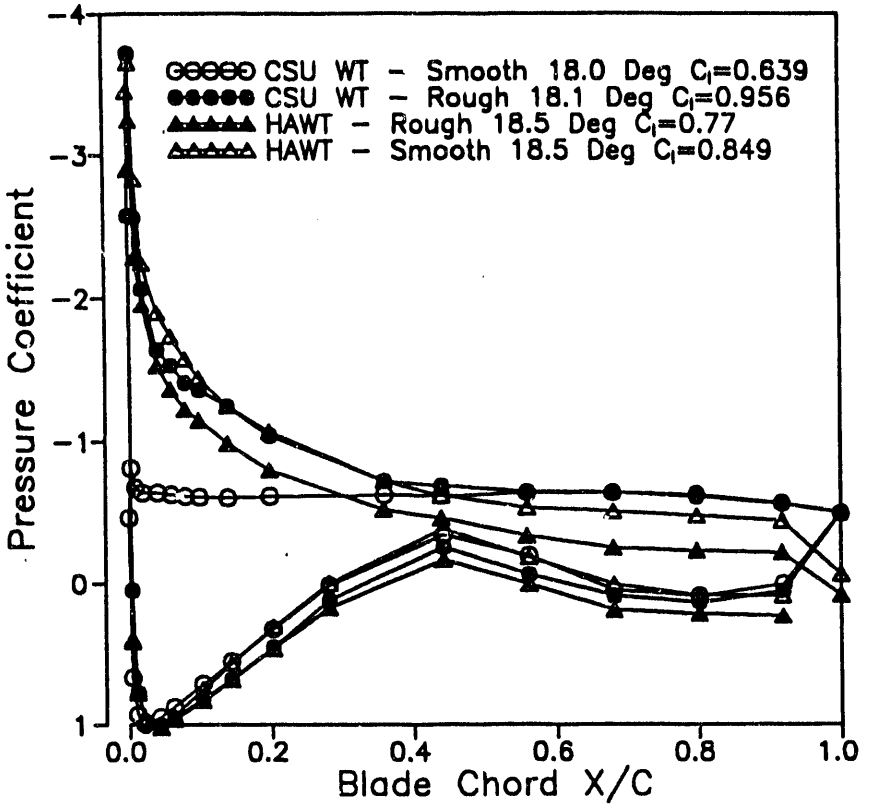

Figure 8-11. A comparison of pressure distributions for 18° angle of attack

airfoil. On close examination, one can see that the rough wind turbine pressure data meet that flat region about .10 x/c further toward the trailing edge than the non-rotating case. This implies that slightly delayed separation may result from blade rotation.

Both smooth curves (open symbols) in Figure 8-9 show significantly lower (i.e., higher negative) pressures in the low-pressure, leading edge region. Again, the rotating wind turbine blade data show a delayed separation when compared to the wind tunnel data. The lower pressures in the leading edge region on the smooth airfoils caused higher smooth lift coefficients. Both smooth curves resulted in C_Ls that were 25% higher than the rough cases (see legend in Figure 8-9 for values of C_L).

Figure 8-10 shows pressure distributions for 14-deg AOA. Here, a larger difference in leading suction peak and separation point can be seen. The smooth curves show a C_p of -4.3 and -4.8 for the rotating blade and the wind tunnel, respectively. Both rough cases show a maximum negative peak C_p of -3.3. Again, the separation point was delayed about .10 x/c for the rotating blade cases over their respective wind tunnel cases. As would be predicted from Figure 8-6, both smooth cases show higher negative pressures over the first half of the low-pressure side of the airfoil. This difference is due to attached flow extending further toward the trailing edge for the smooth cases. For the wind tunnel cases, this resulted in a C_L that was 40% greater for the smooth case than the rough case. For the rotating cases, the difference between rough and smooth C_L was only 25%.

At 18-deg AOA (Figure 8-11), the smooth wind tunnel data show a complete loss of suction peak. The distribution of pressures on the low-pressure side of the airfoil is nearly flat from the leading edge to the trailing edge. This is caused by complete flow separation starting at the leading edge.

On the other three curves, high, negative pressures associated with high-velocity attached flow are evident. The rough wind tunnel data still show a strong suction peak, explaining the high C_L at 18 deg in Figure 8-6. Now, C_L for the rough case is 49% higher than the smooth case. It is probable that turbulence resulting from roughness at the leading edge has caused energy from the outer flow to be introduced into the inner boundary layer flow at this Reynolds number. This energy modified the boundary layer velocity profile, making it similar to the effect of a vortex generator. The modified velocity profile appears to have delayed flow separation and maintained the pressure peak at the leading edge well beyond the normal stall angle.

For the smooth rotating blade, the separation point appears to be further aft than the rough rotating case, but no sharp transition from attached flow (decreasing pressures) to separated flow (flat pressures) is visible in these curves. This may be an anomaly of the averaging process, or it may be caused by 3D rotational effects. Further research is under way that is targeted at understanding the rotational and unsteady effects of these pressure measurements and will be the subject of future reports.

Further efforts to quantify the differences in roughness sensitivity between LS(1) and the NREL airfoils should be made using the same roughness conditions under similar conditions. It is important that a realistic roughness distribution, appropriate for wind turbines, be used in these experiments.

9.0 References

Akins, R. E., 1987, *Evaluation of SERI/PSC Pressure System* (Unpublished), NREL, Golden, CO.

APEX Systems, Inc., 1988, *PCM Decoder Card Manual,* APEX Systems, Inc., Boulder, CO.

Bendat, J. S., and Piersol, A. G., 1980, *Engineering Applications of Correlation and Spectral Analysis,* A Wiley-Interscience Publication, John Wiley & Sons, New York.

Bragg, M. B., and Gregorek, G. M., 1989, "Environmentally Induced Surface Roughness Effects on Laminar Flow Airfoils: Implications for Flight Safety," *Proceedings of AIAA, Aircraft Design, Systems and Operations Conference,* Seattle, WA, July 31-Aug. 2, 1989, published by AIAA, 370 L'Enfant Promenade, S.W., Washington, D.C. 20004.

Butterfield, C. P., Scott, G. N., and Musial, W., 1990, *Comparison of Wind Tunnel Airfoil Performance Data with Wind Turbine Blade Data,* TP-254-3799, NREL, Golden, CO.

Butterfield, C. P., 1989b, *Three-Dimensional Airfoil Performance Measurements on a Rotating Wing,* TP-217-3505, NREL, Golden, CO.

Butterfield, C. P., Jenks, M. D., Simms, D. A., and Musial, W. P., 1990, *Aerodynamic Pressure Measurements on a Rotating Wind Turbine Blade,* TP-257-3695, NREL, Golden, CO.

Butterfield, C. P., 1989a, "Aerodynamic Pressure and Flow Visualization Measurements from a Rotating Wind Turbine Blade," *Proceedings of the Eighth ASME Wind Energy Symposium,* Houston, TX, January 22-25, 1989, Vol. 7, pp. 245-255.

Butterfield, C. P., and Nelson, E. N., 1990, *Aerodynamic Testing of a Rotating Wind Turbine Blade,* TP-257-3490, NREL, Golden, CO.

Fairchild Weston Systems, Inc., 1985, *PCM Data Collection and Reduction System for the Solar Energy Research Institute: Operating Manual,* Fairchild Weston Systems, Inc., Sarasota, FL.

Gregorek, G. M., Hoffman, M. J., and Mulh, K. E., 1991, *Wind Tunnel Tests of the S809 Airfoil Model,* NREL, Golden, CO.

Hoerner, S. F., 1975, *Fluid-Dynamic Lift,* Hoerner Fluid Dynamics, Brick Town, NJ.

Holtz, R., 1988, "The Effect of Blade Surface Roughness on the Lead-Lag Bending Moments of a U.S. Windpower 56-100 Wind Turbine," *Proceedings of the Seventh ASME Wind Energy Symposium,* American Society of Mechanical Engineers, New Orleans, Louisiana, Jan. 10-13, 1988, pp. 95-99.

Irwin, H., Cooper, K. R., and Hirard, R., 1979, "Correction of Distortion Effects Caused by Tubing Systems in Measurements of Fluctuating Pressures," *Journal of Industrial Aerodynamics* 5, pp. 93-107.

Lenschow, D. H., 1971, "Vanes for Sensing Incidence Angles of the Air from an Aircraft," *Journal of Applied Meteorology,* Vol. 10, No. 6, pp. 1339-1343.

Loral Instrumentation, *D/PAD Mark II Manual,* Loral Instrumentation, San Diego, CA.

Madsen, H. A., Rasmussen, F., and Pedersen, T. F., 1988, *Aerodynamics of a Full-Scale HAWT Blade,* Riso National Laboratory, Roskilde, Denmark.

McGhee, R. J., Beasley, W. D., and Somers, D. M., 1977, *Low-Speed Aerodynamic Characteristics of a 13-Percent-Thick Airfoil Section Designed for General Aviation Applications,* NASA TM X-72697, Langley Research Center, Hampton, VA.

McGhee, R. J., and Beasley, W. D., 1981, *Wind Tunnel Results for a Modified 17-Percent Thick Low-Speed Airfoil Section,* Technical Paper 1919, National Aeronautics and Space Administration, Houston, TX.

Miley S. J., 1982, *A Catalog of Low Reynolds Number Airfoil Data for Wind Turbine Applications,* RFP-3387, U.S. Department of Energy, Washington, D.C.

Musial, W. D., Butterfield C. P., and Jenks, M. D., 1989, *Effects of Leading-edge Roughness on S809 Airfoil Rotor Performance,* TP-217-3563, NREL, Golden, CO.

Musial, W., and Butterfield, C. P., 1990, *A Comparison of Two- and Three- Dimensional S809 Airfoil Properties for Rough and Smooth HAWT Rotor Operation,* TP-257-3603, NREL, Golden, CO.

Rae, H. W., and Pope, A., 1984, *Low-Speed Wind Tunnel Testing, Second Edition,* John Wiley & Sons, New York.

Rae, W. H., Jr., and Pope, A., 1984, *Low-Speed Wind Tunnel Testing, Second Edition,* John Wiley & Sons, New York, p. 133.

Simms, D. A., and Butterfield, C. P., 1990, *Unsteady Aero Experiment Test Plan* (Unpublished), NREL, Golden, CO.

Simms, D. A., 1990, *PC-Based PCM Telemetry Data Reduction System Software,* TP-257-3663, NREL, Golden, CO.

Simms, D. A., and Butterfield, C. P., 1990, *PC-Based PCM Telemetry Data Reduction System Hardware,* TP-257-3662, NREL, Golden, CO.

Somers, D. M., 1989, *Design and Experimental Results for the S809 Airfoil* (Unpublished), NREL, Golden, CO.

Somers, D. M., 1991, *Design and Experimental Results for the S809 Airfoil,* NREL report, to be published.

Strock, O. J., 1983, *Telemetry Computer Systems: An Introduction,* Prentice-Hall, Inc., Englewood Cliffs, NJ.

Tangler, J. L., 1983, *Horizontal-Axis Wind System Rotor Performance Model Comparison - A Compendium,* RFP-3508, Rockwell International.

Viterna, L. A., and Corrigan, R. D., 1981, "Fixed Pitch Rotor Performance of Large Horizontal Axis Wind Turbines," DOE/NASA Workshop on Large Horizontal Axis Wind Turbines, Cleveland, OH, July 28-30.

Yekutieli, O., and Clark, R. N., 1987, "Influence of Blade Surface Roughness on the Performance of Wind Turbines," *Proceedings of the Sixth ASME Wind Energy Symposium*, pp. 181-187, American Society of Mechanical Engineers, Dallas TX, Feb. 15-18, 1987.

Appendix A

Combined/Unsteady Aero Experiment High and Low Cal Setups for PCM600

Combined/Unsteady Aero Experiment

High and Low Cal Setups for PCM600

Data Stream #1

PCM Ch #	Description	Input Range	Low Cal Input Voltage	Low Cal Output Counts	High Cal Input Voltage	High Cal Output Counts	Gain	Offset	Filter
1	20m Hot Film (Not Used)	0-10 V	0 V	50	+10 V	4049	1	-5 V	10 Hz
2	18m Sonic A (Not Used)	+/-5 V	0 V	2050	+5 V	4049	1	0 V	10 Hz
3	18m Sonic B (Not Used)	+/-5 V	0 V	2050	+5 V	4049	1	0 V	10 Hz
4	18m Sonic C (Not Used)	+/-5 V	0 V	2050	+5 V	4049	1	0 V	10 Hz
5	5m WD	0-5 V	0 V	50	+5 V	4049	2	-5 V	1 Hz
6	5m WS	0-5 V	0 V	50	+5 V	4049	2	-5 V	1 Hz
7	10m WD	0-5 V	0 V	50	+5 V	4049	2	-5 V	1 Hz
8	10m WS	0-5 V	0 V	50	+5 V	4049	2	-5 V	1 Hz
9	20m WD	0-5 V	0 V	50	+5 V	4049	2	-5 V	1 Hz
10	20m WS	0-5 V	0 V	50	+5 V	4049	2	-5 V	1 Hz
11	50m WD	0-5 V	0 V	50	+5 V	4049	2	-5 V	1 Hz
12	50m WS	0-5 V	0 V	50	+5 V	4049	2	-5 V	1 Hz
13	5m Air Temperature	0-5 V	0 V	50	+5 V	4049	2	-5 V	1 Hz
14	Delta Temp(T50-T5)	0-5 V	0 V	50	+5 V	4049	2	-5 V	1 Hz
15	5m Dew Point (Not Used)	+/-5 V	0 V	2050	+5 V	4049	1	0 V	1 Hz
16	Baro Pressure	0-5 V	0 V	50	+5 V	4049	2	-5 V	1 Hz

Note: All voltages are "DC" unless otherwise stated.

Bit Rate = 7.5k bits/second (1.92MHz/256)
Sample Rate = 34.72 samples/second
Bits/Word = 12
Words/Frame = 18 (16 data channels + 2 frame sync)
Frame Sync Code = 000 110 101 110 010 100 011 010

Combined/Unsteady Aero Experiment

High and Low Cal Setups for PCM600

Data Stream #2

PCM Ch #	Description	Input Range	Low Cal Input Voltage	Low Cal Output Counts	High Cal Input Voltage	High Cal Output Counts	Gain	Offset	Filter
1	Propvane Anem. WS1	0-10 V	0 V	50	+10 V	4049	1	-5 V	2 Hz
2	Propvane Anem. WS2	0-10 V	0 V	50	+10 V	4049	1	-5 V	2 Hz
3	Propvane Anem. WS3	0-10 V	0 V	50	+10 V	4049	1	-5 V	2 Hz
4	Propvane Anem. WS4	0-10 V	0 V	50	+10 V	4049	1	-5 V	2 Hz
5	Propvane Anem. WS5	0-10 V	0 V	50	+10 V	4049	1	-5 V	2 Hz
6	Propvane Anem. WS6	0-10 V	0 V	50	+10 V	4049	1	-5 V	2 Hz
7	Propvane Anem. WS7	0-10 V	0 V	50	+10 V	4049	1	-5 V	2 Hz
8	Propvane Anem. WS8	0-10 V	0 V	50	+10 V	4049	1	-5 V	2 Hz
9	Propvane Anem. WS9	0-10 V	0 V	50	+10 V	4049	1	-5 V	2 Hz
10	Propvane Anem. WD9	0-10 V	0 V	50	+10 V	4049	1	-5 V	2 Hz
11	Bivane WS12	0-10 V	0 V	50	+10 V	4049	1	-5 V	2 Hz
12	Bivane WD12	0-2 V	0 V	50	+2.5 V	4049	4	-5 V	2 Hz
13	Bivane WE12	0-2 V	0 V	50	+2.5 V	4049	4	-5 V	2 Hz
14	Bivane WS13	0-10 V	0 V	50	+10 V	4049	1	-5 V	2 Hz
15	Bivane WD13	0-2 V	0 V	50	+2.5 V	4049	4	-5 V	2 Hz
16	Bivane WE13	0-2 V	0 V	50	+2.5 V	4049	4	-5 V	2 Hz

Note: All voltages are "DC" unless otherwise stated.

Bit Rate = 15k bits/second (1.92MHz/128)
Sample Rate = 69.44 samples/second
Bits/Word = 12
Words/Frame = 18 (16 data channels + 2 frame sync)
Frame Sync Code = 000 110 101 110 010 100 011 010

Combined/Unsteady Aero Experiment

High and Low Cal Setups for PCM600

Data Stream #3

PCM Ch #	Description	Input Range	Low Cal Input Voltage	Low Cal Output Counts	High Cal Input Voltage	High Cal Output Counts	Gain	Offset	Filter
1	Propvane Anem. WS10	0-10 V	0 V	50	+10 V	4049	1	-5 V	2 Hz
2	Propvane Anem. WS11	0-10 V	0 V	50	+10 V	4049	1	-5 V	2 Hz
3	LSS Azimuth	0-5 V	0 V	50	+5 V	4049	2	-5 V*	130 Hz
4	Yaw Bending	+/- 24.75 mV	-24.75 mV	50	+24.75 mV	4049	202	0 V	40 Hz
5	Tower Bending N-S	+/- 5.05 mV	-5.05 mV	50	+5.05 mV	4049	990	0 V	40 Hz
6	Tower Bending E-W	+5.03/-5 mV	-5 mV	50	+5.03 mV	4049	997	0 V	40 Hz
7	Yaw Angle	0-10 V	0 V	50	+10 V	4049	1	-5 V	10 Hz
8	Generator Power	+/- 5 V	0 V	2050	+5 V	4049	1	0 V	55 Hz
9	LSS Speed (Not Used)	0-10 V	0 V	50	+8 V	3277	1	-5 V	10 Hz
10	TSI X-Film 1X (Not Used)	2.1-5.7 V	3.9 V	2048	+5.0 V	3277	2.778	-10.8 V	55 Hz
11	TSI X-Film 1Y (Not Used)	2.1-5.7 V	3.9 V	2048	+5.0 V	3277	2.778	-10.8 V	55 Hz
12	TSI X-Film 2X (Not Used)	2.1-5.7 V	3.9 V	2048	+5.0 V	3277	2.778	-10.8 V	55 Hz
13	TSI X-Film 2Y (Not Used)	2.1-5.7 V	3.9 V	2048	+5.0 V	3277	2.778	-10.8 V	55 Hz
14	Sonic U-Axis (Not Used)	+/- 5 V	0 V	2048	+3 V	3277	1	0 V	12 Hz
15	Sonic V-Axis (Not Used)	+/- 5 V	0 V	2048	+3 V	3277	1	0 V	12 Hz
16	Sonic W-Axis (Not Used)	+/- 5 V	0 V	2048	+3 V	3277	1	0 V	12 Hz

Note: All voltages are "DC" unless otherwise stated.

There are only 8 of 16 channels installed in this PCM Stream (3) the signal conditioners are removed until there is a need for channels 9-16.

Bit Rate = 60k bits/second (1.92MHz/32)
Sample Rate = 277.78 samples/second
Bits/Word = 12
Words/Frame = 18 (16 data channels + 2 frame sync)
Frame Sync Code = 000 110 101 110 010 100 011 010

Combined/Unsteady Aero Experiment

High and Low Cal Setups for PCM600

Data Stream #4

PCM Ch #	Description	Input Range	Low Cal Input Voltage	Low Cal Output Counts	High Cal Input Voltage	High Cal Output Counts	Gain	Offset	Filter
1	Root Flap "RTFBM-A"	±6.25 mV	0 V	2048	-	-	800	0 V	40 Hz
2	Root Flap "RTFBM-B"	±5.0 mV	0 V	2048	-	-	1000	0 V	40 Hz
3	Root Fl Blade 2 "RTFBM-2"	±5.0 mV	0 V	2048	-	-	1000	0 V	40 Hz
4	Root Fl Blade 3 "RTFBM-3"	±6.25 mV	0 V	2048	-	-	800	0 V	40 Hz
5	20% Flap "20FBM"	±5.0 mV	0 V	2048	-	-	1000	0 V	40 Hz
6	40% Flap "40FBM"	±10.0 mV	0 V	2048	-	-	500	0 V	40 Hz
7	50% Flap "50FBM"	±7.0 mV	0 V	2048	-	-	700	0 V	40 Hz
8	60% Flap "60FBM" (Not Used)	-	-	-	-	-	-	-	-
9	70% Flap "70FBM"	±5.0 mV	0 V	2048	-	-	1000	0 V	40 Hz
10	75% Flap "75FBM" (Not Used)	-	-	-	-	-	-	-	-
11	80% Flap "80FBM" (Not Used)	-	-	-	-	-	-	-	-
12	85% Flap "85FBM" (Not Used)	-	-	-	-	-	-	-	-
13	90% Flap "90FBM"	±2.5 mV	0 V	2048	-	-	2000	0 V	40 Hz
14	Root Edge "RTEBM-A"	±6.25 mV	0 V	2048	-	-	800	0 V	40 Hz
15	20% Edge "20EBM"	±7.0 mV	0 V	2048	-	-	700	0 V	40 Hz
16	50% Edge "50EBM"	±10.0 mV	0 V	2048	-	-	500	0 V	40 Hz
17	70% Blade Torque "70TQ"	±2.5 mV	0 V	2048	-	-	2000	0 V	40 Hz
18	85% Edge "85EBM" (Not Used)	-	-	-	-	-	-	-	-
19	Root Torque (Link) "RTTQ"	±2.5 mV	0 V	2048	-	-	2000	0 V	40 Hz
20	50% Torsion "50TQ"	±2.5 mV	0 V	2048	-	-	2000	0 V	100 Hz
21	X-X LSS "LSSX-X"	±10.0 mV	0 V	2048	-	-	500	0 V	40 Hz
22	Y-Y LSS "LSSY-Y"	±10.0 mV	0 V	2048	-	-	500	0 V	40 Hz
23	LSS Torque "LSSTQ-A"	±5.0 mV	0 V	2048	-	-	1000	0 V	40 Hz
24	LSS Torque "LSSTQ-B"	±5.0 mV	0 V	2048	-	-	1000	0 V	100 Hz
25	85% RTD (Not Used)	-	-	-	-	-	-	-	-
26	Load Cell for Blade Pull Testing (Cal Only)		-	-	-	-	-	-	-
27-58	Pressure Taps	±5.0 V	-	-	-	-	1	0 V	100 Hz
59	Absolute Pressure	0-5 V	-	-	-	-	2	-5 V	1.5 kHz
60	Cal Pressure	±2.5 V	-	-	-	-	2	0 V	1.5 kHz
61	Pitch Angle	0-5 V	-	-	-	-	1	0 V	-
62	PCM Voltage Monitor	0-28 V	-	-	-	-	.2	0 V	-

Note: All voltages are "DC" unless otherwise stated.

Bit Rate = 400k bits/second
Sample Rate = 520.83 samples/second
Bits/Word = 12
Words/Frame = 64 (62 data channels + 2 frame sync)
Frame Sync Code = 111 110 10. 111 001 100 100 000

Combined/Unsteady Aero Experiment

High and Low Cal Setups for PCM600

Data Stream #8

PCM Ch #	Description	Input Range	Low Cal Input Voltage	Low Cal Output Counts	High Cal Input Voltage	High Cal Output Counts	Gain	Offset	Filter
1	Absolute Pressure	0-5 V	-	-	-	-	2	-5 V	1.5 kHz
2	Cal Pressure	±2.5 V	-	-	-	-	2	0 V	1.5 kHz
3	Spare	-	-	-	-	-	-	-	-
4-62	Pressure Taps	±5.0 V	-	-	-	-	1	0 V	100 Hz

Data Stream #9

PCM Ch #	Description	Input Range	Low Cal Input Voltage	Low Cal Output Counts	High Cal Input Voltage	High Cal Output Counts	Gain	Offset	Filter
1-34	Pressure Taps	±5.0 V	-	-	-	-	1	0 V	100 Hz
35	86% AOA	±10.0 V	-	-	-	-	1	0 V	-
36	Spare	-	-	-	-	-	-	-	-
37	67.3% AOA	±10.0 V	-	-	-	-	1	0 V	-
38	Spare	-	-	-	-	-	-	-	-
39	Spare	-	-	-	-	-	-	-	-
40	Spare	-	-	-	-	-	-	-	-
41	34% AOA	±10.0 V	-	-	-	-	1	0 V	-
42-45	Spare	-	-	-	-	-	-	-	-
46	50.6% AOA	±10.0 V	-	-	-	-	1	0 V	-
47-52	Spare	-	-	-	-	-	-	-	-
53	Absolute Pressure	0-5 V	-	-	-	-	2	-5 V	1.5 kHz
54	Cal Pressure	±2.5 V	-	-	-	-	2	0 V	1.5 kHz
55-62	Spare	-	-	-	-	-	-	-	-

Note: All voltages are "DC" unless otherwise stated.

Bit Rate = 400k bits/second
Sample Rate = 520.83 samples/second
Bits/Word = 12
Words/Frame = 64 (62 data channels + 2 frame sync)
Frame Sync Code = 111 110 101 111 001 100 100 000

Appendix B

Unsteady Aero Experiment Measurement Tolerances

Unsteady Aero Experiment Measurement Tolerances*

Quick Look Number	Description	Cal Procedure #	Measurement Range Max (EU)	Measurement Range Calibrated (EU)	Allowable Error (%)	Accuracy Req'd (±EU)	Max std error (EU)
PCM1: North Met Tower (7.5 Kb/s, 34.72 Hz, 28.8 ms):							
101	20 M Hot Film (Not Used)	-	-	-	-	-	-
102	18 M Sonic Channel A (Not Used)	-	-	-	-	-	-
103	18 M Sonic Channel B (Not Used)	-	-	-	-	-	-
104	18 M Sonic Channel C (Not Used)	-	-	-	-	-	-
105	5 M Wind Direction (Not Used)	-	-	-	-	-	-
106	5 M Wind Speed (m/s)	M1,E1	0 to 90	0 to 25	1.1	.5	.25
107	10 M Wind Direction (Not Used)	-	-	-	-	-	-
108	10 M Wind Speed (m/s)	M1,E1	0 to 90	0 to 25	1.1	.5	.25
109	20 M Wind Direction (Not Used)	-	-	-	-	-	-
110	20 M Wind Speed (m/s)	M1,E1	0 to90	0 to 25	1.1	.5	.25
111	50 M Wind Direction (Not Used)	-	-	-	-	-	-
112	50 M Wind Speed (m/s)	M1,E1	0 to 90	0 to 25	1.1	.5	.25
113	5 M Air Temperature (C)	M1,E5	±50	±50	2.0	1.0	.5
114	Delta Temperature (C)	M1,E4	-4.4 to 6.7	-4.4 to 3.3	1.8	.1	.05
115	5 M DP (Not Used)	-	-	-	-	-	-
116	Baro Pressure (mb)	M1,E3	700 to 930	711 to 914	1.7	2.0	1.5
PCM2: Vertical Plane Array (15.0 Kb/s, 69.44 Hz, 14.4 ms):							
201	VPA Prop Vane WS-1 (m/s)	A1,E1	0 to 37	0 to 25	2.7	.5	.25
202	VPA Prop Vane WS-2 (m/s)	A1,E1	0 to 37	0 to 25	2.7	.5	.25
203	VPA Prop Vane WS-3 (m/s)	A1,E1	0 to 37	0 to 25	2.7	.5	.25
204	VPA Prop Vane WS-4 (m/s)	A1,E1	0 to 37	0 to 25	2.7	.5	.25
205	VPA Prop Vane WS-5 (m/s)	A1,E1	0 to 37	0 to 25	2.7	.5	.25
206	VPA Prop Vane WS-6 (m/s)	A1,E1	0 to 37	0 to 25	2.7	.5	.25
207	VPA Prop Vane WS-7 (m/s)	A1,E1	0 to 37	0 to 25	2.7	.5	.25
208	VPA Prop Vane WS-8 (m/s)	A1,E1	0 to 37	0 to 25	2.7	.5	.25
209	VPA PV Hub Height WS-9 (m/s)	A1,E1	0 to 37	0 to 25	2.7	.5	.25
210	VPA PV Hub Height WD-9 (deg)	A1,M6	0 to 360	112 to 292	.56 (f)	2.0	1.0
211	VPA Bi-Vane WS-12 (m/s)	A1,E1	0 to 37	0 to 25	2.7	.5	.25
212	VPA Bi-Vane WD-12 (deg)	A1,M6	0 to 360	112 to 292	.56 (f)	2.0	1.0
213	VPA Bi-Vane Wa-12 (deg)	A1,M7	±50	±20	2.0	.5	.25
214	VPA Bi-Vane WS-13 (m/s)	A1,E1	0 to 37	0 to 25	2.7	.5	.25
215	VPA Bi-Vane WD-13 (deg)	A1,M6	0 to 360	112 to 292	.56 (f)	2.0	1.0
216	VPA Bi-Vane Wa-13 (deg)	A1,M7	±50	±20	2.0	.5	.25
PCM3: VPA, Local Met, Tower, Turbine (60.0 Kb/s, 277.78 Hz, 3.6 ms):							
301	VPA Prop Vane WS-10 (m/s)	A1,E1	0 to 37	0 to 25	2.7	.5	.25
302	VPA Prop Vane WS-11 (m/s)	A1,E1	0 to 37	0 to 25	2.7	.5	.25
303	LSS Azimuth Angle (deg)	A1,M5	0 to 360	90 to 270	.28 (f)	1.0	.5
304	Yaw Moment (NT-m)	A1,M10	±3500		5.0	175	88
305	Tower Bending E-W (NT-m)	A1,M9	±55000	±5200	5.0	2750	1375
306	Tower Bending N-S (NT-m)	A1,M9	±55000	±5200	5.0	2750	1375
307	Yaw Angle (deg)	A1,M4	0 to 360	112 to 292	.56 (f)	2.0	1.0
308	Generator Power (Kw)	A1,E6	±40	±80	1.25	.5	.25
309	LSS Speed (Not Used)	-	-	-	-	-	-
310	TSI (South) X-Film U (Not Used)	-	-	-	-	-	-
311	TSI (South) X-Film W (Not Used)	-	-	-	-	-	-
312	TSI (North) X-Film U (Not Used)	-	-	-	-	-	-
313	TSI (North) X-Film W (Not Used)	-	-	-	-	-	-
314	Sonic Anemometer Ch A (Not Used)	-	-	-	-	-	-
315	Sonic Anemometer Ch B (Not Used)	-	-	-	-	-	-
316	Sonic Anemometer Ch C (Not Used)	-	-	-	-	-	-

Unsteady Aero Experiment Measurement Tolerances* (continued)

Quick Look Number	Description	Cal Procedure #	Measurement Range Max (EU)	Measurement Range Calibrated (EU)	Allowable Error (%)	Accuracy Req'd (±EU)	Max std error (EU)
PCM4: Rotating Strain Gages, 80% Pressures (400.0 Kb/s, 520.83 Hz, 1.92 ms):							
401	Root Flap Bending "RTFBM-A" (NT-m)	A2,M8	±3200	0 to 1800	5.0	160	80
402	Root Flap Bending "RTFBM-B" (NT-m)	A2,M8	±3200	0 to 1800	5.0	160	80
403	Root Flap Blade 2 "RTFBM-2" (NT-m)	A2,M8	±3200	0 to 1800	5.0	160	80
404	Root Flap Blade 3 "RTFBM-3" (NT-m)	A2,M8	±3200	0 to 1800	5.0	160	80
405	20% Flap Bending "20FBM" (NT-m)	A2,M8	±3000	0 to 1555	5.0	150	75
406	40% Flap Bending "40FBM" (NT-m)	A2,M8	±2300	0 to 1150	5.0	115	58
407	50% Flap Bending "50FBM" (NT-m)	A2,M8	±1400	0 to 950	5.0	70	35
408	60% Flap Bending "60FBM" (Not Used)	-	-	-	-	-	-
409	70% Flap Bending "70FBM" (NT-m)	A2,M8	±800	0 to 550	5.0	40	20
410	75% Flap Bending "75FBM" (Not Used)	-	-	-	-	-	-
411	80% Flap Bending "80FBM" (Not Used)	-	-	-	-	-	-
412	85% Flap Bending "85FBM" (Not Used)	-	-	-	-	-	-
413	90% Flap Bending "90FBM" (NT-m)	A2,M8	±300	0 to 145	5.0	15	8
414	Root Edge Bending "RTEBM-A" (NT-m)	A2,M8	±3200	0 to 1800	5.0	160	80
415	20% Edge Bending "20EBM" (NT-m)	A2,M8	±3000	0 to 1555	5.0	150	75
416	50% Edge Bending "50EBM" (NT-m)	A2,M8	±1400	0 to 950	5.0	70	35
417	70% Blade Torque "70TQ" (NT-m)	A2,M8	±1100	0 to 550	5.0	55	28
418	85% Edge Bending "85EBM" (Not Used)	-	-	-	-	-	-
419	Root Torque (Link) "RTTQ" (NT-m)	A2,M8	±205	0 to 480	5.0	10	5
420	50% Torsion "50TQ" (NT-m)	A2,M8	±300	0 to 480	5.0	15	8
421	X-X LSS Bending "LSSX-X" (NT-m)	A2,M8	±13000		5.0	650	325
422	Y-Y LSS Bending "LSSY-Y" (NT-m)	A2,M8	±13000		5.0	650	325
423	LSS Torque "LSSTQ-A" (NT-m)	A2,M8	±6500	0 to 2000	5.0	325	163
424	LSS Torque "LSSTQ-B" (NT-m)	A2,M8	±6500	0 to 2000	5.0	325	163
425	85% RTD (Not Used)	-	-	-	-	-	-
426	Load Cell for Blade Pull Testing (NT)	A2,M8	0-900	0 to 900	2.0 (f)	18	9
427	Pressure #1 StaPT10, 100% trailing (psi)	A3,A4	±1.2	±0.3	.579	.00695	.00347
428	Pressure #2 StaPT10, 92% upper (psi)	A3,A4	±1.2	±0.3	.579	.00695	.00347
429	Pressure #4 StaPT10, 80% upper (psi)	A3,A4	±1.2	±0.3	.579	.00695	.00347
430	Pressure #6 StaPT10, 68% upper (psi)	A3,A4	±1.2	±0.3	.579	.00695	.00347
431	Pressure #8 StaPT10, 56% upper (psi)	A3,A4	±1.2	±0.3	.579	.00695	.00347
432	Pressure #10 StaPT10, 44% upper (psi)	A3,A4	±1.2	±0.3	.579	.00695	.00347
433	Pressure #11 StaPT10, 36% upper (psi)	A3,A4	±1.2	±0.3	.579	.00695	.00347
434	Pressure #12 StaPT10, 28% upper (psi)	A3,A4	±1.2	±0.3	.579	.00695	.00347
435	Pressure #13 StaPT10, 20% upper (psi)	A3,A4	±1.2	±0.3	.579	.00695	.00347
436	Pressure #14 StaPT10, 14% upper (psi)	A3,A4	±1.2	±0.3	.579	.00695	.00347
437	Pressure #15 StaPT10, 10% upper (psi)	A3,A4	±1.2	±0.3	.579	.00695	.00347
438	Pressure #16 StaPT10, 8% upper (psi)	A3,A4	±1.2	±0.3	.579	.00695	.00347
439	Pressure #17 StaPT10, 6% upper (psi)	A3,A4	±1.2	±0.3	.579	.00695	.00347
440	Pressure #18 StaPT10, 4% upper (psi)	A3,A4	±1.2	±0.3	.579	.00695	.00347
441	Pressure #19 StaPT10, 2% upper (psi)	A3,A4	±1.2	±0.3	.579	.00695	.00347
442	Pressure #20 StaPT10, 1% upper (psi)	A3,A4	±1.2	±0.3	.579	.00695	.00347
443	Pressure #21 StaPT10, 0.5% upper (psi)	A3,A4	±1.2	±0.3	.579	.00695	.00347
444	Pressure #22 StaPT10, 0% leading (psi)	A3,A4	±1.2	±0.3	.579	.00695	.00347
445	Pressure #23 StaPT10, 0.5% lower (psi)	A3,A4	±1.2	±0.3	.579	.00695	.00347
446	Pressure #24 StaPT10, 1% lower (psi)	A3,A4	±1.2	±0.3	.579	.00695	.00347
447	Pressure #25 StaPT10, 2% lower (psi)	A3,A4	±1.2	±0.3	.579	.00695	.00347
448	Pressure #26 StaPT10, 4% lower (psi)	A3,A4	±1.2	±0.3	.579	.00695	.00347
449	Pressure #28 StaPT10, 8% lower (psi)	A3,A4	±1.2	±0.3	.579	.00695	.00347
450	Pressure #30 StaPT10, 14% lower (psi)	A3,A4	±1.2	±0.3	.579	.00695	.00347
451	Pressure #32 StaPT10, 28% lower (psi)	A3,A4	±1.2	±0.3	.579	.00695	.00347
452	Pressure #34 StaPT10, 44% lower (psi)	A3,A4	±1.2	±0.3	.579	.00695	.00347

Unsteady Aero Experiment Measurement Tolerances* (continued)

Quick Look Number	Description	Cal Procedure #	Measurement Range Max (EU)	Measurement Range Calibrated (EU)	Allowable Error (%)	Accuracy Req'd (±EU)	Max std error (EU)
PCM4: Continued (400.0 Kb/s, 520.83 Hz, 1.92 ms)							
453	Pressure #36 StaPT10, 68% lower (psi)	A3,A4	±1.2	±0.3	.579	.00695	.00347
454	Pressure #38 StaPT10, 92% lower (psi)	A3,A4	±1.2	±0.3	.579	.00695	.00347
455	Pressure #18 StaPT9, 4% upper (psi)	A3,A4	±1.2	±0.3	.500	.00600	.00300
456	Pressure #11 StaPT9, 36% upper (psi)	A3,A4	±1.2	±0.3	.500	.00600	.00300
457	Pressure #11 StaPT8, 36% upper (psi)	A3,A4	±1.2	±0.3	.439	.00527	.00264
458	Total Pressure Probe, 86% span (psi)	A3,A4	±1.2	±0.3	.579	.00695	.00347
459	Absolute Reference Pressure (mb)	E3	800-1100	711-914	2.0	3.0	1.5
460	Calibration Pressure (psi) (Cal Only)	E2	±0.3	±0.5	.222 (f)	.00133	.00044**
461	Pitch Angle (degrees)	M3	-106 to 71	-10 to 20	1.0	1.0	.5
462	PCM Voltage Monitor (Quick-Look Only)	-	±140		10	14	7
PCM8: Rotating 30% and 40% Pressures (400.0 Kb/s, 520.83 Hz, 1.92 ms):							
801	Absolute Reference Pressure (Not Used)	-	-	-	-	-	-
802	Calibration Pressure (Cal Only)	E2	±0.3	±0.5	.222 (f)	.00133	.00044**
803	Spare	-	-	-	-	-	-
804	Pressure #1 StaPT1, 100% trailing (psi)	A2,A3	±0.43	±0.3	.310	.00133	.00067
805	Pressure #4 StaPT1, 80% upper (psi)	A2,A3	±0.43	±0.3	.310	.00133	.00067
806	Pressure #6 StaPT1, 68% upper (psi)	A2,A3	±0.43	±0.3	.310	.00133	.00067
807	Pressure #8 StaPT1, 56% upper (psi)	A2,A3	±0.43	±0.3	.310	.00133	.00067
808	Pressure #10 StaPT1, 44% upper (psi)	A2,A3	±0.43	±0.3	.310	.00133	.00067
809	Pressure #11 StaPT1, 36% upper (psi)	A2,A3	±0.43	±0.3	.310	.00133	.00067
810	Pressure #13 StaPT1, 20% upper (psi)	A2,A3	±0.43	±0.3	.310	.00133	.00067
811	Pressure #14 StaPT1, 14% upper (psi)	A2,A3	±0.43	±0.3	.310	.00133	.00067
812	Pressure #15 StaPT1, 10% upper (psi)	A2,A3	±0.43	±0.3	.310	.00133	.00067
813	Pressure #16 StaPT1, 8% upper (psi)	A2,A3	±0.43	±0.3	.310	.00133	.00067
814	Pressure #17 StaPT1, 6% upper (psi)	A2,A3	±0.43	±0.3	.310	.00133	.00067
815	Pressure #18 StaPT1, 4% upper (psi)	A2,A3	±0.43	±0.3	.310	.00133	.00067
816	Pressure #19 StaPT1, 2% upper (psi)	A2,A3	±0.43	±0.3	.310	.00133	.00067
817	Pressure #21 StaPT1, 0.5% upper (psi)	A2,A3	±0.43	±0.3	.310	.00133	.00067
818	Pressure #22 StaPT1, 0% leading (psi)	A2,A3	±0.43	±0.3	.310	.00133	.00067
819	Pressure #23 StaPT1, 0.5% lower (psi)	A2,A3	±0.43	±0.3	.310	.00133	.00067
820	Pressure #24 StaPT1, 1% lower (psi)	A2,A3	±0.43	±0.3	.310	.00133	.00067
821	Pressure #25 StaPT1, 2% lower (psi)	A2,A3	±0.43	±0.3	.310	.00133	.00067
822	Pressure #26 StaPT1, 4% lower (psi)	A2,A3	±0.43	±0.3	.310	.00133	.00067
823	Pressure #28 StaPT1, 8% lower (psi)	A2,A3	±0.43	±0.3	.310	.00133	.00067
824	Pressure #30 StaPT1, 14% lower (psi)	A2,A3	±0.43	±0.3	.310	.00133	.00067
825	Pressure #31 StaPT1, 20% lower (psi)	A2,A3	±0.43	±0.3	.310	.00133	.00067
826	Pressure #34 StaPT1, 44% lower (psi)	A2,A3	±0.43	±0.3	.310	.00133	.00067
827	Pressure #36 StaPT1, 68% lower (psi)	A2,A3	±0.43	±0.3	.310	.00133	.00067
828	Pressure #38 StaPT1, 92% lower (psi)	A2,A3	±0.43	±0.3	.310	.00133	.00067
829	Pressure #18 StaPT2, 4% upper (psi)	A2,A3	±0.43	±0.3	.404	.00174	.00087
830	Pressure #11 StaPT2, 36% upper (psi)	A2,A3	±0.43	±0.3	.404	.00174	.00087
831	Pressure #11 StaPT3, 36% upper (psi)	A2,A3	±0.43	±0.3	.495	.00213	.00106
832	Total Pressure Probe, 34% span (psi)	A2,A3	±0.43	±0.3	.310	.00133	.00067
833	Pressure #1 StaPT4, 100% trailing (psi)	A2,A3	±0.43	±0.3	.620	.00267	.00133
834	Pressure #2 StaPT4, 92% upper (psi)	A2,A3	±0.43	±0.3	.620	.00267	.00133
835	Pressure #4 StaPT4, 80% upper (psi)	A2,A3	±0.43	±0.3	.620	.00267	.00133
836	Pressure #6 StaPT4, 68% upper (psi)	A2,A3	±0.43	±0.3	.620	.00267	.00133
837	Pressure #8 StaPT4, 56% upper (psi)	A2,A3	±0.43	±0.3	.620	.00267	.00133
838	Pressure #10 StaPT4, 44% upper (psi)	A2,A3	±0.43	±0.3	.620	.00267	.00133
839	Pressure #11 StaPT4, 36% upper (psi)	A2,A3	±0.43	±0.3	.620	.00267	.00133
840	Pressure #12 StaPT4, 28% upper (psi)	A2,A3	±0.43	±0.3	.620	.00267	.00133

Unsteady Aero Experiment Measurement Tolerances* (continued)

Quick Look Number	Description	Cal Procedure #	Measurement Range Max (EU)	Measurement Range Calibrated (EU)	Allowable Error (%)	Accuracy Req'd (±EU)	Max std error (EU)
PCM8: Continued (400.0 Kb/s, 520.83 Hz, 1.92 ms):							
841	Pressure #13 StaPT4, 20% upper (psi)	A2,A3	±0.43	±0.3	.620	.00267	.00133
842	Pressure #14 StaPT4, 14% upper (psi)	A2,A3	±0.43	±0.3	.620	.00267	.00133
843	Pressure #15 StaPT4, 10% upper (psi)	A2,A3	±0.43	±0.3	.620	.00267	.00133
844	Pressure #16 StaPT4, 8% upper (psi)	A2,A3	±0.43	±0.3	.620	.00267	.00133
845	Pressure #17 StaPT4, 6% upper (psi)	A2,A3	±0.43	±0.3	.620	.00267	.00133
846	Pressure #18 StaPT4, 4% upper (psi)	A2,A3	±0.43	±0.3	.620	.00267	.00133
847	Pressure #19 StaPT4, 2% upper (psi)	A2,A3	±0.43	±0.3	.620	.00267	.00133
848	Pressure #20 StaPT4, 1% upper (psi)	A2,A3	±0.43	±0.3	.620	.00267	.00133
849	Pressure #21 StaPT4, 0.5% upper (psi)	A2,A3	±0.43	±0.3	.620	.00267	.00133
850	Pressure #22 StaPT4, 0% leading (psi)	A2,A3	±0.43	±0.3	.620	.00267	.00133
851	Pressure #23 StaPT4, 0.5% lower (psi)	A2,A3	±0.43	±0.3	.620	.00267	.00133
852	Pressure #25 StaPT4, 2% lower (psi)	A2,A3	±0.43	±0.3	.620	.00267	.00133
853	Pressure #26 StaPT4, 4% lower (psi)	A2,A3	±0.43	±0.3	.620	.00267	.00133
854	Pressure #27 StaPT4, 6% lower (psi)	A2,A3	±0.43	±0.3	.620	.00267	.00133
855	Pressure #28 StaPT4, 8% lower (psi)	A2,A3	±0.43	±0.3	.620	.00267	.00133
856	Pressure #30 StaPT4, 14% lower (psi)	A2,A3	±0.43	±0.3	.620	.00267	.00133
857	Pressure #32 StaPT4, 28% lower (psi)	A2,A3	±0.43	±0.3	.620	.00267	.00133
858	Pressure #34 StaPT4, 44% lower (psi)	A2,A3	±0.43	±0.3	.620	.00267	.00133
859	Pressure #36 StaPT4, 68% lower (psi)	A2,A3	±0.43	±0.3	.620	.00267	.00133
860	Pressure #38 StaPT4, 92% lower (psi)	A2,A3	±0.43	±0.3	.620	.00267	.00133
861	Pressure #18 StaPT3, 4% upper (psi)	A2,A3	±0.43	±0.3	.495	.00213	.00106
862	Total Pressure Probe, 50.6% span (psi)	A2,A3	±0.43	±0.3	.620	.00267	.00133
PCM9: Rotating 63% Pressures, Angle of Attack (400.0 Kb/s, 520.83 Hz, 1.92 ms):							
901	Pressure #11 StaPT5, 36% upper (psi)	A2,A3	±1.2	±0.3	.262	.00317	.00159
902	Pressure #18 StaPT5, 4% upper (psi)	A2,A3	±1.2	±0.3	.262	.00317	.00159
903	Pressure #1 StaPT7, 100% trailing (psi)	A2,A3	±1.2	±0.3	.372	.00447	.00223
904	Pressure #2 StaPT7, 92% upper (psi)	A2,A3	±1.2	±0.3	.372	.00447	.00223
905	Pressure #4 StaPT7, 80% upper (psi)	A2,A3	±1.2	±0.3	.372	.00447	.00223
906	Pressure #6 StaPT7, 68% upper (psi)	A2,A3	±1.2	±0.3	.372	.00447	.00223
907	Pressure #8 StaPT7, 56% upper (psi)	A2,A3	±1.2	±0.3	.372	.00447	.00223
908	Pressure #10 StaPT7, 44% upper (psi)	A2,A3	±1.2	±0.3	.372	.00447	.00223
909	Pressure #11 StaPT7, 36% upper (psi)	A2,A3	±1.2	±0.3	.372	.00447	.00223
910	Pressure #12 StaPT7, 28% upper (psi)	A2,A3	±1.2	±0.3	.372	.00447	.00223
911	Pressure #13 StaPT7, 20% upper (psi)	A2,A3	±1.2	±0.3	.372	.00447	.00223
912	Pressure #14 StaPT7, 14% upper (psi)	A2,A3	±1.2	±0.3	.372	.00447	.00223
913	Pressure #15 StaPT7, 10% upper (psi)	A2,A3	±1.2	±0.3	.372	.00447	.00223
914	Pressure #16 StaPT7, 8% upper (psi)	A2,A3	±1.2	±0.3	.372	.00447	.00223
915	Pressure #17 StaPT7, 6% upper (psi)	A2,A3	±1.2	±0.3	.372	.00447	.00223
916	Pressure #18 StaPT7, 4% upper (psi)	A2,A3	±1.2	±0.3	.372	.00447	.00223
917	Pressure #19 StaPT7, 2% upper (psi)	A2,A3	±1.2	±0.3	.372	.00447	.00223
918	Pressure #20 StaPT7, 1% upper (psi)	A2,A3	±1.2	±0.3	.372	.00447	.00223
919	Pressure #21 StaPT7, 0.5% upper (psi)	A2,A3	±1.2	±0.3	.372	.00447	.00223
920	Pressure #22 StaPT7, 0% leading (psi)	A2,A3	±1.2	±0.3	.372	.00447	.00223
921	Pressure #23 StaPT7, 0.5% lower (psi)	A2,A3	±1.2	±0.3	.372	.00447	.00223
922	Pressure #24 StaPT7, 1% lower (psi)	A2,A3	±1.2	±0.3	.372	.00447	.00223
923	Pressure #25 StaPT7, 2% lower (psi)	A2,A3	±1.2	±0.3	.372	.00447	.00223
924	Pressure #26 StaPT7, 4% lower (psi)	A2,A3	±1.2	±0.3	.372	.00447	.00223
925	Pressure #28 StaPT7, 8% lower (psi)	A2,A3	±1.2	±0.3	.372	.00447	.00223
926	Pressure #30 StaPT7, 14% lower (psi)	A2,A3	±1.2	±0.3	.372	.00447	.00223
927	Pressure #32 StaPT7, 28% lower (psi)	A2,A3	±1.2	±0.3	.372	.00447	.00223
928	Pressure #34 StaPT7, 44% lower (psi)	A2,A3	±1.2	±0.3	.372	.00447	.00223

Unsteady Aero Experiment Measurement Tolerances* (continued)

Quick Look Number	Description	Cal Procedure #	Measurement Range Max (EU)	Measurement Range Calibrated (EU)	Allowable Error (%)	Accuracy Req'd (±EU)	Max std error (EU)
PCM9: Continued (400.0 Kb/s, 520.83 Hz, 1.92 ms):							
929	Pressure #36 StaPT7, 68% lower (psi)	A2,A3	±1.2	±0.3	.372	.00447	.00223
930	Pressure #38 StaPT7, 92% lower (psi)	A2,A3	±1.2	±0.3	.372	.00447	.00223
931	Pressure #18 StaPT6, 4% upper (psi)	A2,A3	±1.2	±0.3	.321	.00386	.00192
932	Pressure #18 StaPT8, 4% upper (psi)	A2,A3	±1.2	±0.3	.439	.00527	.00264
933	Pressure #11 StaPT6, 36% upper (psi)	A2,A3	±1.2	±0.3	.321	.00386	.00192
934	Total Pressure Probe, 67.3% span (psi)	A2,A3	±1.2	±0.3	.372	.00447	.00223
935	Angle-of-Attack, 86% span (degrees)	M2	-22 to 55	-20 to 40	2.6	1.0	.5
936	Ground	-	-	-	-	-	-
937	Angle-of-Attack, 67.3% span (degrees)	M2	-22 to 55	-20 to 40	2.6	1.0	.5
938	Ground	-	-	-	-	-	-
939	Do Not Use (Bad channel)	-	-	-	-	-	-
940	Ground	-	-	-	-	-	-
941	Angle-of-Attack, 34% span (degrees)	M2	-22 to 55	-20 to 40	2.6	1.0	.5
942	Ground	-	-	-	-	-	-
943	Nitrogen Pressure (psi) (Quick-Look Only)	-	±2000		10	200	100
944	+15 Volt Power Monitor (V) (Quick-Look Only)	-	±20		10	1.5	.8
945	-15 Volt Power Monitor (V) (Quick-Look Only)	-	±20		10	1.5	.8
946	Angle-of-Attack, 50.6% span (degrees)	M2	-22 to 55	-20 to 40	2.6	1.0	.5
947	DC Ground Monitor (counts) (Quick-Look Only)	-	0 to 4095				
948	Spare	-	-	-	-	-	-
949	Spare	-	-	-	-	-	-
950	Spare	-	-	-	-	-	-
951	Spare	-	-	-	-	-	-
952	Spare	-	-	-	-	-	-
953	Absolute Reference Pressure	E3	800-1100	711-914	2.0	3.0	1.5
954	Calibration Pressure (Cal Only)	E4	±0.3	±0.5	.222 (f)	.00133	.00044**
955	Spare	-	-	-	-	-	-
956	Spare	-	-	-	-	-	-
957	Spare	-	-	-	-	-	-
958	Spare	-	-	-	-	-	-
959	Spare	-	-	-	-	-	-
960	Spare	-	-	-	-	-	-
961	Spare	-	-	-	-	-	-
962	Spare	-	-	-	-	-	-

Notes

* All measured channels and their corresponding calibration requirements are listed here. The first column shows channel ID number as it is referenced by the Quick-Look system. The first digit is the PCM stream number and the next two digits are the PCM frame number. Column 2 contains channel descriptions and units. Each channel has defined calibration procedures identified in column 3 which are performed to measure the end to end accuracy of all channels. The procedures are identified by the letter A, E or M, followed by a number. The letter designates 3 basic types of calibrations An "E" designates those channels in which the transducer requires an external calibration, such as anamometers in the wind tunnel. An "A" designates an automatic calibration in which many incoming signals can be automatically placed in a known calibration state. An "M" designates calibrations which require manual placement of transducers into a position to enable calibrating. The number which follows identifies a specific procedure to be followed in order to calibrate that channel. These are described in detail in Appendix D. Channels with type "E" calibrations are done in two parts in which the transducer and electronics are calibrated separately, then RMS summed to determine overall channel accuracy. All other channels are end-to-end calibrated to directly measure the full channel response. Some channels (such as pressures and strain-gages) require two end-to-end cals, one to calculate slope, and another to calculate offset.

The next two columns show the measurement range. Column 4 shows the full data range by identifying estimated data extremes over which accurate measurements can be made. Column 5 shows the range over which the channel transducer is typically calibrated. Since all incoming signals are linear, calibration coefficients are theoretically accurate over the full measurement range. However, a higher level of confidence is associated with measurements of demonstrated accuracy made within the calibration range.

Channel measurement tolerances can be defined in terms of required absolute measurement accuracy. For example, it could be specified that temperature measurements made over the range of Y_{min} to Y_{max} be accurate to $\pm Q_{acc}$ degrees C. Column 7 shows the required overall measurement accuracy $\pm Q_{acc}$ for each channel in engineering units over the data range of column 4. The requirements are based on subsequent processed data needs.

It may not always be desirable to express measurement tolerances in engineering units. It is often necessary to quantify the accuracy of intermediate processes which occur prior to engineering unit conversion. For this reason, measurement tolerances are also specified in terms of percent acceptable error over a given measurement range. For example, wind speed measurement errors can be specified not to exceed $\pm Q_{err}$ percent of a given measurement range. Column 6 lists the maximum allowable error $\pm Q_{err}$ for each channel. Q_{err} is specified as a percentage of either half or full measurement range.

Most channels are set up to provide data measurements over a large range to cover all possible conditions. Typical values, however, occur only within a small portion of the full range. Excursions to range extremes can be measured, but seldom occur. It is therefore not practical to base calibration requirements on the full data range. Rather, measurement errors for these types of channels are defined not exceed $\pm Q_{err}$ percent of half the measurement range of $\frac{1}{2}(Y_{max}-Y_{min})$. Examples are wind speed and blade pressure measurements. Most of the channels in the table use the half-range error criteria. Some channels, however, require the specified accuracy across the full measurement range. For these, the required accuracy is $\pm Q_{err}$ percent of the full range of $Y_{max}-Y_{min}$. Examples of channels using the full-range criteria are azimuth angle and wind direction, and are identified with by a (f) in column 6.

The relationship between Q_{err} and Q_{acc} is a function of the measurement range, and is defined as:

$$Q_{acc} = Q_{err}\ \tfrac{1}{2}(Y_{max} - Y_{min}) \qquad \text{for half-range accuracy}$$
$$Q_{acc} = Q_{err}\ (Y_{max} - Y_{min}) \qquad \text{for full-range accuracy}$$

To check acceptable channel drift tolerances, the error level in column 6 defines maximum allowable slope difference between results of two successive slope calibration sequences. Typically, for each data interval, a pre and post calibration sequence is conducted. If the percent difference between slopes calculated at each time has not changed beyond the specified level, then the drift is not significant, and the data is considered valid. Similarly, maximum allowable offset difference is defined by the maximum measurement accuracy value in column 7.

All calibration measurements should be made within the required accuracy to a 95% or greater statistical degree of confidence. This means that there should be at least a 95% probability that calibration measurements fall within the specified error band. The 95.45% range is defined as $\pm 2S_{yx}$ where S_{yx} is the standard error (also called the sample standard deviation). This identity is used to determine the acceptable error range. Maximum allowable standard errors to achieve the 95% confidence level are shown for each channel in the last column, and were calculated from:

$$S_{yx} = \frac{Q_{err}}{2}$$

The Unsteady Aero Experiment requires many calibrations to be quickly conducted in the field. To ensure accuracy and verify calibration results, standard error values from column 8 are compared to those calculated in the field during Quick-Look calibration sequences. This provides test engineers with an immediate estimation of calibration validity. A full rigorous statistical analysis could also be conducted in order to provide additional useful calibration information, including confidence limits for the regression coefficients and individual mean sample values. Due to limitations imposed by PC-based processing, this is not done in the field, but could be

post-calculated if required. 95% confidence limits for least-squares regression slope value m are determined from:

$$m \pm \frac{t_{.975}}{\sqrt{N-2}} \frac{S_{yx}}{S_x}$$

where $t_{.975}$ is the student t distribution for N samples at the .975 level (use 5% significance / 2), and S_x is the standard deviation of the measured X values. Similarly, 95% confidence limits for the mean sample values can be determined using standard statistical techniques:

$$Y_0 \pm \frac{t_{.975}}{\sqrt{N-2}} S_{yx} \sqrt{1+\frac{(X_0-\overline{X})^2}{S_x^2}}$$

where $\overline{X}$ is the mean of the measured X values and Y_0 is the predicted value of Y at $X = X_0$ using the resulting calculated regression slope m and offset b, ie. $Y_0 = mX_0 + b$.

** For calibrating pressures, the refrence transducer is calibrated to a 99% confidence level that measurements can be made to a required accuracy of $\pm$.00133 psi accros the full calibration range of $\pm$.3 psi. The 99.73% level is defined as $\pm 3S_{yx}$, which is typically used when calibrating reference transducers from which other calibrations are derived. For pressure calibrations, required pressure measurement accuracy is 10% of the total induced pressure.

Appendix C

Unsteady Aero Experiment Channel Data Rates

Unsteady Aero Experiment Channel Data Rates

Quick/EXP Look /Tag Number	Description	Filter Setting (Hz)	Dec/BW (Nth Seq/) (Hz)	Sample Rate (Hz)	DT (msec)	No. Per 144 msec record
PCM1: North Met Tower (7.5 Kb/s, 34.72 Hz, 28.8 ms):						
101/1301	20 M Hot Film (Not Used)	-	5/1	6.94	144.0	1
102/1302	18 M Sonic Channel A (Not Used)	-	5/1	6.94	144.0	1
103/1303	18 M Sonic Channel B (Not Used)	-	5/1	6.94	144.0	1
104/1304	18 M Sonic Channel C (Not Used)	-	5/1	6.94	144.0	1
105/1305	5 M Wind Direction (Not Used)	1	5/1	6.94	144.0	1
106/1306	5 M Wind Speed	1	5/1	6.94	144.0	1
107/1307	10 M Wind Direction (Not Used)	1	5/1	6.94	144.0	1
108/1308	10 M Wind Speed	1	5/1	6.94	144.0	1
109/1309	20 M Wind Direction (Not Used)	1	5/1	6.94	144.0	1
110/1310	20 M Wind Speed	1	5/1	6.94	144.0	1
111/1311	50 M Wind Direction (Not Used)	1	5/1	6.94	144.0	1
112/1312	50 M Wind Speed	1	5/1	6.94	144.0	1
113/1313	5 M Air Temperature	1	5/1	6.94	144.0	1
114/1314	Delta Temperature	1	5/1	6.94	144.0	1
115/1315	5 M DP (Not Used)	-	5/1	6.94	144.0	1
116/1316	Baro Pressure	1	5/1	6.94	144.0	1
PCM2: Vertical Plane Array (15.0 Kb/s, 69.44 Hz, 14.4 ms):						
201/0201	VPA Prop Vane WS-1	2	5/2	13.9	72.0	2
202/0202	VPA Prop Vane WS-2	2	5/2	13.9	72.0	2
203/0203	VPA Prop Vane WS-3	2	5/2	13.9	72.0	2
204/0204	VPA Prop Vane WS-4	2	5/2	13.9	72.0	2
205/0205	VPA Prop Vane WS-5	2	5/2	13.9	72.0	2
206/0206	VPA Prop Vane WS-6	2	5/2	13.9	72.0	2
207/0207	VPA Prop Vane WS-7	2	5/2	13.9	72.0	2
208/0208	VPA Prop Vane WS-8	2	5/2	13.9	72.0	2
209/0209	VPA PV Hub Height WS-9	2	5/2	13.9	72.0	2
210/0210	VPA PV Hub Height WD-9	2	5/2	13.9	72.0	2
211/0211	VPA Bi-Vane WS-12	2	5/2	13.9	72.0	2
212/0212	VPA Bi-Vane WD-12	2	5/2	13.9	72.0	2
213/0213	VPA Bi-Vane Wa-12	2	5/2	13.9	72.0	2
214/0214	VPA Bi-Vane WS-13	2	5/2	13.9	72.0	2
215/0215	VPA Bi-Vane WD-13	2	5/2	13.9	72.0	2
216/0216	VPA Bi-Vane Wa-13	2	5/2	13.9	72.0	2
PCM3: VPA, Local Met, Tower, Turbine (60.0 Kb/s, 277.78 Hz, 3.6 ms):						
301/0301	VPA Prop Vane WS-10	2	20/2	13.9	72.0	2
302/0302	VPA Prop Vane WS-11	2	20/2	13.9	72.0	2
303/0303	LSS Azimuth Angle	32	0/54	277.78	3.6	40
304/0304	Yaw Moment	40	0/54	277.78	3.6	40
305/0305	Tower Bending E-W	40	0/54	277.78	3.6	40
306/0306	Tower Bending N-S	40	0/54	277.78	3.6	40
307/0307	Yaw Angle	10	5/11	55.56	18.8	8
308/0308	Generator Power	54	0/54	277.78	3.6	40
309/0309	LSS Speed (Not Used)	-	40/1	6.94	144.0	1
310/0310	TSI (South) X-Film U (Not Used)	-	40/1	6.94	144.0	1
311/0311	TSI (South) X-Film W (Not Used)	-	40/1	6.94	144.0	1
312/0312	TSI (North) X-Film U (Not Used)	-	40/1	6.94	144.0	1
313/0313	TSI (North) X-Film W (Not Used)	-	40/1	6.94	144.0	1
314/0314	Sonic Anemometer Ch A (Not Used)	-	40/1	6.94	144.0	1
315/0315	Sonic Anemometer Ch B (Not Used)	-	40/1	6.94	144.0	1
316/0316	Sonic Anemometer Ch C (Not Used)	-	40/1	6.94	144.0	1

Unsteady Aero Experiment Channel Data Rates (Continued)

Quick/EXP Look /Tag Number	Description	Filter Setting (Hz)	Dec/BW (Nth Seq/) (Hz)	Sample Rate (Hz)	DT (msec)	No. Per 144 msec record
PCM4: Rotating Strain Gages, 80% Pressures (400.0 Kb/s, 520.83 Hz, 1.92 ms):						
401/1101	Root Flap Bending "RTFBM-A"	100	0/104	520.83	1.92	75
402/1102	Root Flap Bending "RTFBM-B"	100	0/104	520.83	1.92	75
403/1103	Root Flap Blade 2 "RTFBM-2"	100	0/104	520.83	1.92	75
404/1104	Root Flap Blade 3 "RTFBM-3"	100	0/104	520.83	1.92	75
405/1105	20% Flap Bending "20FBM"	100	0/104	520.83	1.92	75
406/1106	40% Flap Bending "40FBM"	100	0/104	520.83	1.92	75
407/1107	50% Flap Bending "50FBM"	100	0/104	520.83	1.92	75
408/1108	60% Flap Bending "60FBM" (Not Used)	-	75/1	6.94	144.0	1
409/1109	70% Flap Bending "70FBM"	100	0/104	520.83	1.92	75
410/1110	75% Flap Bending "75FBM" (Not Used)	-	75/1	6.94	144.0	1
411/1111	80% Flap Bending "80FBM" (Not Used)	-	75/1	6.94	144.0	1
412/1112	85% Flap Bending "85FBM" (Not Used)	-	75/1	6.94	144.0	1
413/1113	90% Flap Bending "90FBM"	100	0/104	520.83	1.92	75
414/1114	Root Edge Bending "RTEBM-A"	100	0/104	520.83	1.92	75
415/1115	20% Edge Bending "20EBM"	100	0/104	520.83	1.92	75
416/1116	50% Edge Bending "50EBM"	100	0/104	520.83	1.92	75
417/1117	70% Blade Torque "70TQ"	100	0/104	520.83	1.92	75
418/1118	85% Edge Bending "85EBM" (Not Used)	-	75/1	6.94	144.0	1
419/1119	Root Torque (Link) "RTTQ"	100	0/104	520.83	1.92	75
420/1120	50% Torsion "50TQ"	100	0/104	520.83	1.92	75
421/1121	X-X LSS Bending "LSSX-X"	100	0/104	520.83	1.92	75
422/1122	Y-Y LSS Bending "LSSY-Y"	100	0/104	520.83	1.92	75
423/1123	LSS Torque "LSSTQ-A"	100	0/104	520.83	1.92	75
424/1124	LSS Torque "LSSTQ-B"	100	0/104	520.83	1.92	75
425/1125	85% RTD (Not Used)	-	75/1	6.94	144.0	1
426/1126	Load Cell for Blade Pull Testing (Cal Only)	-	75/1	6.94	144.0	1
427/1127	Pressure #1 StaPT10, 100% trailing	100	0/104	520.83	1.92	75
428/1128	Pressure #2 StaPT10, 92% upper	100	0/104	520.83	1.92	75
429/1129	Pressure #4 StaPT10, 80% upper	100	0/104	520.83	1.92	75
430/1130	Pressure #6 StaPT10, 68% upper	100	0/104	520.83	1.92	75
431/1131	Pressure #8 StaPT10, 56% upper	100	0/104	520.83	1.92	75
432/1132	Pressure #10 StaPT10, 44% upper	100	0/104	520.83	1.92	75
433/1133	Pressure #11 StaPT10, 36% upper	100	0/104	520.83	1.92	75
434/1134	Pressure #12 StaPT10, 28% upper	100	0/104	520.83	1.92	75
435/1135	Pressure #13 StaPT10, 20% upper	100	0/104	520.83	1.92	75
436/1136	Pressure #14 StaPT10, 14% upper	100	0/104	520.83	1.92	75
437/1137	Pressure #15 StaPT10, 10% upper	100	0/104	520.83	1.92	75
438/1138	Pressure #16 StaPT10, 8% upper	100	0/104	520.83	1.92	75
439/1139	Pressure #17 StaPT10, 6% upper	100	0/104	520.83	1.92	75
440/1140	Pressure #18 StaPT10, 4% upper	100	0/104	520.83	1.92	75
441/1141	Pressure #19 StaPT10, 2% upper	100	0/104	520.83	1.92	75
442/1142	Pressure #20 StaPT10, 1% upper	100	0/104	520.83	1.92	75
443/1143	Pressure #21 StaPT10, 0.5% upper	100	0/104	520.83	1.92	75
444/1144	Pressure #22 StaPT10, 0% leading	100	0/104	520.83	1.92	75
445/1145	Pressure #23 StaPT10, 0.5% lower	100	0/104	520.83	1.92	75
446/1146	Pressure #24 StaPT10, 1% lower	100	0/104	520.83	1.92	75
447/1147	Pressure #25 StaPT10, 2% lower	100	0/104	520.83	1.92	75
448/1148	Pressure #26 StaPT10, 4% lower	100	0/104	520.83	1.92	75
449/1149	Pressure #28 StaPT10, 8% lower	100	0/104	520.83	1.92	75
450/1150	Pressure #30 StaPT10, 14% lower	100	0/104	520.83	1.92	75
451/1151	Pressure #32 StaPT10, 28% lower	100	0/104	520.83	1.92	75

Unsteady Aero Experiment Channel Data Rates (Continued)

Quick/EXP Look /Tag Number	Description	Filter Setting (Hz)	Dec/BW (Nth Seq/) (Hz)	Sample Rate (Hz)	DT (msec)	No. Per 144 msec record
PCM4: Continued (400.0 Kb/s, 520.83 Hz, 1.92 ms):						
452/1152	Pressure #34 StaPT10, 44% lower	100	0/104	520.83	1.92	75
453/1153	Pressure #36 StaPT10, 68% lower	100	0/104	520.83	1.92	75
454/1154	Pressure #38 StaPT10, 92% lower	100	0/104	520.83	1.92	75
455/1155	Pressure #18 StaPT9, 4% upper	100	0/104	520.83	1.92	75
456/1156	Pressure #11 StaPT9, 36% upper	100	0/104	520.83	1.92	75
457/1157	Pressure #11 StaPT8, 36% upper	100	0/104	520.83	1.92	75
458/1158	Total Pressure Probe, 86% span	100	0/104	520.83	1.92	75
459/1159	Absolute Reference Pressure	100	0/104	520.83	1.92	75
460/1160	Calibration Pressure (Cal Only)	-	75/1	6.94	144.0	1
461/1161	Pitch Angle	100	0/104	520.83	1.92	75
462/1162	PCM Voltage Monitor (Quick-Look Only)	-	75/1	6.94	144.0	1
PCM8: Rotating 30% and 40% Pressures (400.0 Kb/s, 520.83 Hz, 1.92 ms):						
801/1201	Absolute Reference Pressure (Not Used)	-	75/1	6.94	144.0	1
802/1202	Calibration Pressure (Cal Only)	-	75/1	6.94	144.0	1
803/1203	Spare	-	75/1	6.94	144.0	1
804/1204	Pressure #1 StaPT1, 100% trailing	100	0/104	520.83	1.92	75
805/1205	Pressure #4 StaPT1, 80% upper	100	0/104	520.83	1.92	75
806/1206	Pressure #6 StaPT1, 68% upper	100	0/104	520.83	1.92	75
807/1207	Pressure #8 StaPT1, 56% upper	100	0/104	520.83	1.92	75
808/1208	Pressure #10 StaPT1, 44% upper	100	0/104	520.83	1.92	75
809/1209	Pressure #11 StaPT1, 36% upper	100	0/104	520.83	1.92	75
810/1210	Pressure #13 StaPT1, 20% upper	100	0/104	520.83	1.92	75
811/1211	Pressure #14 StaPT1, 14% upper	100	0/104	520.83	1.92	75
812/1212	Pressure #15 StaPT1, 10% upper	100	0/104	520.83	1.92	75
813/1213	Pressure #16 StaPT1, 8% upper	100	0/104	520.83	1.92	75
814/1214	Pressure #17 StaPT1, 6% upper	100	0/104	520.83	1.92	75
815/1215	Pressure #18 StaPT1, 4% upper	100	0/104	520.83	1.92	75
816/1216	Pressure #19 StaPT1, 2% upper	100	0/104	520.83	1.92	75
817/1217	Pressure #21 StaPT1, 0.5% upper	100	0/104	520.83	1.92	75
818/1218	Pressure #22 StaPT1, 0% leading	100	0/104	520.83	1.92	75
819/1219	Pressure #23 StaPT1, 0.5% lower	100	0/104	520.83	1.92	75
820/1220	Pressure #24 StaPT1, 1% lower	100	0/104	520.83	1.92	75
821/1221	Pressure #25 StaPT1, 2% lower	100	0/104	520.83	1.92	75
822/1222	Pressure #26 StaPT1, 4% lower	100	0/104	520.83	1.92	75
823/1223	Pressure #28 StaPT1, 8% lower	100	0/104	520.83	1.92	75
824/1224	Pressure #30 StaPT1, 14% lower	100	0/104	520.83	1.92	75
825/1225	Pressure #31 StaPT1, 20% lower	100	0/104	520.83	1.92	75
826/1226	Pressure #34 StaPT1, 44% lower	100	0/104	520.83	1.92	75
827/1227	Pressure #36 StaPT1, 68% lower	100	0/104	520.83	1.92	75
828/1228	Pressure #38 StaPT1, 92% lower	100	0/104	520.83	1.92	75
829/1229	Pressure #18 StaPT2, 4% upper	100	0/104	520.83	1.92	75
830/1230	Pressure #11 StaPT2, 36% upper	100	0/104	520.83	1.92	75
831/1231	Pressure #11 StaPT3, 36% upper	100	0/104	520.83	1.92	75
832/1232	Total Pressure Probe, 34% span	100	0/104	520.83	1.92	75
833/1233	Pressure #1 StaPT4, 100% trailing	100	0/104	520.83	1.92	75
834/1234	Pressure #2 StaPT4, 92% upper	100	0/104	520.83	1.92	75
835/1235	Pressure #4 StaPT4, 80% upper	100	0/104	520.83	1.92	75
836/1236	Pressure #6 StaPT4, 68% upper	100	0/104	520.83	1.92	75
837/1237	Pressure #8 StaPT4, 56% upper	100	0/104	520.83	1.92	75
838/1238	Pressure #10 StaPT4, 44% upper	100	0/104	520.83	1.92	75
839/1239	Pressure #11 StaPT4, 36% upper	100	0/104	520.83	1.92	75

Unsteady Aero Experiment Channel Data Rates (Continued)

Quick/EXP Look /Tag Number	Description	Filter Setting (Hz)	Dec/BW (Nth Seq/) (Hz)	Sample Rate (Hz)	DT (msec)	No. Per 144 msec record
PCM8: Continued (400.0 Kb/s, 520.83 Hz, 1.92 ms):						
840/1240	Pressure #12 StaPT4, 28% upper	100	0/104	520.83	1.92	75
841/1241	Pressure #13 StaPT4, 20% upper	100	0/104	520.83	1.92	75
842/1242	Pressure #14 StaPT4, 14% upper	100	0/104	520.83	1.92	75
843/1243	Pressure #15 StaPT4, 10% upper	100	0/104	520.83	1.92	75
844/1244	Pressure #16 StaPT4, 8% upper	100	0/104	520.83	1.92	75
845/1245	Pressure #17 StaPT4, 6% upper	100	0/104	520.83	1.92	75
846/1246	Pressure #18 StaPT4, 4% upper	100	0/104	520.83	1.92	75
847/1247	Pressure #19 StaPT4, 2% upper	100	0/104	520.83	1.92	75
848/1248	Pressure #20 StaPT4, 1% upper	100	0/104	520.83	1.92	75
849/1249	Pressure #21 StaPT4, 0.5% upper	100	0/104	520.83	1.92	75
850/1250	Pressure #22 StaPT4, 0% leading	100	0/104	520.83	1.92	75
851/1251	Pressure #23 StaPT4, 0.5% lower	100	0/104	520.83	1.92	75
852/1252	Pressure #25 StaPT4, 2% lower	100	0/104	520.83	1.92	75
853/1253	Pressure #26 StaPT4, 4% lower	100	0/104	520.83	1.92	75
854/1254	Pressure #27 StaPT4, 6% lower	100	0/104	520.83	1.92	75
855/1255	Pressure #28 StaPT4, 8% lower	100	0/104	520.83	1.92	75
856/1256	Pressure #30 StaPT4, 14% lower	100	0/104	520.83	1.92	75
857/1257	Pressure #32 StaPT4, 28% lower	100	0/104	520.83	1.92	75
858/1258	Pressure #34 StaPT4, 44% lower	100	0/104	520.83	1.92	75
859/1259	Pressure #36 StaPT4, 68% lower	100	0/104	520.83	1.92	75
860/1260	Pressure #38 StaPT4, 92% lower	100	0/104	520.83	1.92	75
861/1261	Pressure #18 StaPT3, 4% upper	100	0/104	520.83	1.92	75
862/1262	Total Pressure Probe, 50.6% span	100	0/104	520.83	1.92	75
PCM9: Rotating 63% Pressures, Angle of Attack (400.0 Kb/s, 520.83 Hz, 1.92 ms):						
901/0101	Pressure #11 StaPT5, 36% upper	100	0/104	520.83	1.92	75
902/0102	Pressure #18 StaPT5, 4% upper	100	0/104	520.83	1.92	75
903/0103	Pressure #1 StaPT7, 100% trailing	100	0/104	520.83	1.92	75
904/0104	Pressure #2 StaPT7, 92% upper	100	0/104	520.83	1.92	75
905/0105	Pressure #4 StaPT7, 80% upper	100	0/104	520.83	1.92	75
906/0106	Pressure #6 StaPT7, 68% upper	100	0/104	520.83	1.92	75
907/0107	Pressure #8 StaPT7, 56% upper	100	0/104	520.83	1.92	75
908/0108	Pressure #10 StaPT7, 44% upper	100	0/104	520.83	1.92	75
909/0109	Pressure #11 StaPT7, 36% upper	100	0/104	520.83	1.92	75
910/0110	Pressure #12 StaPT7, 28% upper	100	0/104	520.83	1.92	75
911/0111	Pressure #13 StaPT7, 20% upper	100	0/104	520.83	1.92	75
912/0112	Pressure #14 StaPT7, 14% upper	100	0/104	520.83	1.92	75
913/0113	Pressure #15 StaPT7, 10% upper	100	0/104	520.83	1.92	75
914/0114	Pressure #16 StaPT7, 8% upper	100	0/104	520.83	1.92	75
915/0115	Pressure #17 StaPT7, 6% upper	100	0/104	520.83	1.92	75
916/0116	Pressure #18 StaPT7, 4% upper	100	0/104	520.83	1.92	75
917/0117	Pressure #19 StaPT7, 2% upper	100	0/104	520.83	1.92	75
918/0118	Pressure #20 StaPT7, 1% upper	100	0/104	520.83	1.92	75
919/0119	Pressure #21 StaPT7, 0.5% upper	100	0/104	520.83	1.92	75
920/0120	Pressure #22 StaPT7, 0% leading	100	0/104	520.83	1.92	75
921/0121	Pressure #23 StaPT7, 0.5% lower	100	0/104	520.83	1.92	75
922/0122	Pressure #24 StaPT7, 1% lower	100	0/104	520.83	1.92	75
923/0123	Pressure #25 StaPT7, 2% lower	100	0/104	520.83	1.92	75
924/0124	Pressure #26 StaPT7, 4% lower	100	0/104	520.83	1.92	75
925/0125	Pressure #28 StaPT7, 8% lower	100	0/104	520.83	1.92	75
926/0126	Pressure #30 StaPT7, 14% lower	100	0/104	520.83	1.92	75
927/0127	Pressure #32 StaPT7, 28% lower	100	0/104	520.83	1.92	75

Unsteady Aero Experiment Channel Data Rates (Continued)

Quick/EXP Look /Tag Number	Description	Filter Setting (Hz)	Dec/BW (Nth Seq/) (Hz)	Sample Rate (Hz)	DT (msec)	No. Per 144 msec record
PCM9: Continued (400.0 Kb/s, 520.83 Hz, 1.92 ms):						
928/0128	Pressure #34 StaPT7, 44% lower	100	0/104	520.83	1.92	75
929/0129	Pressure #36 StaPT7, 68% lower	100	0/104	520.83	1.92	75
930/0130	Pressure #38 StaPT7, 92% lower	100	0/104	520.83	1.92	75
931/0131	Pressure #18 StaPT6, 4% upper	100	0/104	520.83	1.92	75
932/0132	Pressure #18 StaPT8, 4% upper	100	0/104	520.83	1.92	75
933/0133	Pressure #11 StaPT6, 36% upper	100	0/104	520.83	1.92	75
934/0134	Total Pressure Probe, 67.3% span	100	0/104	520.83	1.92	75
935/0135	Angle-of-Attack, 86% span	100	0/104	520.83	1.92	75
936/0136	Not Used (Ground)	-	75/1	6.94	144.0	1
937/0137	Angle-of-Attack, 67.3% span	100	0/104	520.83	1.92	75
938/0138	Not Used (Ground)	-	75/1	6.94	144.0	1
939/0139	RTD 50% span (Not Used)	100	0/104	520.83	1.92	75
940/0140	Not Used (Ground)	-	75/1	6.94	144.0	1
941/0141	Angle-of-Attack, 34% span	100	0/104	520.83	1.92	75
942/0142	Not Used (Ground)	-	75/1	6.94	144.0	1
943/0143	Nitrogen Pressure (Quick-Look Only)	-	75/1	6.94	144.0	1
944/0144	+15 Volt Power Monitor (Quick-Look Only)	-	75/1	6.94	144.0	1
945/0145	-15 Volt Power Monitor (Quick-Look Only)	-	75/1	6.94	144.0	1
946/0146	Angle-of-Attack, 50.6% span	100	0/104	520.83	1.92	75
947/0147	DC Ground Monitor #1 (V) (Quick-Look Only)	-	75/1	6.94	144.0	1
948/0148	Spare	-	75/1	6.94	144.0	1
949/0149	Spare	-	75/1	6.94	144.0	1
950/0150	Spare	-	75/1	6.94	144.0	1
951/0151	Spare	-	75/1-	6.94	144.0	1
952/0152	Spare	-	75/1	6.94	144.0	1
953/0153	Absolute Reference Pressure	100	0/104	520.83	1.92	75
954/0154	Calibration Pressure (Cal Only)	-	75/1	6.94	144.0	1
955/0155	Spare	-	75/1	6.94	144.0	1
956/0156	Spare	-	75/1-	6.94	144.0	1
957/0157	Spare	-	75/1	6.94	144.0	1
958/0158	Spare	-	75/1	6.94	144.0	1
959/0159	Spare	-	75/1	6.94	144.0	1
960/0160	Spare	-	75/1	6.94	144.0	1
961/0161	Spare	-	75/1	6.94	144.0	1
962/0162	Spare	-	75/1	6.94	144.0	1

Appendix D

Design and Experimental Results for the S809 Airfoil

AIRFOILS, INCORPORATED
617 WILLOW OAKS BOULEVARD
HAMPTON, VIRGINIA 23669
(804) 851-9338

DESIGN AND EXPERIMENTAL RESULTS FOR THE S809 AIRFOIL

Dan M. Somers

March 1989

ABSTRACT

A 21-percent-thick, laminar-flow airfoil for horizontal-axis wind-turbine applications, the S809, has been designed and analyzed theoretically and verified experimentally in the low-turbulence wind tunnel of the Delft University of Technology Low Speed Laboratory, The Netherlands. The two primary objectives of restrained maximum lift, insensitive to roughness, and low profile drag have been achieved. The airfoil also exhibits a docile stall. Comparisons of the theoretical and experimental results show good agreement. Comparisons with other airfoils illustrate the restrained maximum lift coefficient as well as the lower profile-drag coefficients, thus confirming the achievement of the primary objectives.

INTRODUCTION

The majority of the airfoils in use on horizontal-axis wind turbines today were originally developed for airplanes. The design requirements for these airfoils, primarily National Advisory Committee for Aeronautics (NACA) and National Aeronautics and Space Administration (NASA) airfoils (refs. 1 through 6), are significantly different from those for wind-turbine airfoils. Accordingly, two sets of thick airfoils were designed, using the method of references 7 and 8, specifically for horizontal-axis wind-turbine applications. (See ref. 9.) The major, distinguishing feature between the two sets is the maximum lift coefficients of the airfoils for the outboard portion of the wind-turbine blade. The first set produces relatively low ("restrained") maximum lift coefficients outboard whereas the second set produces maximum lift coefficients outboard which are 0.2 higher than those produced by the first set.

In conjunction with this effort, the primary airfoil (0.75 blade radial station) of the first set was selected for experimental verification. An investigation was conducted in the low-turbulence wind tunnel of the Delft University of Technology Low Speed Laboratory (ref. 10), The Netherlands, to obtain the basic, low-speed, two-dimensional aerodynamic characteristics of this airfoil. The results have been compared with the predictions from the method of references 7 and 8 and also with data from another low-turbulence wind tunnel for other airfoils.

The specific tasks performed under this study are described in Solar Energy Research Institute (SERI) Subcontract Number HK-6-06075-1.

EXPERIMENTAL PROCEDURE

WIND TUNNEL

The low-turbulence wind tunnel (ref. 10) of the Delft University of Technology Low Speed Laboratory, The Netherlands, is a closed-throat, single-return, atmospheric tunnel (fig. 3). The turbulence level in the test section varies from .0.02 percent at 10 m/s (33 ft./s) to 0.04 percent at 60 m/s (200 ft./s).

The octagonal test section is 180.0 cm (70.87 in.) wide by 125.0 cm (49.21 in.) high. Electrically actuated turntables provide positioning and attachment for the two-dimensional model. The turntables are flush with the top and bottom tunnel walls and rotate with the model. The axis of rotation coincided with the quarter chord of the model which was mounted vertically between the turntables. (See fig. 4.) The gaps between the model and the turntables were sealed.

MODEL

The aluminum, wind-tunnel model was constructed by the Deutsche Forschungs- und Versuchsanstalt fuer Luft- und Raumfahrt e.V. (DFVLR), Braunschweig, Federal Republic of Germany. The model had a chord of 600.00 mm (23.622 in.) and a span of 1248 mm (49.13 in.). Chordwise orifices were located in the upper and lower surfaces to one side of the midspan at the staggered positions listed in table III. Spanwise orifices were located in the upper surface only in order to monitor the two-dimensionality of the flow at high angles of attack. All the orifices were 0.40 mm (0.016 in.) in diameter with their axes perpendicular to the surface. The measured model contour was generally within 0.1 mm (0.004 in.) of the prescribed shape.

WAKE RAKE

A total-pressure, a static-pressure, and an integrating wake rake were mounted on a strut between the tunnel sidewalls (figs. 4 and 5). The strut could be positioned spanwise and streamwise in the test section. Movement of the strut provided positioning of the wake rakes normal to the sidewalls. The tips of the total-pressure tubes were located downstream of the trailing edge of the model. The details of the wake rakes are shown in figures 6 and 7. The integrating wake rake was not used in this investigation.

INSTRUMENTATION

Measurements of the basic tunnel pressures, the static pressures on the model surfaces, and the wake-rake pressures were made by a multitube manometer which was read automatically using photoelectric cells. Data were obtained and recorded by an electronic data-acquisition system.

METHODS

The static-pressure measurements on the model surface were reduced to standard pressure coefficients and numerically integrated to obtain section normal-force coefficients and section pitching-moment coefficients about the quarter-chord point. Section profile-drag coefficients were computed from the wake-rake total and static pressures by the method of reference 12. Standard, low-speed, wind-tunnel boundary corrections (ref. 13) have been applied to the data. The following procedure was used. The uncorrected force, moment, and pressure coefficients are referred to the apparent dynamic pressure as measured tunnel empty at the model position. The lift, profile-drag, pitching-moment, and airfoil pressure coefficients and the angle of attack are then corrected by the method of reference 13. The corrected values are plotted. Finally, as a check, the corrected airfoil pressure distribution is numerically integrated to obtain the corrected normal-force (and pitching-moment) coefficient which, together with the corrected profile-drag coefficient and angle of attack, yields the corrected lift coefficient (and chord-force coefficient).

At high angles of attack, the wake becomes wider than the wake rake. When this occurs, the drag is obtained from a parabolic extrapolation of the measured wake pressures. At even higher angles of attack, the total-pressure coefficients measured in the wake become negative, making calculation of the drag impossible. In these cases, an uncorrected profile-drag coefficient of 0.3 (estimated from ref. 14) is assumed.

TESTS

The model was tested at Reynolds numbers based on airfoil chord from 1,000,000 to 3,000,000. The model was tested smooth (transition free) and with transition fixed by roughness at 0.02c on the upper surface and 0.03c on the lower surface. The grit roughness was sized by the method of reference 15 and sparsely distributed along 3-mm (0.1-in.) wide strips applied to the model with lacquer. (See table IV.)

Starting from zero degrees, the angle of attack was increased until the entire upper surface was separated and then decreased in order to determine hysteresis. The same procedure was followed for the negative angles of attack. For the Reynolds numbers of 2,500,000 and 3,000,000, the static pressures on the upper surface could not be measured by the manometer at high angles of attack because the differences between those pressures and the free-stream static pressure were too great.

For several test runs, the model surfaces were coated with oil to determine the location, as well as the nature, of the boundary-layer transition from laminar to turbulent flow (ref. 16). Transition was also located using a probe containing a microphone, which was positioned near the leading edge and then moved slowly downstream along the model surface. Two span stations, corresponding to the wake-rake position and the chordwise orifice row, were surveyed. The beginning of the turbulent boundary layer was detected as an increase in noise level over that for the laminar boundary layer which was essentially silent. (See ref. 17.)

Two turbulators, zig-zag tape (ref. 18), were placed on the model, one between 0.43c and 0.45c on the upper surface and the other between 0.42c and 0.44c on the lower surface, in order to determine their effect on laminar separation bubbles and section characteristics. The details of the 0.25-mm (0.010-in.) thick tape are shown in the following sketch.

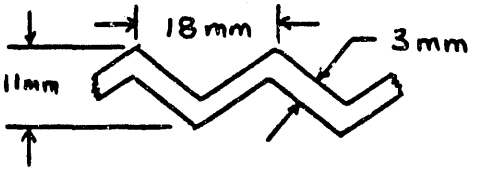

Sketch 4

PRESENTATION OF RESULTS

The principal results of this investigation are presented in the following figures:

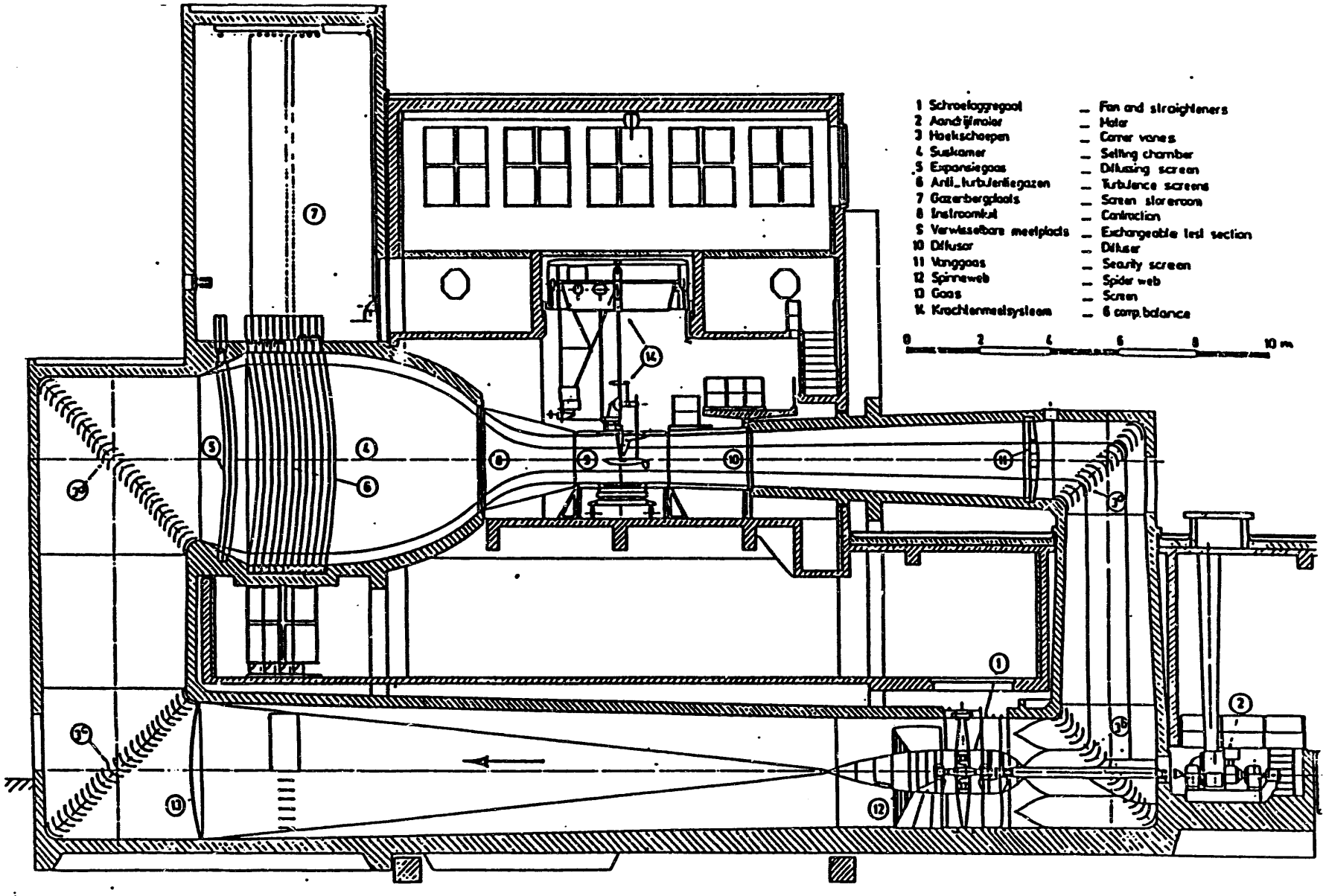

Figure 3.- Delft University of Technology 1.80- x 1.25-m low-speed wind tunnel.

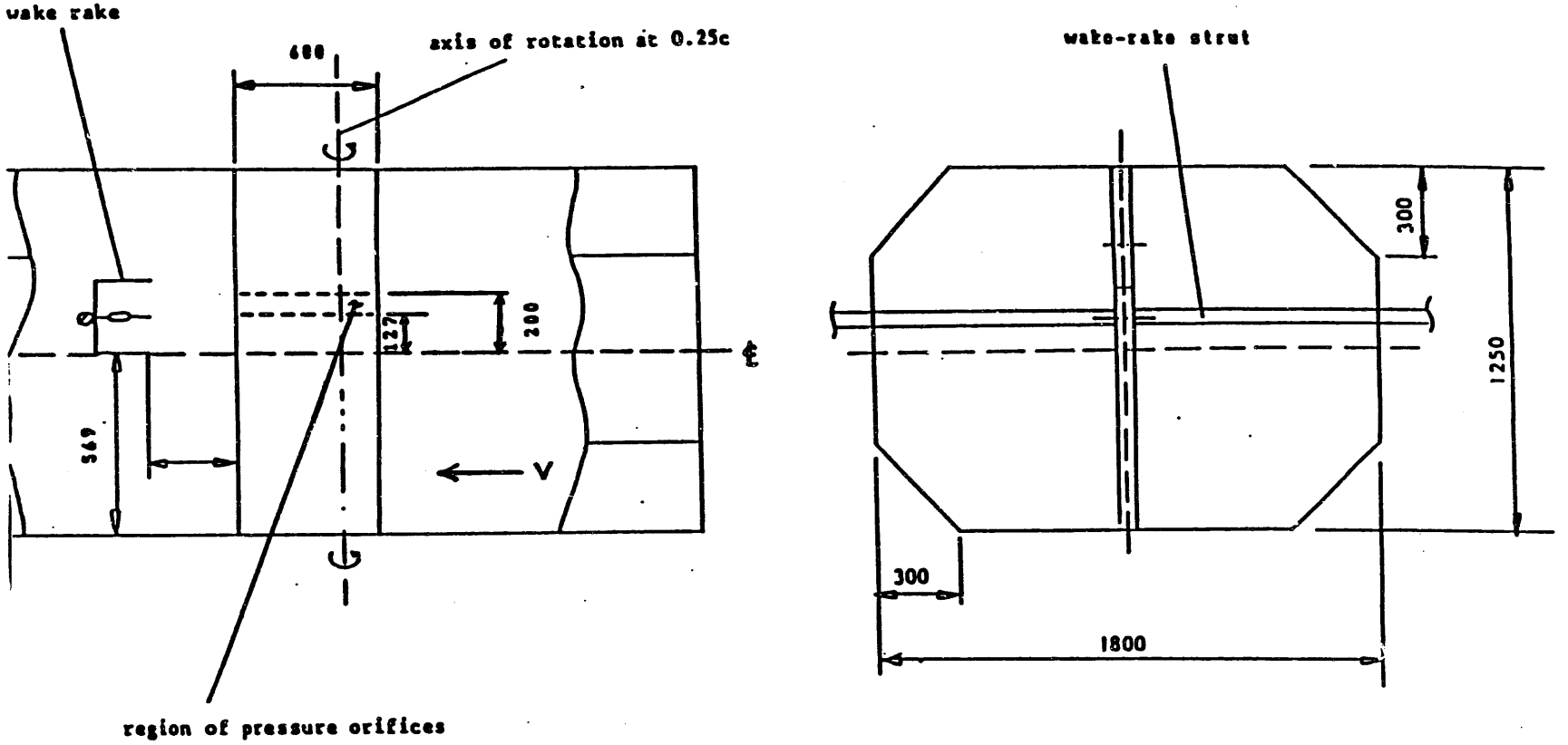

Figure 4.- Model and wake rakes mounted in test section. All dimensions are in mm.

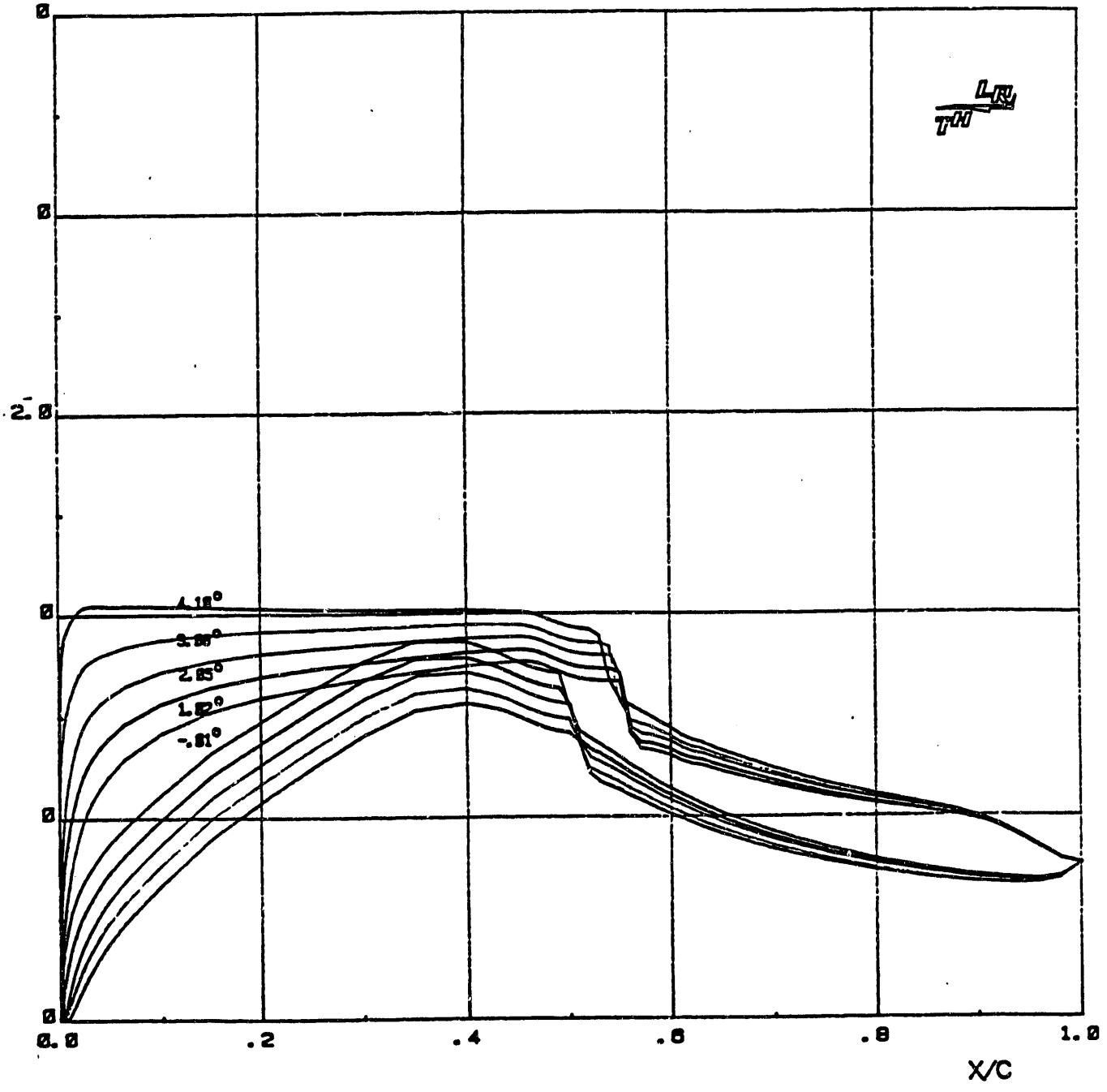

(a) α = -0.01, 1.02, 2.05, 3.08, and 4.10 degrees.

Figure 8.- Pressure distributions for R = 2,000,000. Arrows indicate direction of angle-of-attack change (for determination of hysteresis).

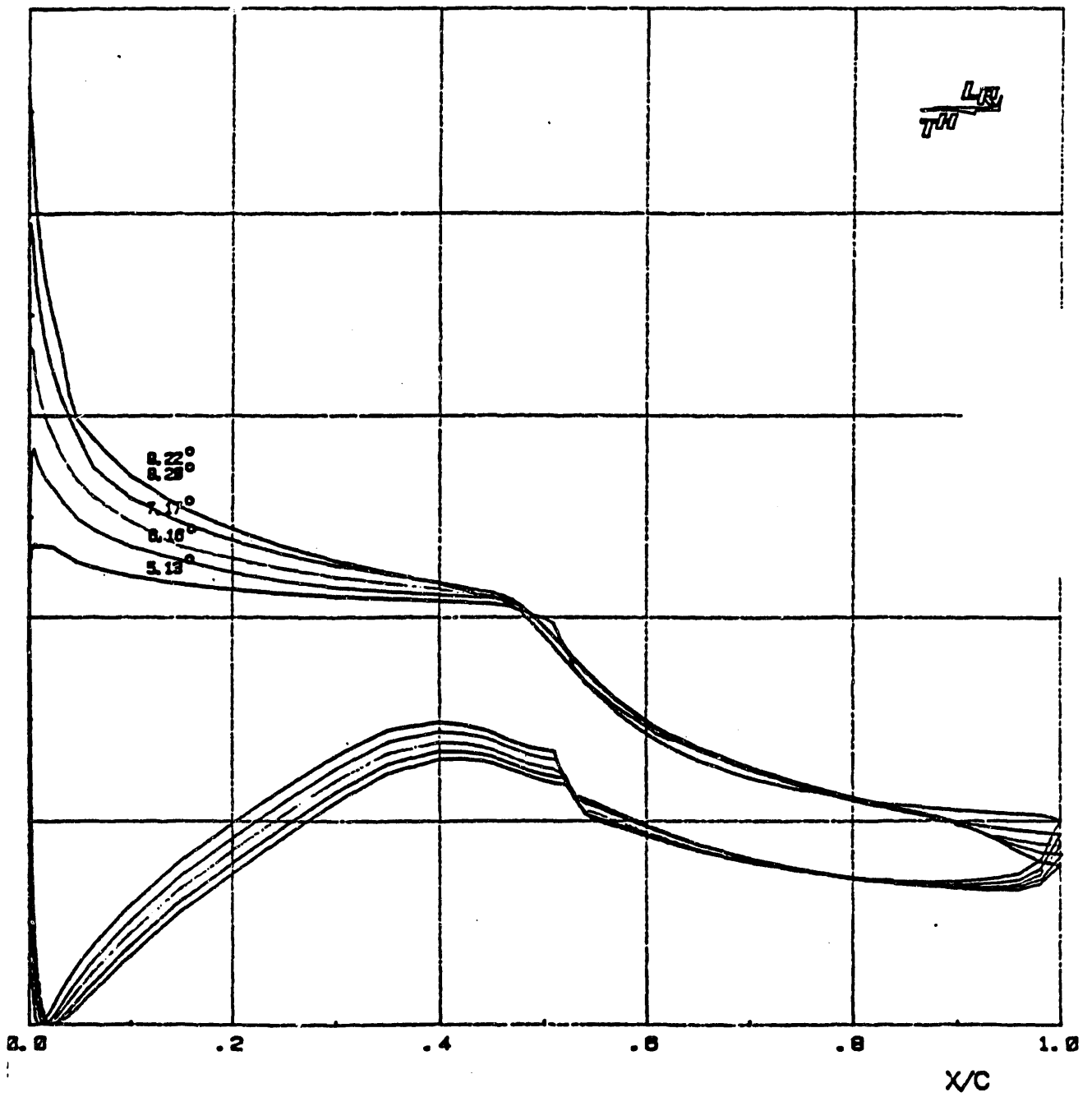

(b) α = 5.13, 6.16, 7.17, 8.20, and 9.22 degrees.

Figure 8.- Continued.

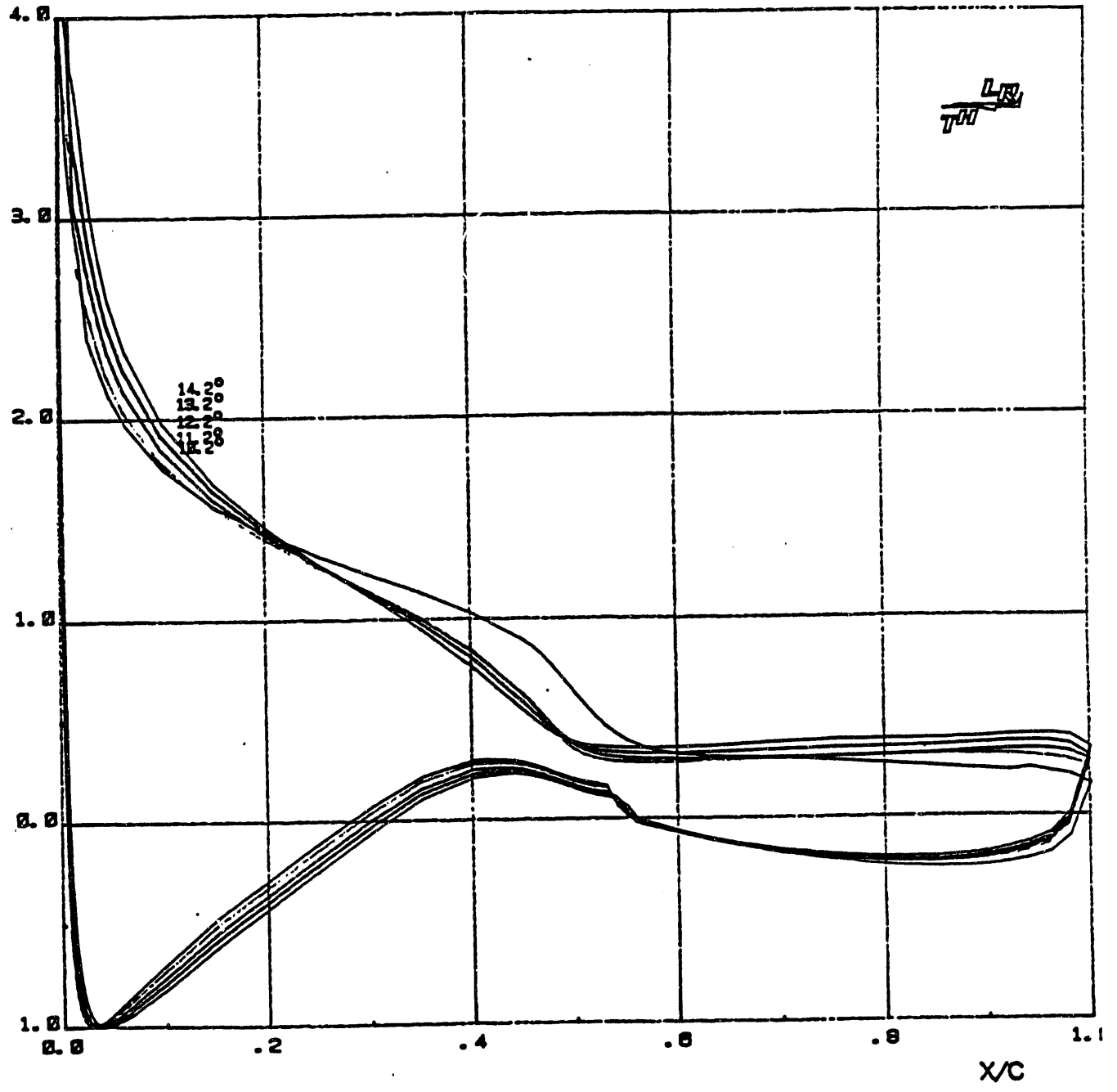

(c) α = 10.21, 11.21, 12.22, 13.24, and 14.24 degrees.

Figure 8.- Continued.

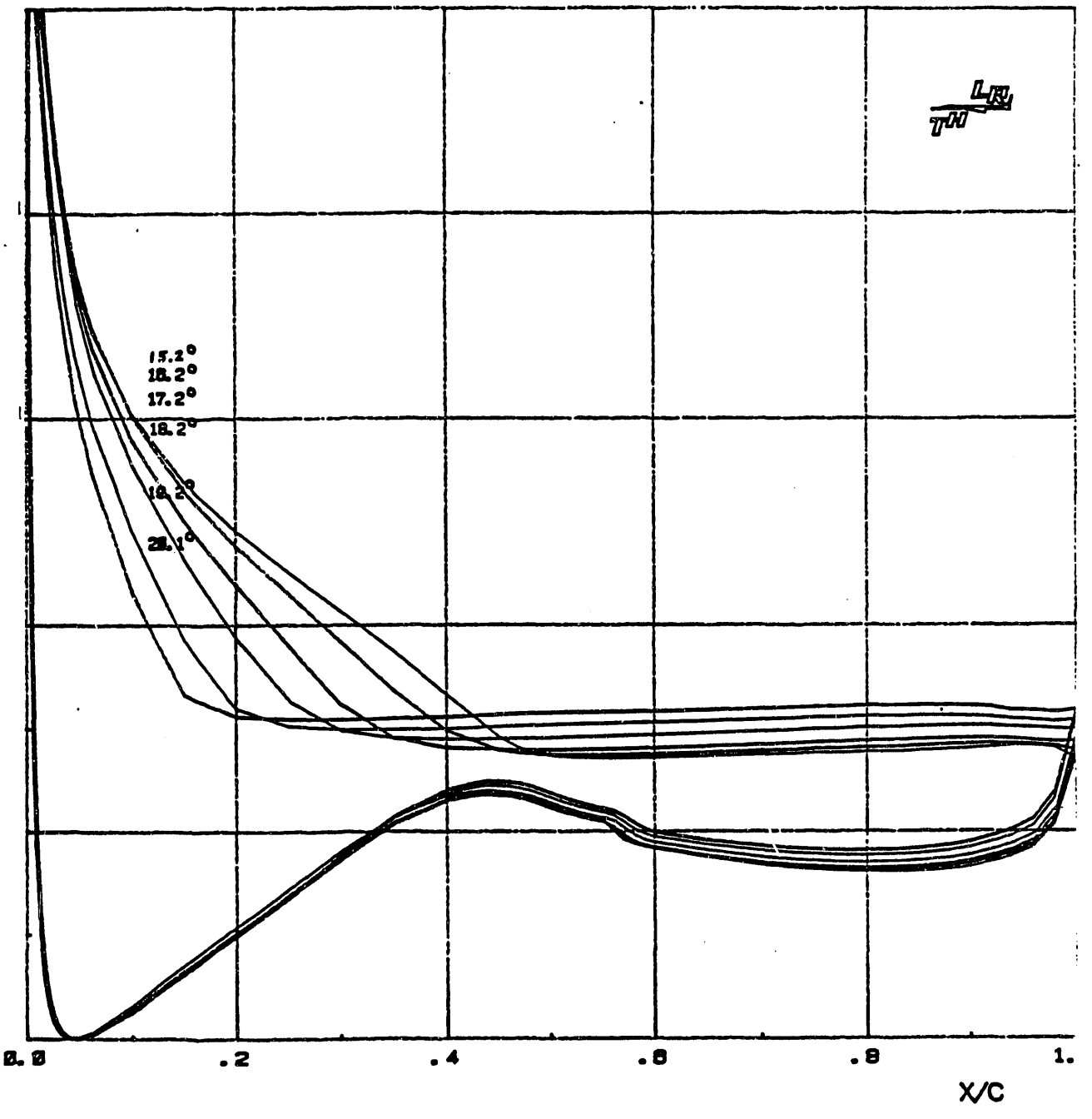

(d) α = 15.24, 16.24, 17.23, 18.20, 19.17, and 20.15 degrees.

Figure 8.- Continued.

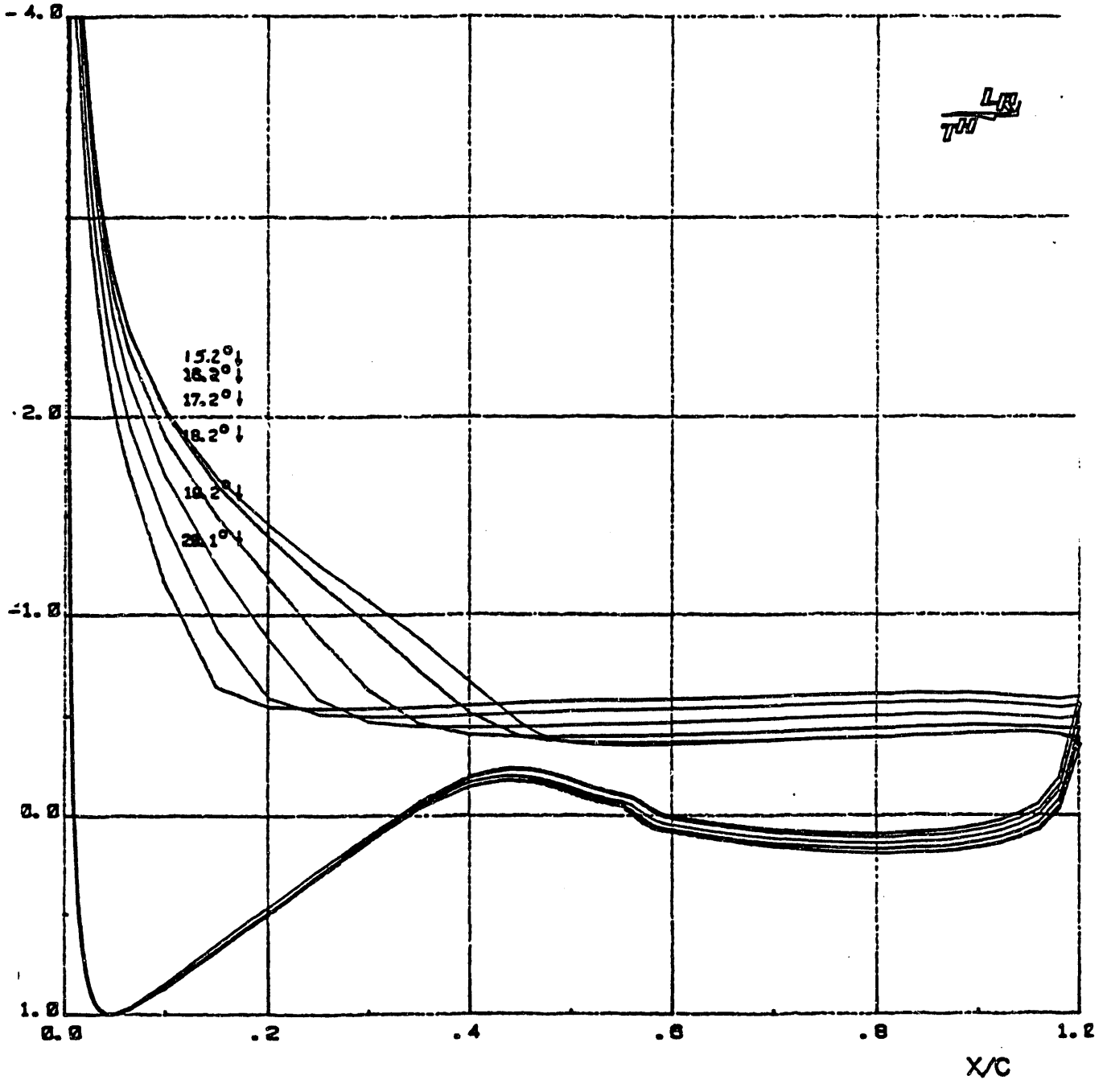

(e) α = 20.14↓, 19.16↓, 18.19↓, 17.22↓, 16.24↓, and 15.24↓ degrees.

Figure 8.- Continued.

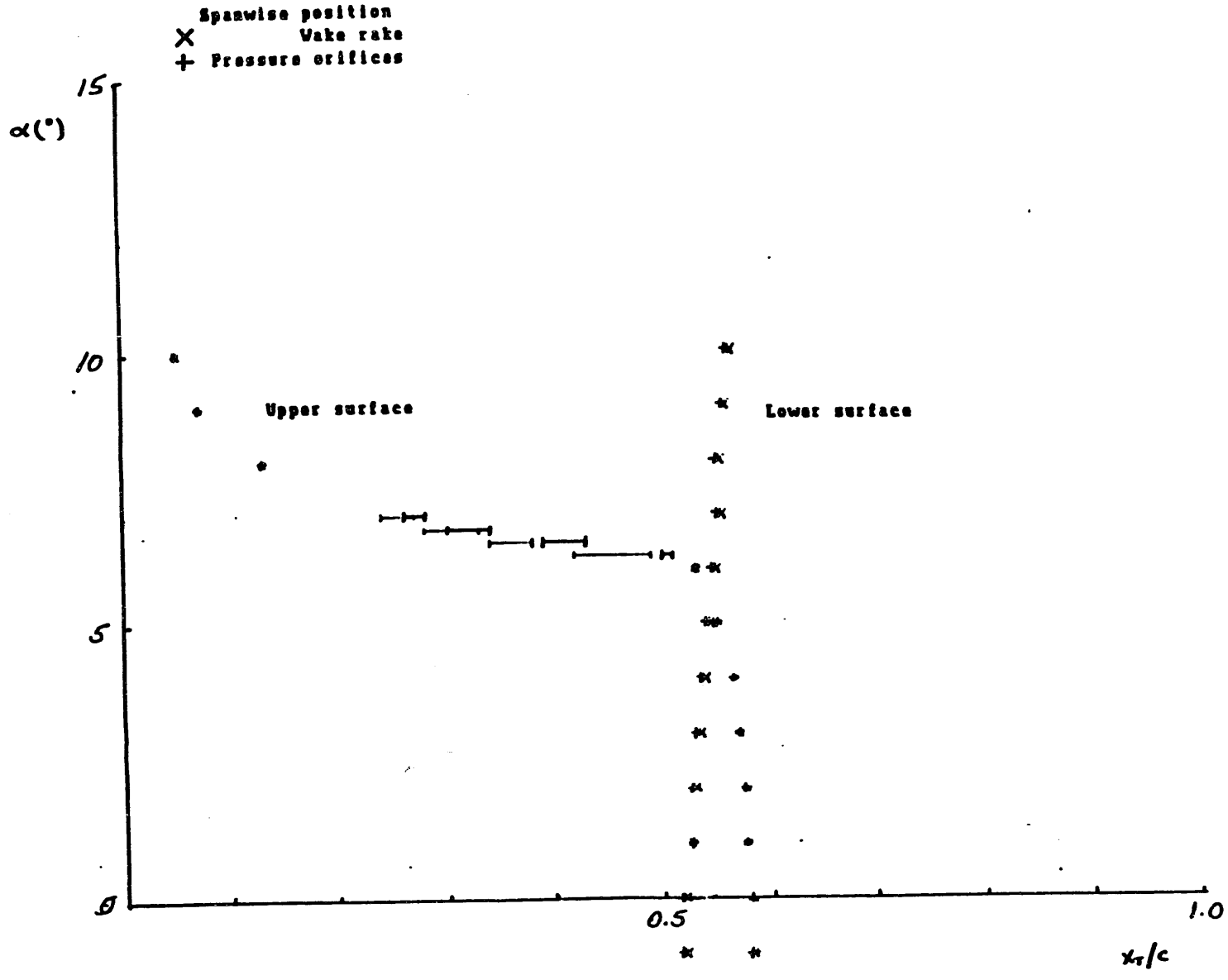
Spanwise position
Wake rake
Pressure orifices
α(°)
15
10
5
0
Upper surface
Lower surface
0.5
1.0
x_T/c

(a) R = 1,000,000.

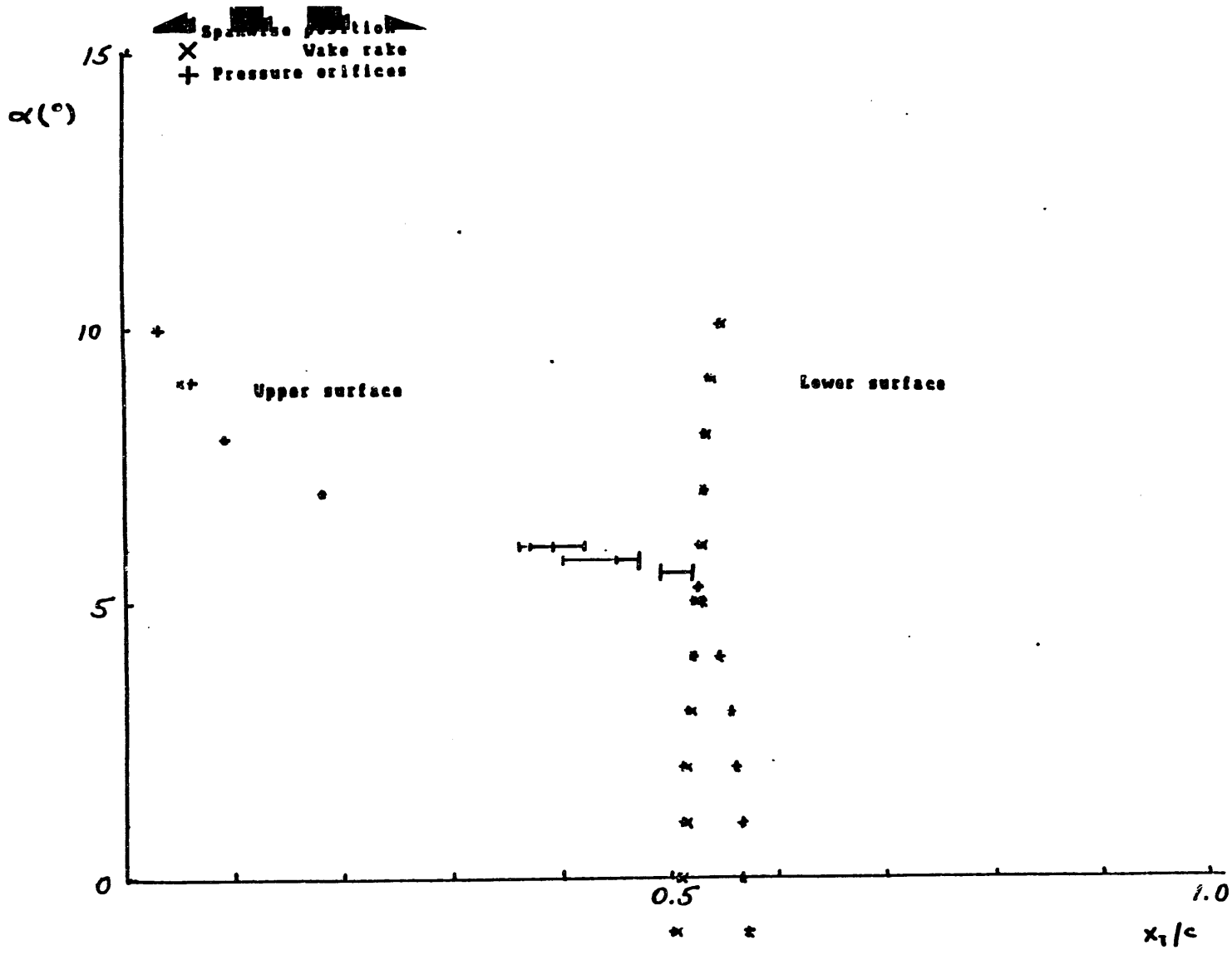

(b) R = 1,500,000.

Figure 15.- Continued.

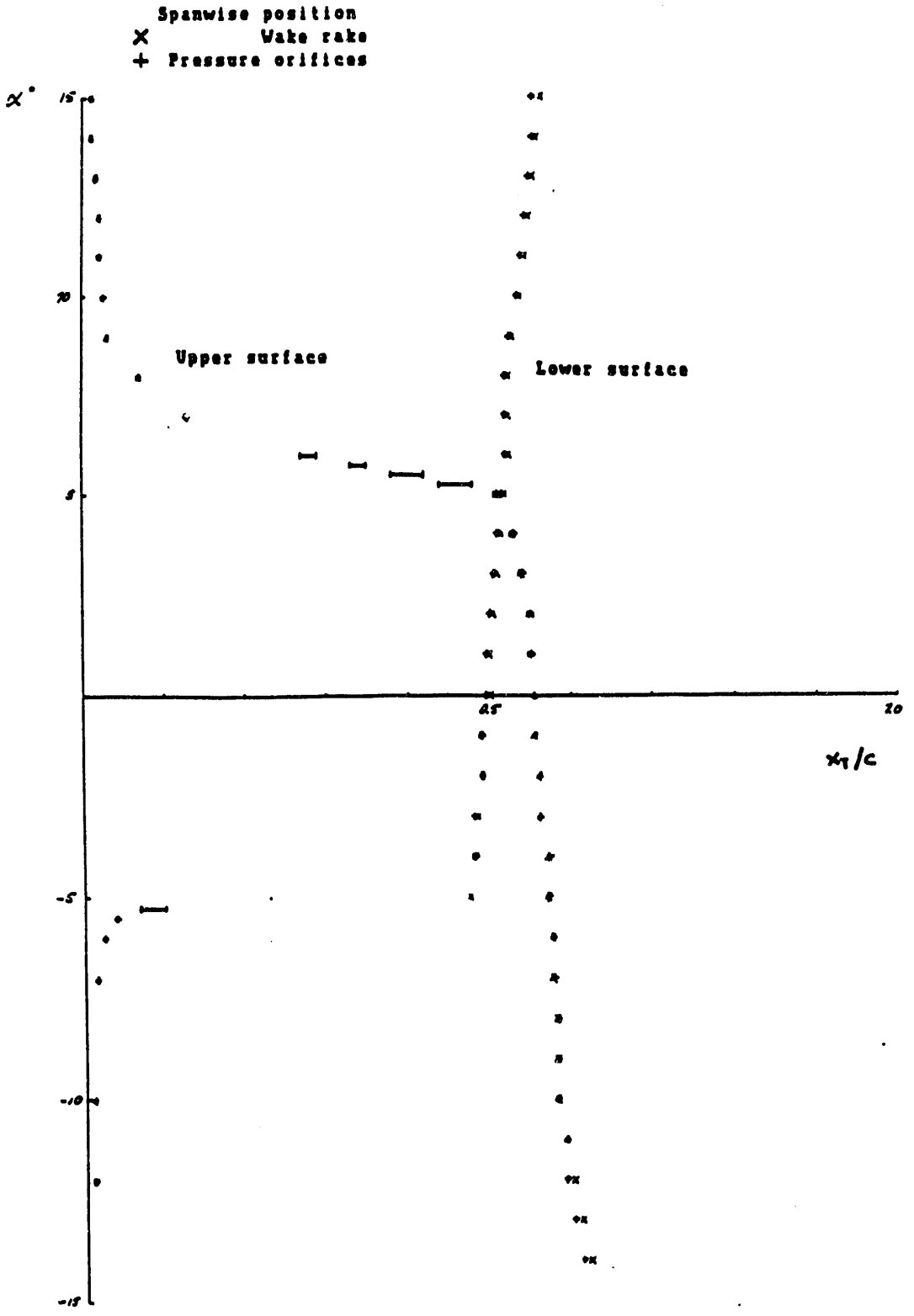

(c) R = 2,000,000.

Figure 15.- Continued.

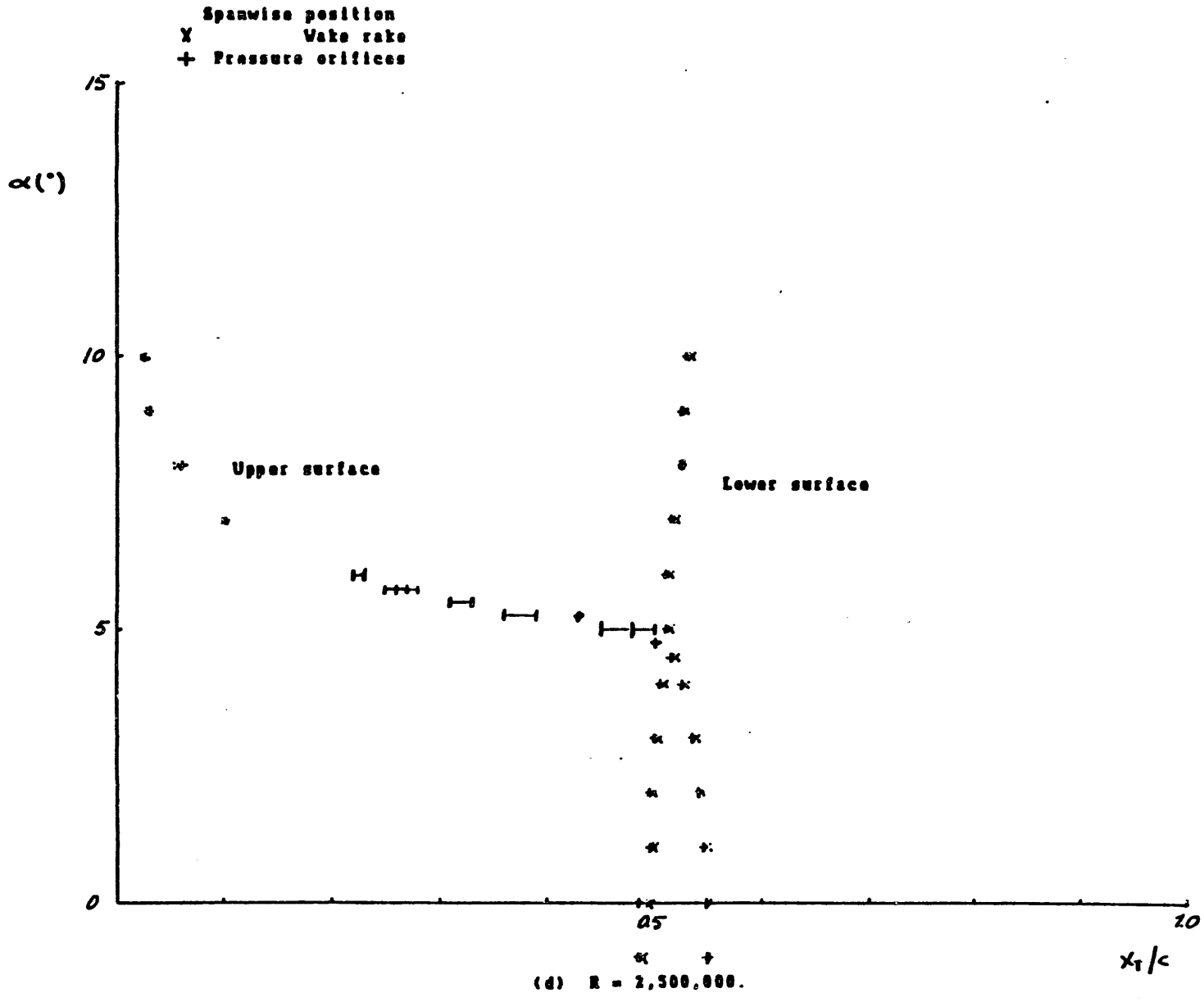
Spanwise position
X Wake rake
+ Pressure orifices
15
10
5
0
α(°)
Upper surface
Lower surface
.5
1.0
x_1/c

(d) R = 2,500,000.

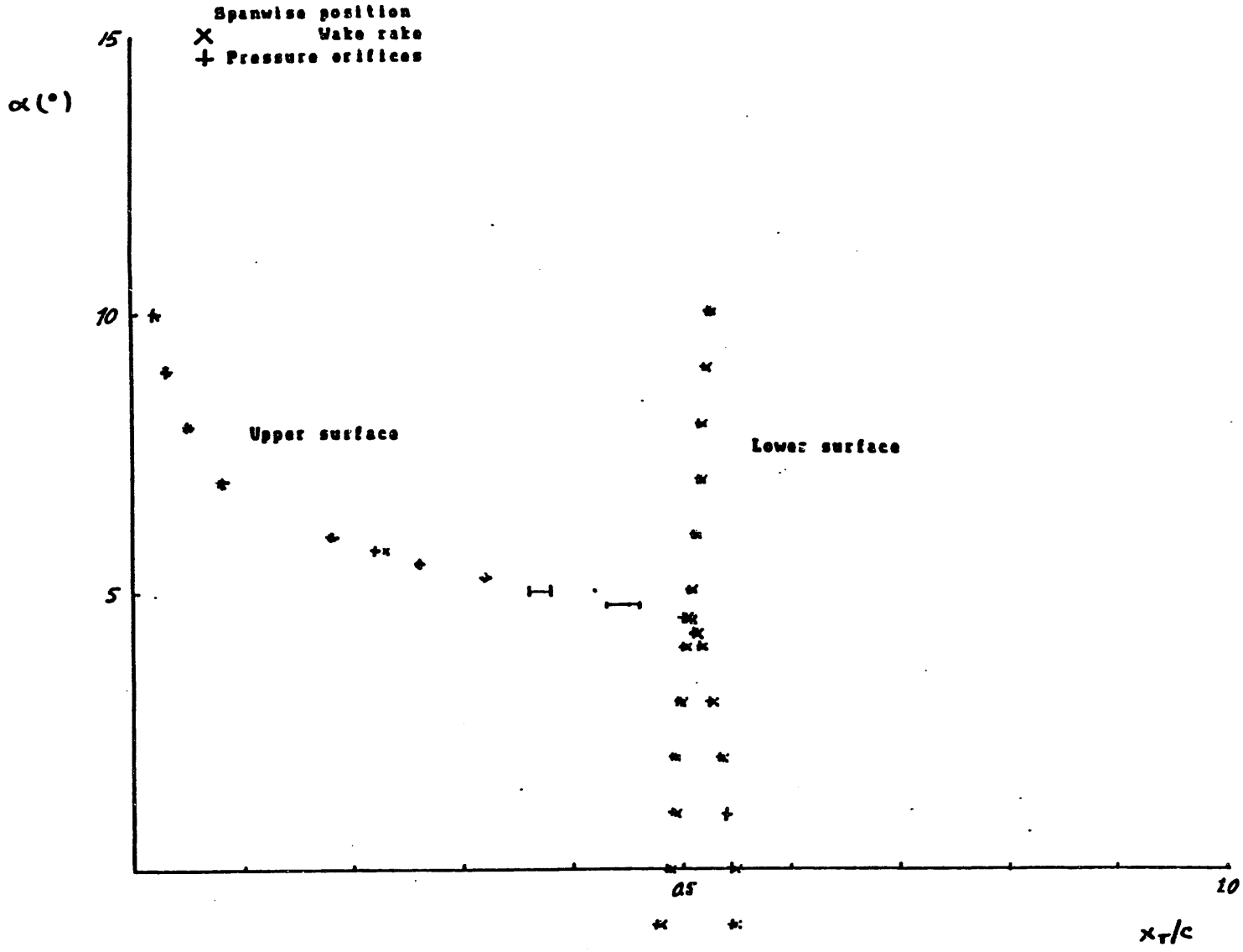

(a) R = 3,000,000.

Figure 15.- Concluded.

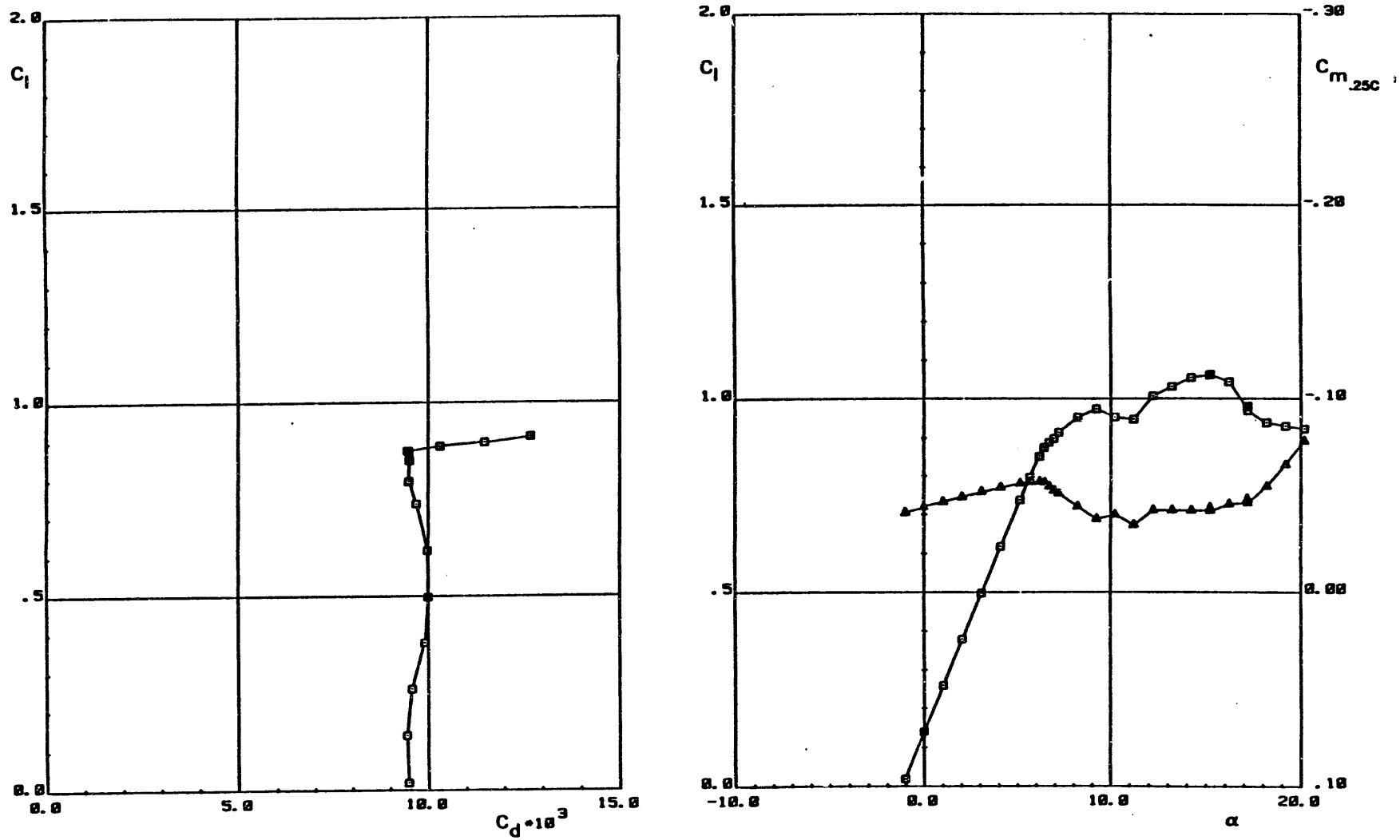

(a) R = 1,000,000.

Figure 17.- Section characteristics.

Delft University of Technology Low Speed Laboratory

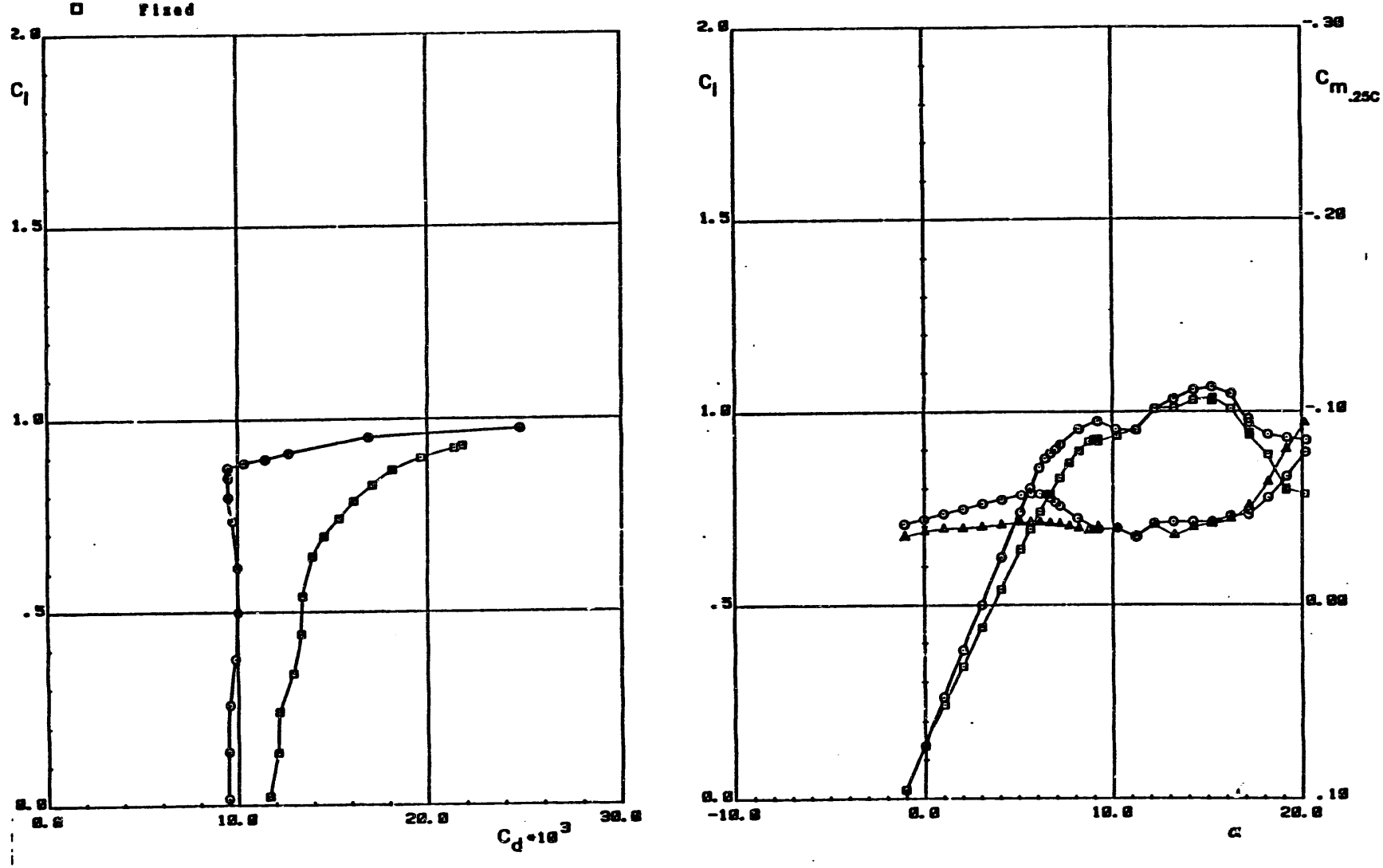

(a) R = 1,000,000.

Appendix E

Wind Tunnel Tests of the S809 Airfoil Model

THE OHIO STATE UNIVERSITY

Aeronautical and Astronautical
Research Laboratory

2300 West Case Road
Columbus, OH 43235-1949
Phone 614-292-5491

WIND TUNNEL TESTS OF THE S809 AIRFOIL MODEL

G. M. GREGOREK
M. J. HOFFMANN
K. E. MULH

THE AERONAUTICAL & ASTRONAUTICAL RESEARCH LABORATORY
THE OHIO STATE UNIVERSITY
COLUMBUS, OHIO

APRIL 1991

Prepared for: SOLAR ENERGY RESEARCH INSTITUTE
MIDWEST RESEARCH INSTITUTE
CONTRACT XL-9-19011-1

FOREWARD

This is the Final Report on Midwest Research Institute Grant XL-9-19011-1 Entitled "Wind Tunnel Testing on the S809 Airfoil Model". (OSU Research Foundation Project 721623). Mr. Sandy Butterfield was the Technical Monitor for the Solar Energy Research Institute for the period November 1988 to June 1989.

TABLE OF CONTENTS

LIST OF FIGURES

ABSTRACT

A wind tunnel test program to calibrate a vane-type angle of attack sensor that is in use on the rotor of the HAWT undergoing field tests at Rocky Flats was conducted in the 3'x 5' Subsonic Wind Tunnel of The Ohio State University. The sensor was mounted on a boom extending from the leading edge of an 18" chord, two-dimensional model of the S809 airfoil. Static calibration of the vane produced two distinct linear relationships between vane angle and model angle of attack. Between a model angle of attack from -5° to +7°, this linear calibration is represented by:

$$\alpha_{model}=0.590 * \alpha_{probe} + 0.4°;$$

while the model angle region from +7° to +15° is represented by:

$$\alpha_{model}=0.799 * \alpha_{probe} - 2.0°.$$

When the vane was disturbed from it's equilibrium position during tunnel tests with the model at a fixed angle of attack a damped oscillation with period of 0.10 seconds was recorded, with time to damp to half amplitude of 0.073 seconds. Vane response was also measured as the model was sinusoidally oscillated ±3° about a mean angle at frequencies of 0.2, 0.9, and 1.2 Hz. To extend the data base on the S809 airfoil, surface pressures and wake total pressure surveys were measured during the steady state calibration of the vane. These pressures were integrated to yield lift pitching moment and total drag coefficients at the test condition of $Re=1.0x10^6$.

I. INTRODUCTION

The S809 airfoil is an airfoil tailored for Horizontal Axis Wind Turbine (HAWT) rotors. It is presently being used on the HAWT at Rocky Flats and is undergoing extensive field tests. This rotor on the field test machine has a vane projecting from the leading edge of the airfoil to be used as an angle of attack measuring device. The upwash from the airfoil alters the flow field of the vane, necessitating a calibration of the vane versus model angle of attack. The purpose of the experimental program conducted at the Aeronautical and Astronautical Research Laboratory (AARL) of The Ohio State University (OSU) reported here, is to provide this calibration for both steady and unsteady flow conditions. In addition, during the steady state tests, surface pressures are obtained and wake pressures measured to supplement the existing data base on the aerodynamic characteristics of the S809 airfoil.

The OSU 3'x 5' Subsonic Wind Tunnel was used for the test program. Test conditions were at a Reynolds number of $1x10^6$ based on an 18" model chord. Steady state pressures were measured at angles of attack from -8° to +15° and were reduced to lift and pitching moment coefficients. A wake survey probe provided total drag for the steady state test sequence. Unsteady information was obtained by oscillating the model with a sinusoidal wave form of amplitude ±3°. During the oscillations both vane angle and model angle of attack were recorded. These data, coupled with the steady state calibration of the vane versus model angle of attack provide the needed calibration.

A description of the experimental program, wind tunnel and model, fabricated earlier from the same mold used to produce the HAWT rotor being field tested, follows. Results of the test are presented in both tabular and graphic form and include a short test sequence of the dynamic response of the vane. An Appendix includes the airfoil coordinates and location of the pressure taps on the model to complete the report.

II. RESEARCH PROGRAM

A. Test Program

The main purpose of the present test program was the calibration of the angle of attack vane relative to the airfoil angle of attack. These calibrations were to be performed in steady state and in an unsteady condition with the airfoil oscillating sinusoidally at a nominal ±3° angle of attack. During the steady state tests, surface pressures were to be recorded as well as airfoil and vane angle of attack to provide pressure distributions which could be integrated to lift, moment and pressure drag coefficients. A wake survey would also be conducted to determine the total drag of the airfoil. These steady state data were to supplement data obtained from the model in an earlier test series.

All tests were conducted at a nominal Reynolds number of 1×10^6 based on the 18" model chord.

B. Experimental Facilities

The Subsonic Wind Tunnel at AARL is shown schematically in Figure 1. It is an open-circuit, atmospheric wind tunnel of the Eiffel type, powered by a 125 hp AC motor driving an 8' diameter, 6 blade fan. The blade angle can be set, manually, to produce velocities from 20 to 200 ft/sec. Test section turbulence level is low; four 40 mesh seamless stainless steel screens and a 4 inch thick honeycomb of 1/4 inch cells upstream of the contraction maintains a turbulence level measured below 0.1%.

The test section geometry is rectangular, with filleted corners; dimensions of the test section are 55" wide and 39" high.

Because of this orientation, two dimensional airfoil models are mounted vertically in the facility. A horizontally traversing single total pressure probe is used to survey the wake behind the airfoil to measure total airfoil drag. Wind tunnel test conditions are monitored by a single total probe mounted off the wall and by two static ports mounted in each side wall as shown in the schematic.

Two pressure sensing systems can be used to measure airfoil pressure distributions. For steady state measurements a single pressure transducer is coupled to a 48 port scanning system located outside of the wind tunnel to make the surface measurements. When unsteady pressure are required, two electronically scanned pressure modules can be mounted inside the model to reduce the length of pressure tubing and to provide the necessary rapid response.

These unsteady airfoil tests are performed on pressure tapped airfoil models mounted on the oscillating rig shown in Figure 2. The rig is driven by a 5 hp AC motor that is controllable over a wide range of frequencies. Because large airfoil models are being studied, frequencies from 0.1 to 2 Hz are pertinent for the wind turbine applications of interest. Amplitude and wave form during the oscillation are controlled by specially designed face cams. Sinusoidal wave forms and other more complex wave shapes are available.

The two dimensional model of 18" chord studied in this experimental series has the specially designed S809 contour. It's coordinates are listed in Table I of the appendix. Table II in the appendix gives the location of the 31 pressure taps used in the steady state surface pressure measurements. A sketch of the

model showing the location of the total pressure probe and the angle of attack vane is presented in Figure 3.

C. Data Acquisition And Reduction

As noted in Figure 4, the data from each test run was recorded by an IBM PC-XT and processed by the AARL Harris H800 computer. The output from the wind tunnel pressure transducers, vane and model angle of attack sensors, electronically scanned pressure module, and wake probe pressure and position were recorded on the PC disc for each test run. Prior to the start of each run a calibration of all the pressure instrumentation was also printed on the disc. A test run for this test program consisted of one of two modes; a steady state mode in which the surface pressures and wake total pressure survey were obtained at a fixed model angle of attack, and an unsteady mode during which the model was oscillated ±3° about a mean angle of attack at a specific frequency and the angle of attack sensors measured as a function of time. During the unsteady test mode, the surface pressures were not measured.

As a series of test runs are completed and stored on disc, for example, after 5 steady state angles of attack or frequencies of oscillation, the electronic data was processed by the Harris H800 into engineering units to produce the required hard copy tables and plots of the test results. These surface pressure distributions, lift, drag, and pitching moment coefficients as a function of angle of attack for the steady case and vane and model angle of attack time-histories were available within a few minutes of completion of a test sequence.

III. RESULTS AND DISCUSSIONS

A. Steady State Test Sequence

Sixteen surface pressure distributions taken during an angle of attack sweep from a nominal -8° to +19° are presented in Figure 5. A legend accompanies each distribution to give the angle of attack, test Reynolds number, lift coefficient, pressure drag coefficient and pitching moment coefficient. Note that the triangles with the vortex pointing up represent the upper surface pressures while the triangular symbols with the downward pointing vortex are the lower surface pressures.

The pressure distributions can provide insight into the aerodynamic behavior of the airfoil. For example, Run 558, the first distribution presented is at a negative angle of attack (-8.1°) so the lower surface pressures are negative yielding a negative lift coefficient (C_l=-0.57). Further, the airfoil is near its stall at this negative angle as determined by the constant pressure plateau of C_p=-0.3 representing flow separation for the aft 50% of chord. When the angle of attack increases 2° to -6.1°, the lower surface pressure is now attached, with the pressure plateau eliminated and the trailing edge pressure becoming positive. As the angle of attack becomes more positive, the lower surface leading edge pressure spike gradually decreases, disappearing near -2° and providing smooth pressure distributions on both upper and lower surfaces, favoring natural laminar boundary layer development for the forward 45% of airfoil chord. The favorable pressure gradients persist on both surfaces until nearing 5°, where a pressure spike begins to develop in the upper surface leading edge. This pressure peak increases with angle of

attack. At 7.1° the flow is attached up to the trailing edge, but by 9.2° the flow has separated past the 55% chord of the upper surface. In spite of this flow separation the low pressure spike continues to increase, with a corresponding modest increase in lift coefficient until complete separation occurs on the upper surface as shown at angle of attack 16.8°, and the lift coefficient falls.

The integrated surface pressure distributions are presented in Figures 6 to 9. Figures 6 and 7 indicate the lift and pitching moment coefficient versus angle of attack. The total drag coefficient obtained from integration of the momentum deficit in the wake is illustrated in Figure 8; the pressure drag coefficient is not shown since the pressure taps on the model were not felt to be sufficient to determine a reliable value of pressure drag. A drag polar is given in Figure 9. From this information, pertinent aerodynamic characteristics for this airfoil are summarized in Table I below:

TABLE I

S809 Measured Aerodynamic Coefficients At Re= 1.05×10^6

C_{lmax}	0.91 @ α=7°, 1.03 @ α=15°
$dC_l/d\alpha$	0.121
α_{lo}	-1.0
C_{Mo}	-0.035
C_{dmin}	0.0069 @ α=5°
$(C_l/C_d)_{mx}$	107 @ α=5°
$-C_{lmx}$	-0.57 @ α=-8°

Table II lists the complete aerodynamic coefficients as a function of model angle of attack. The table includes the vane angle of attack.

TABLE II

SERI Steady State Reduced Data

RUN #	α_{model}	α_{vane}	C_l	C_{dw}	C_m	Rex10^6
557	3.5	5.42	0.545	0.0078	-0.0449	1.07
558	-8.1	-13.38	-0.574	0.0742	0.0028	1.06
559	-6.1	-10.66	-0.547	------	0.0161	1.06
560	-4.2	-7.75	-0.416	0.0117	-0.0176	1.06
561	-2.6	-4.98	-0.198	0.0114	-0.0266	1.06
562	-0.5	-1.45	0.056	0.0109	-0.0341	1.06
563	1.5	1.70	0.286	0.0102	-0.0373	1.06
564	3.6	5.33	0.535	0.0091	-0.0426	1.06
565	5.1	7.87	0.737	0.0069	-0.0510	1.05
566	7.1	11.41	0.914	0.0088	-0.0385	1.05
567	9.2	13.96	0.946	0.0525	-0.0396	1.05
568	11.2	16.50	0.967	------	-0.0314	1.04
569	12.7	18.34	1.000	------	-0.0279	1.04
570	14.9	21.17	1.029	------	-0.0440	1.05
571	16.8	22.76	0.723	------	-0.1272	1.04
572	18.6	24.33	0.726	------	-0.1268	1.03

B. Vane Calibration

Steady State Calibration

From the steady state tests described above, the calibration of the sensed angle of the vane compared to the geometric angle of attack can be obtained. Figure 10 presents this data for the angle of attack ranging from -8° to +19°. It can be noted that this curve appears to have two distinct linear portions, represented by the two equations below:

From $-5° < \alpha < +7°$ $\alpha_{model} = .590 * \alpha_{probe} + 0.4$

From $+7° < \alpha < 15°$ $\alpha_{model} = .799 * \alpha_{probe} - 2.0$

The two equations represent the experimental data with ±0.1° in their range of applicability.

The two segment behavior of the vane calibration is related to the loss of circulation as the flow separates from the airfoil. Referring back to the pressure distributions, the angles of attack between -5° and +7° all have positive pressures at the trailing edge, indicating attached flow to the trailing edge and a corresponding linear increase in lift with angle. At angles above 7°, up to 14.9°, a low pressure plateau exists on the upper aft airfoil surface with a leading edge pressure spike increasing with angle. The pressure spike collapses at 16.8° and, again, the vane calibration reflects this flow behavior by departing from the linear equation. A similar separation pattern exists at the negative angles of attack when the angle exceeds -5°, with the vane calibrations again becoming non-linear.

Vane Response

A limited test sequence was performed to examine the response of the vane. With the model fixed at an angle of attack and the tunnel operating, a clip restraining the vane was released, allowing the vane to respond to the flow field about the airfoil. Figures 11 and 12 illustrate the probe angle of attack as a function of time. The vane responds with a damped oscillation as shown. Two other trials at this wind tunnel test condition were made, then two more such vane response checks were made at a lower speed, corresponding to Re = 0.74×10^6. Table III summarizes this response data.

TABLE III

VANE RESPONSE

RUN #	PERIOD (sec)	AMPLITUDE (deg)	TIME TO 1/2 AMP. (sec)
574	0.107	9.35	0.072
575	0.100	9.25	0.075
576	0.097	7.0	0.073
579	0.120	9.5	0.103

The average of the three trials at Re= $1x10^6$ yields an oscillation period of 0.101 seconds; frequency of 9.9 Hz with 0.073 seconds and 0.72 cycles to damp to half amplitude. Only one of the vane response tests at the lower speed was recovered (Run 579). This single vane test indicates a period of 0.120 seconds with a frequency of 8.33 Hz and 0.103 seconds and 0.85 cycles required to damp to half amplitude.

The longer period and decreased damping of the vane found during the lower speed tests are attributed to the decrease in dynamic pressure. Although vane inertia about the near frictionless period remains the same, the restoring aerodynamic moment is decreased.

C. Unsteady Vane Measurements

Four tests were made with the airfoil oscillating ±3° about a 7° mean angle of attack. The frequency of this sinusoidal motion was varied from 0.2, 0.6, 0.9 and 1.2 Hz. Those of the time histories of model and vane angle of attack are shown in Figures 13, 14, and 15; the data for the 0.6 Hz test run could not be recovered because of instrumentation problems.

In all three cases the vane angle lags the sinusoidal oscilla-

tions of the models. Examination of the digital data for each test case indicates a phase lag of approximately 0.28 seconds for the 0.2 Hz test, 0.05 seconds for the 0.9 Hz test and 0.03 seconds for the 1.2 Hz case. These values for phase shift of the vane time-history must be taken as approximate times; however, since both angle of attack sensor outputs appear to have a sizable noise level. The follower on the face cam that drives the model angle of attack causes some "chatter" in the model angle of attack signal. When that "chatter" is coupled with the motion of the vane that has the damped oscillation noted earlier, the vane and model outputs are difficult to interpret.

Attempts to use the steady state calibrations of Figure 10 to predict the model angle of attack from the vane output met with mixed success. By applying the phase shift, using the static calibration and the vane measured angle, the model angle of attack many times could be predicted within ±0.2° of the measured model angle. At other times, the predicted values were more than 1° off, usually due to noise in the digital output. It appears that a smoothing routine must be applied to the vane output to reduce the scatter in the vane output data. As of this writing it does appear that the static calibrations may be used to predict the model angle of attack when the frequency dependent phase lag of the vane is used to adjust prediction.

IV. SUMMARY

A two dimensional model of the S809 airfoil has been tested in the OSU 3'x 5' Subsonic Wind Tunnel. The experimental program was performed to calibrate an angle of attack vane mounted on the model and to provide additional aerodynamic data on the S809 characteristics.

Under steady state conditions, the vane angle versus model angle resolved into two linear regions. In the model angle of attack range from -5° to +7°,

$$\alpha_{model} = 0.590 * \alpha_{probe} + 0.4$$

In the model angle of attack range from +7° to +15°

$$\alpha_{model} = 0.799 * \alpha_{probe} - 2.0$$

In terms of probe angle measurements, the first equation applies from a probe angle of -9° to +11°, the latter equation applies when probe output is +11° to +21°. Outside these angle of attack ranges, the calibrations are non-linear.

Unsteady tests measured the dynamic response of the vane when freed suddenly from a restraint while the tunnel was operating and the model held at a fixed angle of attack. The period of the damped oscillating response averaged 0.101 seconds for three response trials at Re = $1x10^6$. Time to damp to half amplitude averaged 0.073 seconds. At a lower Reynolds number ($.74x10^6$) a single trial resulted in increase in both the period and half amplitude time. A second unsteady series of tests put the model in sinusoidal motion. The vane followed this motion, lagging the model by approximately .28, .05 and .03 seconds for the three recorded oscillation frequencies of 0.2, 0.9 and 1.2 Hz, respec-

tively. Application of the steady state vane calibration using these phase lags appeared to yield adequate predictions of model angle of attack for selected trials. However, both sets of sensed angle data, vane and model, require smoothing and additional analysis to improve the calibrations.

The measured steady state pressure distributions verified the favorable laminar flow pressure gradients and the limited maximum lift designed into the S809 airfoil for HAWT applications. The minimum drag coefficient measured was $C_d = 0.0069$, producing a maximum lift to drag ratio of 107 at $\alpha = 5°$. At $\alpha = 7°$ flow separation occurred to initiate a limited maximum lift with full separation from the upper surface at $\alpha = 14.9°$ holding the maximum value of lift coefficient to $C_l = 1.029$.

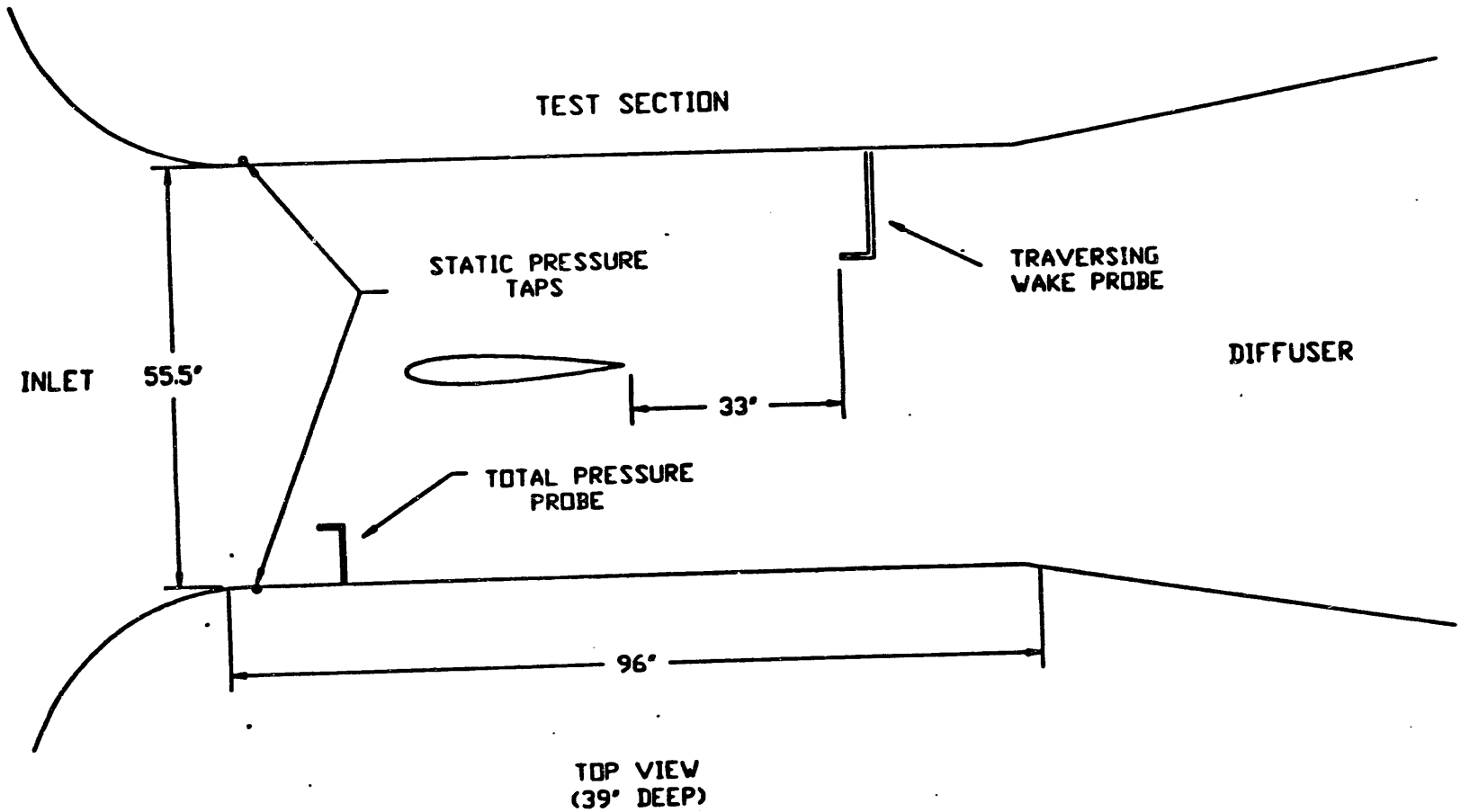

FIGURE 1. LOW SPEED WIND TUNNEL TEST-SECTION DESIGN

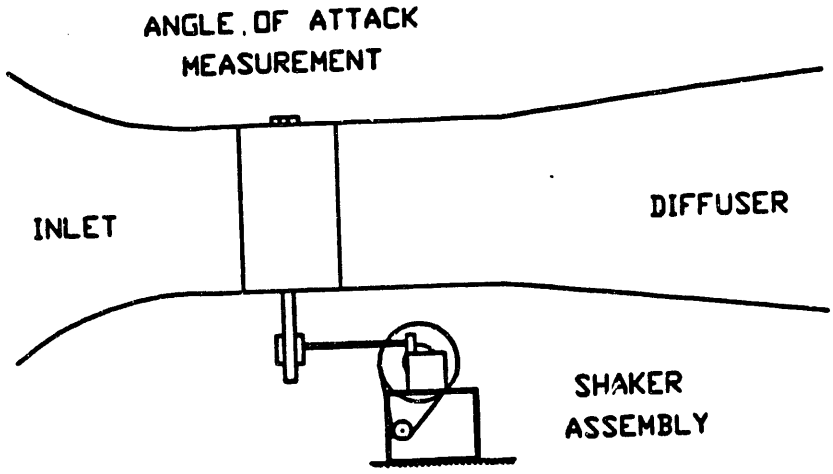

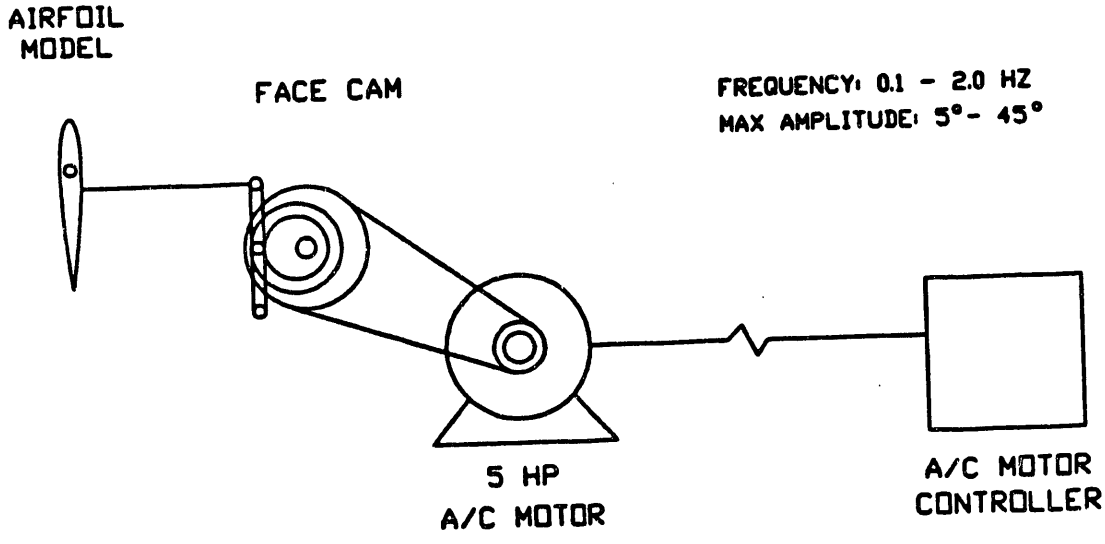

FIGURE 2. OSCILLATORY SYSTEM DESIGN

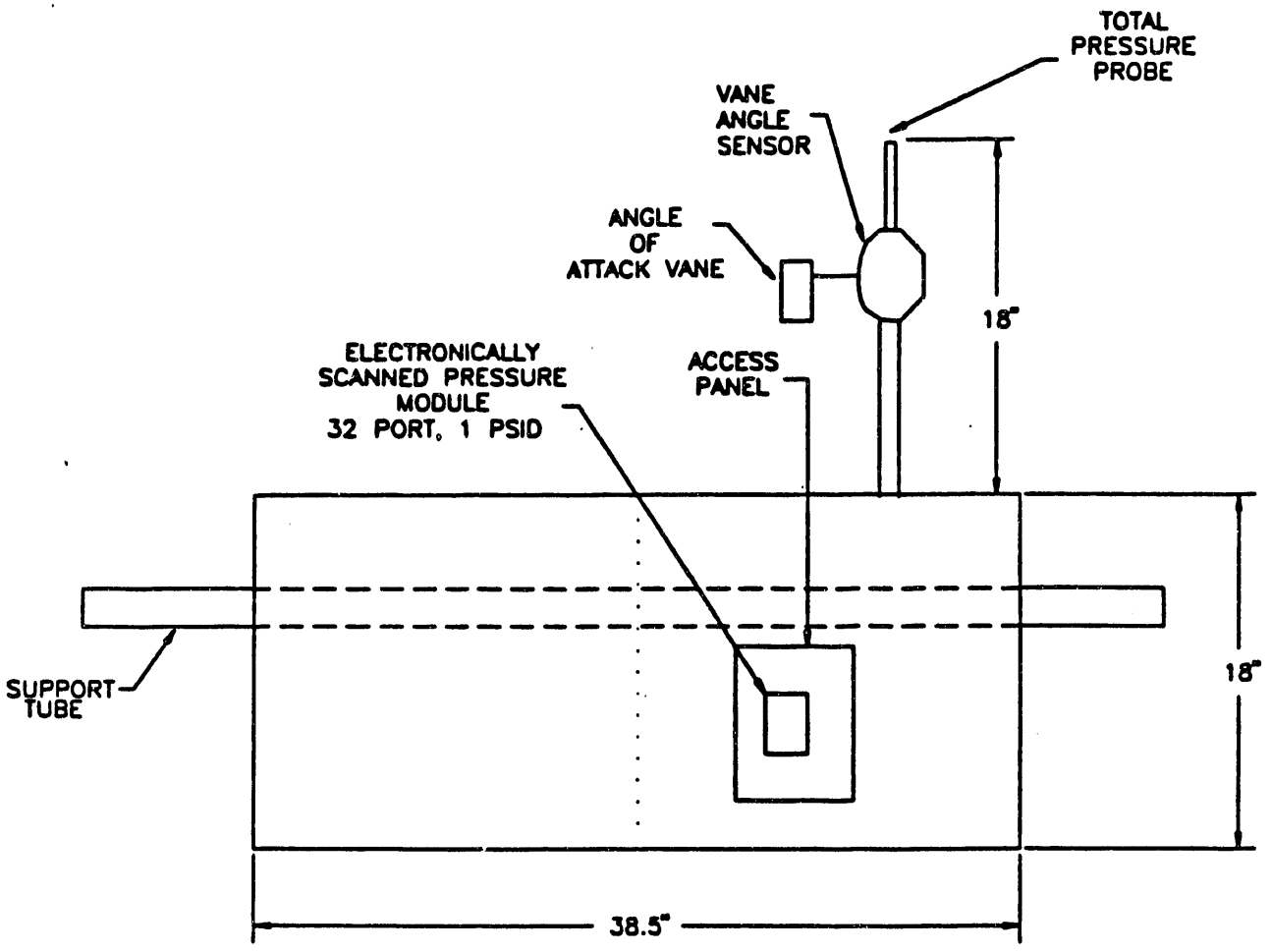

FIGURE 3. S-809 MODEL SCHEMATIC

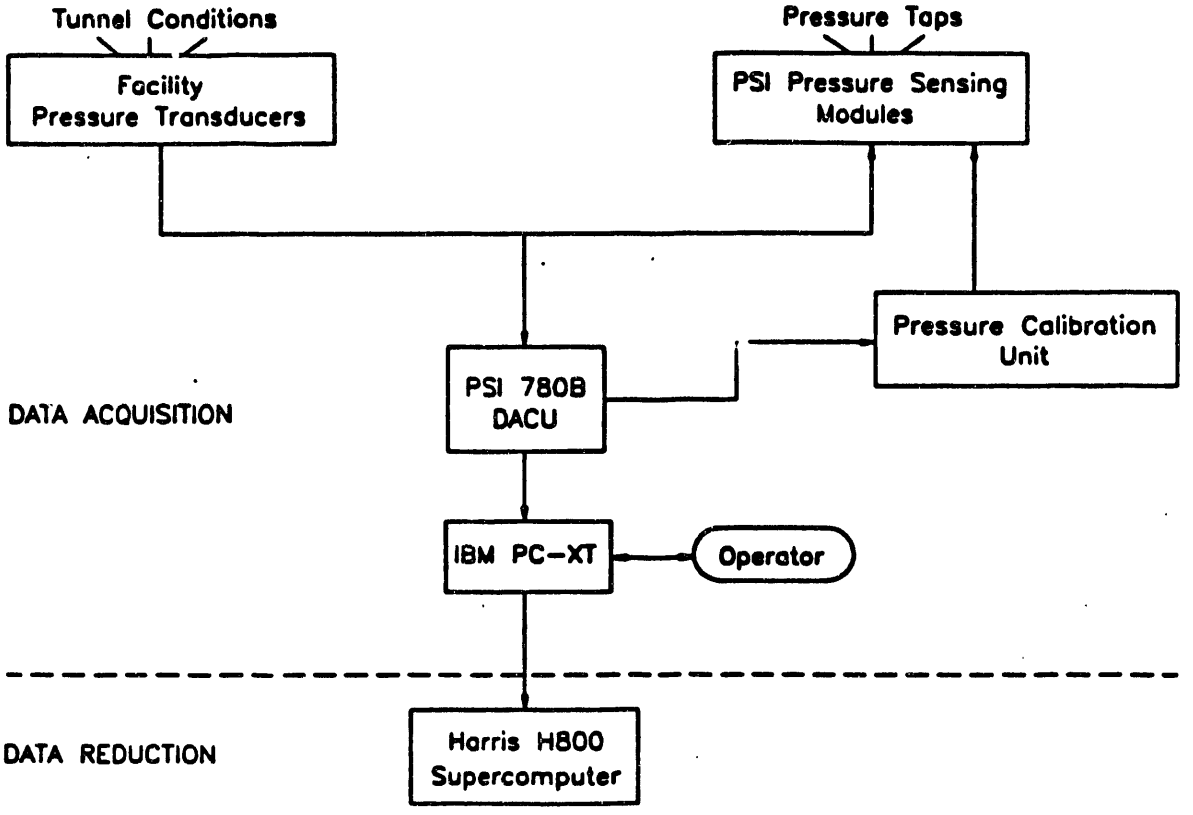

FIGURE 4. DATA ACQUISITION AND REDUCTION SYSTEM

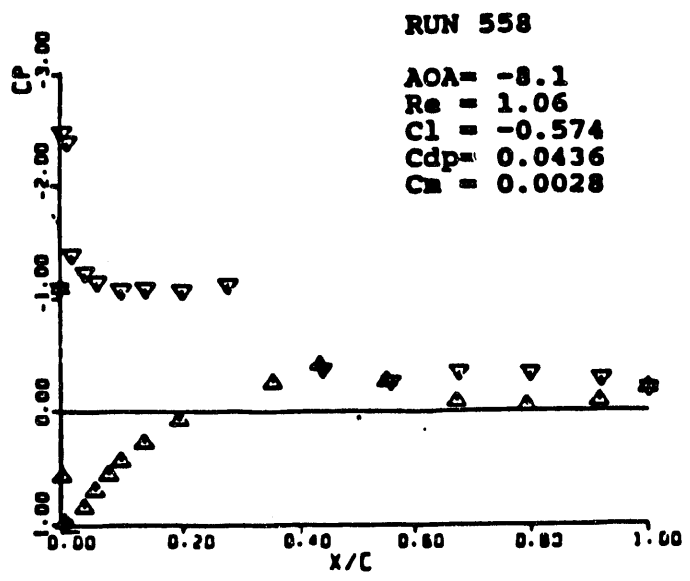

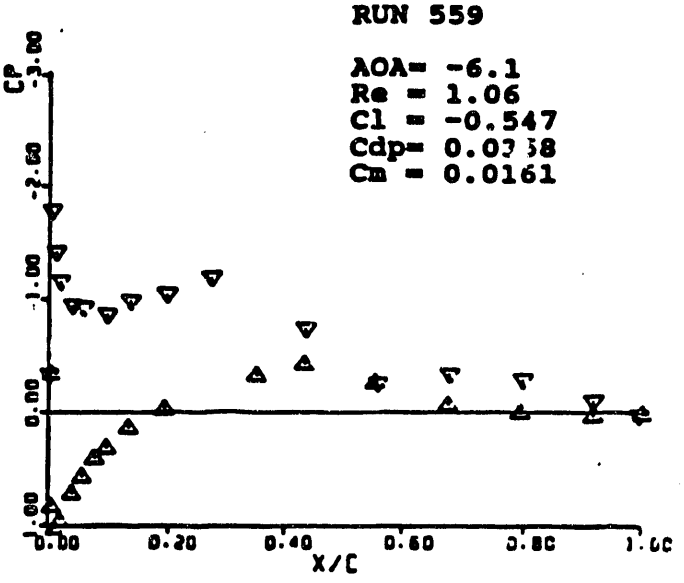

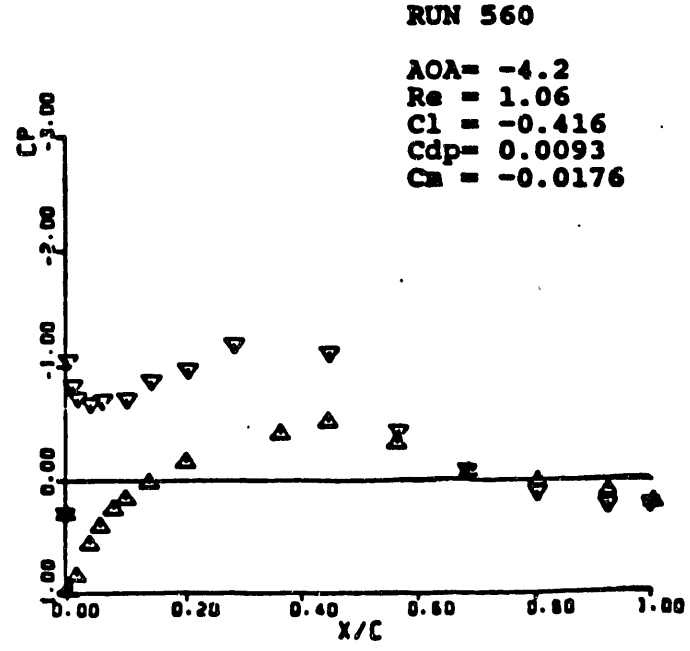

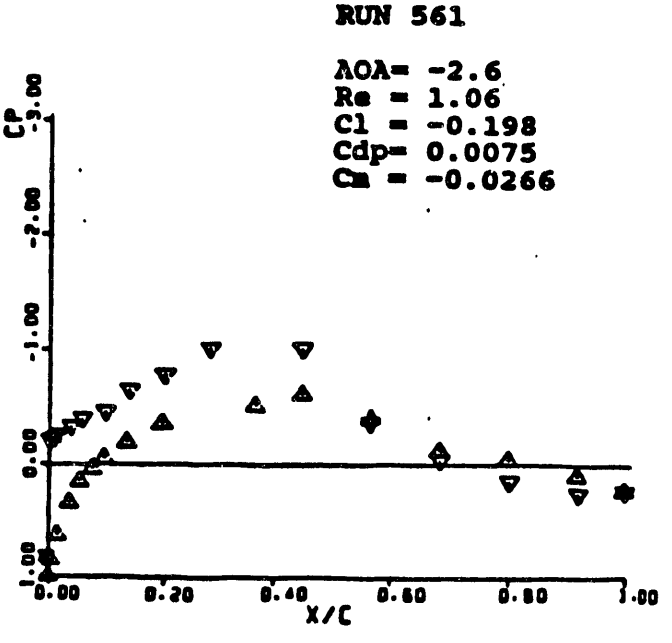

FIGURE 5: SURFACE PRESSURE DISTRIBUTIONS

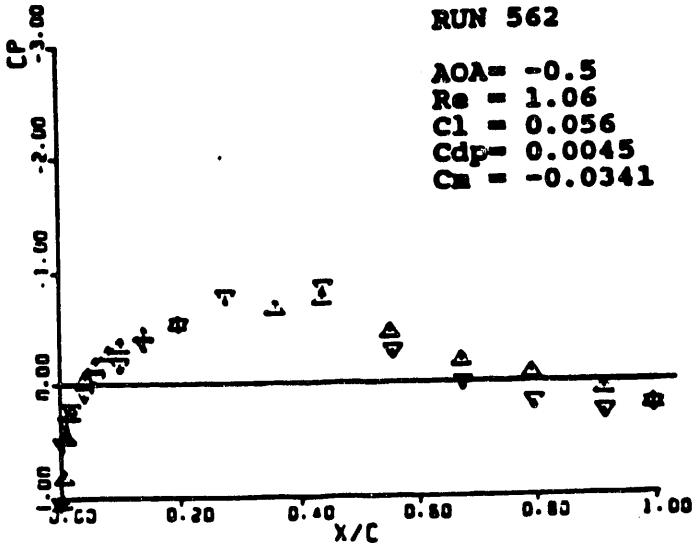

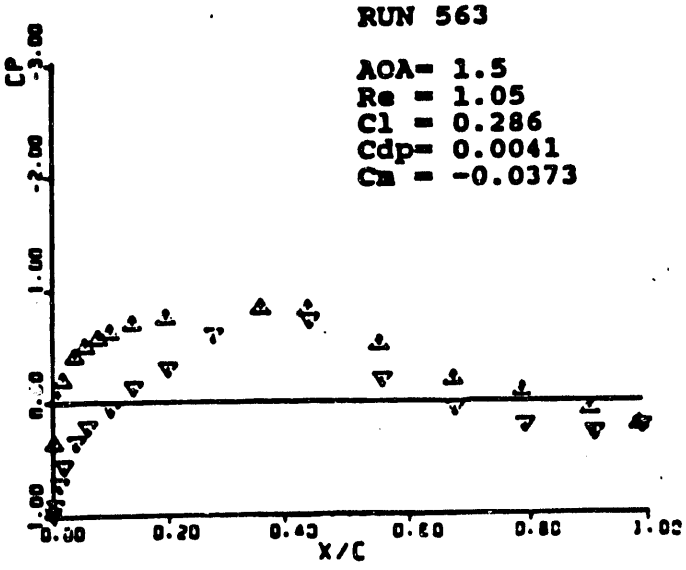

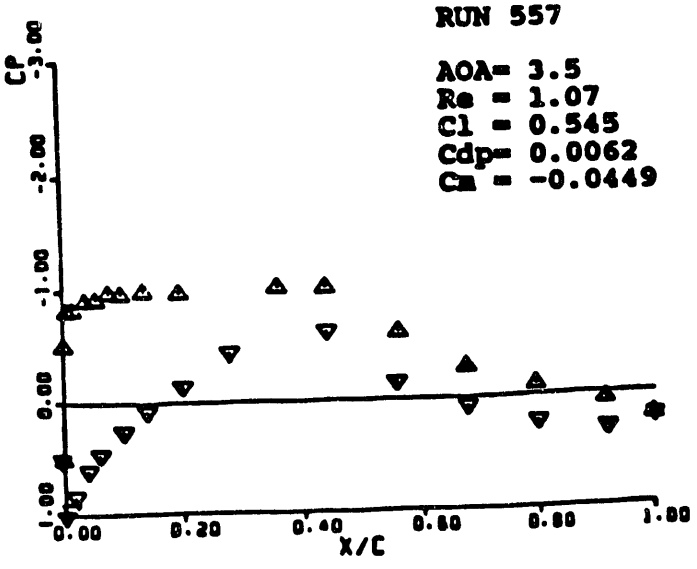

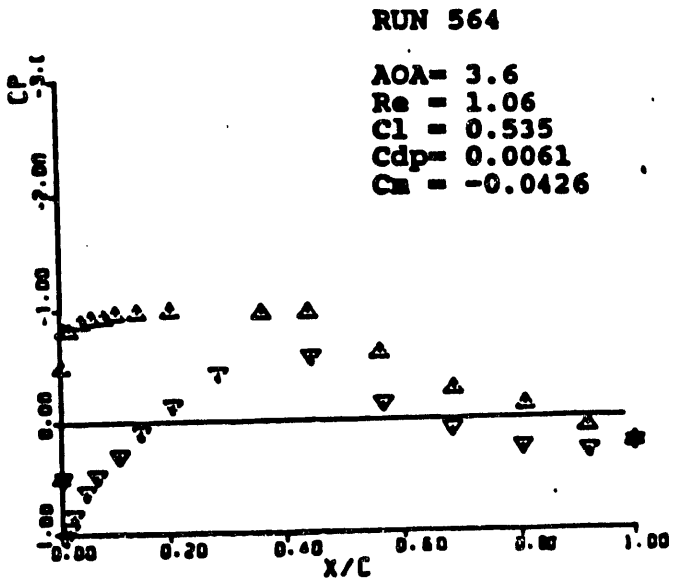

FIGURE 5: SURFACE PRESSURE DISTRIBUTIONS (contd)

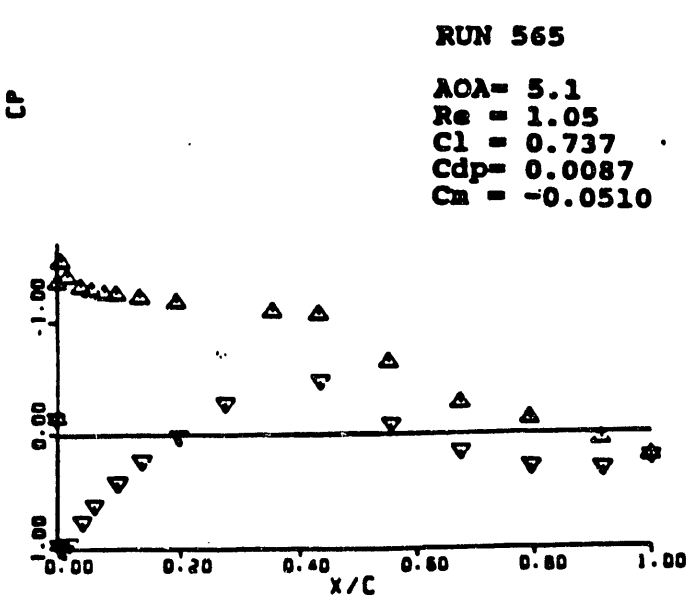

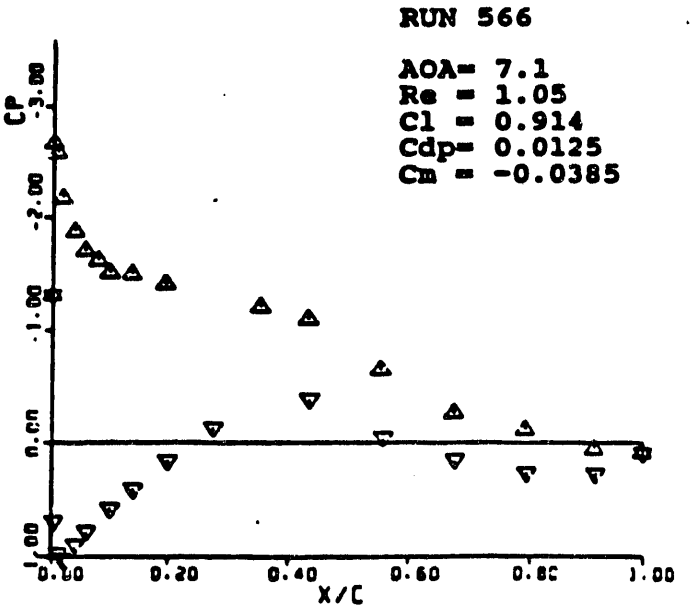

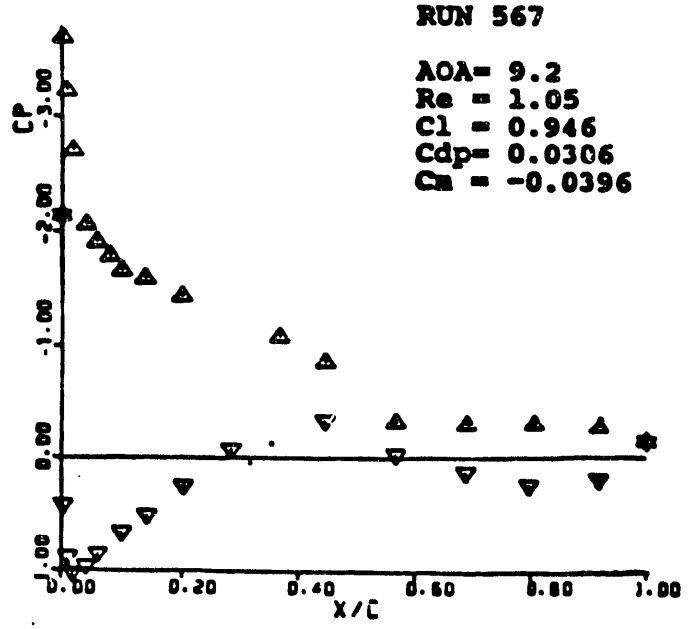

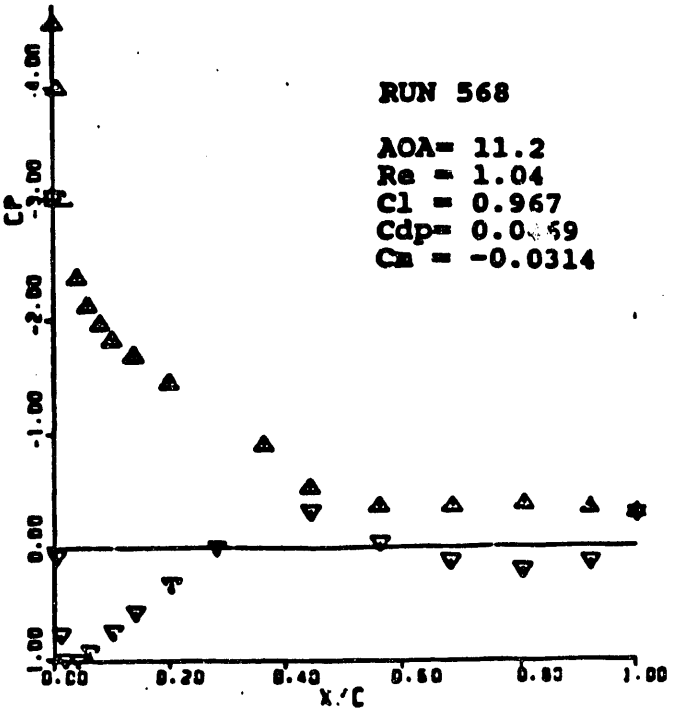

FIGURE 5: SURFACE PRESSURE DISTRIBUTIONS (contd)

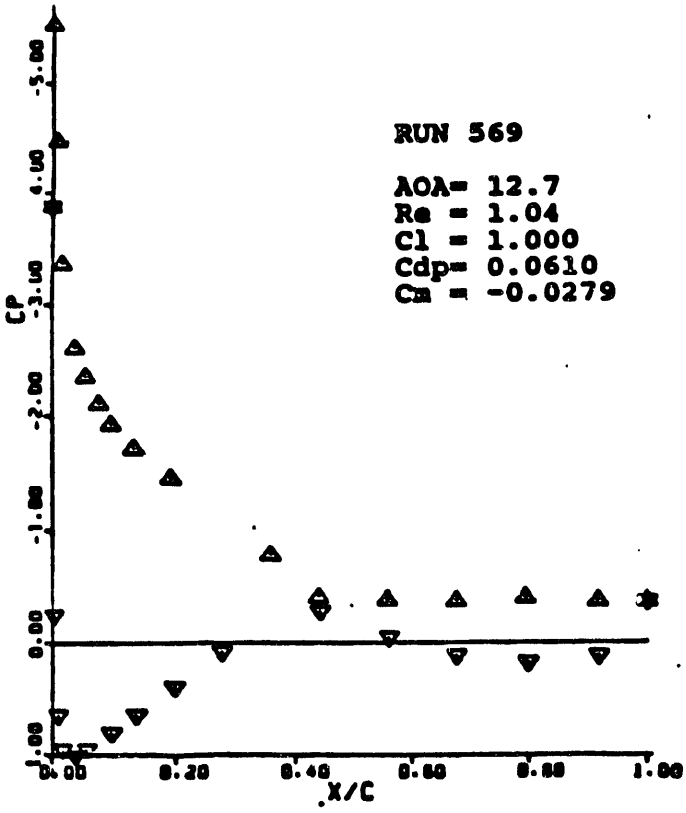

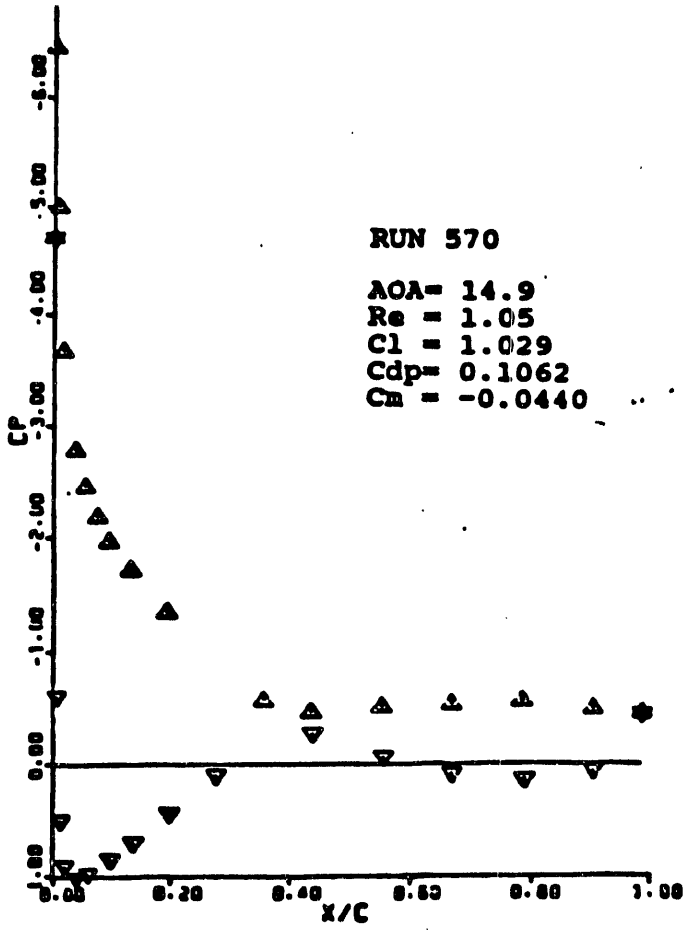

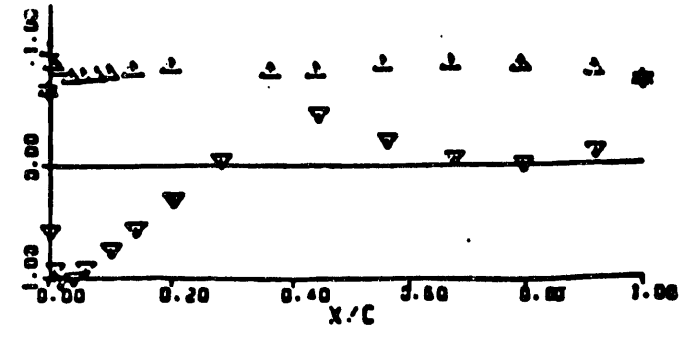

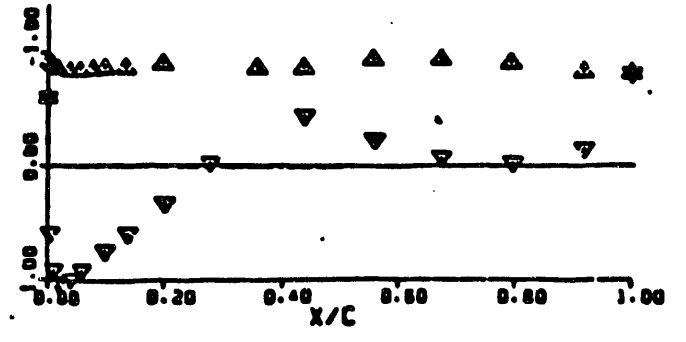

FIGURE 5: SURFACE PRESSURE DISTRIBUTIONS (contd)

FIGURE 6: LIFT COEFFICIENT –VS– ANGLE OF ATTACK

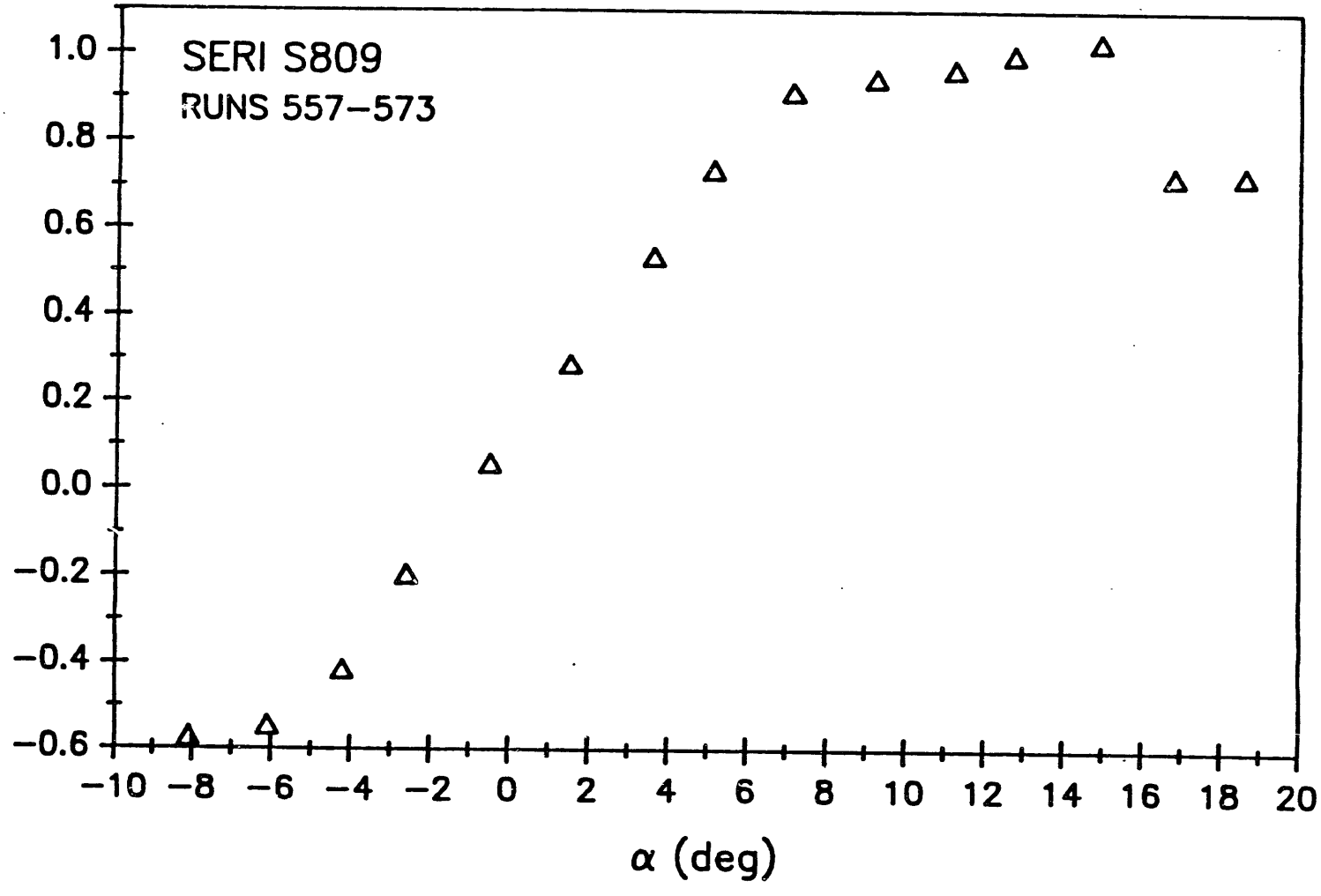

FIGURE 7: MOMENT COEFFICIENT –VS– ANGLE OF ATTACK

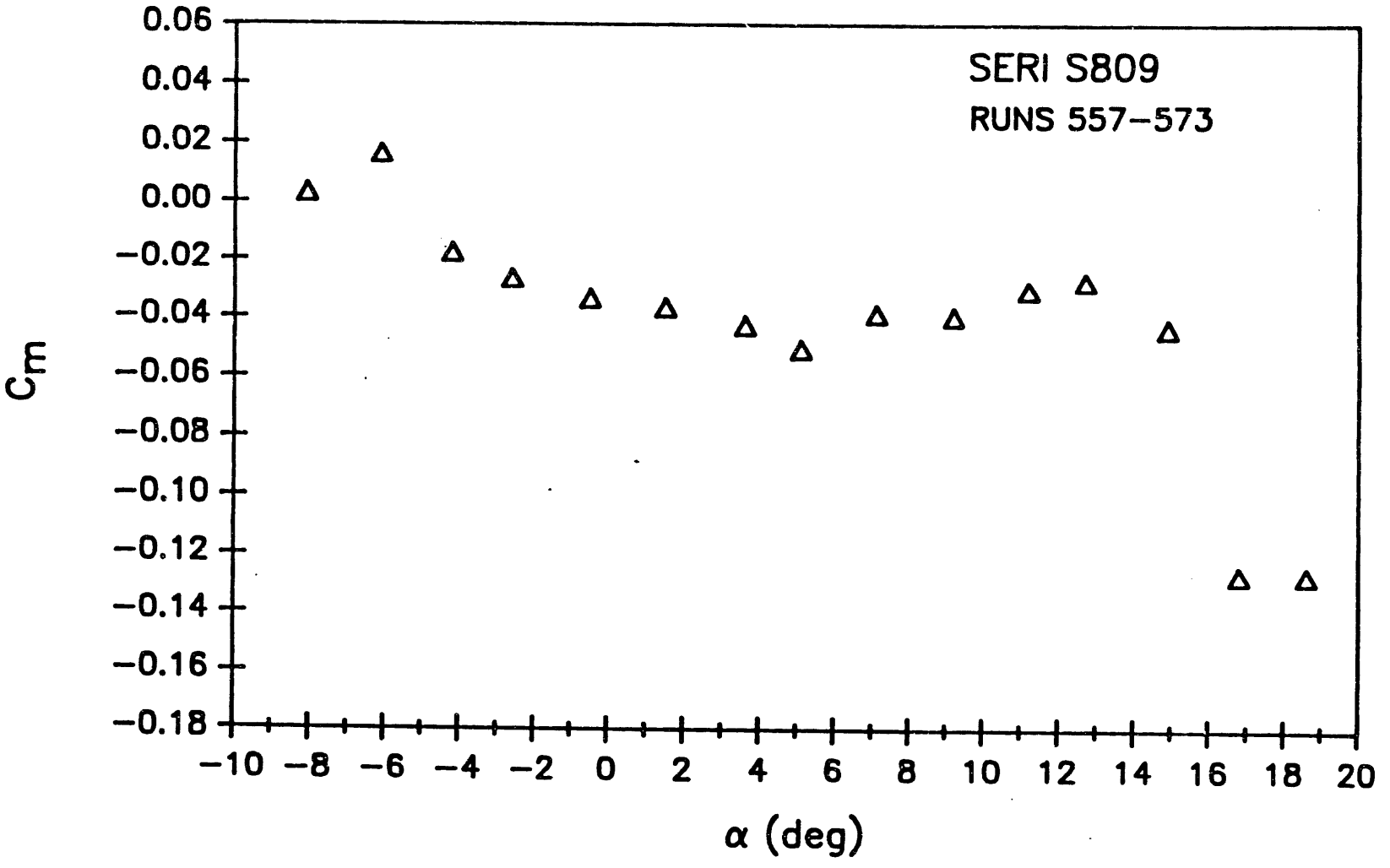

FIGURE 8: DRAG COEFFICIENT –VS– ANGLE OF ATTACK

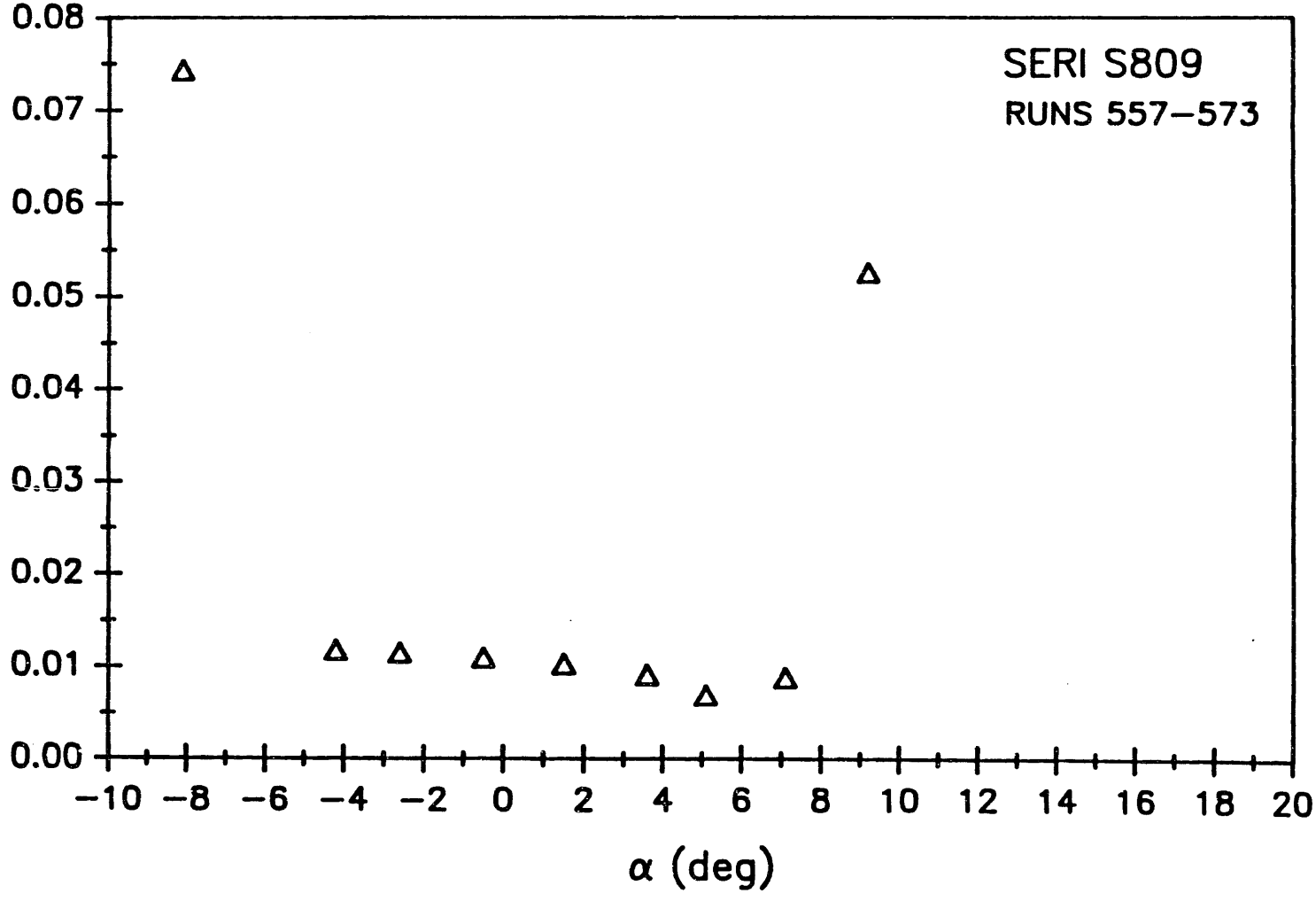

FIGURE 9: DRAG POLAR

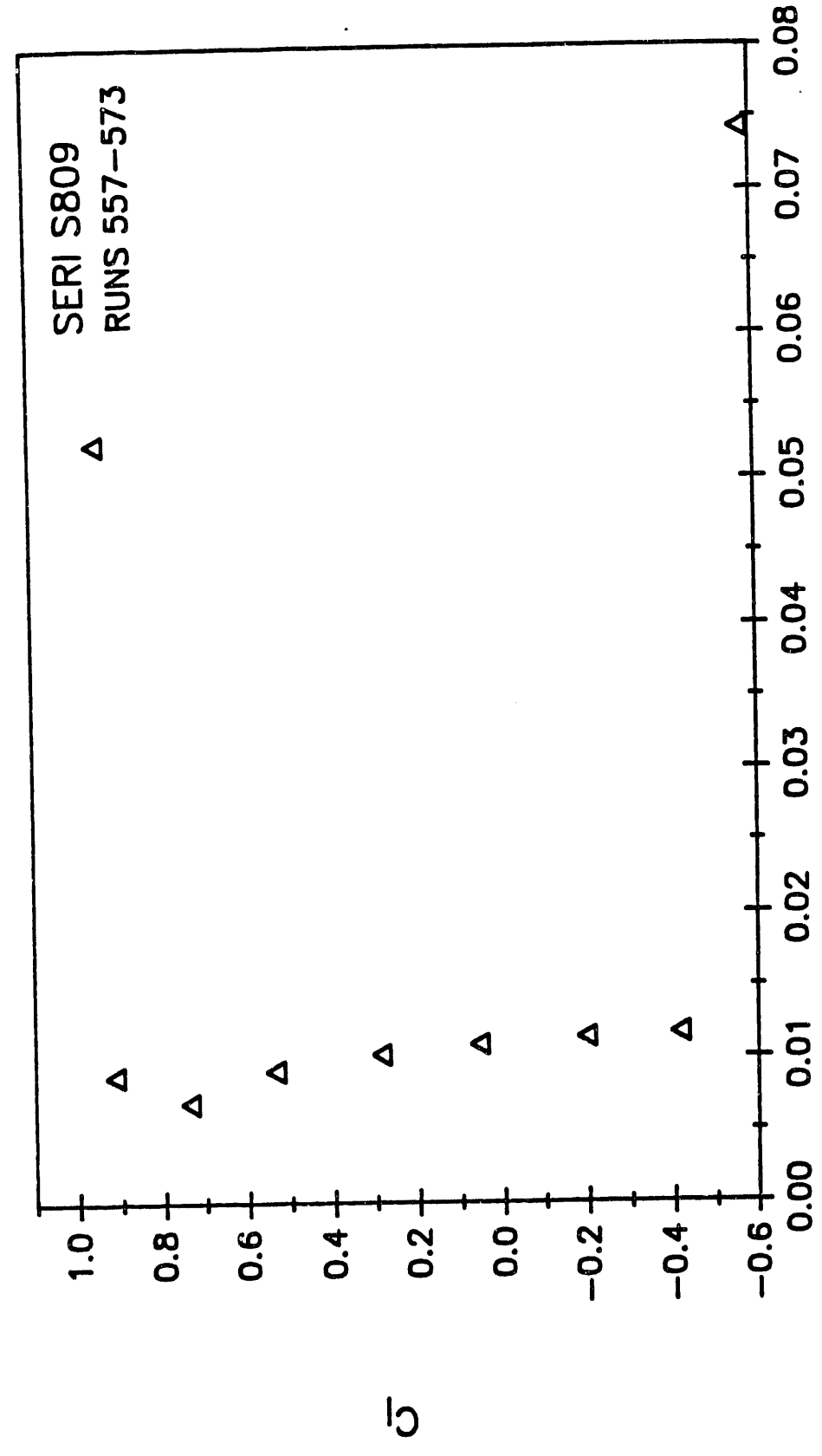

FIGURE 10: CALIBRATION OF ANGLE OF ATTACK PROBE
–VS– MODEL ANGLE

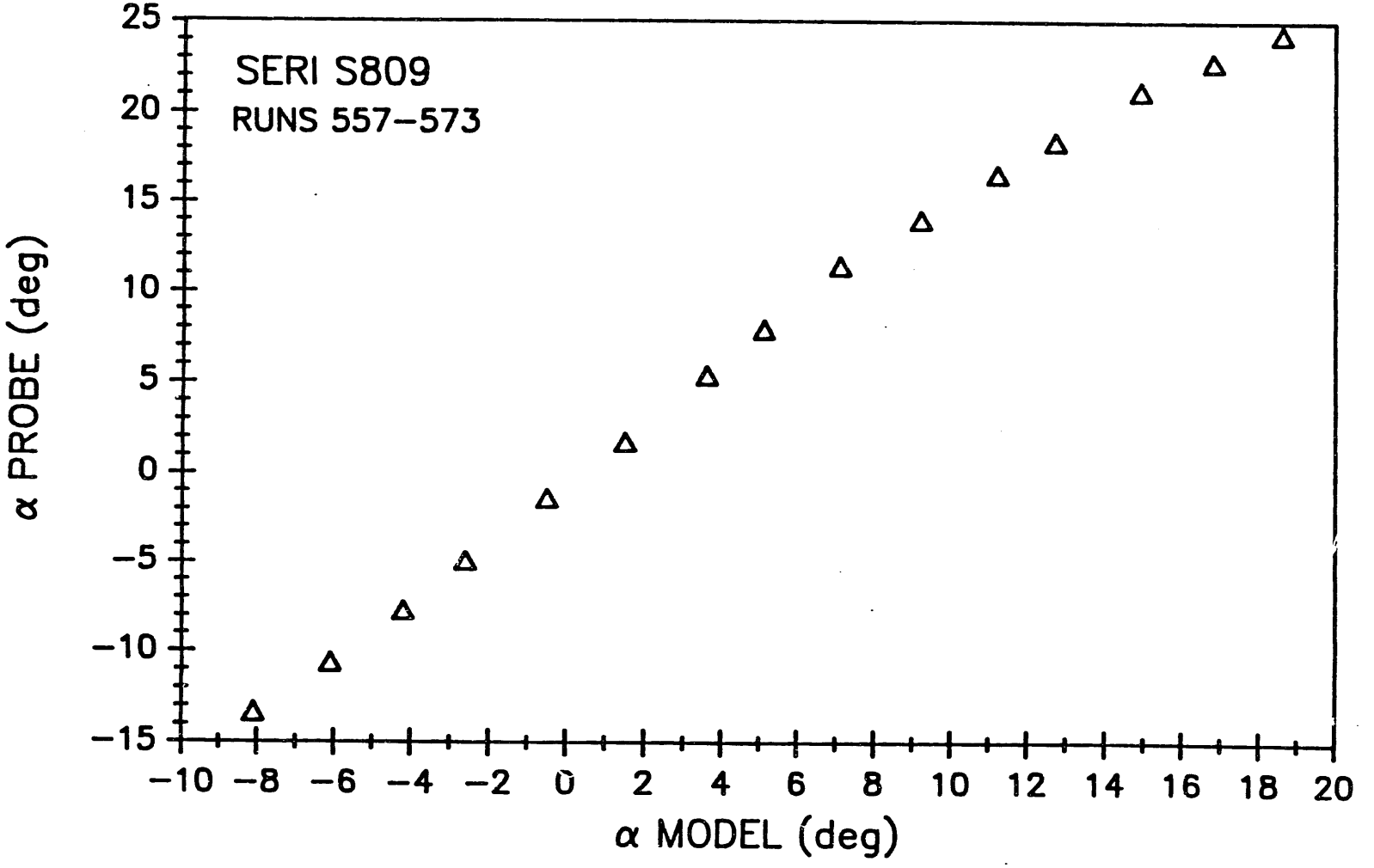

FIGURE 11: PROBE ANGLE –VS– TIME AT Re=1.0 X 10^6

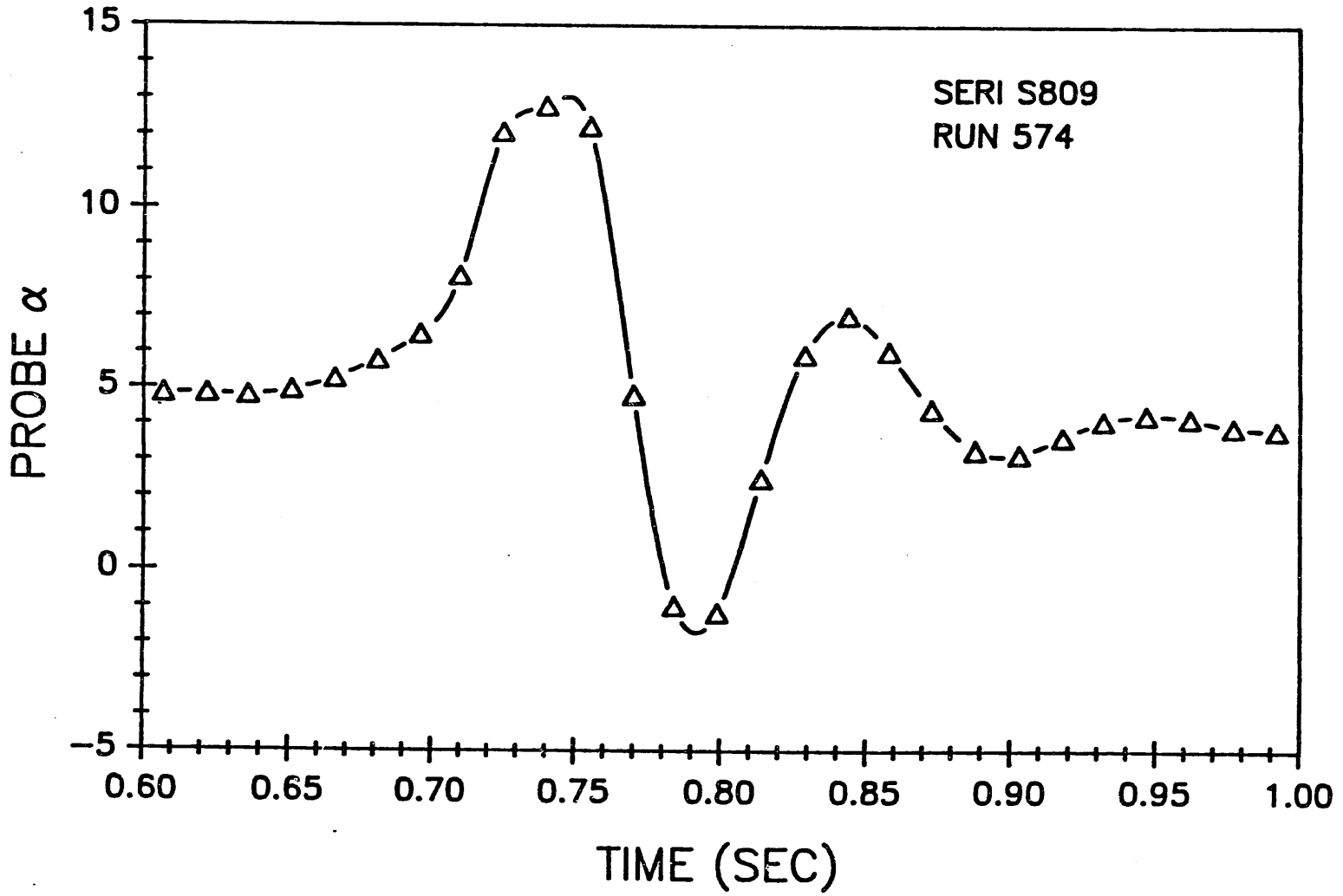

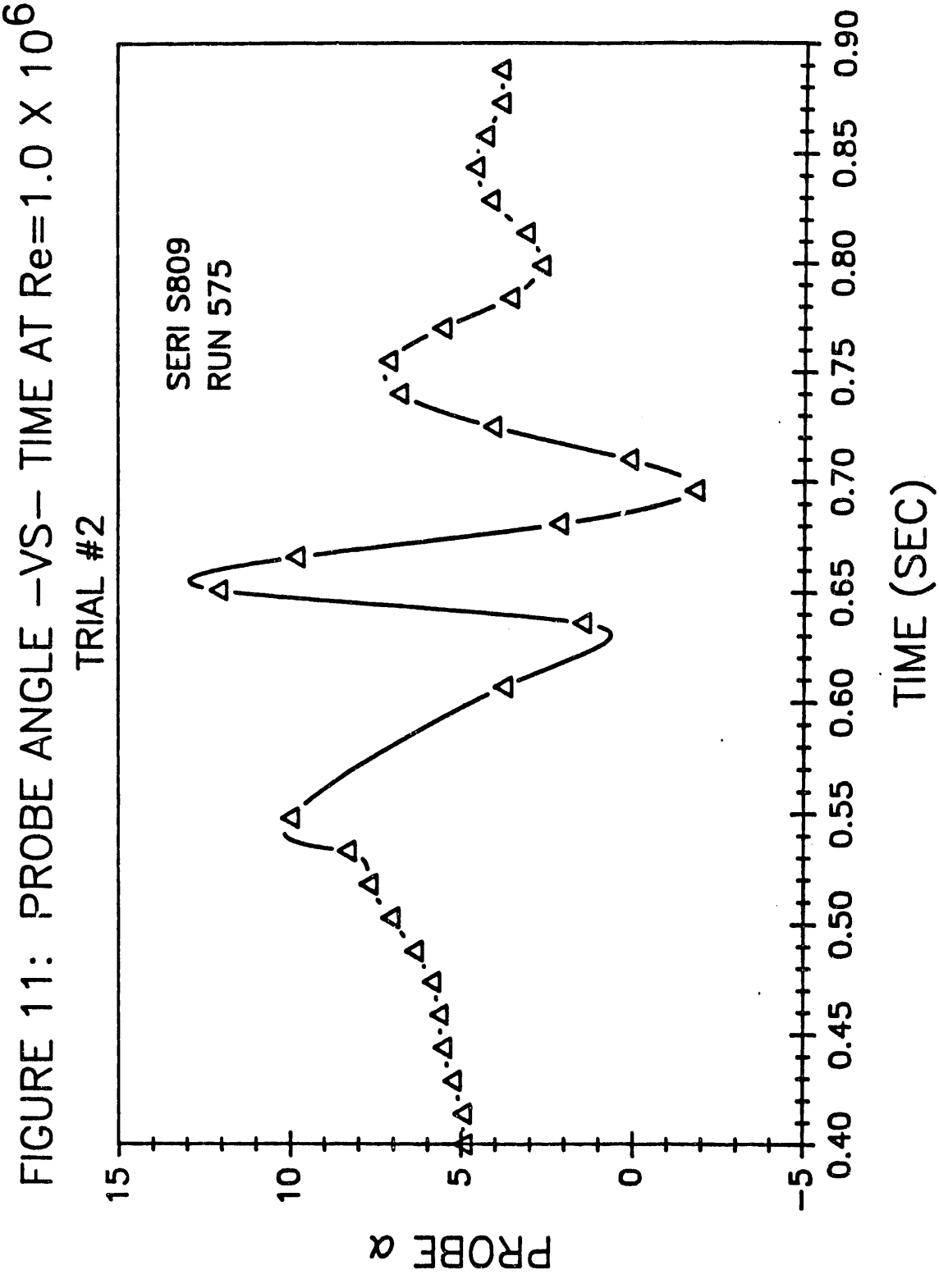
FIGURE 11: PROBE ANGLE –VS– TIME AT Re=1.0 X 10^6
TRIAL #2
SERI S809
RUN 575
PROBE α
TIME (SEC)
15
10
5
0
-5
0.40
0.45
0.50
0.55
0.60
0.65
0.70
0.75
0.80
0.85
0.90

FIGURE 11: PROBE ANGLE –VS– TIME AT Re=1.0 X 10^6

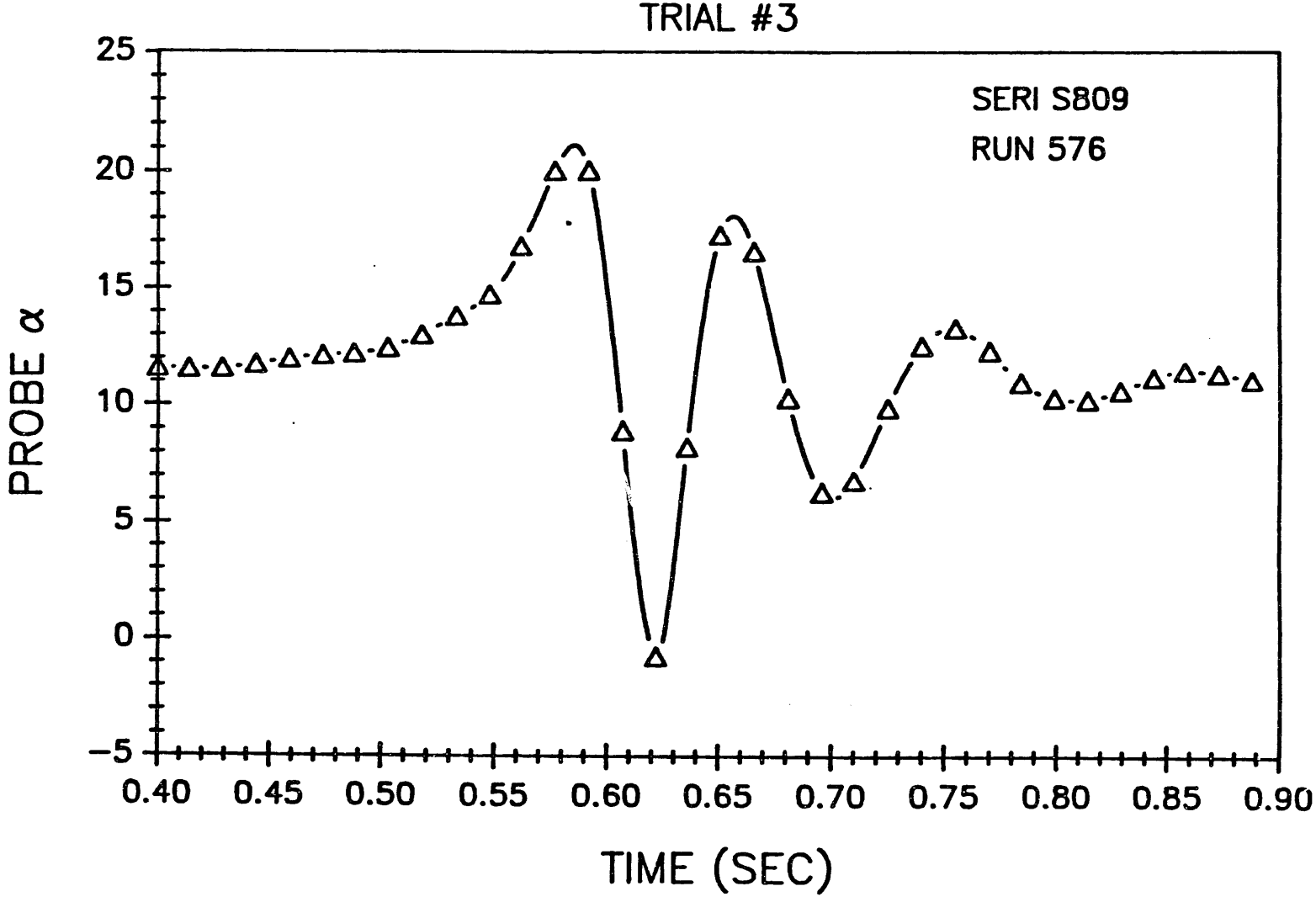

FIGURE 12: PROBE ANGLE –VS– TIME AT Re=0.74 X 10^6

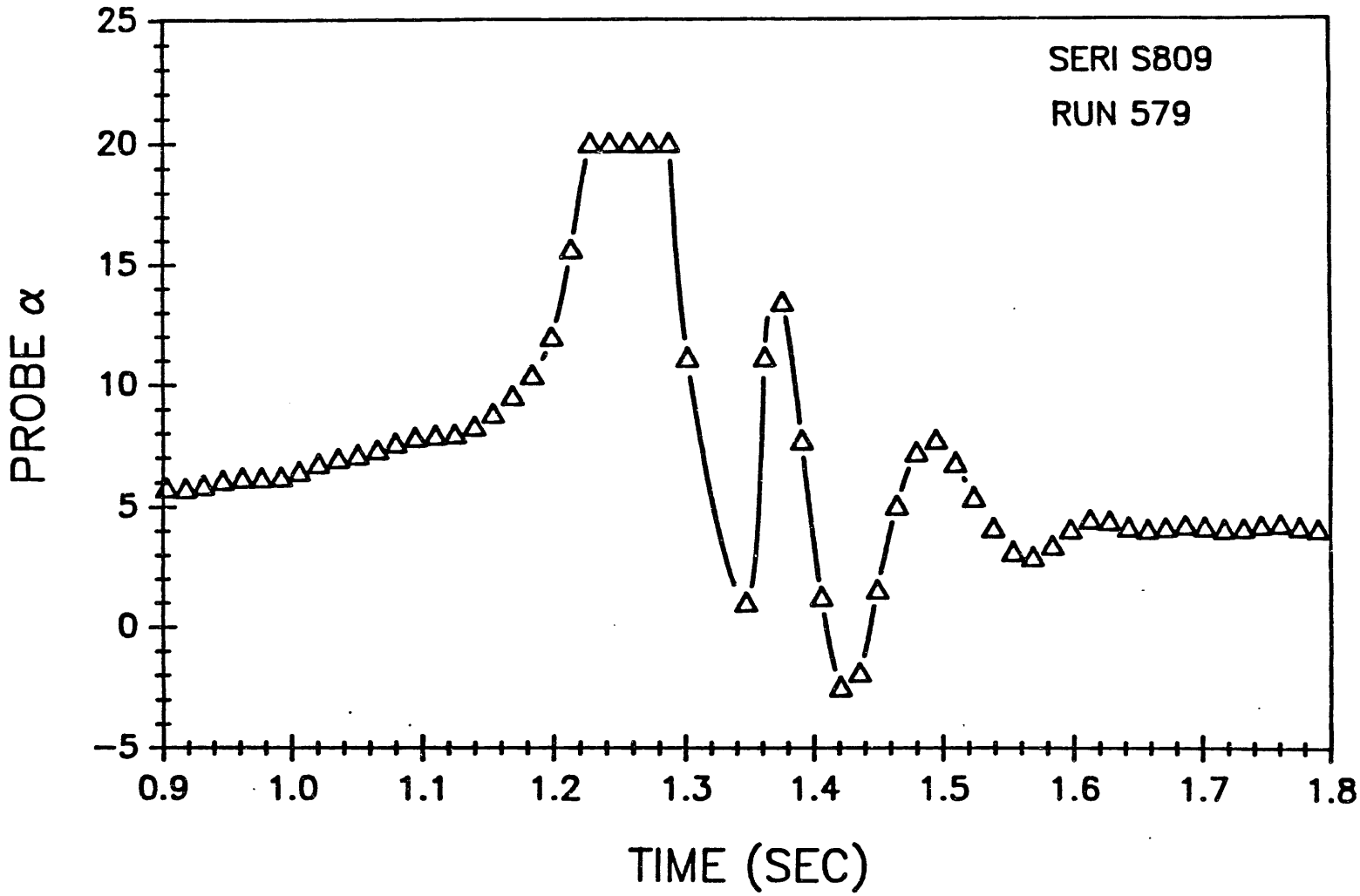

FIGURE 13: PROBE AND MODEL ANGLE OF ATTACK
–VS– TIME AT 0.2 Hz

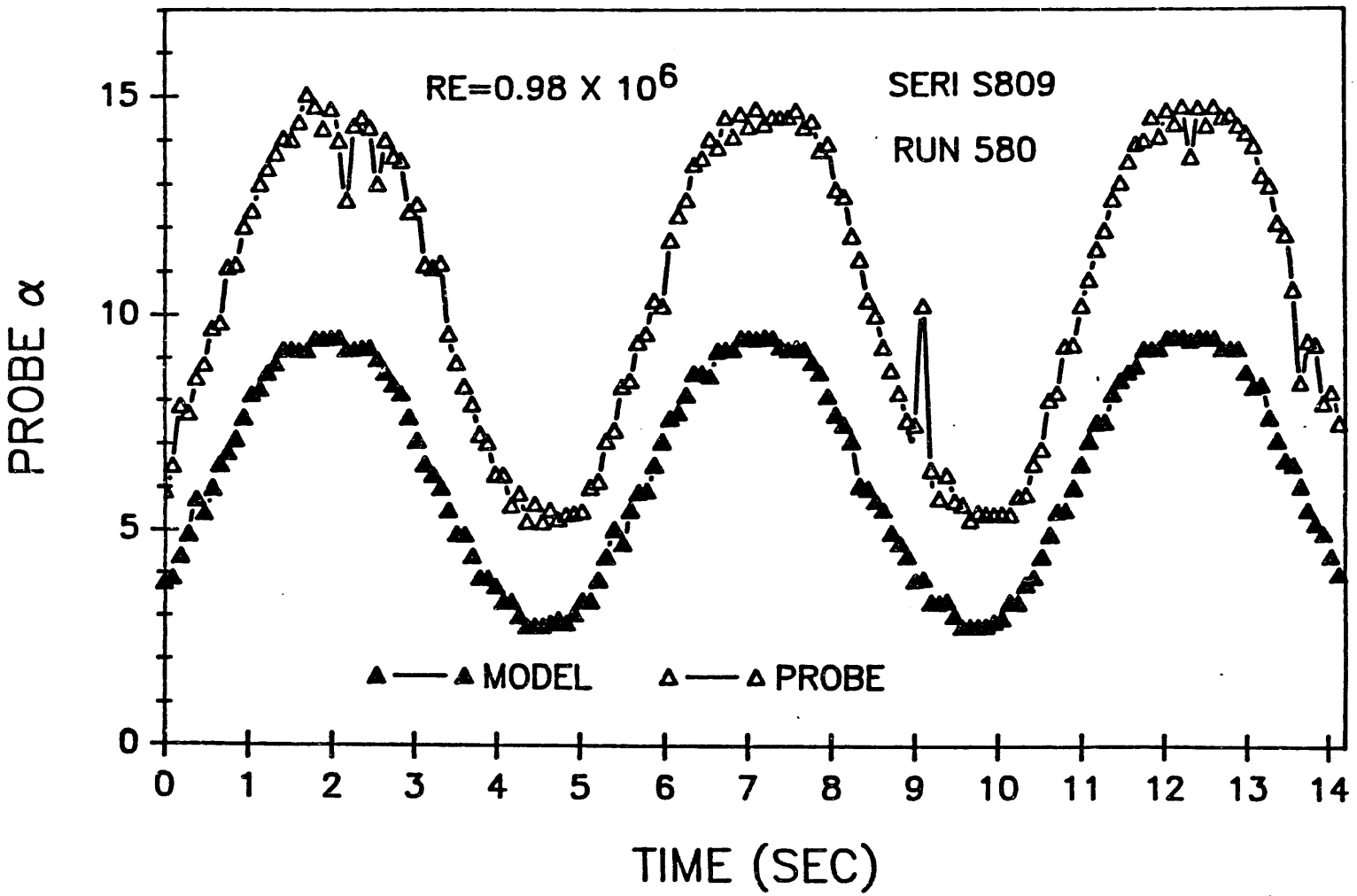

FIGURE 14: PROBE AND MODEL ANGLE OF ATTACK
–VS– TIME AT .9 Hz

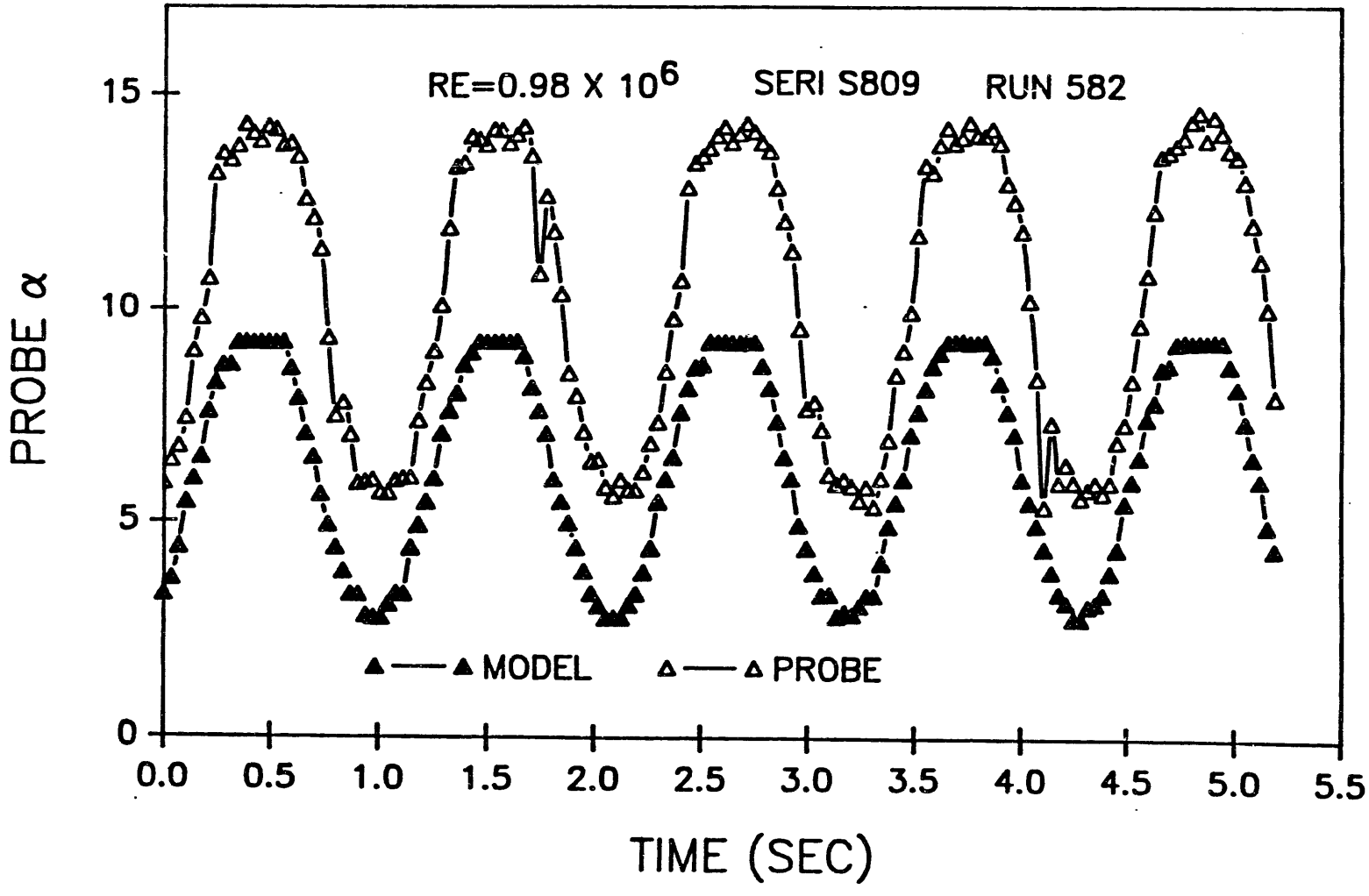

FIGURE 15: PROBE AND MODEL ANGLE OF ATTACK
—VS— TIME AT 1.2 Hz

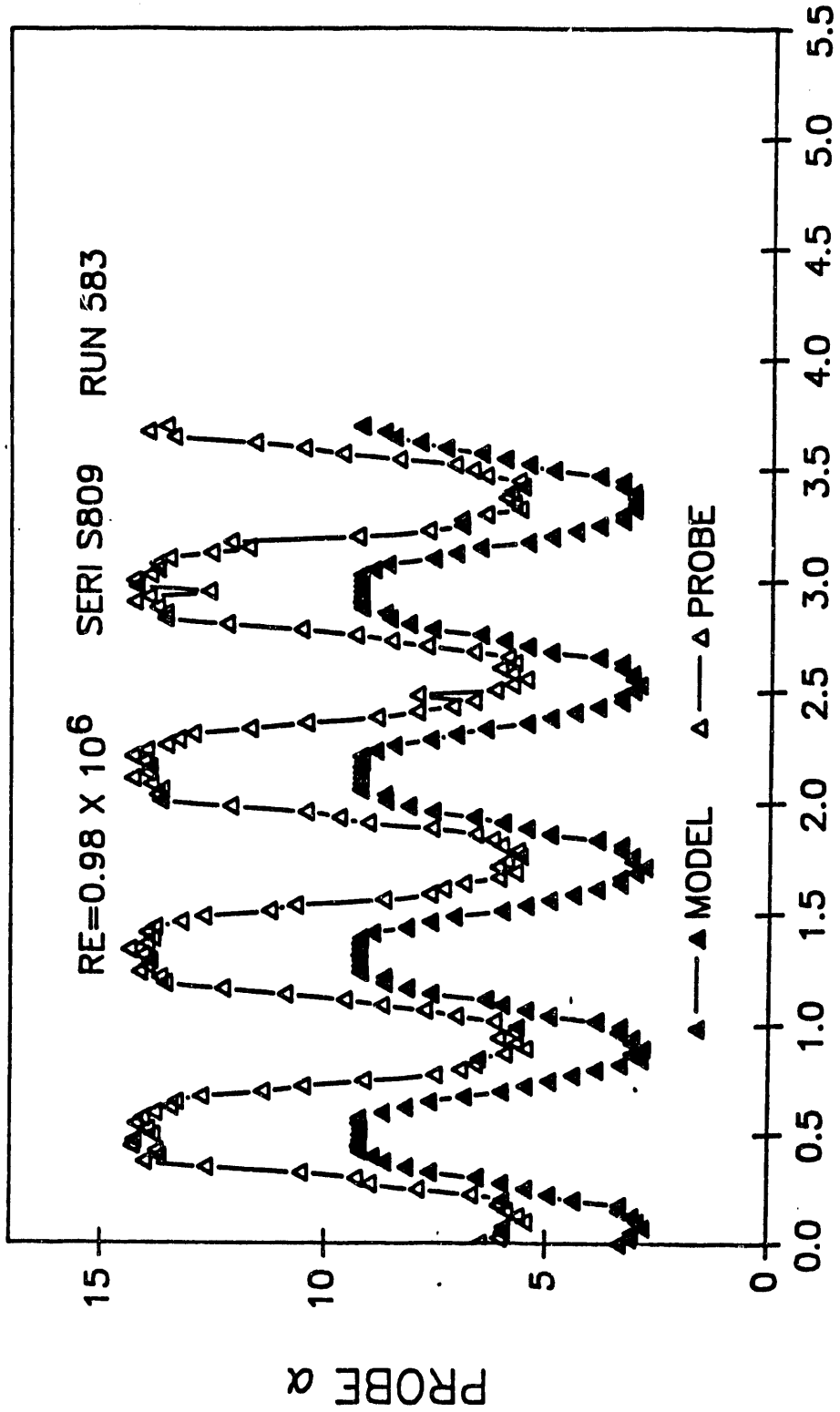

APPENDICES

TABLE I: S809 AIRFOIL COORDINATES

COORDINATES FOR UPPER SURFACE		COORDINATES FOR LOWER SURFACE	
X (in)	Y (in)	X (in)	Y (in)
0.006660	0.049500	0.025200	-0.089640
0.103500	0.209880	0.167940	-0.228960
0.292680	0.383940	0.417780	-0.389160
0.568440	0.564480	0.760140	-0.565920
0.926460	0.745740	1.184220	-0.755820
1.362240	0.923760	1.678500	-0.954180
1.870200	1.094760	2.231460	-1.153440
2.444400	1.254960	2.835360	-1.344060
3.078540	1.401480	3.485160	-1.520460
3.765600	1.530900	4.171500	-1.678680
4.497660	1.640340	4.883220	-1.810800
5.266620	1.726920	5.613840	-1.906020
6.064020	1.787940	6.359040	-1.955880
6.880140	1.819620	7.117380	-1.951560
7.705620	1.818180	7.889760	-1.887120
8.529120	1.771740	8.682120	-1.756080
9.360900	1.662660	9.510660	-1.565460
10.224180	1.504080	10.379340	-1.339560
11.114460	1.328220	11.276820	-1.100160
12.009240	1.152540	12.187800	-0.862560
12.889080	0.983160	13.095360	-0.640440
13.736520	0.824040	13.980240	-0.443880
14.536080	0.676980	14.822640	-0.280620
15.273720	0.543060	15.601860	-0.154620
15.936660	0.420300	16.298100	-0.066600
16.517340	0.304920	16.893360	-0.013500
17.014140	0.198180	17.371620	0.009720
17.423820	0.108000	17.720280	0.011700
17.735040	0.044100	17.930160	0.004320
17.932140	0.009720	18.000000	0.000000
18.000000	0.000000		

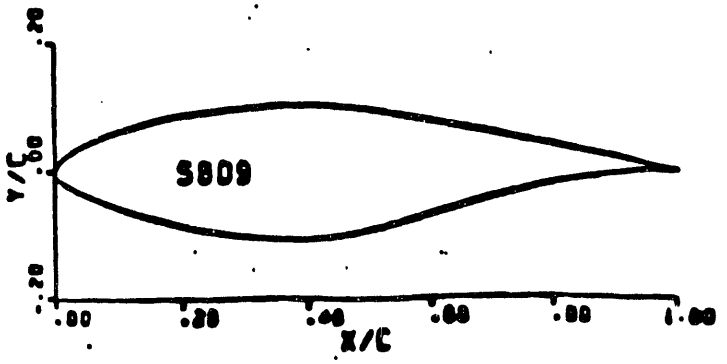

TABLE II: S809 TAP FILE

SERI S809 18 INCH CHORD MODEL FOR 3X5

PRESSURE TRANSDUCER PORT NUMBER	MODEL TAP NUMBER	X/C	Y/C
1	1	1.0000000	-0.0000400
2	2	0.9180000	0.0167000
4	3	0.7970000	0.0395000
6	4	0.6789000	0.0616000
8	5	0.5588000	0.0854000
10	6	0.4394000	0.1006000
11	7	0.3594000	0.1004000
13	8	0.1984000	0.0831000
14	9	0.1389000	0.0705000
15	10	0.0992000	0.0595000
16	11	0.0792000	0.0527000
17	12	0.0589000	0.0448000
18	13	0.0398000	0.0357000
19	14	0.0189000	0.0228000
20	15	0.0089000	0.0151000
21	16	0.0027000	0.0072000
22	17	0.0000000	0.0000000
23	18	0.0040000	-0.0091000
24	19	0.0111000	-0.0140000
25	20	0.0210000	-0.0200000
26	21	0.0421000	-0.0314000
27	22	0.0613000	-0.0400000
29	23	0.1024000	-0.0563000
30	24	0.1425000	-0.0700000
31	25	0.2017000	-0.0864000
32	26	0.2809000	-0.1019000
34	27	0.4416000	-0.1044000
35	28	0.5611000	-0.0783000
36	29	0.6803000	-0.0471000
37	30	0.8009000	-0.0198000
38	31	0.9194000	-0.0023000
39	32	1.1000000	-0.0001000

Appendix F

Integrated Coefficients from all Tests

Plots of Integrated Coefficients

Colorado State University Environmental Wind Tunnel Test Results
SERI S809 Airfoil
Reynolds Number = 650,000

alpa	Cn	Ct	Cl	Cdp	LFA	Tunnel Q	Probe Q
deg					deg	psi	psi
-0.25	0.151	-0.002	0.151	0.002	0.808	0.047	0.047
1.75	0.354	0.01	0.354	0.001	4.09	0.048	0.048
3.81	0.56	0.035	0.561	0.002	7.62	0.048	0.048
5.92	0.762	0.073	0.765	0.006	10.9	0.049	0.049
7.94	0.854	0.104	0.86	0.015	13.8	0.05	0.05
9.98	0.841	0.116	0.848	0.031	16.4	0.049	0.048
11	0.884	0.128	0.892	0.043	17.4	0.049	0.049
12	0.879	0.136	0.888	0.049	18.4	0.049	0.048
13	0.918	0.145	0.927	0.043	19.7	0.049	0.049
14	0.901	0.148	0.91	0.075	20.8	0.051	0.051
15	0.914	0.148	0.91	0.075	20.8	0.051	0.051
16	0.922	0.153	0.928	0.107	22.9	0.049	0.049
17	0.737	-0.066	0.686	0.278	23.3	0.048	0.047
18	0.693	-0.065	0.639	0.276	24.1	0.048	0.047
19	0.634	-0.07	0.576	0.273	25	0.047	0.046
20	0.613	-0.07	0.552	0.275	26	0.048	0.046
22	0.673	-0.076	0.596	0.323	28.4	0.045	0.044
23.9	0.743	-0.075	0.649	0.37	31.2	0.046	0.044
26	0.794	-0.076	0.68	0.417	33.9	0.045	0.041
30	1.02	-0.073	0.851	0.576	39.3	0.045	0.041
35	1.28	-0.067	1.01	0.789	45.7	0.042	0.035
40	1.52	-0.064	1.12	1.03	51.5	0.039	0.029
45	1.64	-0.05	1.12	1.19	57	0.037	0.021
50	1.75	-0.032	1.1	1.36	59.1	0.035	0.012
55.3	1.92	-0.018	1.08	1.58			
60.2	1.87	0.002	0.931	1.62			
65.2	2.22	0.038	0.968	2			
70.2	2.18	0.039	0.776	2.04			
75.2	2.22	0.062	0.63	2.13			
80.2	2.37	0.082	0.485	2.32			
85.1	2.15	0.107	0.289	2.14			
90.2	2.27	0.116	0.109	2.27			

Colorado State University Environmental Wind Tunnel Test Results
SERI S809 Airfoil
Reynolds Number =500,000
Smooth

alpha	Cn	Ct	Ci	Cdp	LFA
deg					deg
-2.23	-0.06	-0.004	-0.06	0.006	-2.34
-0.161	0.156	-0.005	0.156	0.004	0.8
1.84	0.369	0.005	0.369	0.006	4.13
3.88	0.571	0.031	0.571	0.008	7.44
5.89	0.752	0.068	0.755	0.009	10.5
7.89	0.854	0.101	0.86	0.017	13.7
8.95	0.88	0.115	0.887	0.024	14.5
9.91	0.862	0.115	0.869	0.035	15.7
10.9	0.86	0.126	0.868	0.039	16.9
12	0.885	0.138	0.894	0.048	17.9
12.9	0.928	0.15	0.938	0.061	19.1
14	0.919	0.153	0.929	0.074	20
14.9	0.9	0.151	0.908	0.08	21
16	0.906	0.15	0.912	0.106	22.5
17	0.705	-0.07	0.655	0.271	23
18	0.641	-0.07	0.588	0.265	23.6
19	0.646	-0.075	0.587	0.281	24.5
20	0.663	-0.076	0.597	0.298	25.7
22	0.681	-0.076	0.603	0.326	28
24	0.744	-0.079	0.647	0.375	30.5
26	0.798	-0.077	0.683	0.419	32.9
28.1	0.884	-0.075	0.745	0.482	36.3
30	0.994	-0.073	0.824	0.56	38
35	1.33	-0.063	1.05	0.817	39.6
40	1.54	-0.058	1.14	1.03	39.6
45	1.74	-0.046	1.2	1.26	39.6
50	1.77	-0.031	1.12	1.38	39.6
55	2.07	-0.014	1.17	1.7	39.6
60	2.16	0.002	1.08	1.87	39.6
65	2.19	0.012	0.94	1.98	39.6
70	2.35	0.056	0.857	2.19	39.6
74.9	2.27	0.078	0.666	2.17	39.6
79.9	2.26	0.076	0.472	2.21	39.6
84.8	2.34	0.146	0.356	2.32	39.6
89.9	2.09	0.139	0.142	2.09	39.6

Colorado State University Environmental Wind Tunnel Test Data
SERI S809 Airfoil
Reynolds Number = 300,000
Smooth

alpha	Cn	Ct	Cl	Cdp	LFA
deg					deg
0	0.105	-0.0116	0.105	0.0117	1.13
1.99	0.308	0	0.307	0.0116	3.59
4.08	0.544	0.025	0.545	0.0139	8.42
6.11	0.745	0.066	0.748	0.0135	10.7
8.14	0.874	0.105	0.88	0.0198	14.6
10.2	0.87	0.119	0.878	0.036	16.9
11.2	0.862	0.129	0.87	0.0446	17.4
12.2	0.846	0.132	0.854	0.0496	17.9
13.1	0.868	0.139	0.877	0.0619	20.5
14.1	0.884	0.148	0.894	0.0731	21
15.2	0.882	0.15	0.891	0.0865	22.4
16.3	0.777	0.003	0.745	0.22	23
17.2	0.638	-0.062	0.591	0.248	23.3
18.1	0.645	-0.067	0.592	0.265	23.7
19.2	0.64	-0.073	0.58	0.279	24.5
20.2	0.67	-0.071	0.604	0.298	26
22.1	0.666	-0.077	0.582	0.323	28.2
26.2	0.782	-0.075	0.669	0.412	34.3
30.2	1.14	-0.071	0.946	0.633	39.2
35.2	1.3	-0.063	1.02	0.799	46.1
40.3	1.46	-0.051	1.08	0.983	51.8
45.2	1.79	-0.05	1.23	1.31	56.7
45.1	1.66	-0.054	1.13	1.21	56.2
50	1.94	-0.047	1.21	1.51	59.1
60	2.14	-0.019	1.05	1.86	59.1
69.9	2.41	-0.024	0.805	2.27	59.1
80	2.2	0.076	0.456	2.16	59.1
90	2.24	0.132	0.128	2.24	59.1

Colorado State University Environmental Wind Tunnel Test Data
SERI S809 Airfoil
Reynolds Number = 650,000
Wind Turbine Roughness (Very Rough, LE Wrap Around)

alpha	Cn	Ct	Cl	Cdp	LFA	Pdyn	Ptp
deg					deg	psi	psi
0	0.115	-0.009	0.115	0.009	0.956	0.044	0.044
1.8	0.291	-0.0001	0.291	0.009	3.8	0.045	0.046
3.98	0.483	0.022	0.483	0.012	7.52	0.046	0.046
6.01	0.603	0.043	0.604	0.02	10.6	0.046	0.046
8	0.672	0.058	0.674	0.036	13.1	0.045	0.046
10.1	0.696	0.075	0.699	0.047	15.7	0.046	0.046
11.1	0.724	0.082	0.726	0.059	17	0.047	0.047
12.2	0.709	0.08	0.71	0.071	17.9	0.047	0.047
13.1	0.681	0.063	0.677	0.092	18.7	0.047	0.047
14.1	0.647	0.041	0.638	0.119	19.8	0.046	0.048
15.2	0.657	0.014	0.637	0.158	21	0.047	0.048
16.2	0.852	0.019	0.823	0.219	22.7	0.047	0.048
17.1	0.951	0.022	0.915	0.259	24	0.046	0.045
18.2	0.988	0.054	0.956	0.257	24.7	0.046	0.045
19.2	0.957	0.035	0.915	0.282	25.6	0.045	0.042
20.2	0.784	-0.048	0.719	0.316	26.5	0.045	0.045
22.2	0.774	-0.049	0.698	0.338	29.1	0.044	0.042
24.2	0.736	-0.076	0.639	0.371	31.1	0.044	0.044

Colorado State University Environmental Wind Tunnel Test Data
SERI S809 Airfoil
Reynolds Number = 500,000
Very Rough LE Wrap Around

alpha	Cn	Ct	Cl	Cdp	LFA
deg					deg
0.17	0.113	-0.009	0.113	0.009	0.983
2.12	0.288	0.0001	0.288	0.01	3.73
4.16	0.473	0.021	0.473	0.013	7.54
6.25	0.591	0.043	0.592	0.022	10.7
8.2	0.667	0.058	0.668	0.037	13.2
10.2	0.705	0.076	0.707	0.049	15.7
11.3	0.705	0.083	0.707	0.056	17
12.3	0.704	0.081	0.706	0.071	17.9
14.3	0.642	0.05	0.634	0.109	19.8
15.2	0.632	0.02	0.615	0.146	20.8
16.3	0.698	0.02	0.676	0.175	22.5
17.2	0.786	-0.012	0.747	0.245	23.8
18.2	0.77	-0.045	0.717	0.283	25
19.2	0.726	-0.058	0.666	0.294	25.9
20.3	0.723	-0.075	0.653	0.321	27.1
22.2	0.676	-0.076	0.598	0.326	29.3
24.2	0.733	-0.078	0.636	0.372	30.9

Colorado State University Environmental Wind Tunnel Test Data
SERI S809 Airfoil
Reynolds Number = 300,000
Very Rough LE Wrap Around

alpha	Cn	Ct	Cl	Cdp	LFA
deg					deg
-0.09	0.111	-0.007	0.111	0.007	0.905
1.87	0.295	0.003	0.295	0.006	3.42
3.96	0.472	0.019	0.473	0.013	9.01
6.04	0.618	0.047	0.62	0.017	11
7.98	0.696	0.061	0.698	0.036	13.6
10.1	0.715	0.08	0.718	0.046	15.9
11	0.733	0.086	0.736	0.056	17.4
12.1	0.75	0.091	0.753	0.068	18
13.1	0.739	0.088	0.74	0.081	18.8
14.1	0.76	0.088	0.758	0.099	20.1
15	0.719	0.068	0.712	0.121	21.7
16.1	0.636	-0.071	0.591	0.245	22.8
17.1	0.625	-0.065	0.578	0.247	23.8
18.1	0.639	-0.074	0.584	0.27	24.6
19.2	0.719	-0.05	0.662	0.283	25.5
20.1	0.668	-0.078	0.6	0.305	26.6
22.2	0.685	-0.079	0.605	0.331	29.6
24.2	0.771	-0.076	0.672	0.386	30.4

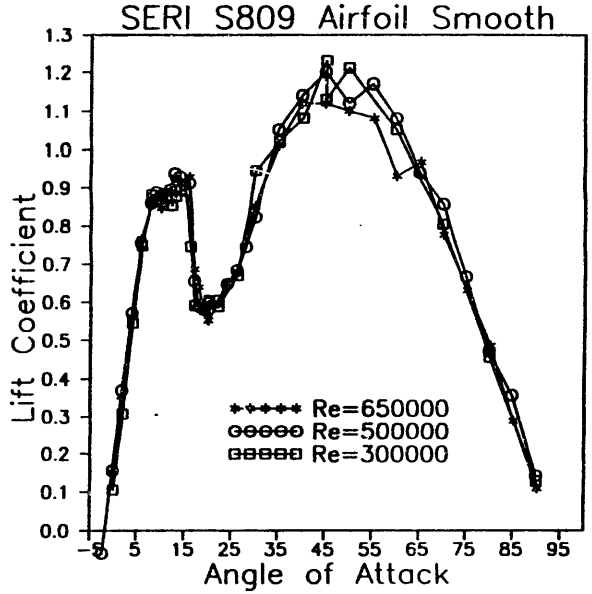
SERI S809 Airfoil Smooth
Lift Coefficient
Angle of Attack
Re=650000
Re=500000
Re=300000

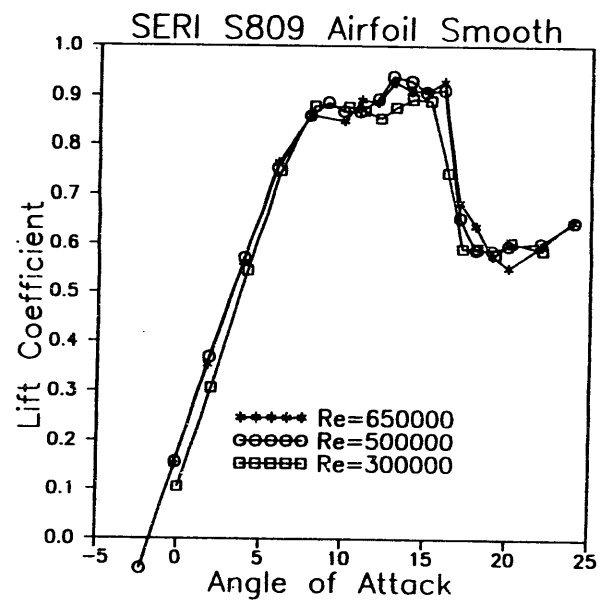
SERI S809 Airfoil Smooth
Lift Coefficient
Angle of Attack
Re=650000
Re=500000
Re=300000

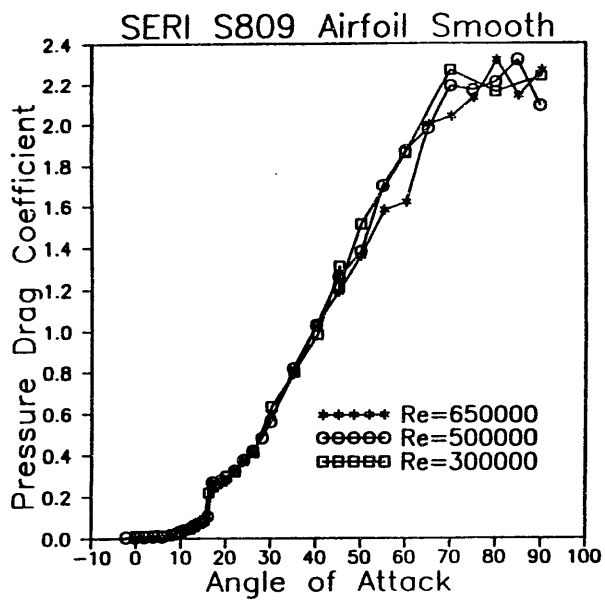
SERI S809 Airfoil Smooth
Pressure Drag Coefficient
Angle of Attack
Re=650000
Re=500000
Re=300000

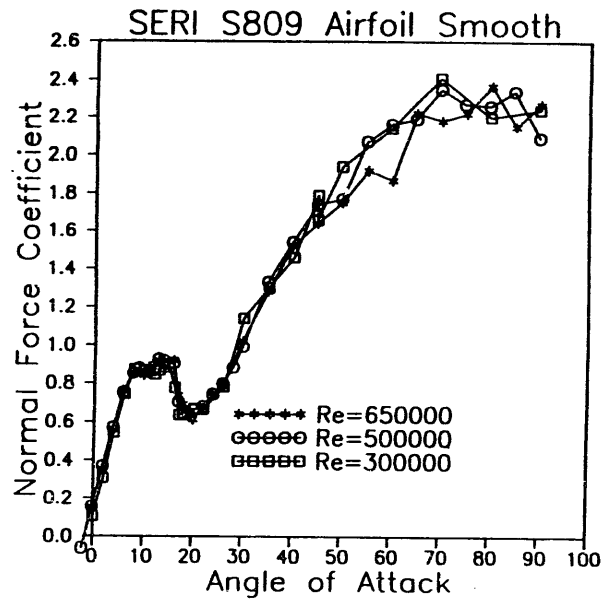
SERI S809 Airfoil Smooth
Normal Force Coefficient
Angle of Attack
Re=650000
Re=500000
Re=300000

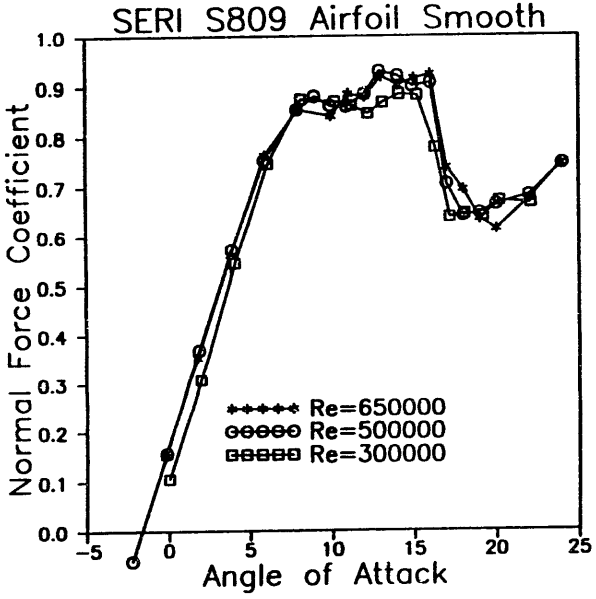
SERI S809 Airfoil Smooth
Normal Force Coefficient
Angle of Attack
Re=650000
Re=500000
Re=300000

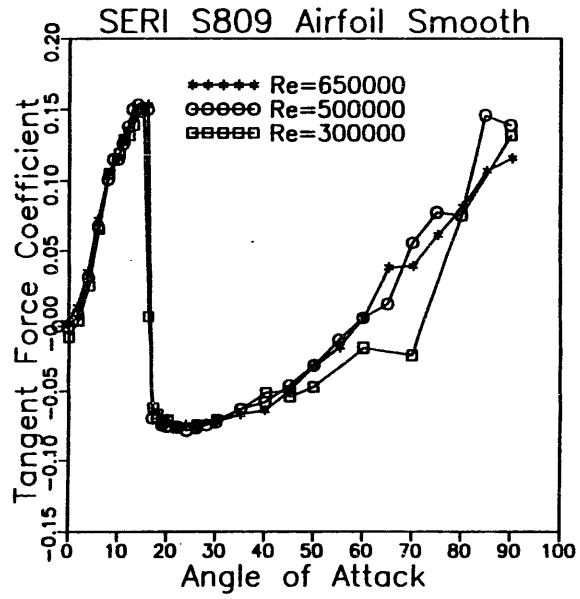
SERI S809 Airfoil Smooth
Tangent Force Coefficient
Angle of Attack
Re=650000
Re=500000
Re=300000

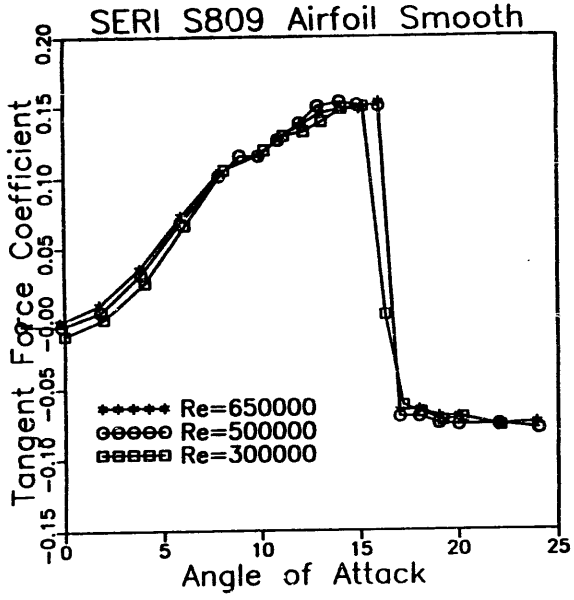
SERI S809 Airfoil Smooth
Tangent Force Coefficient
Angle of Attack
Re=650000
Re=500000
Re=300000

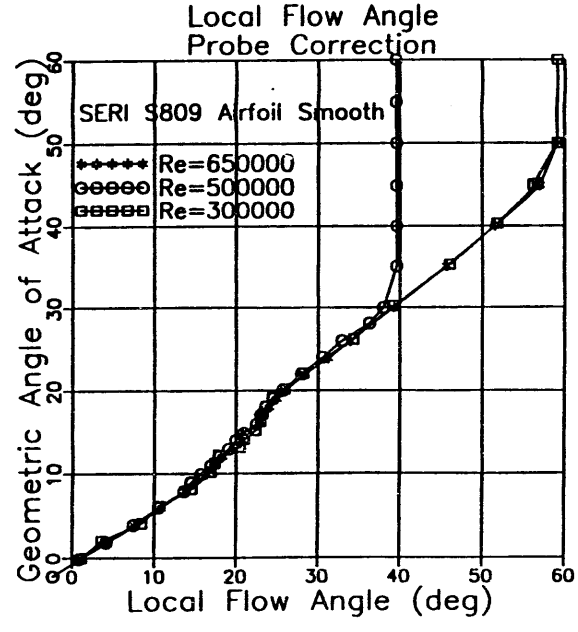
Local Flow Angle
Probe Correction
SERI S809 Airfoil Smooth
Re=650000
Re=500000
Re=300000
Geometric Angle of Attack (deg)
Local Flow Angle (deg)

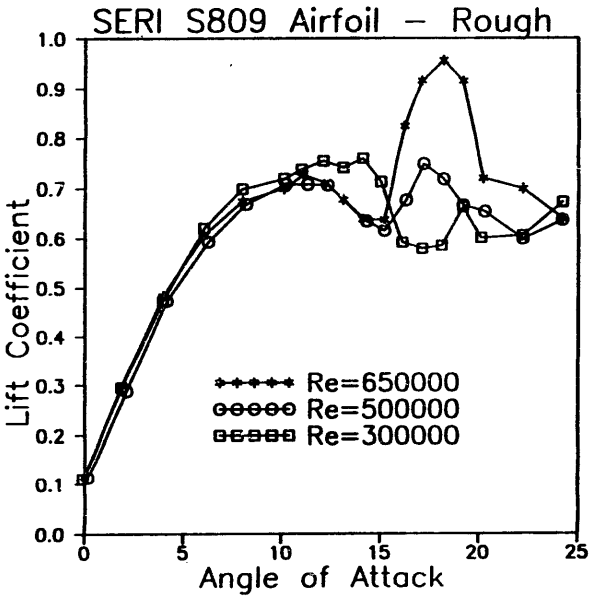
SERI S809 Airfoil – Rough
Lift Coefficient
Angle of Attack
Re=650000
Re=500000
Re=300000

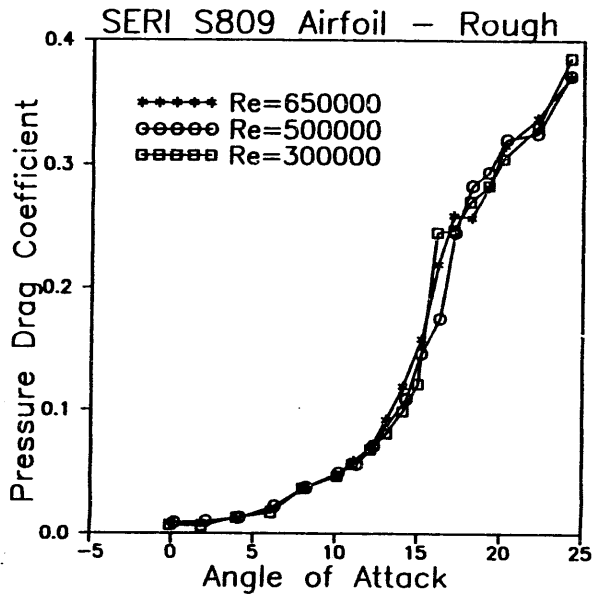
SERI S809 Airfoil – Rough
Pressure Drag Coefficient
Angle of Attack
Re=650000
Re=500000
Re=300000

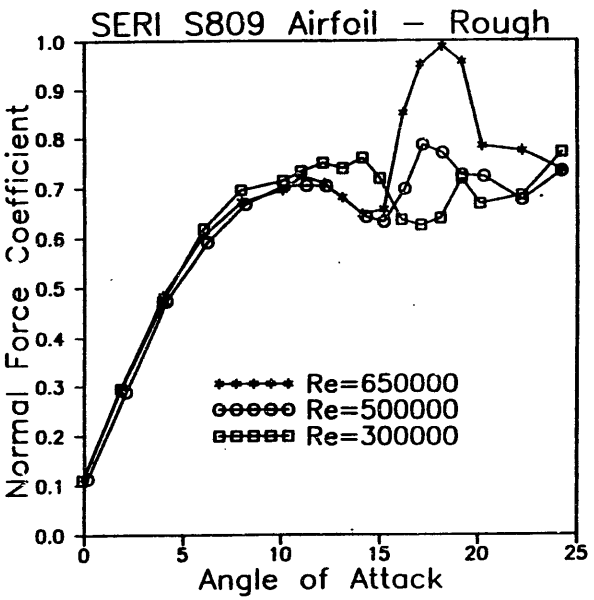
SERI S809 Airfoil – Rough
Normal Force Coefficient
Angle of Attack
Re=650000
Re=500000
Re=300000

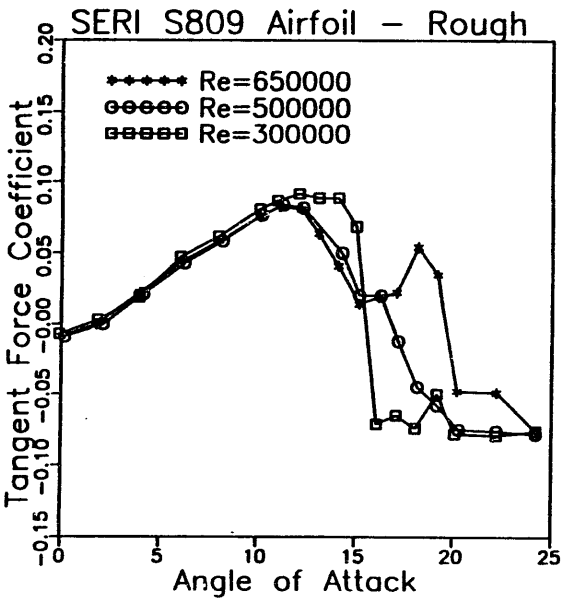
SERI S809 Airfoil – Rough
Tangent Force Coefficient
Angle of Attack
Re=650000
Re=500000
Re=300000

Appendix G

Pressure Distributions for Reynolds Number 650,000 Smooth

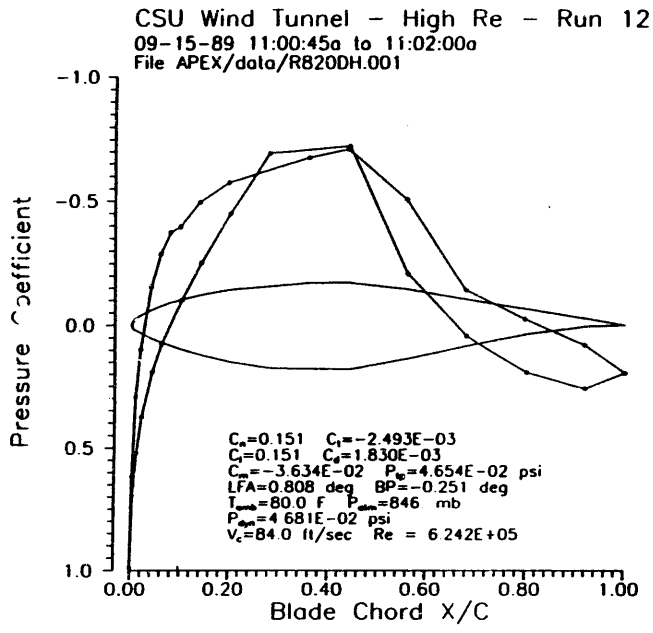
CSU Wind Tunnel – High Re – Run 12
09-15-89 11:00:45a to 11:02:00a
File APEX/data/R820DH.001
Pressure Coefficient
Blade Chord X/C
C_n=0.151 C_t=-2.493E-03
C_l=0.151 C_d=1.830E-03
C_m=-3.634E-02 P_{tp}=4.654E-02 psi
LFA=0.808 deg BP=-0.251 deg
T_{amb}=80.0 F P_{atm}=846. mb
P_{dyn}=4.681E-02 psi
V_c=84.0 ft/sec Re = 6.242E+05

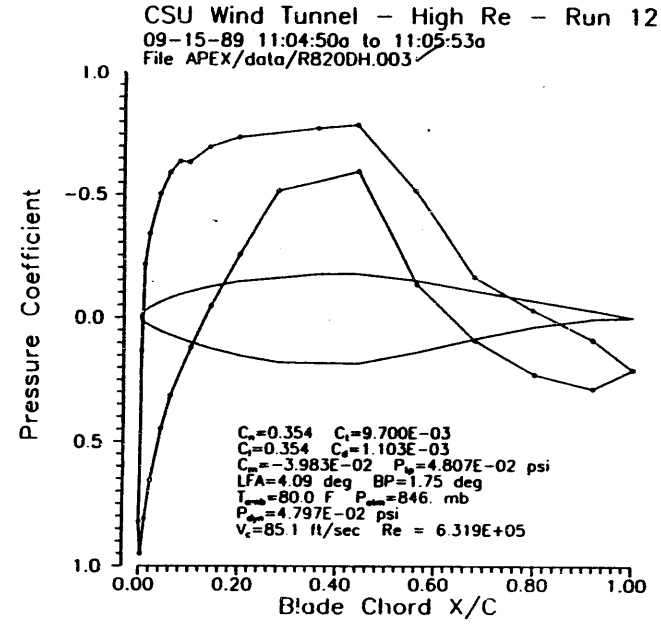
CSU Wind Tunnel – High Re – Run 12
09-15-89 11:04:50a to 11:05:53a
File APEX/data/R820DH.003
Pressure Coefficient
Blade Chord X/C
C_n=0.354 C_t=9.700E-03
C_l=0.354 C_d=1.103E-03
C_m=-3.983E-02 P_{tp}=4.807E-02 psi
LFA=4.09 deg BP=1.75 deg
T_{amb}=80.0 F P_{atm}=846. mb
P_{dyn}=4.797E-02 psi
V_c=85.1 ft/sec Re = 6.319E+05

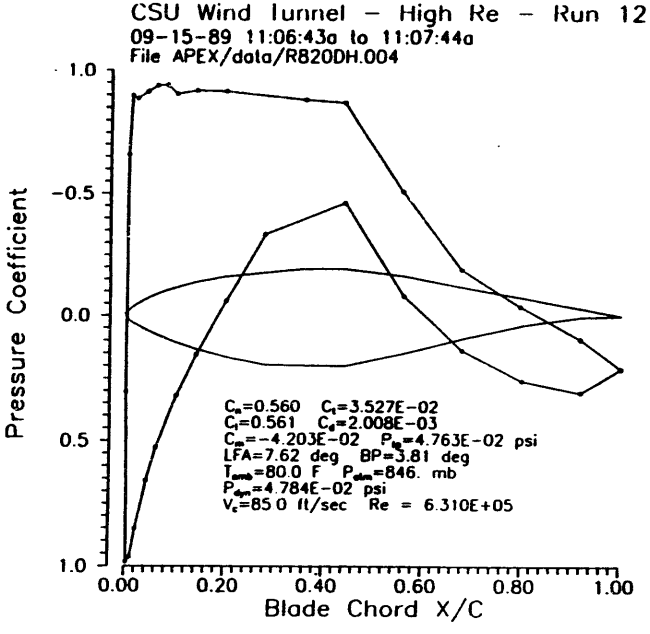
CSU Wind Tunnel – High Re – Run 12
09-15-89 11:06:43a to 11:07:44a
File APEX/data/R820DH.004
Pressure Coefficient
Blade Chord X/C
C_n=0.560 C_t=3.527E-02
C_l=0.561 C_d=2.008E-03
C_m=-4.203E-02 P_{tp}=4.763E-02 psi
LFA=7.62 deg BP=3.81 deg
T_{amb}=80.0 F P_{atm}=846. mb
P_{dyn}=4.784E-02 psi
V_c=85.0 ft/sec Re = 6.310E+05

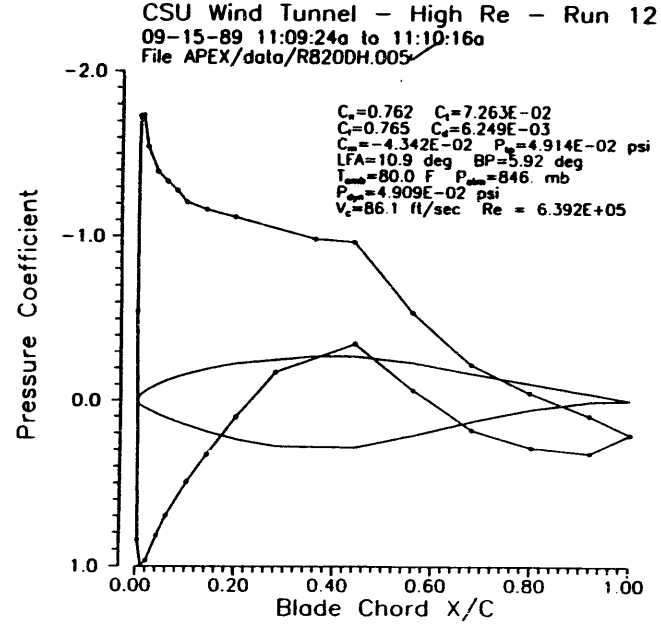
CSU Wind Tunnel – High Re – Run 12
09-15-89 11:09:24a to 11:10:16a
File APEX/data/R820DH.005
Pressure Coefficient
Blade Chord X/C
C_n=0.762 C_t=7.263E-02
C_l=0.765 C_d=6.249E-03
C_m=-4.342E-02 P_{tp}=4.914E-02 psi
LFA=10.9 deg BP=5.92 deg
T_{amb}=80.0 F P_{atm}=846. mb
P_{dyn}=4.909E-02 psi
V_c=86.1 ft/sec Re = 6.392E+05

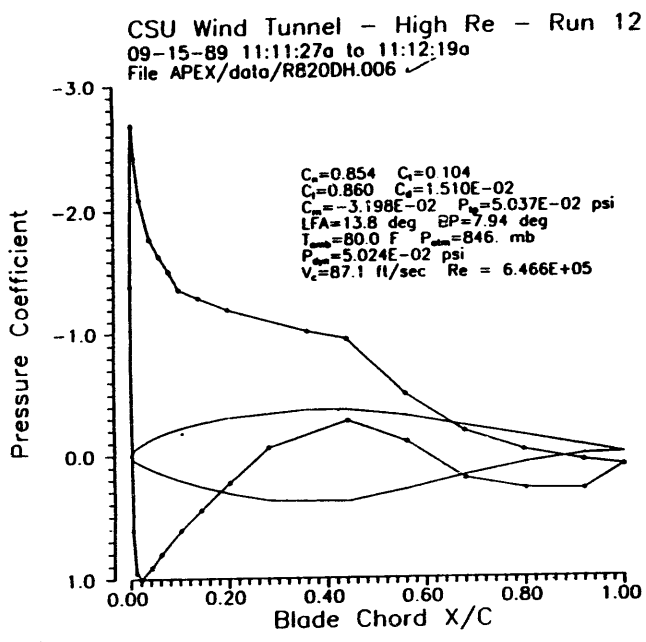
CSU Wind Tunnel – High Re – Run 12
09-15-89 11:11:27a to 11:12:19a
File APEX/data/R820DH.006
C_n=0.854 C_t=0.104
C_l=0.860 C_d=1.510E-02
C_{cm}=-3.198E-02 P_{tp}=5.037E-02 psi
LFA=13.8 deg BP=7.94 deg
T_{amb}=80.0 F P_{atm}=846. mb
P_{dyn}=5.024E-02 psi
V_c=87.1 ft/sec Re = 6.466E+05
Pressure Coefficient
-3.0
-2.0
-1.0
0.0
1.0
0.00
0.20
0.40
0.60
0.80
1.00
Blade Chord X/C

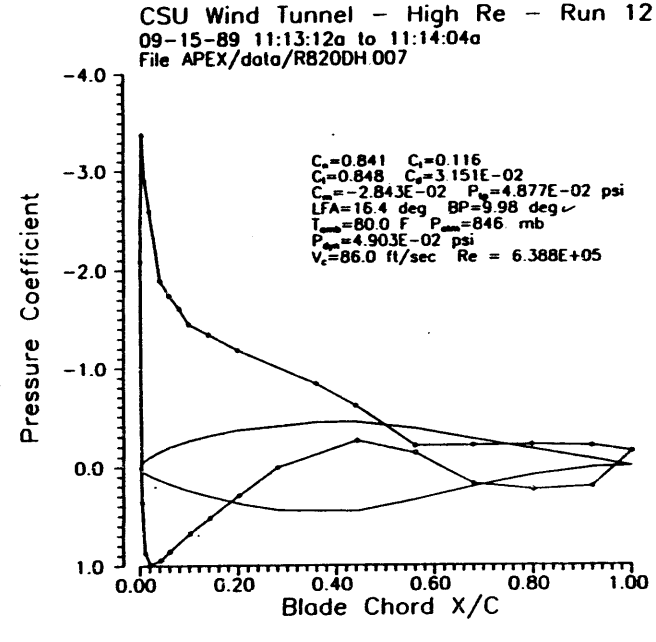
CSU Wind Tunnel – High Re – Run 12
09-15-89 11:13:12a to 11:14:04a
File APEX/data/R820DH.007
C_n=0.841 C_t=0.116
C_l=0.848 C_d=3.151E-02
C_{cm}=-2.843E-02 P_{tp}=4.877E-02 psi
LFA=16.4 deg BP=9.98 deg
T_{amb}=80.0 F P_{atm}=846. mb
P_{dyn}=4.903E-02 psi
V_c=86.0 ft/sec Re = 6.388E+05
Pressure Coefficient
-4.0
-3.0
-2.0
-1.0
0.0
1.0
0.00
0.20
0.40
0.60
0.80
1.00
Blade Chord X/C

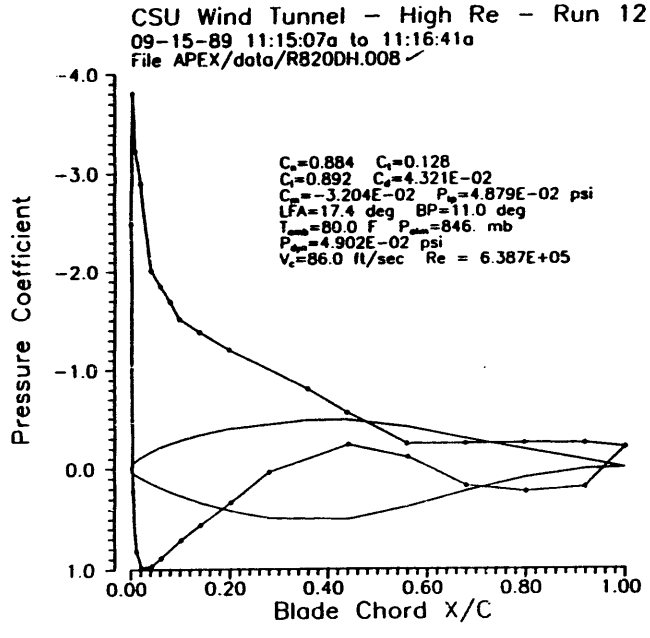
CSU Wind Tunnel – High Re – Run 12
09-15-89 11:15:07a to 11:16:41a
File APEX/data/R820DH.008
C_n=0.884 C_t=0.128
C_l=0.892 C_d=4.321E-02
C_{cm}=-3.204E-02 P_{tp}=4.879E-02 psi
LFA=17.4 deg BP=11.0 deg
T_{amb}=80.0 F P_{atm}=846. mb
P_{dyn}=4.902E-02 psi
V_c=86.0 ft/sec Re = 6.387E+05
Pressure Coefficient
-4.0
-3.0
-2.0
-1.0
0.0
1.0
0.00
0.20
0.40
0.60
0.80
1.00
Blade Chord X/C

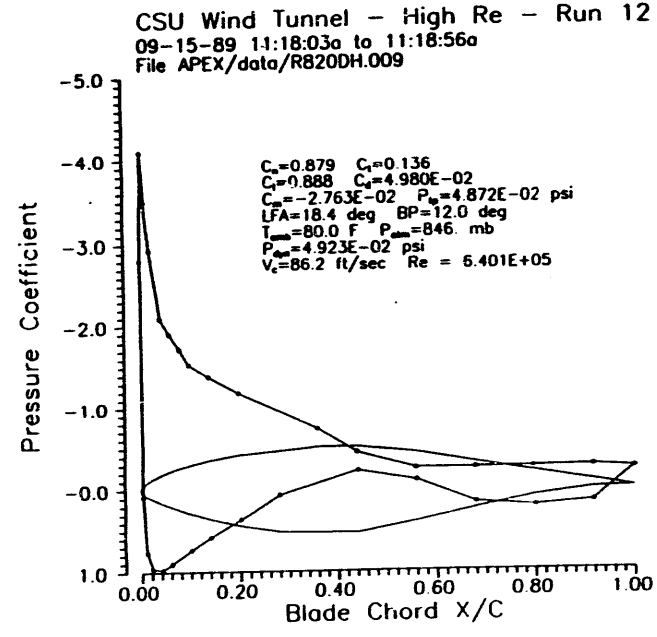
CSU Wind Tunnel – High Re – Run 12
09-15-89 11:18:03a to 11:18:56a
File APEX/data/R820DH.009
C_n=0.879 C_t=0.136
C_l=0.888 C_d=4.980E-02
C_{cm}=-2.763E-02 P_{tp}=4.872E-02 psi
LFA=18.4 deg BP=12.0 deg
T_{amb}=80.0 F P_{atm}=846. mb
P_{dyn}=4.923E-02 psi
V_c=86.2 ft/sec Re = 6.401E+05
Pressure Coefficient
-5.0
-4.0
-3.0
-2.0
-1.0
-0.0
1.0
0.00
0.20
0.40
0.60
0.80
1.00
Blade Chord X/C

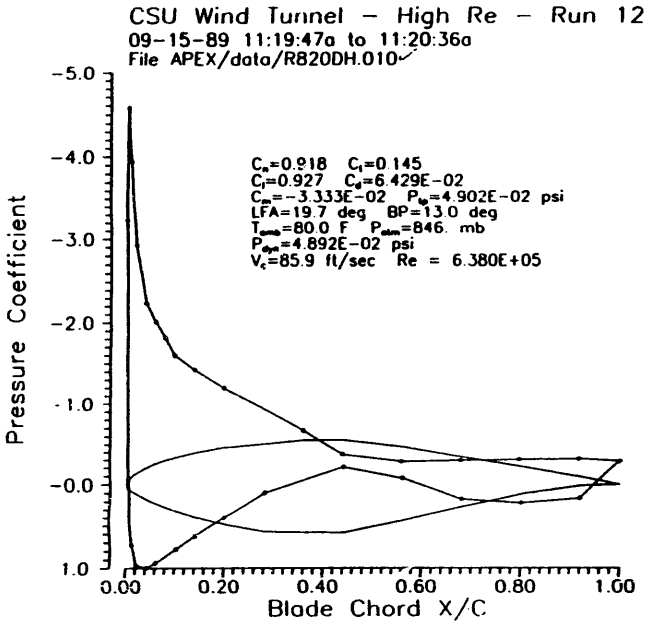
CSU Wind Tunnel – High Re – Run 12
09-15-89 11:19:47a to 11:20:36a
File APEX/data/R820DH.010
C_n=0.918 C_t=0.145
C_l=0.927 C_d=6.429E-02
C_m=-3.333E-02 P_{tp}=4.902E-02 psi
LFA=19.7 deg BP=13.0 deg
T_{amb}=80.0 F P_{atm}=846. mb
P_{dyn}=4.892E-02 psi
V_c=85.9 ft/sec Re = 6.380E+05
Pressure Coefficient
-5.0
-4.0
-3.0
-2.0
-1.0
-0.0
1.0
0.00
0.20
0.40
0.60
0.80
1.00
Blade Chord X/C

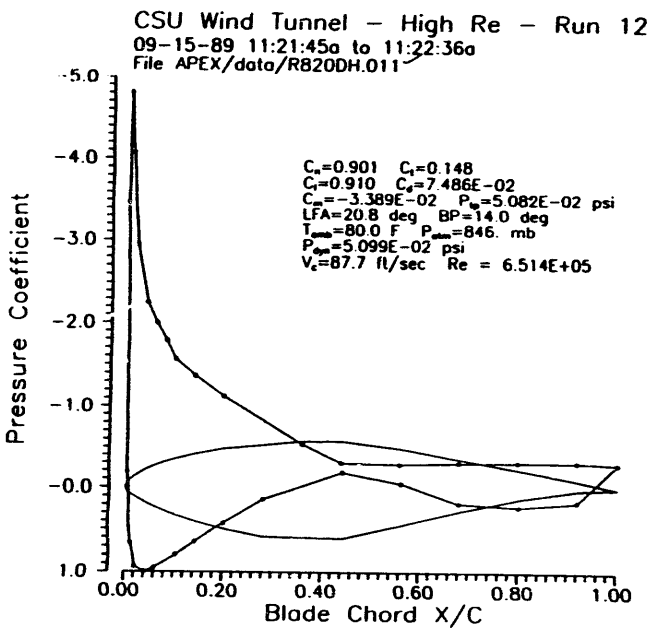
CSU Wind Tunnel – High Re – Run 12
09-15-89 11:21:45a to 11:22:36a
File APEX/data/R820DH.011
C_n=0.901 C_t=0.148
C_l=0.910 C_d=7.486E-02
C_m=-3.389E-02 P_{tp}=5.082E-02 psi
LFA=20.8 deg BP=14.0 deg
T_{amb}=80.0 F P_{atm}=846. mb
P_{dyn}=5.099E-02 psi
V_c=87.7 ft/sec Re = 6.514E+05
Pressure Coefficient
-5.0
-4.0
-3.0
-2.0
-1.0
-0.0
1.0
0.00
0.20
0.40
0.60
0.80
1.00
Blade Chord X/C

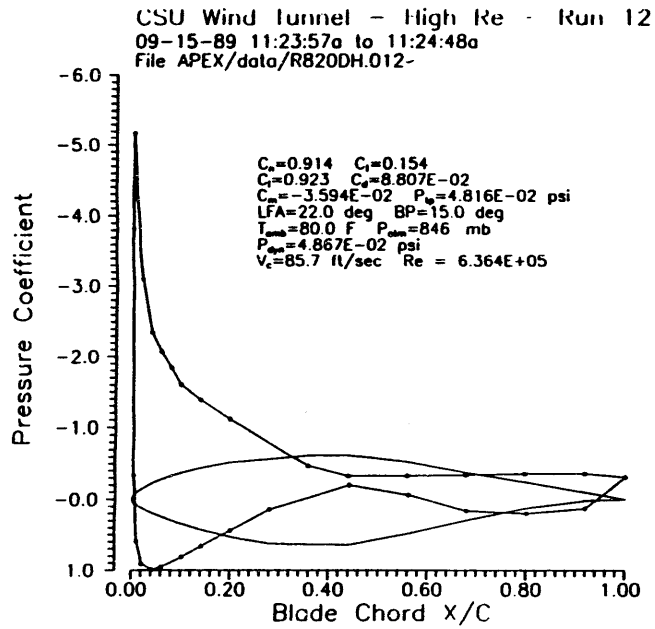
CSU Wind Tunnel – High Re – Run 12
09-15-89 11:23:57a to 11:24:48a
File APEX/data/R820DH.012
C_n=0.914 C_t=0.154
C_l=0.923 C_d=8.807E-02
C_m=-3.594E-02 P_{tp}=4.816E-02 psi
LFA=22.0 deg BP=15.0 deg
T_{amb}=80.0 F P_{atm}=846 mb
P_{dyn}=4.867E-02 psi
V_c=85.7 ft/sec Re = 6.364E+05
Pressure Coefficient
-6.0
-5.0
-4.0
-3.0
-2.0
-1.0
-0.0
1.0
0.00
0.20
0.40
0.60
0.80
1.00
Blade Chord X/C

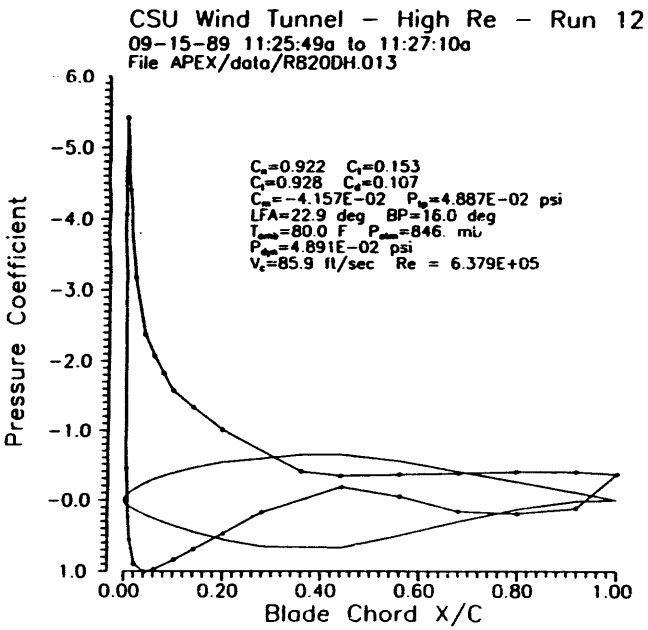
CSU Wind Tunnel – High Re – Run 12
09-15-89 11:25:49a to 11:27:10a
File APEX/data/R820DH.013
C_n=0.922 C_t=0.153
C_l=0.928 C_d=0.107
C_m=-4.157E-02 P_{tp}=4.887E-02 psi
LFA=22.9 deg BP=16.0 deg
T_{amb}=80.0 F P_{atm}=846. mb
P_{dyn}=4.891E-02 psi
V_c=85.9 ft/sec Re = 6.379E+05
Pressure Coefficient
6.0
-5.0
-4.0
-3.0
-2.0
-1.0
-0.0
1.0
0.00
0.20
0.40
0.60
0.80
1.00
Blade Chord X/C

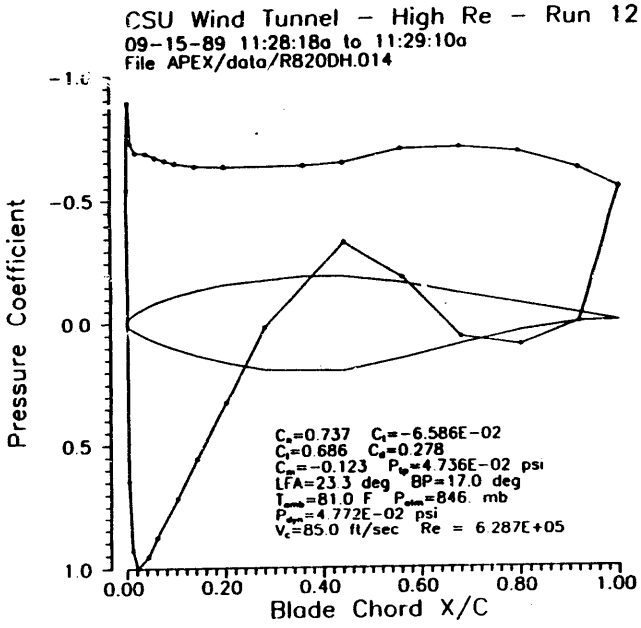
CSU Wind Tunnel – High Re – Run 12
09-15-89 11:28:18a to 11:29:10a
File APEX/data/R820DH.014
Pressure Coefficient
Blade Chord X/C
C_n=0.737 C_t=-6.586E-02
C_l=0.686 C_d=0.278
C_m=-0.123 P_{tp}=4.736E-02 psi
LFA=23.3 deg BP=17.0 deg
T_{amb}=81.0 F P_{atm}=846. mb
P_{dyn}=4.772E-02 psi
V_c=85.0 ft/sec Re = 6.287E+05

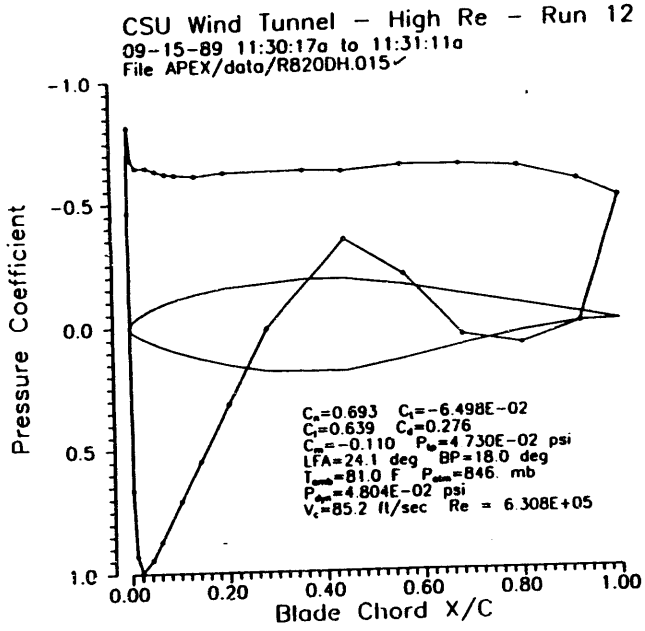
CSU Wind Tunnel – High Re – Run 12
09-15-89 11:30:17a to 11:31:11a
File APEX/data/R820DH.015
Pressure Coefficient
Blade Chord X/C
C_n=0.693 C_t=-6.498E-02
C_l=0.639 C_d=0.276
C_m=-0.110 P_{tp}=4.730E-02 psi
LFA=24.1 deg BP=18.0 deg
T_{amb}=81.0 F P_{atm}=846. mb
P_{dyn}=4.804E-02 psi
V_c=85.2 ft/sec Re = 6.308E+05

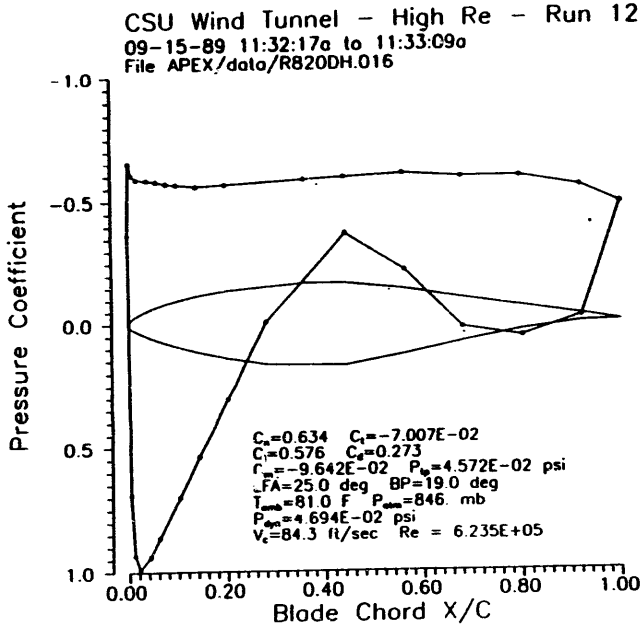
CSU Wind Tunnel – High Re – Run 12
09-15-89 11:32:17a to 11:33:09a
File APEX/data/R820DH.016
Pressure Coefficient
Blade Chord X/C
C_n=0.634 C_t=-7.007E-02
C_l=0.576 C_d=0.273
C_m=-9.642E-02 P_{tp}=4.572E-02 psi
LFA=25.0 deg BP=19.0 deg
T_{amb}=81.0 F P_{atm}=846. mb
P_{dyn}=4.694E-02 psi
V_c=84.3 ft/sec Re = 6.235E+05

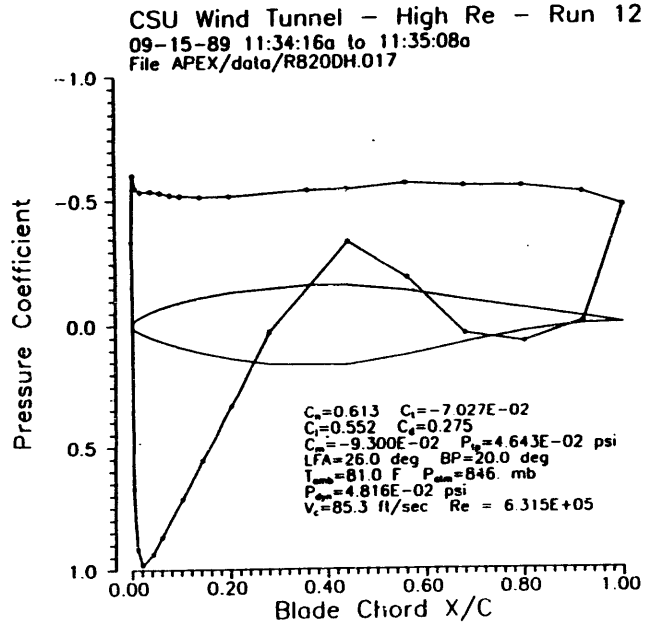
CSU Wind Tunnel – High Re – Run 12
09-15-89 11:34:16a to 11:35:08a
File APEX/data/R820DH.017
Pressure Coefficient
Blade Chord X/C
C_n=0.613 C_t=-7.027E-02
C_l=0.552 C_d=0.275
C_m=-9.300E-02 P_{tp}=4.643E-02 psi
LFA=26.0 deg BP=20.0 deg
T_{amb}=81.0 F P_{atm}=846. mb
P_{dyn}=4.816E-02 psi
V_c=85.3 ft/sec Re = 6.315E+05

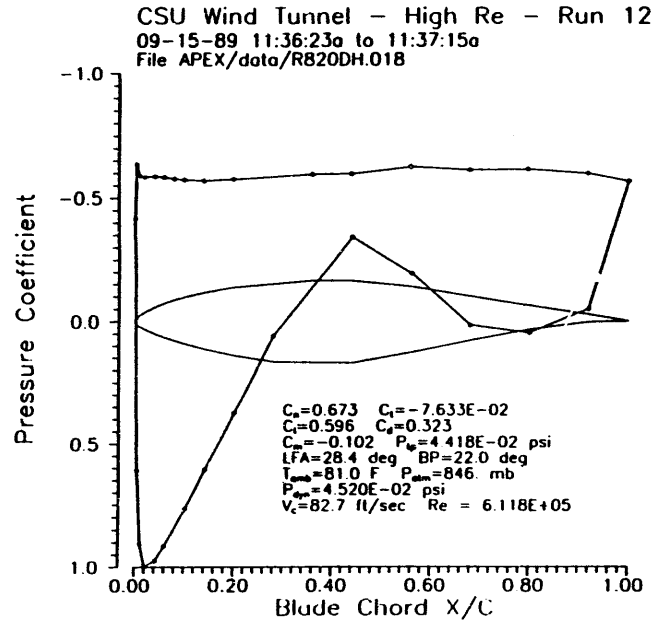
CSU Wind Tunnel – High Re – Run 12
09-15-89 11:36:23a to 11:37:15a
File APEX/data/R820DH.018
Pressure Coefficient
-1.0
-0.5
0.0
0.5
1.0
0.00
0.20
0.40
0.60
0.80
1.00
Blade Chord X/C
C_n=0.673 C_t=-7.633E-02
C_l=0.596 C_d=0.323
C_m=-0.102 P_{tp}=4.418E-02 psi
LFA=28.4 deg BP=22.0 deg
T_{amb}=81.0 F P_{atm}=846. mb
P_{dyn}=4.520E-02 psi
V_c=82.7 ft/sec Re = 6.118E+05

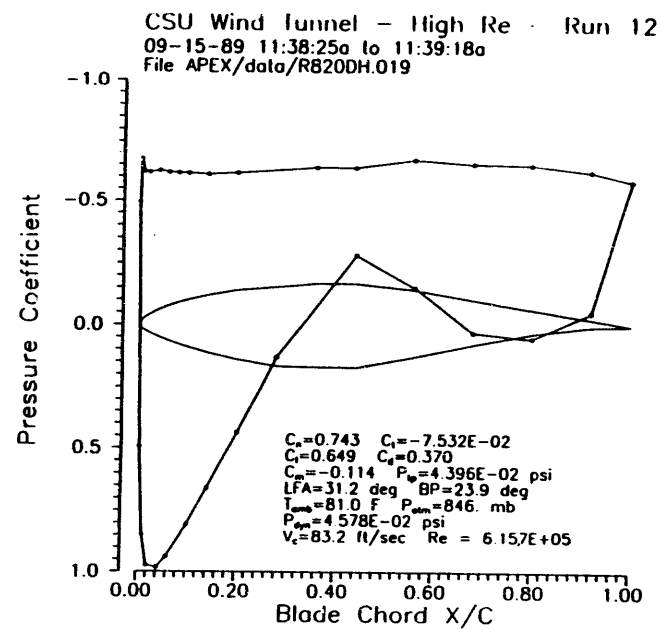
CSU Wind Tunnel – High Re – Run 12
09-15-89 11:38:25a to 11:39:18a
File APEX/data/R820DH.019
Pressure Coefficient
-1.0
-0.5
0.0
0.5
1.0
0.00
0.20
0.40
0.60
0.80
1.00
Blade Chord X/C
C_n=0.743 C_t=-7.532E-02
C_l=0.649 C_d=0.370
C_m=-0.114 P_{tp}=4.396E-02 psi
LFA=31.2 deg BP=23.9 deg
T_{amb}=81.0 F P_{atm}=846. mb
P_{dyn}=4.578E-02 psi
V_c=83.2 ft/sec Re = 6.157E+05

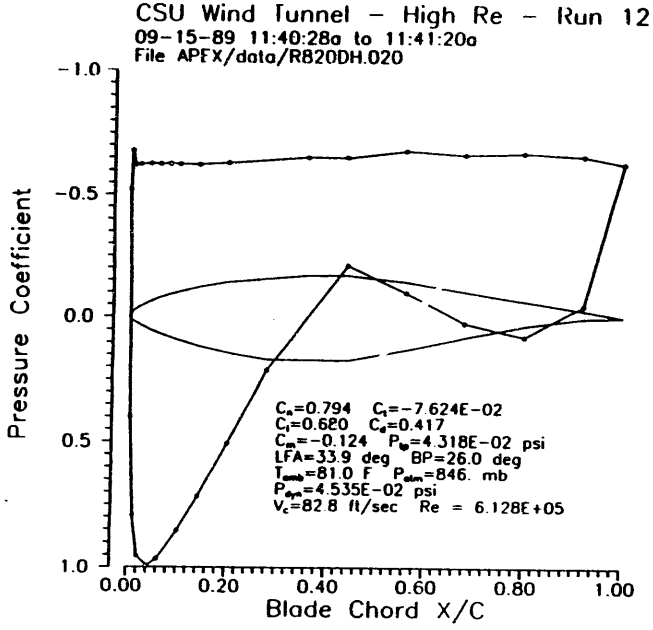
CSU Wind Tunnel – High Re – Run 12
09-15-89 11:40:28a to 11:41:20a
File APEX/data/R820DH.020
Pressure Coefficient
-1.0
-0.5
0.0
0.5
1.0
0.00
0.20
0.40
0.60
0.80
1.00
Blade Chord X/C
C_n=0.794 C_t=-7.624E-02
C_l=0.680 C_d=0.417
C_m=-0.124 P_{tp}=4.318E-02 psi
LFA=33.9 deg BP=26.0 deg
T_{amb}=81.0 F P_{atm}=846. mb
P_{dyn}=4.535E-02 psi
V_c=82.8 ft/sec Re = 6.128E+05

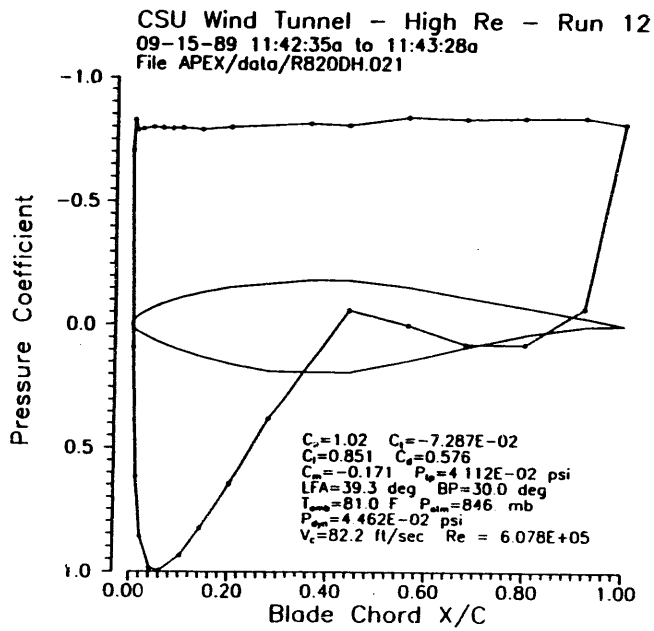
CSU Wind Tunnel – High Re – Run 12
09-15-89 11:42:35a to 11:43:28a
File APEX/data/R820DH.021
Pressure Coefficient
-1.0
-0.5
0.0
0.5
1.0
0.00
0.20
0.40
0.60
0.80
1.00
Blade Chord X/C
C_n=1.02 C_t=-7.287E-02
C_l=0.851 C_d=0.576
C_m=-0.171 P_{tp}=4.112E-02 psi
LFA=39.3 deg BP=30.0 deg
T_{amb}=81.0 F P_{atm}=846 mb
P_{dyn}=4.462E-02 psi
V_c=82.2 ft/sec Re = 6.078E+05

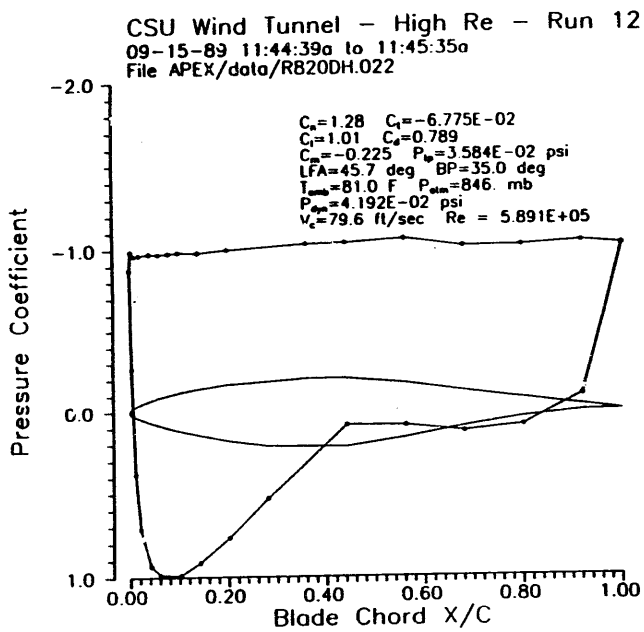
CSU Wind Tunnel – High Re – Run 12
09-15-89 11:44:39a to 11:45:35a
File APEX/data/R820DH.022
C_n=1.28 C_t=-6.775E-02
C_l=1.01 C_d=0.789
C_m=-0.225 P_{tp}=3.584E-02 psi
LFA=45.7 deg BP=35.0 deg
T_{amb}=81.0 F P_{atm}=846. mb
P_{dyn}=4.192E-02 psi
V_c=79.6 ft/sec Re = 5.891E+05
Pressure Coefficient
-2.0
-1.0
0.0
1.0
0.00
0.20
0.40
0.60
0.80
1.00
Blade Chord X/C

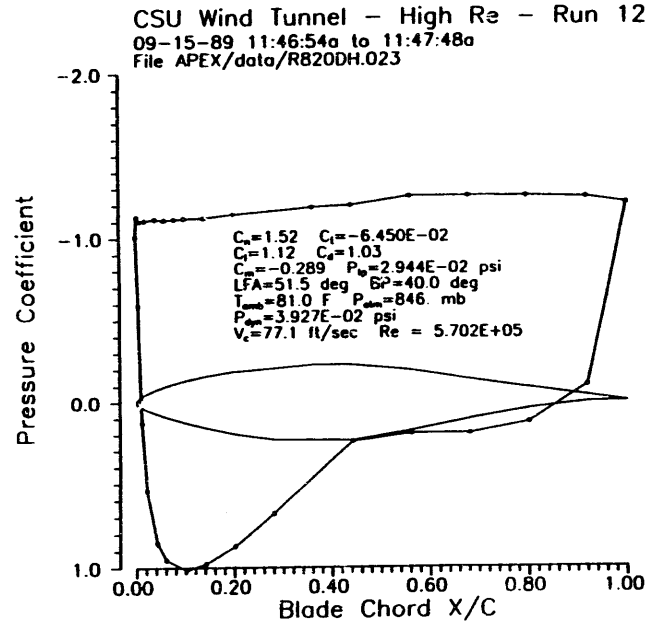
CSU Wind Tunnel – High Re – Run 12
09-15-89 11:46:54a to 11:47:48a
File APEX/data/R820DH.023
C_n=1.52 C_t=-6.450E-02
C_l=1.12 C_d=1.03
C_m=-0.289 P_{tp}=2.944E-02 psi
LFA=51.5 deg BP=40.0 deg
T_{amb}=81.0 F P_{atm}=846. mb
P_{dyn}=3.927E-02 psi
V_c=77.1 ft/sec Re = 5.702E+05
Pressure Coefficient
-2.0
-1.0
0.0
1.0
0.00
0.20
0.40
0.60
0.80
1.00
Blade Chord X/C

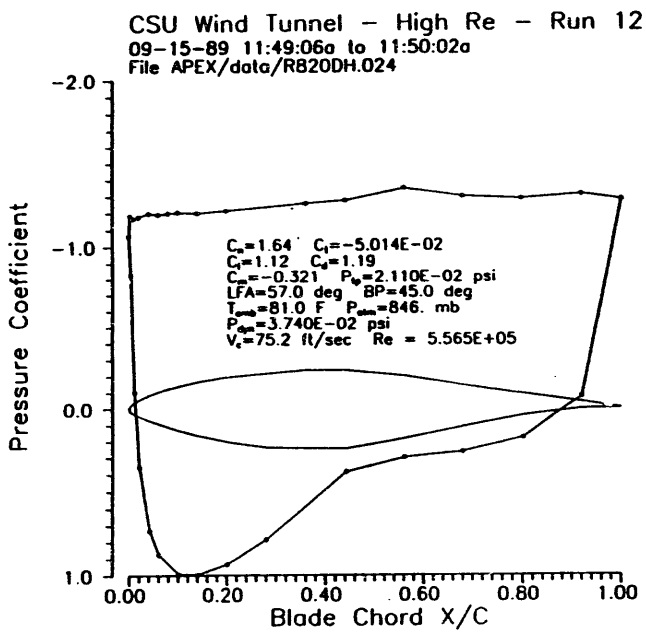
CSU Wind Tunnel – High Re – Run 12
09-15-89 11:49:06a to 11:50:02a
File APEX/data/R820DH.024
C_n=1.64 C_t=-5.014E-02
C_l=1.12 C_d=1.19
C_m=-0.321 P_{tp}=2.110E-02 psi
LFA=57.0 deg BP=45.0 deg
T_{amb}=81.0 F P_{atm}=846. mb
P_{dyn}=3.740E-02 psi
V_c=75.2 ft/sec Re = 5.565E+05
Pressure Coefficient
-2.0
-1.0
0.0
1.0
0.00
0.20
0.40
0.60
0.80
1.00
Blade Chord X/C

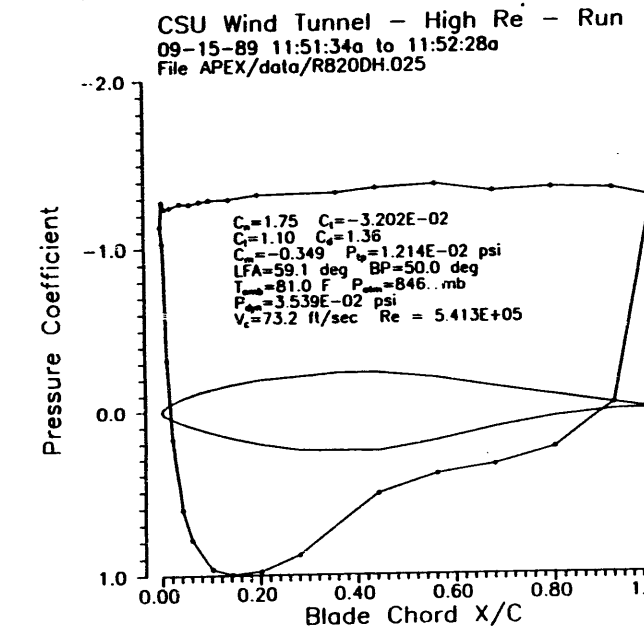
CSU Wind Tunnel – High Re – Run 12
09-15-89 11:51:34a to 11:52:28a
File APEX/data/R820DH.025
C_n=1.75 C_t=-3.202E-02
C_l=1.10 C_d=1.36
C_m=-0.349 P_{tp}=1.214E-02 psi
LFA=59.1 deg BP=50.0 deg
T_{amb}=81.0 F P_{atm}=846. mb
P_{dyn}=3.539E-02 psi
V_c=73.2 ft/sec Re = 5.413E+05
Pressure Coefficient
-2.0
-1.0
0.0
1.0
0.00
0.20
0.40
0.60
0.80
1.00
Blade Chord X/C

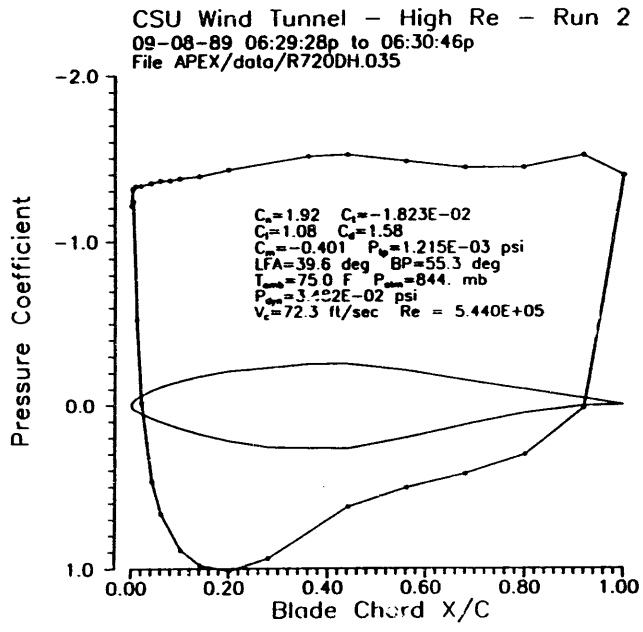
CSU Wind Tunnel – High Re – Run 2
09-08-89 06:29:28p to 06:30:46p
File APEX/data/R720DH.035
C_n=1.92 C_t=-1.823E-02
C_l=1.08 C_d=1.58
C_m=-0.401 P_{tp}=1.215E-03 psi
LFA=39.6 deg BP=55.3 deg
T_{amb}=75.0 F P_{atm}=844. mb
P_{dyn}=3.482E-02 psi
V_c=72.3 ft/sec Re = 5.440E+05
Pressure Coefficient
-2.0
-1.0
0.0
1.0
0.00
0.20
0.40
0.60
0.80
1.00
Blade Chord X/C

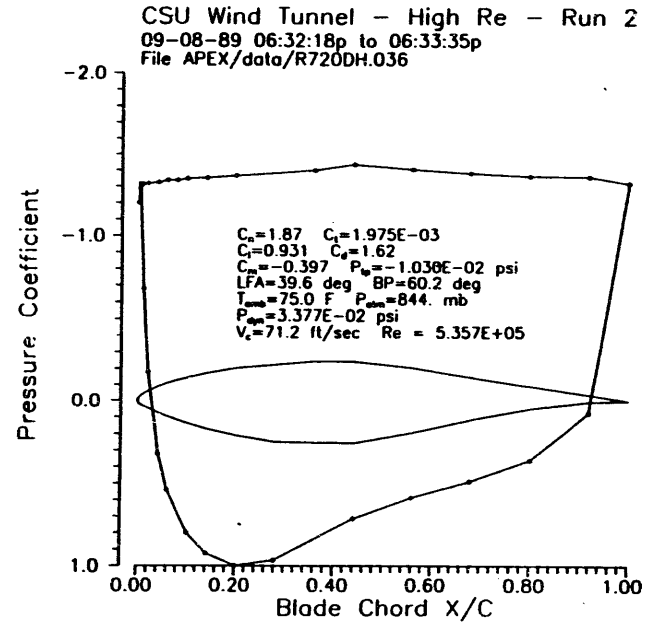
CSU Wind Tunnel – High Re – Run 2
09-08-89 06:32:18p to 06:33:35p
File APEX/data/R720DH.036
C_n=1.87 C_t=1.975E-03
C_l=0.931 C_d=1.62
C_m=-0.397 P_{tp}=-1.038E-02 psi
LFA=39.6 deg BP=60.2 deg
T_{amb}=75.0 F P_{atm}=844. mb
P_{dyn}=3.377E-02 psi
V_c=71.2 ft/sec Re = 5.357E+05
Pressure Coefficient
-2.0
-1.0
0.0
1.0
0.00
0.20
0.40
0.60
0.80
1.00
Blade Chord X/C

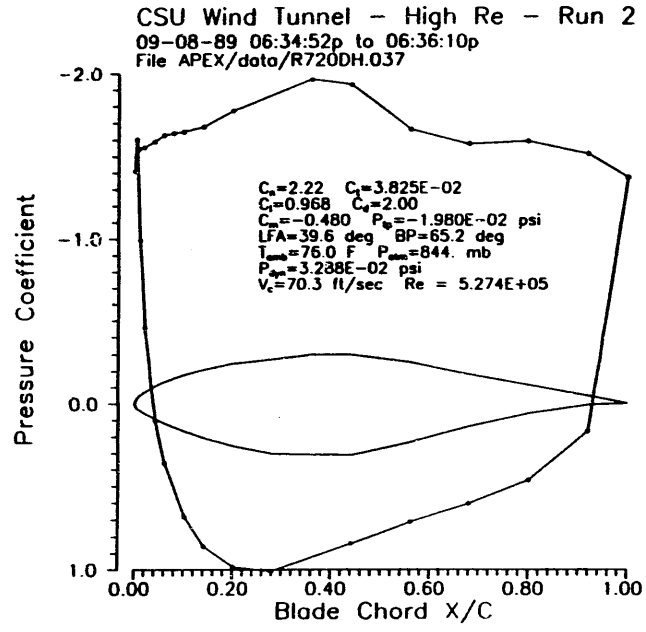
CSU Wind Tunnel – High Re – Run 2
09-08-89 06:34:52p to 06:36:10p
File APEX/data/R720DH.037
C_n=2.22 C_t=3.825E-02
C_l=0.968 C_d=2.00
C_m=-0.480 P_{tp}=-1.980E-02 psi
LFA=39.6 deg BP=65.2 deg
T_{amb}=76.0 F P_{atm}=844. mb
P_{dyn}=3.238E-02 psi
V_c=70.3 ft/sec Re = 5.274E+05
Pressure Coefficient
-2.0
-1.0
0.0
1.0
0.00
0.20
0.40
0.60
0.80
1.00
Blade Chord X/C

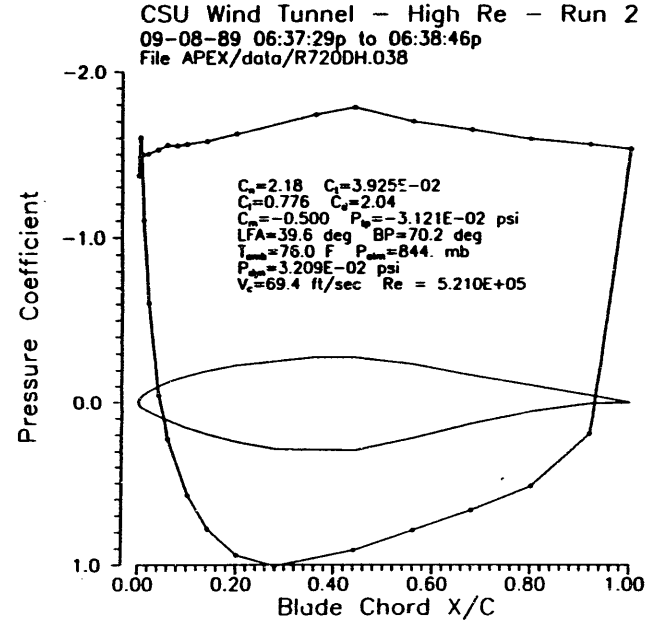
CSU Wind Tunnel – High Re – Run 2
09-08-89 06:37:29p to 06:38:46p
File APEX/data/R720DH.038
C_n=2.18 C_t=3.925E-02
C_l=0.776 C_d=2.04
C_m=-0.500 P_{tp}=-3.121E-02 psi
LFA=39.6 deg BP=70.2 deg
T_{amb}=76.0 F P_{atm}=844. mb
P_{dyn}=3.209E-02 psi
V_c=69.4 ft/sec Re = 5.210E+05
Pressure Coefficient
-2.0
-1.0
0.0
1.0
0.00
0.20
0.40
0.60
0.80
1.00
Blade Chord X/C

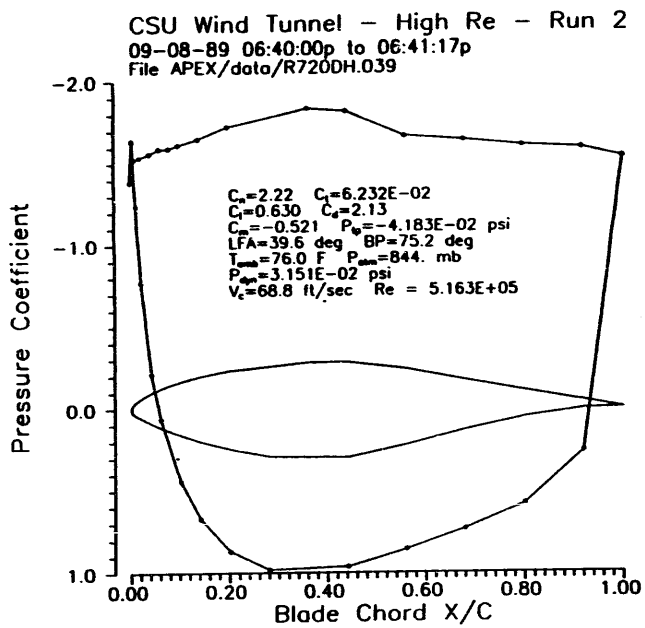
CSU Wind Tunnel – High Re – Run 2
09-08-89 06:40:00p to 06:41:17p
File APEX/data/R720DH.039
C_n=2.22 C_l=6.232E-02
C_l=0.630 C_d=2.13
C_m=-0.521 P_{tp}=-4.183E-02 psi
LFA=39.6 deg BP=75.2 deg
T_{amb}=76.0 F P_{atm}=844. mb
P_{dyn}=3.151E-02 psi
V_c=68.8 ft/sec Re = 5.163E+05
Pressure Coefficient
-2.0
-1.0
0.0
1.0
0.00
0.20
0.40
0.60
0.80
1.00
Blade Chord X/C

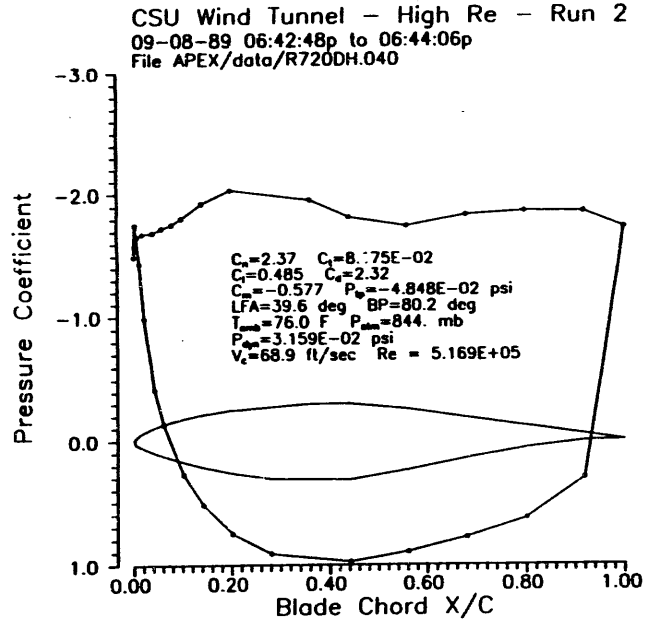
CSU Wind Tunnel – High Re – Run 2
09-08-89 06:42:48p to 06:44:06p
File APEX/data/R720DH.040
C_n=2.37 C_l=8.175E-02
C_l=0.485 C_d=2.32
C_m=-0.577 P_{tp}=-4.848E-02 psi
LFA=39.6 deg BP=80.2 deg
T_{amb}=76.0 F P_{atm}=844. mb
P_{dyn}=3.159E-02 psi
V_c=68.9 ft/sec Re = 5.169E+05
Pressure Coefficient
-3.0
-2.0
-1.0
0.0
1.0
0.00
0.20
0.40
0.60
0.80
1.00
Blade Chord X/C

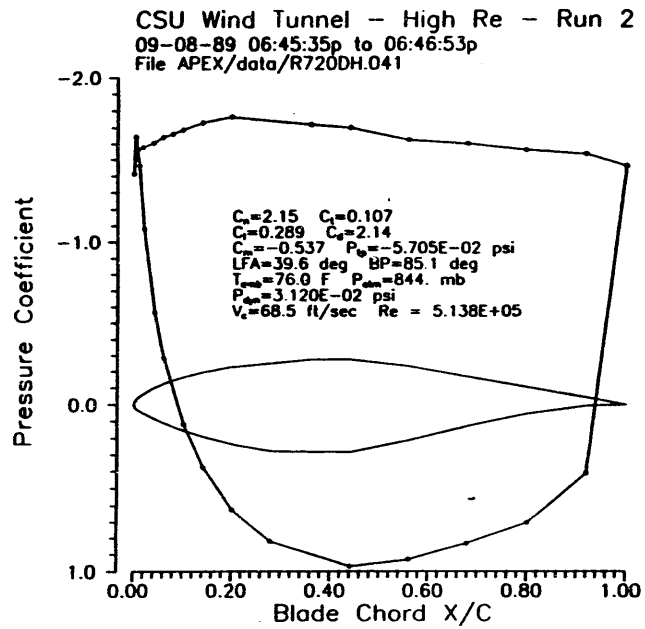
CSU Wind Tunnel – High Re – Run 2
09-08-89 06:45:35p to 06:46:53p
File APEX/data/R720DH.041
C_n=2.15 C_l=0.107
C_l=0.289 C_d=2.14
C_m=-0.537 P_{tp}=-5.705E-02 psi
LFA=39.6 deg BP=85.1 deg
T_{amb}=76.0 F P_{atm}=844. mb
P_{dyn}=3.120E-02 psi
V_c=68.5 ft/sec Re = 5.138E+05
Pressure Coefficient
-2.0
-1.0
0.0
1.0
0.00
0.20
0.40
0.60
0.80
1.00
Blade Chord X/C

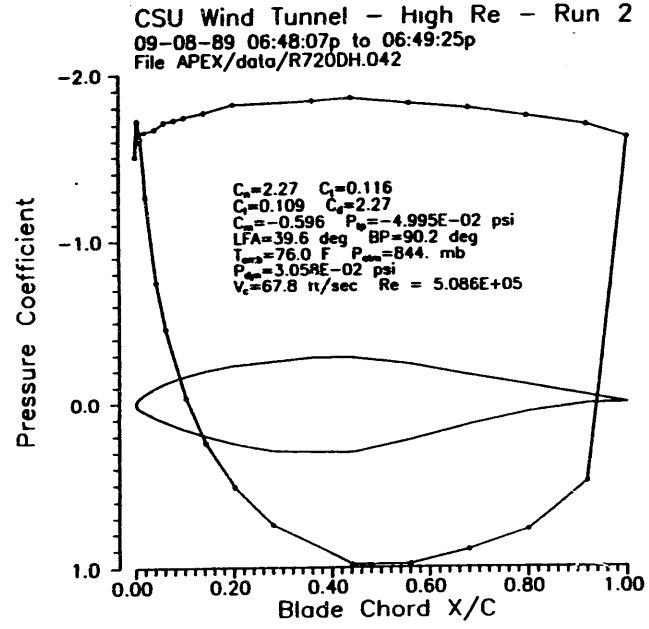
CSU Wind Tunnel – High Re – Run 2
09-08-89 06:48:07p to 06:49:25p
File APEX/data/R720DH.042
C_n=2.27 C_l=0.116
C_l=0.109 C_d=2.27
C_m=-0.596 P_{tp}=-4.995E-02 psi
LFA=39.6 deg BP=90.2 deg
T_{amb}=76.0 F P_{atm}=844. mb
P_{dyn}=3.058E-02 psi
V_c=67.8 ft/sec Re = 5.086E+05
Pressure Coefficient
-2.0
-1.0
0.0
1.0
0.00
0.20
0.40
0.60
0.80
1.00
Blade Chord X/C

Appendix H

Pressure Distributions for Reynolds Number 650,000 Rough

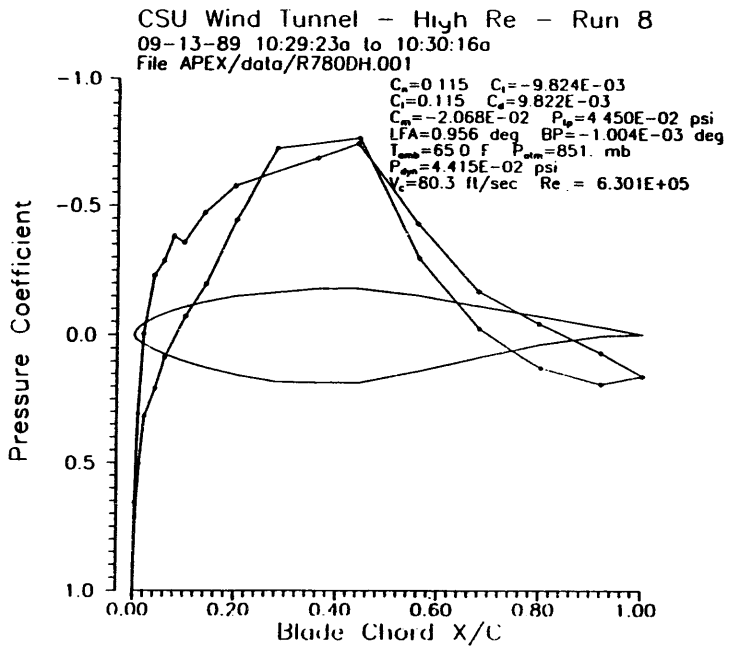
CSU Wind Tunnel – High Re – Run 8
09-13-89 10:29:23a to 10:30:16a
File APEX/data/R780DH.001
C_n=0.115 C_t=-9.824E-03
C_l=0.115 C_d=9.822E-03
C_m=-2.068E-02 P_{tp}=4.450E-02 psi
LFA=0.956 deg BP=-1.004E-03 deg
T_{amb}=65.0 F P_{atm}=851. mb
P_{dyn}=4.415E-02 psi
V_c=80.3 ft/sec Re = 6.301E+05
Pressure Coefficient
-1.0
-0.5
0.0
0.5
1.0
0.00
0.20
0.40
0.60
0.80
1.00
Blade Chord X/C

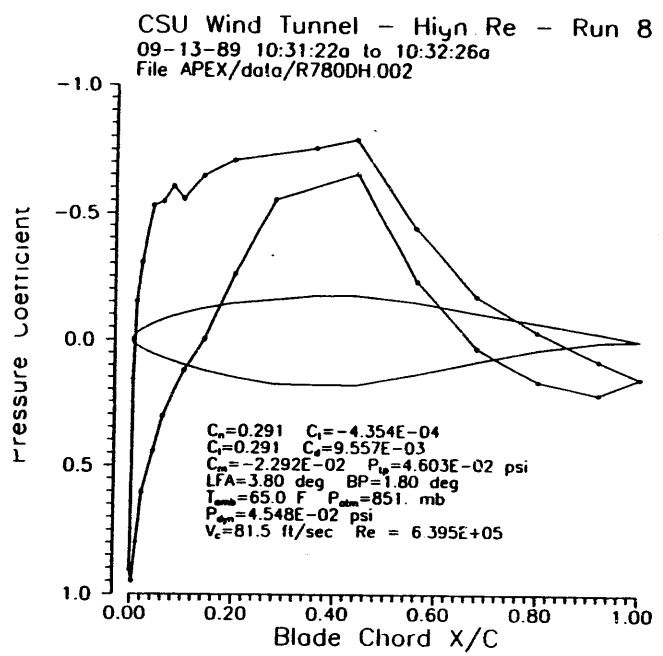
CSU Wind Tunnel – High Re – Run 8
09-13-89 10:31:22a to 10:32:26a
File APEX/data/R780DH.002
C_n=0.291 C_t=-4.354E-04
C_l=0.291 C_d=9.557E-03
C_m=-2.292E-02 P_{tp}=4.603E-02 psi
LFA=3.80 deg BP=1.80 deg
T_{amb}=65.0 F P_{atm}=851. mb
P_{dyn}=4.548E-02 psi
V_c=81.5 ft/sec Re = 6.395E+05
Pressure Coefficient
-1.0
-0.5
0.0
0.5
1.0
0.00
0.20
0.40
0.60
0.80
1.00
Blade Chord X/C

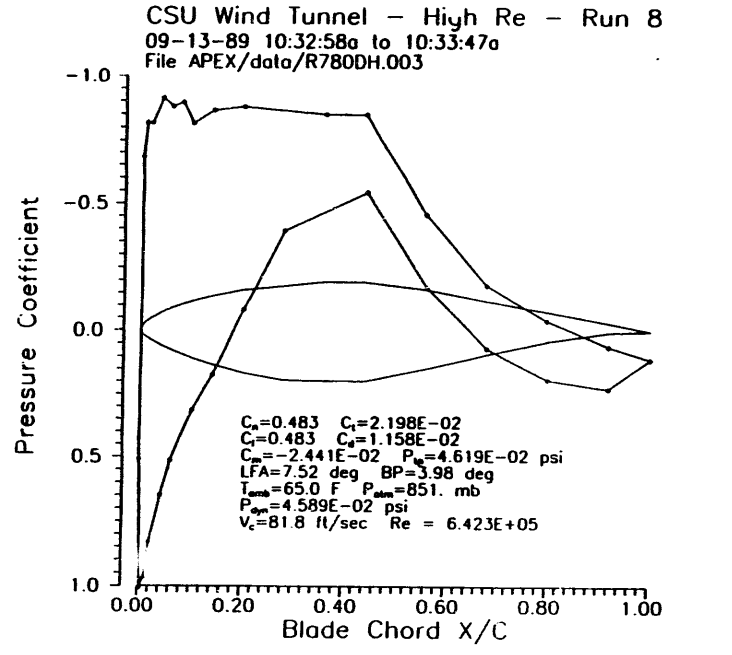
CSU Wind Tunnel – High Re – Run 8
09-13-89 10:32:58a to 10:33:47a
File APEX/data/R780DH.003
C_n=0.483 C_t=2.198E-02
C_l=0.483 C_d=1.158E-02
C_m=-2.441E-02 P_{tp}=4.619E-02 psi
LFA=7.52 deg BP=3.98 deg
T_{amb}=65.0 F P_{atm}=851. mb
P_{dyn}=4.589E-02 psi
V_c=81.8 ft/sec Re = 6.423E+05
Pressure Coefficient
-1.0
-0.5
0.0
0.5
1.0
0.00
0.20
0.40
0.60
0.80
1.00
Blade Chord X/C

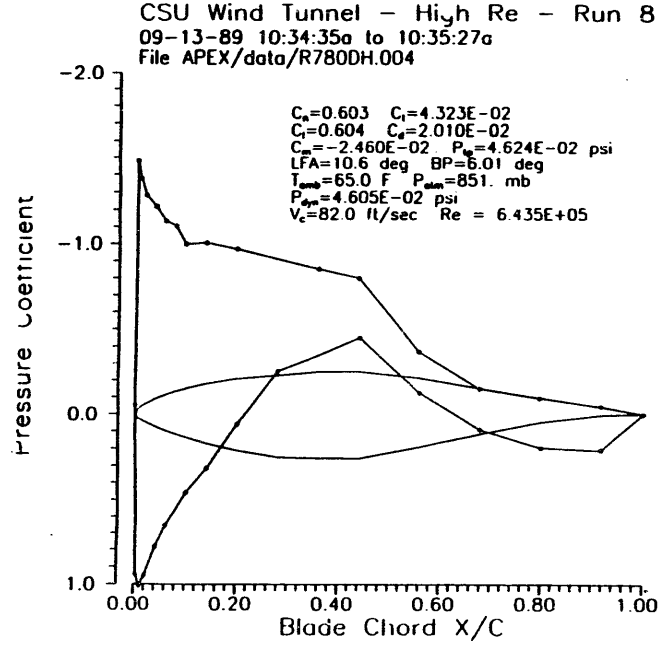
CSU Wind Tunnel – High Re – Run 8
09-13-89 10:34:35a to 10:35:27a
File APEX/data/R780DH.004
C_n=0.603 C_t=4.323E-02
C_l=0.604 C_d=2.010E-02
C_m=-2.460E-02 P_{tp}=4.624E-02 psi
LFA=10.6 deg BP=6.01 deg
T_{amb}=65.0 F P_{atm}=851. mb
P_{dyn}=4.605E-02 psi
V_c=82.0 ft/sec Re = 6.435E+05
Pressure Coefficient
-2.0
-1.0
0.0
1.0
0.00
0.20
0.40
0.60
0.80
1.00
Blade Chord X/C

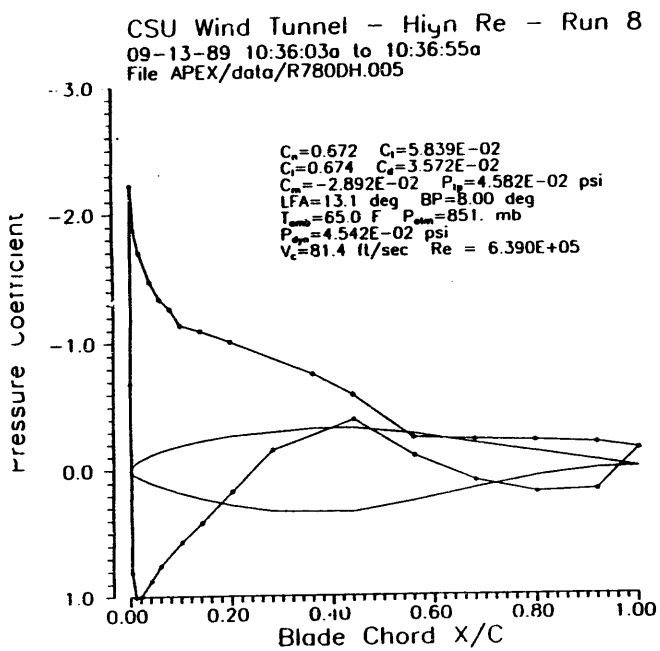
CSU Wind Tunnel - High Re - Run 8
09-13-89 10:36:03a to 10:36:55a
File APEX/data/R780DH.005
C_n=0.672 C_t=5.839E-02
C_l=0.674 C_d=3.572E-02
C_m=-2.892E-02 P_{tp}=4.582E-02 psi
LFA=13.1 deg BP=8.00 deg
T_{amb}=65.0 F P_{atm}=851. mb
P_{dyn}=4.542E-02 psi
V_c=81.4 ft/sec Re = 6.390E+05
Pressure Coefficient
-3.0
-2.0
-1.0
0.0
1.0
0.00
0.20
0.40
0.60
0.80
1.00
Blade Chord X/C

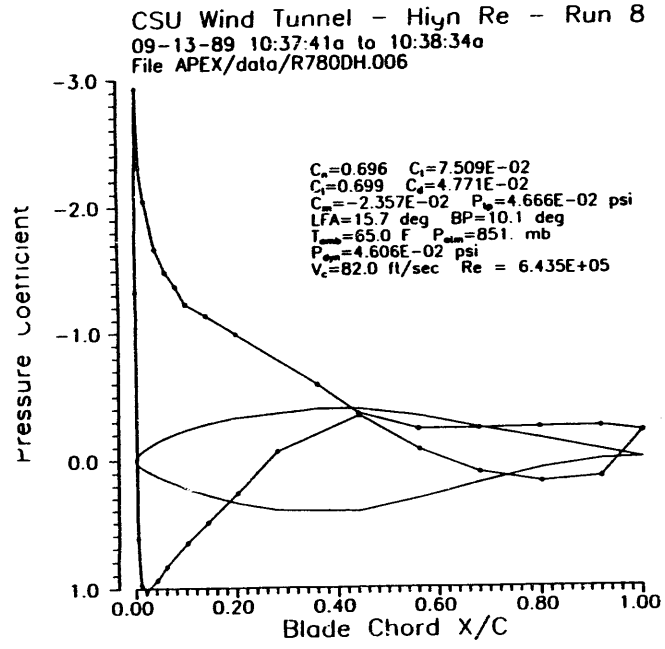
CSU Wind Tunnel - High Re - Run 8
09-13-89 10:37:41a to 10:38:34a
File APEX/data/R780DH.006
C_n=0.696 C_t=7.509E-02
C_l=0.699 C_d=4.771E-02
C_m=-2.357E-02 P_{tp}=4.666E-02 psi
LFA=15.7 deg BP=10.1 deg
T_{amb}=65.0 F P_{atm}=851. mb
P_{dyn}=4.606E-02 psi
V_c=82.0 ft/sec Re = 6.435E+05
Pressure Coefficient
-3.0
-2.0
-1.0
0.0
1.0
0.00
0.20
0.40
0.60
0.80
1.00
Blade Chord X/C

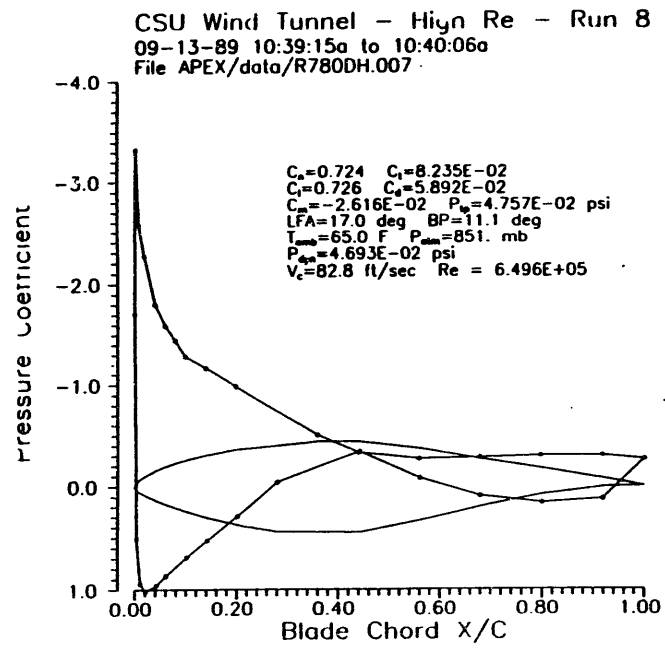
CSU Wind Tunnel - High Re - Run 8
09-13-89 10:39:15a to 10:40:06a
File APEX/data/R780DH.007
C_n=0.724 C_t=8.235E-02
C_l=0.726 C_d=5.892E-02
C_m=-2.616E-02 P_{tp}=4.757E-02 psi
LFA=17.0 deg BP=11.1 deg
T_{amb}=65.0 F P_{atm}=851. mb
P_{dyn}=4.693E-02 psi
V_c=82.8 ft/sec Re = 6.496E+05
Pressure Coefficient
-4.0
-3.0
-2.0
-1.0
0.0
1.0
0.00
0.20
0.40
0.60
0.80
1.00
Blade Chord X/C

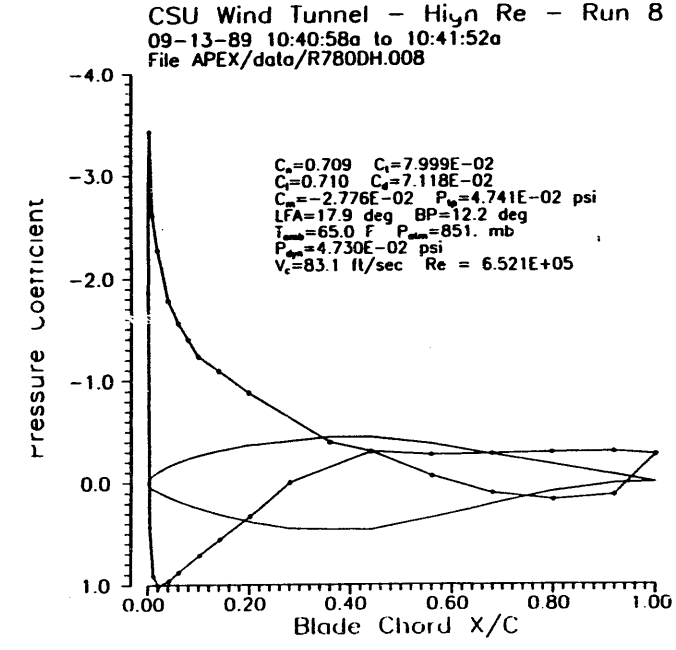
CSU Wind Tunnel - High Re - Run 8
09-13-89 10:40:58a to 10:41:52a
File APEX/data/R780DH.008
C_n=0.709 C_t=7.999E-02
C_l=0.710 C_d=7.118E-02
C_m=-2.776E-02 P_{tp}=4.741E-02 psi
LFA=17.9 deg BP=12.2 deg
T_{amb}=65.0 F P_{atm}=851. mb
P_{dyn}=4.730E-02 psi
V_c=83.1 ft/sec Re = 6.521E+05
Pressure Coefficient
-4.0
-3.0
-2.0
-1.0
0.0
1.0
0.00
0.20
0.40
0.60
0.80
1.00
Blade Chord X/C

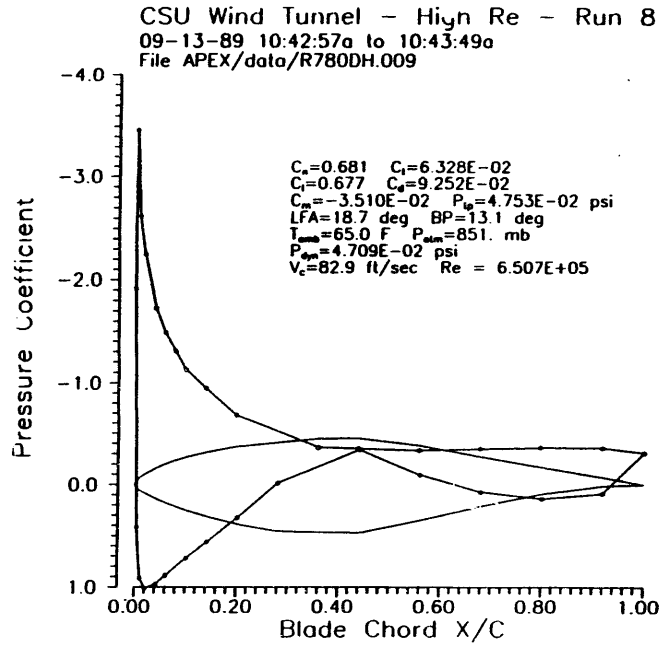
CSU Wind Tunnel – High Re – Run 8
09-13-89 10:42:57a to 10:43:49a
File APEX/data/R780DH.009
C_n=0.681 C_t=6.328E-02
C_l=0.677 C_d=9.252E-02
C_m=-3.510E-02 P_{tp}=4.753E-02 psi
LFA=18.7 deg BP=13.1 deg
T_{amb}=65.0 F P_{atm}=851. mb
P_{dyn}=4.709E-02 psi
V_c=82.9 ft/sec Re = 6.507E+05
Pressure Coefficient
-4.0
-3.0
-2.0
-1.0
0.0
1.0
0.00
0.20
0.40
0.60
0.80
1.00
Blade Chord X/C

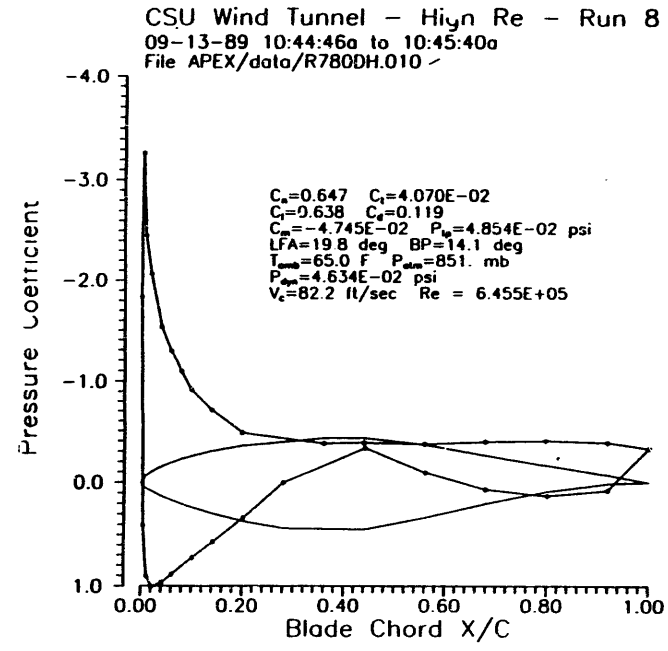
CSU Wind Tunnel – High Re – Run 8
09-13-89 10:44:46a to 10:45:40a
File APEX/data/R780DH.010
C_n=0.647 C_t=4.070E-02
C_l=0.638 C_d=0.119
C_m=-4.745E-02 P_{tp}=4.854E-02 psi
LFA=19.8 deg BP=14.1 deg
T_{amb}=65.0 F P_{atm}=851. mb
P_{dyn}=4.634E-02 psi
V_c=82.2 ft/sec Re = 6.455E+05
Pressure Coefficient
-4.0
-3.0
-2.0
-1.0
0.0
1.0
0.00
0.20
0.40
0.60
0.80
1.00
Blade Chord X/C

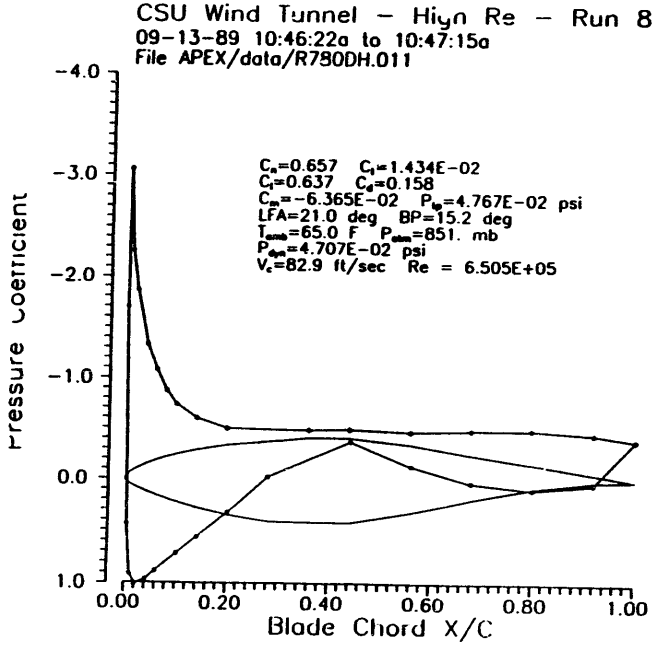
CSU Wind Tunnel – High Re – Run 8
09-13-89 10:46:22a to 10:47:15a
File APEX/data/R780DH.011
C_n=0.657 C_t=1.434E-02
C_l=0.637 C_d=0.158
C_m=-6.365E-02 P_{tp}=4.767E-02 psi
LFA=21.0 deg BP=15.2 deg
T_{amb}=65.0 F P_{atm}=851. mb
P_{dyn}=4.707E-02 psi
V_c=82.9 ft/sec Re = 6.505E+05
Pressure Coefficient
-4.0
-3.0
-2.0
-1.0
0.0
1.0
0.00
0.20
0.40
0.60
0.80
1.00
Blade Chord X/C

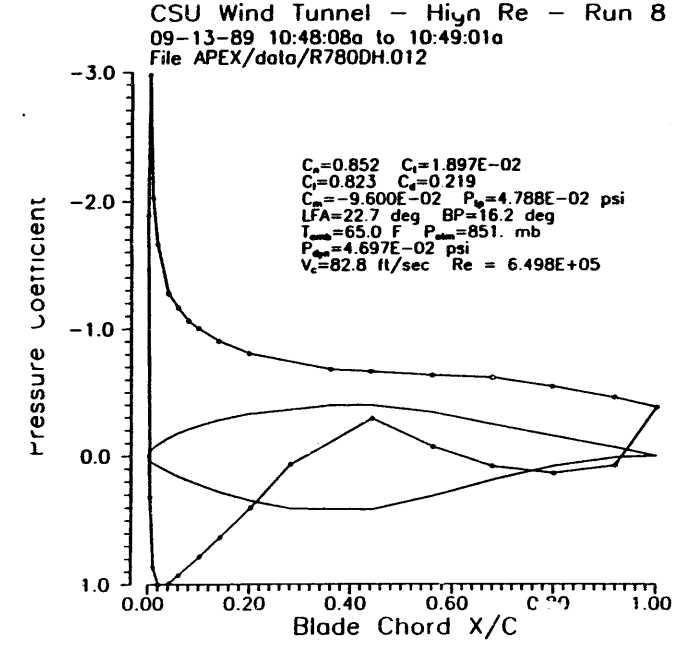
CSU Wind Tunnel – High Re – Run 8
09-13-89 10:48:08a to 10:49:01a
File APEX/data/R780DH.012
C_n=0.852 C_t=1.897E-02
C_l=0.823 C_d=0.219
C_m=-9.600E-02 P_{tp}=4.788E-02 psi
LFA=22.7 deg BP=16.2 deg
T_{amb}=65.0 F P_{atm}=851. mb
P_{dyn}=4.697E-02 psi
V_c=82.8 ft/sec Re = 6.498E+05
Pressure Coefficient
-3.0
-2.0
-1.0
0.0
1.0
0.00
0.20
0.40
0.60
1.00
Blade Chord X/C

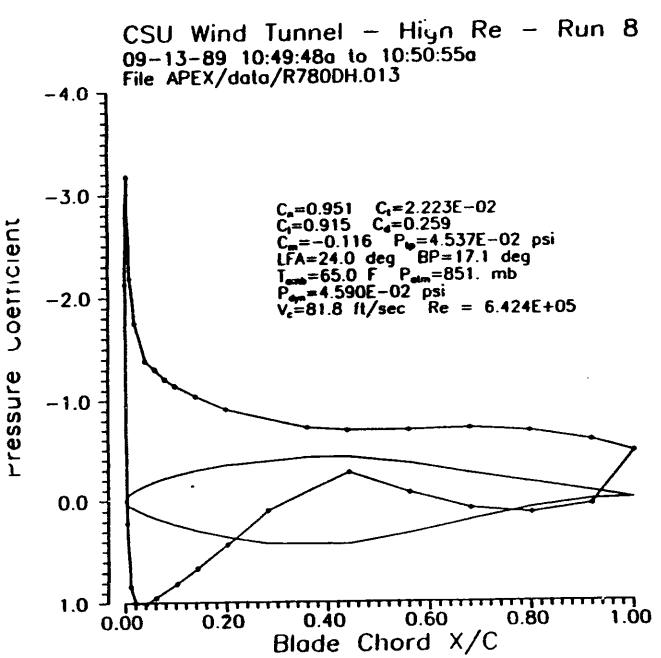
CSU Wind Tunnel - High Re - Run 8
09-13-89 10:49:48a to 10:50:55a
File APEX/data/R780DH.013
C_n=0.951 C_t=2.223E-02
C_l=0.915 C_d=0.259
C_m=-0.116 P_{tp}=4.537E-02 psi
LFA=24.0 deg BP=17.1 deg
T_{amb}=65.0 F P_{atm}=851. mb
P_{dyn}=4.590E-02 psi
V_c=81.8 ft/sec Re = 6.424E+05
Pressure Coefficient
Blade Chord X/C

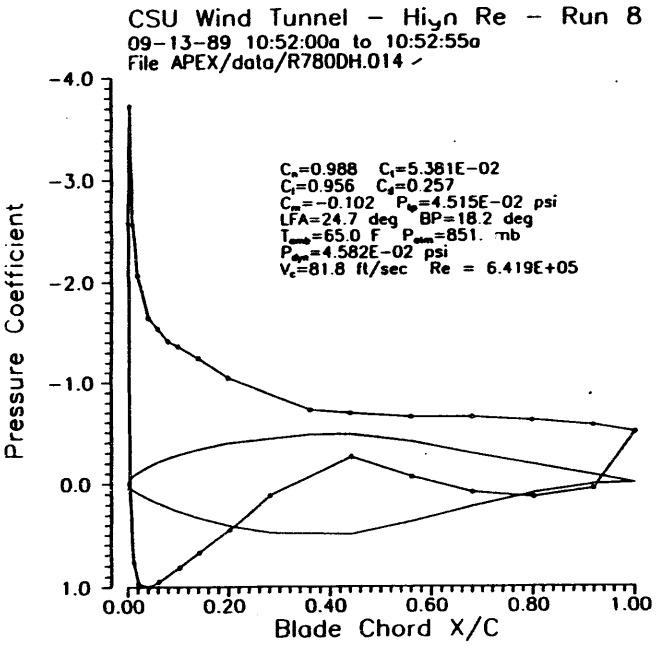
CSU Wind Tunnel - High Re - Run 8
09-13-89 10:52:00a to 10:52:55a
File APEX/data/R780DH.014
C_n=0.988 C_t=5.381E-02
C_l=0.956 C_d=0.257
C_m=-0.102 P_{tp}=4.515E-02 psi
LFA=24.7 deg BP=18.2 deg
T_{amb}=65.0 F P_{atm}=851. mb
P_{dyn}=4.582E-02 psi
V_c=81.8 ft/sec Re = 6.419E+05
Pressure Coefficient
Blade Chord X/C

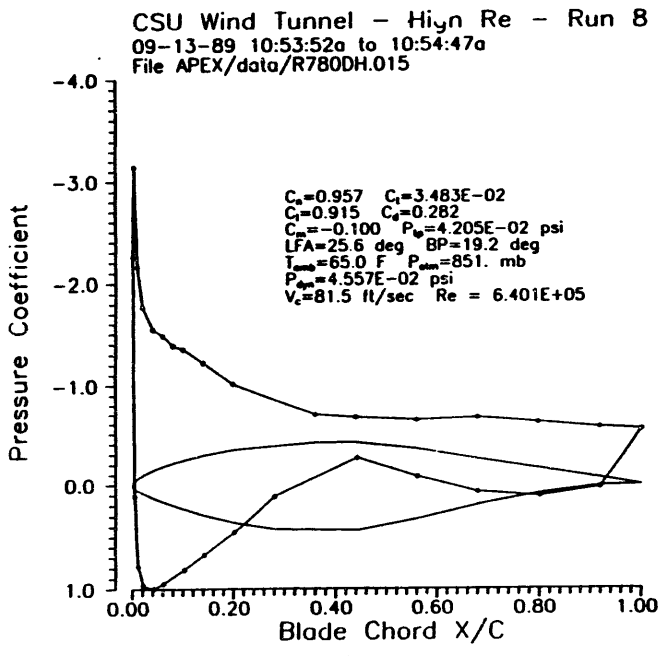
CSU Wind Tunnel - High Re - Run 8
09-13-89 10:53:52a to 10:54:47a
File APEX/data/R780DH.015
C_n=0.957 C_t=3.483E-02
C_l=0.915 C_d=0.282
C_m=-0.100 P_{tp}=4.205E-02 psi
LFA=25.6 deg BP=19.2 deg
T_{amb}=65.0 F P_{atm}=851. mb
P_{dyn}=4.557E-02 psi
V_c=81.5 ft/sec Re = 6.401E+05
Pressure Coefficient
Blade Chord X/C

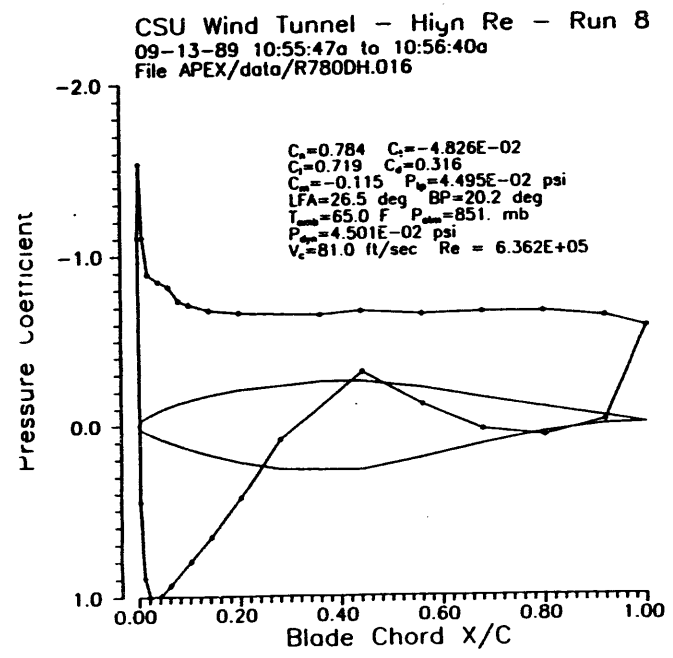
CSU Wind Tunnel - High Re - Run 8
09-13-89 10:55:47a to 10:56:40a
File APEX/data/R780DH.016
C_n=0.784 C_t=-4.826E-02
C_l=0.719 C_d=0.316
C_m=-0.115 P_{tp}=4.495E-02 psi
LFA=26.5 deg BP=20.2 deg
T_{amb}=65.0 F P_{atm}=851. mb
P_{dyn}=4.501E-02 psi
V_c=81.0 ft/sec Re = 6.362E+05
Pressure Coefficient
Blade Chord X/C

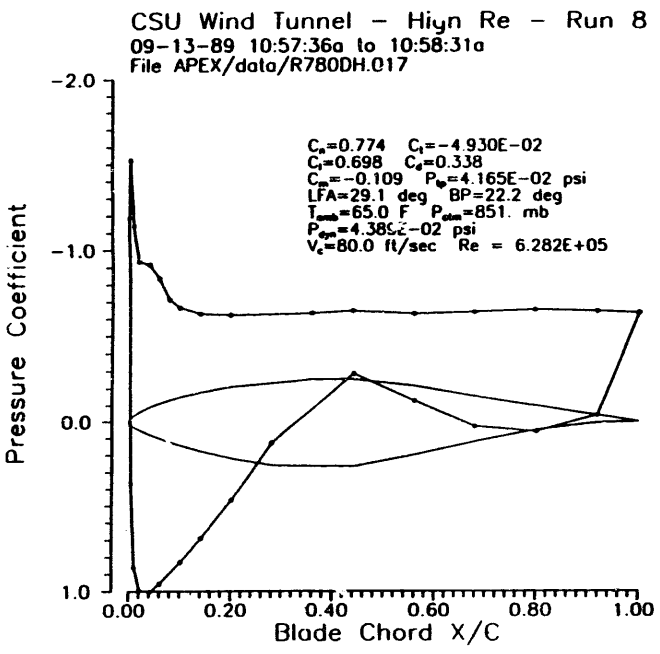
CSU Wind Tunnel - High Re - Run 8
09-13-89 10:57:36a to 10:58:31a
File APEX/data/R780DH.017
C_n=0.774 C_t=-4.930E-02
C_l=0.698 C_d=0.338
C_{cp}=-0.109 P_{tp}=4.165E-02 psi
LFA=29.1 deg BP=22.2 deg
T_{amb}=65.0 F P_{atm}=851. mb
P_{dyn}=4.385E-02 psi
V_c=80.0 ft/sec Re = 6.282E+05
Pressure Coefficient
-2.0
-1.0
0.0
1.0
0.00
0.20
0.40
0.60
0.80
1.00
Blade Chord X/C

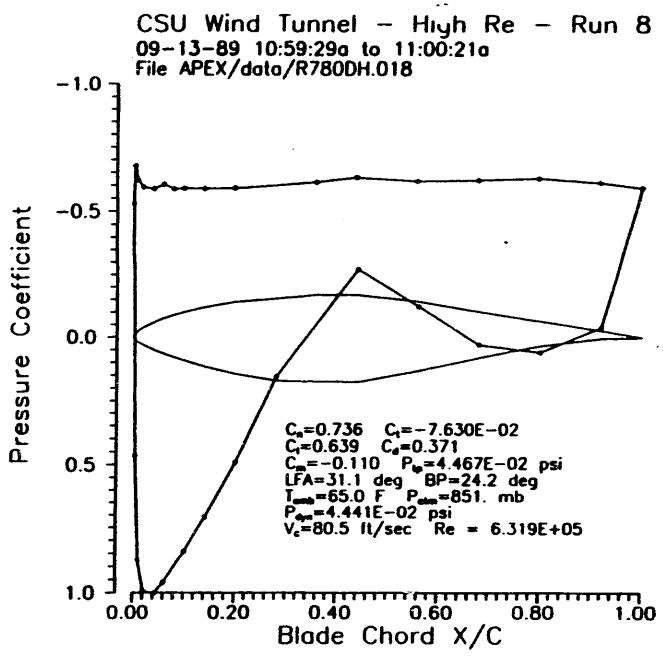
CSU Wind Tunnel - High Re - Run 8
09-13-89 10:59:29a to 11:00:21a
File APEX/data/R780DH.018
C_n=0.736 C_t=-7.630E-02
C_l=0.639 C_d=0.371
C_{cp}=-0.110 P_{tp}=4.467E-02 psi
LFA=31.1 deg BP=24.2 deg
T_{amb}=65.0 F P_{atm}=851. mb
P_{dyn}=4.441E-02 psi
V_c=80.5 ft/sec Re = 6.319E+05
Pressure Coefficient
-1.0
-0.5
0.0
0.5
1.0
0.00
0.20
0.40
0.60
0.80
1.00
Blade Chord X/C

Appendix I

Pressure Distributions for Reynolds Number 500,000 Smooth

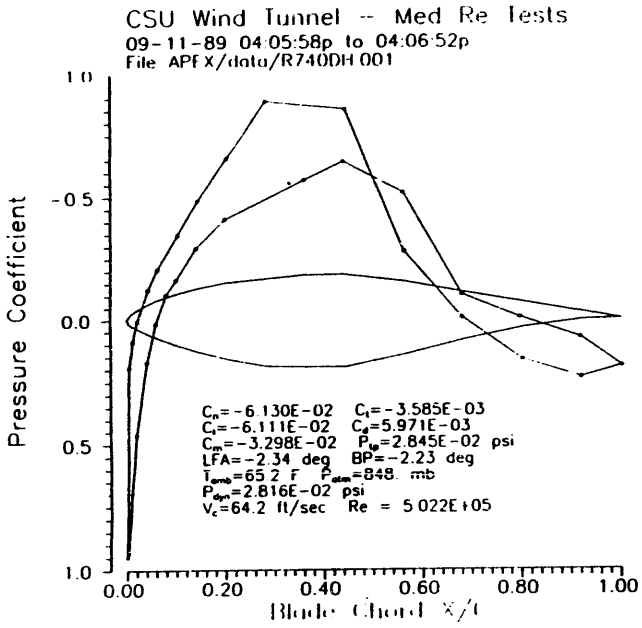
CSU Wind Tunnel -- Med Re Tests
09-11-89 04:05:58p to 04:06:52p
File APEX/data/R740DH.001
Pressure Coefficient
Blade Chord X/C
C_n=-6.130E-02 C_t=-3.585E-03
C_a=-6.111E-02 C_d=5.971E-03
C_m=-3.298E-02 P_{tp}=2.845E-02 psi
LFA=-2.34 deg BP=-2.23 deg
T_{amb}=65.2 F P_{atm}=848. mb
P_{dyn}=2.816E-02 psi
V_c=64.2 ft/sec Re = 5.022E+05

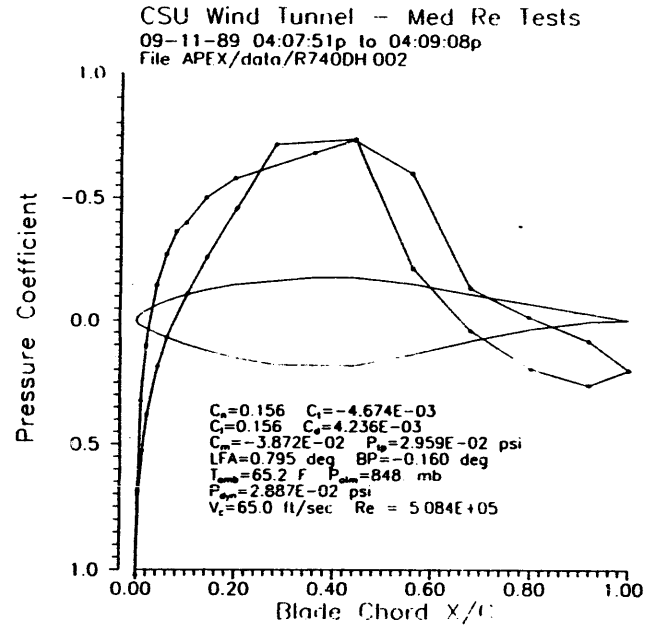
CSU Wind Tunnel -- Med Re Tests
09-11-89 04:07:51p to 04:09:08p
File APEX/data/R740DH.002
Pressure Coefficient
Blade Chord X/C
C_n=0.156 C_t=-4.674E-03
C_l=0.156 C_d=4.236E-03
C_m=-3.872E-02 P_{tp}=2.959E-02 psi
LFA=0.795 deg BP=-0.160 deg
T_{amb}=65.2 F P_{atm}=848. mb
P_{dyn}=2.887E-02 psi
V_c=65.0 ft/sec Re = 5.084E+05

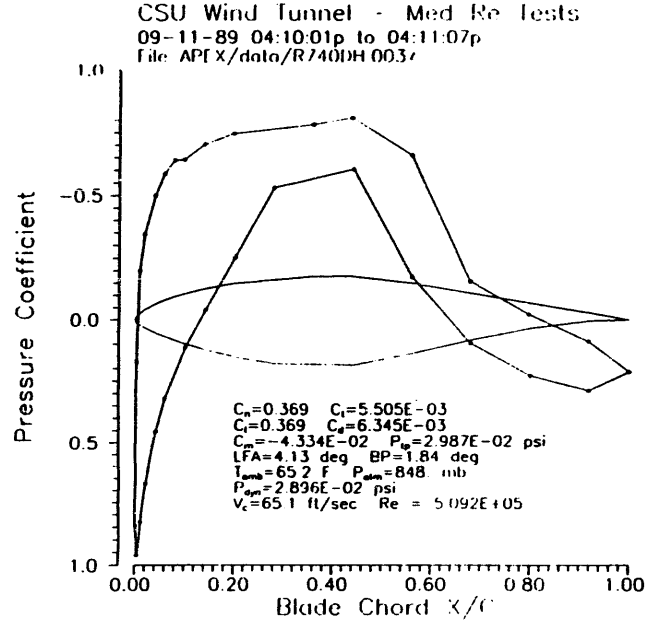
CSU Wind Tunnel -- Med Re Tests
09-11-89 04:10:01p to 04:11:07p
File APEX/data/R740DH.003
Pressure Coefficient
Blade Chord X/C
C_n=0.369 C_t=5.505E-03
C_l=0.369 C_d=6.345E-03
C_m=-4.334E-02 P_{tp}=2.987E-02 psi
LFA=4.13 deg BP=1.84 deg
T_{amb}=65.2 F P_{atm}=848. mb
P_{dyn}=2.896E-02 psi
V_c=65.1 ft/sec Re = 5.092E+05

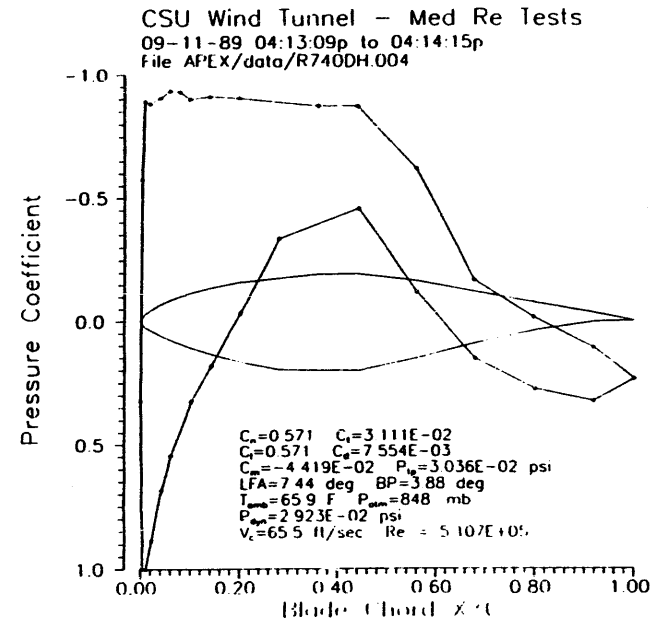
CSU Wind Tunnel -- Med Re Tests
09-11-89 04:13:09p to 04:14:15p
File APEX/data/R740DH.004
Pressure Coefficient
Blade Chord X/C
C_n=0.571 C_t=3.111E-02
C_l=0.571 C_d=7.554E-03
C_m=-4.419E-02 P_{tp}=3.036E-02 psi
LFA=7.44 deg BP=3.88 deg
T_{amb}=65.9 F P_{atm}=848. mb
P_{dyn}=2.923E-02 psi
V_c=65.5 ft/sec Re = 5.107E+05

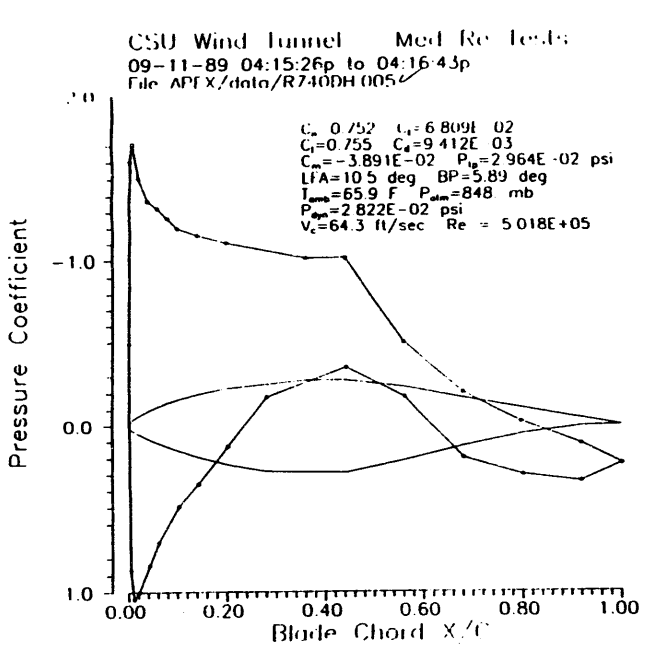
CSU Wind Tunnel Med Re Tests
09-11-89 04:15:26p to 04:16:43p
File APEX/data/R740DH.005
Cn 0.752 Cl=6.809E-02
Ct=0.755 Cd=9.412E-03
Cm=-3.891E-02 Pts=2.964E-02 psi
LFA=10.5 deg BP=5.89 deg
Tamb=65.9 F Patm=848. mb
Pdyn=2.822E-02 psi
Vc=64.3 ft/sec Re = 5.018E+05
Pressure Coefficient
Blade Chord X/C

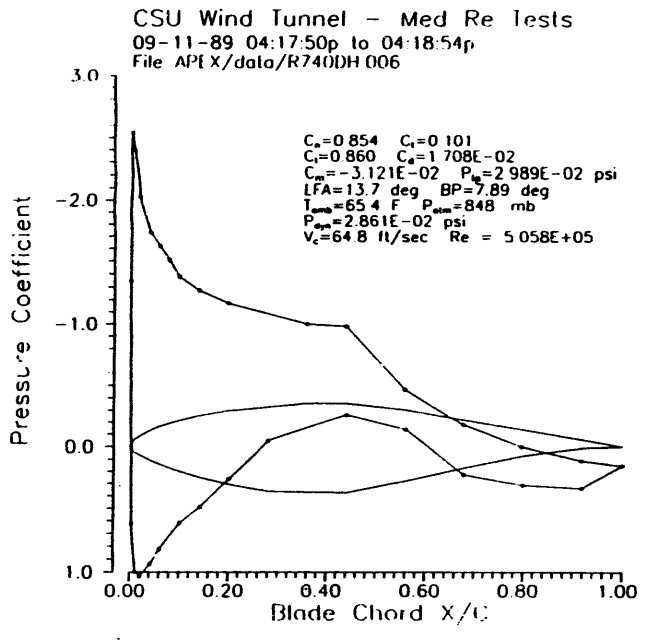
CSU Wind Tunnel - Med Re Tests
09-11-89 04:17:50p to 04:18:54p
File APEX/data/R740DH.006
Cn=0.854 Cl=0.101
Ct=0.860 Cd=1.708E-02
Cm=-3.121E-02 Pts=2.989E-02 psi
LFA=13.7 deg BP=7.89 deg
Tamb=65.4 F Patm=848. mb
Pdyn=2.861E-02 psi
Vc=64.8 ft/sec Re = 5.058E+05
Pressure Coefficient
Blade Chord X/C

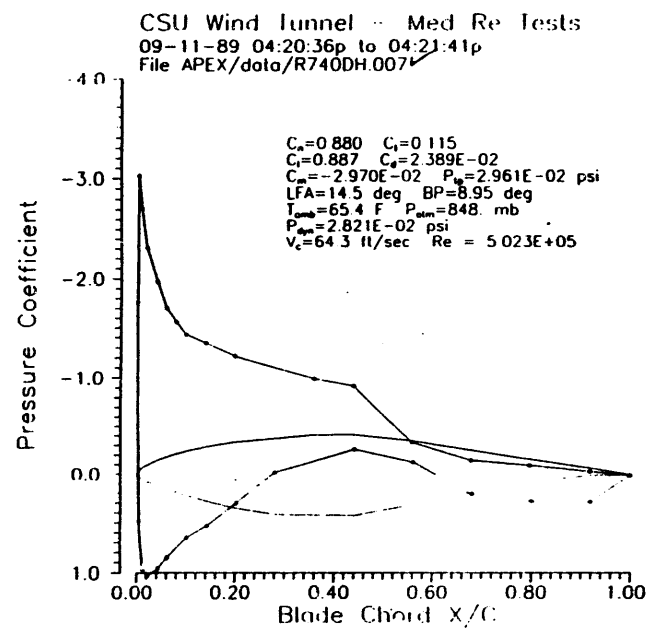
CSU Wind Tunnel - Med Re Tests
09-11-89 04:20:36p to 04:21:41p
File APEX/data/R740DH.007
Cn=0.880 Cl=0.115
Ct=0.887 Cd=2.389E-02
Cm=-2.970E-02 Pts=2.961E-02 psi
LFA=14.5 deg BP=8.95 deg
Tamb=65.4 F Patm=848. mb
Pdyn=2.821E-02 psi
Vc=64.3 ft/sec Re = 5.023E+05
Pressure Coefficient
Blade Chord X/C

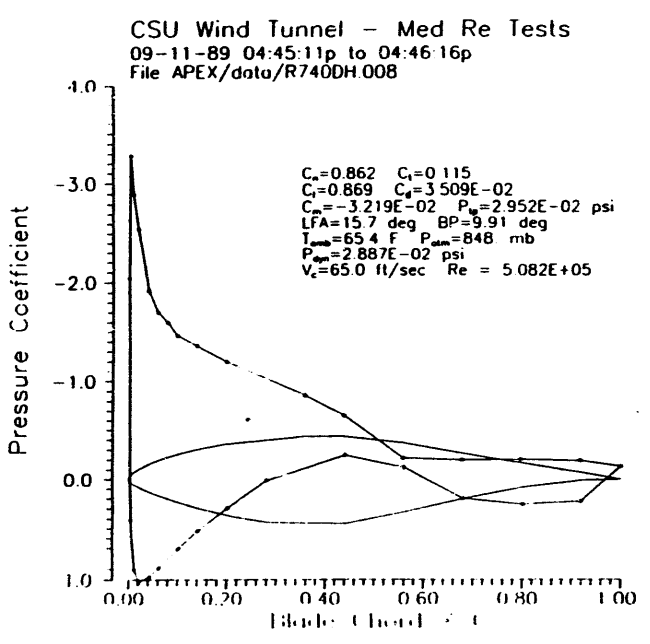
CSU Wind Tunnel - Med Re Tests
09-11-89 04:45:11p to 04:46:16p
File APEX/data/R740DH.008
Cn=0.862 Cl=0.115
Ct=0.869 Cd=3.509E-02
Cm=-3.219E-02 Pts=2.952E-02 psi
LFA=15.7 deg BP=9.91 deg
Tamb=65.4 F Patm=848. mb
Pdyn=2.887E-02 psi
Vc=65.0 ft/sec Re = 5.082E+05
Pressure Coefficient

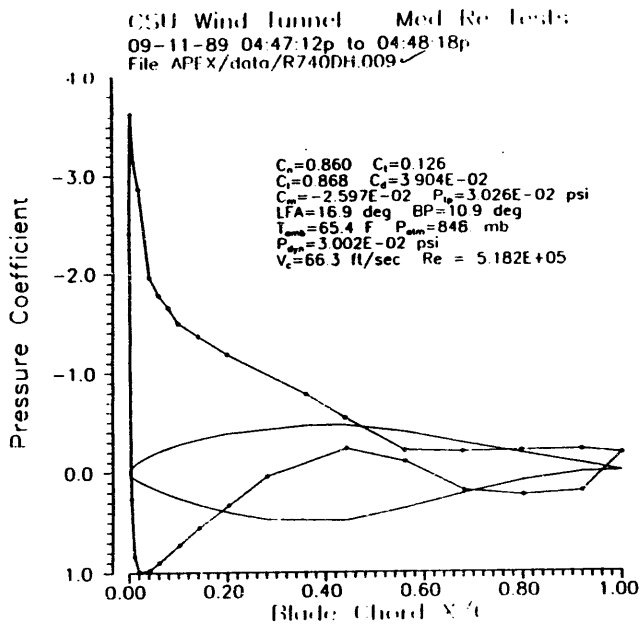
CSU Wind Tunnel Med Re Tests
09-11-89 04:47:12p to 04:48:18p
File APEX/data/R740DH.009
C_n=0.860 C_t=0.126
C_l=0.868 C_d=3.904E-02
C_m=-2.597E-02 P_{tp}=3.026E-02 psi
LFA=16.9 deg BP=10.9 deg
T_{amb}=65.4 F P_{atm}=846 mb
P_{dyn}=3.002E-02 psi
V_c=66.3 ft/sec Re = 5.182E+05
Pressure Coefficient
Blade Chord X/C

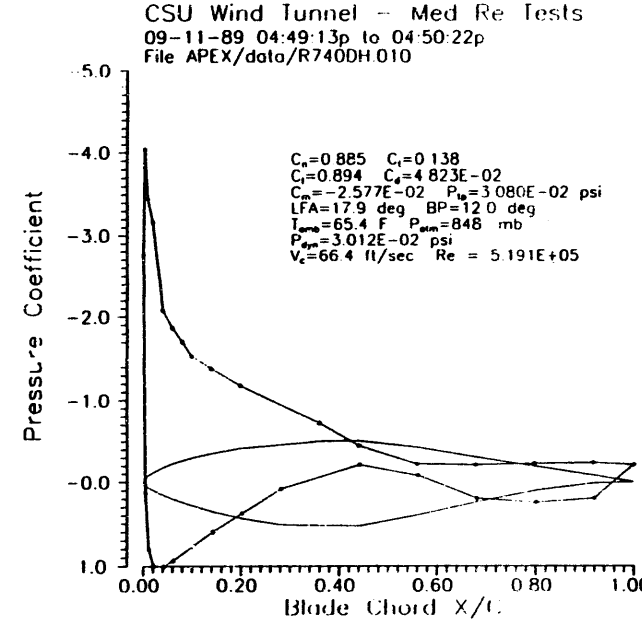
CSU Wind Tunnel - Med Re Tests
09-11-89 04:49:13p to 04:50:22p
File APEX/data/R740DH.010
C_n=0.885 C_t=0.138
C_l=0.894 C_d=4.823E-02
C_m=-2.577E-02 P_{tp}=3.080E-02 psi
LFA=17.9 deg BP=12.0 deg
T_{amb}=65.4 F P_{atm}=848 mb
P_{dyn}=3.012E-02 psi
V_c=66.4 ft/sec Re = 5.191E+05
Pressure Coefficient
Blade Chord X/C

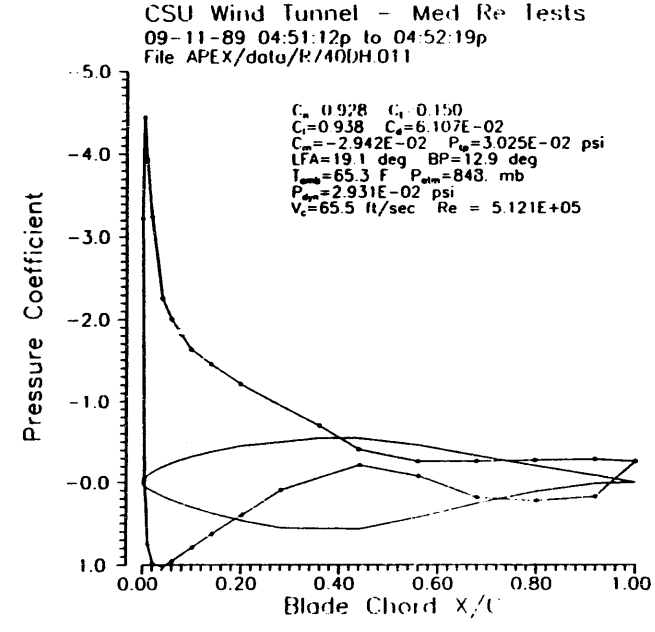
CSU Wind Tunnel - Med Re Tests
09-11-89 04:51:12p to 04:52:19p
File APEX/data/R740DH.011
C_n 0.928 C_t=0.150
C_l=0.938 C_d=6.107E-02
C_m=-2.942E-02 P_{tp}=3.025E-02 psi
LFA=19.1 deg BP=12.9 deg
T_{amb}=65.3 F P_{atm}=848. mb
P_{dyn}=2.931E-02 psi
V_c=65.5 ft/sec Re = 5.121E+05
Pressure Coefficient
Blade Chord X/C

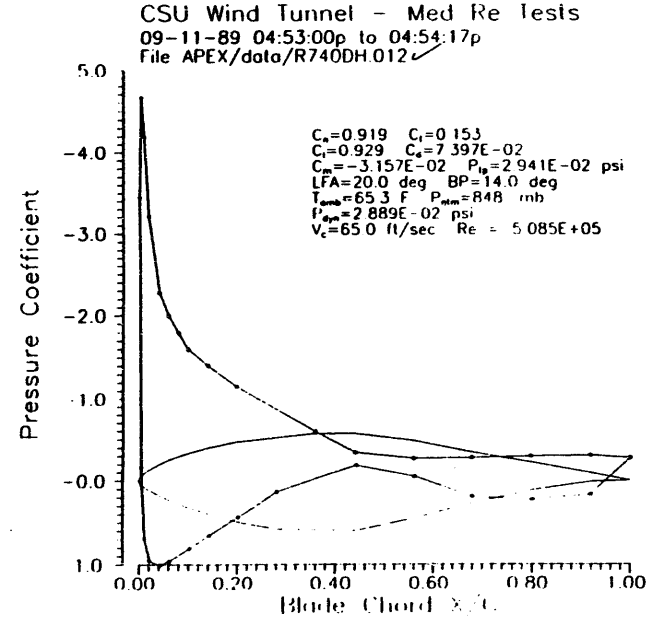
CSU Wind Tunnel - Med Re Tests
09-11-89 04:53:00p to 04:54:17p
File APEX/data/R740DH.012
C_n=0.919 C_t=0.153
C_l=0.929 C_d=7.397E-02
C_m=-3.157E-02 P_{tp}=2.941E-02 psi
LFA=20.0 deg BP=14.0 deg
T_{amb}=65.3 F P_{atm}=848 mb
P_{dyn}=2.889E-02 psi
V_c=65.0 ft/sec Re = 5.085E+05
Pressure Coefficient
Blade Chord X/C

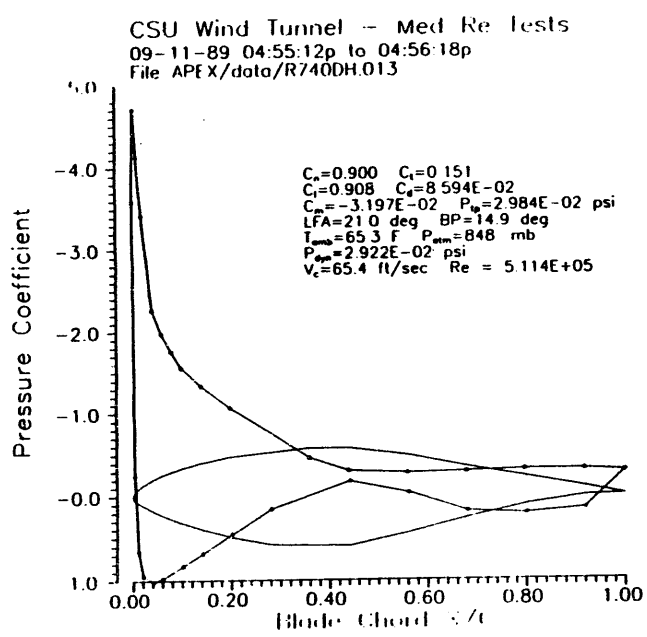
CSU Wind Tunnel - Med Re Tests
09-11-89 04:55:12p to 04:56:18p
File APEX/data/R740DH.013
C_n=0.900 C_t=0.151
C_l=0.908 C_d=8.594E-02
C_m=-3.197E-02 P_{tp}=2.984E-02 psi
LFA=21.0 deg BP=14.9 deg
T_{amb}=65.3 F P_{atm}=848 mb
P_{dyn}=2.922E-02 psi
V_c=65.4 ft/sec Re = 5.114E+05
Pressure Coefficient
Blade Chord X/C

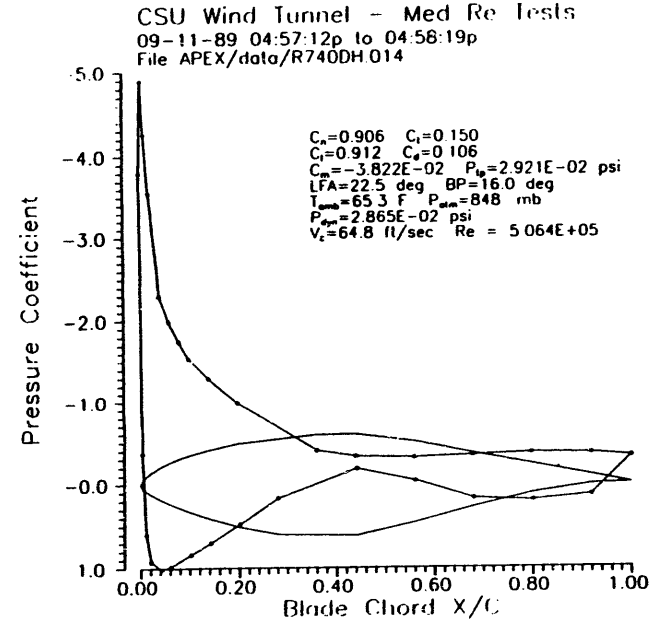
CSU Wind Tunnel - Med Re Tests
09-11-89 04:57:12p to 04:58:19p
File APEX/data/R740DH.014
C_n=0.906 C_t=0.150
C_l=0.912 C_d=0.106
C_m=-3.822E-02 P_{tp}=2.921E-02 psi
LFA=22.5 deg BP=16.0 deg
T_{amb}=65.3 F P_{atm}=848 mb
P_{dyn}=2.865E-02 psi
V_c=64.8 ft/sec Re = 5.064E+05
Pressure Coefficient
Blade Chord X/C

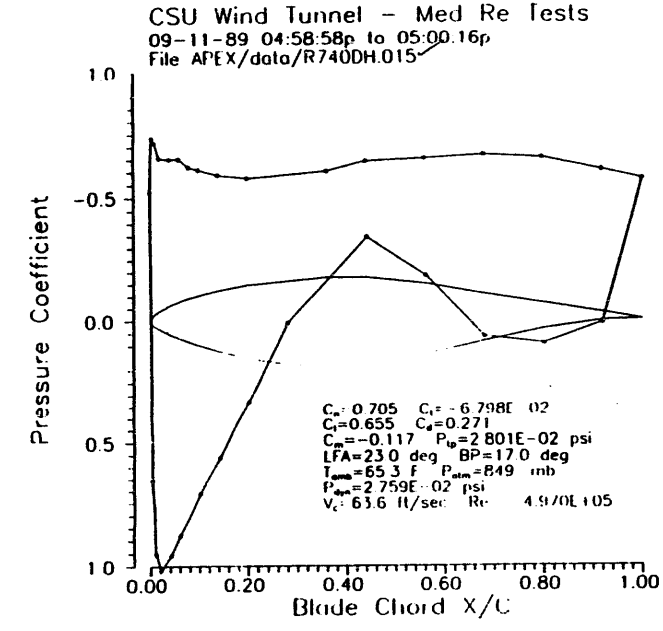
CSU Wind Tunnel - Med Re Tests
09-11-89 04:58:58p to 05:00:16p
File APEX/data/R740DH.015
C_n=0.705 C_t=-6.798E-02
C_l=0.655 C_d=0.271
C_m=-0.117 P_{tp}=2.801E-02 psi
LFA=23.0 deg BP=17.0 deg
T_{amb}=65.3 F P_{atm}=849 mb
P_{dyn}=2.759E-02 psi
V_c=63.6 ft/sec Re = 4.970E+05
Pressure Coefficient
Blade Chord X/C

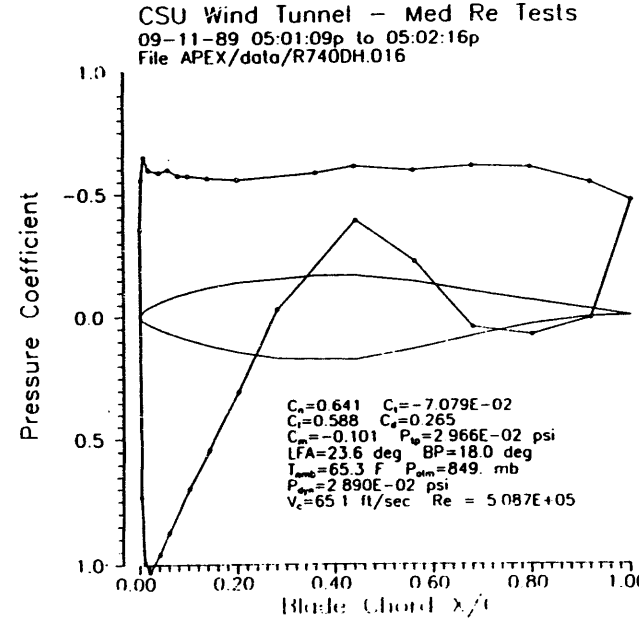
CSU Wind Tunnel - Med Re Tests
09-11-89 05:01:09p to 05:02:16p
File APEX/data/R740DH.016
C_n=0.641 C_t=-7.079E-02
C_l=0.588 C_d=0.265
C_m=-0.101 P_{tp}=2.966E-02 psi
LFA=23.6 deg BP=18.0 deg
T_{amb}=65.3 F P_{atm}=849. mb
P_{dyn}=2.890E-02 psi
V_c=65.1 ft/sec Re = 5.087E+05
Pressure Coefficient
Blade Chord X/C

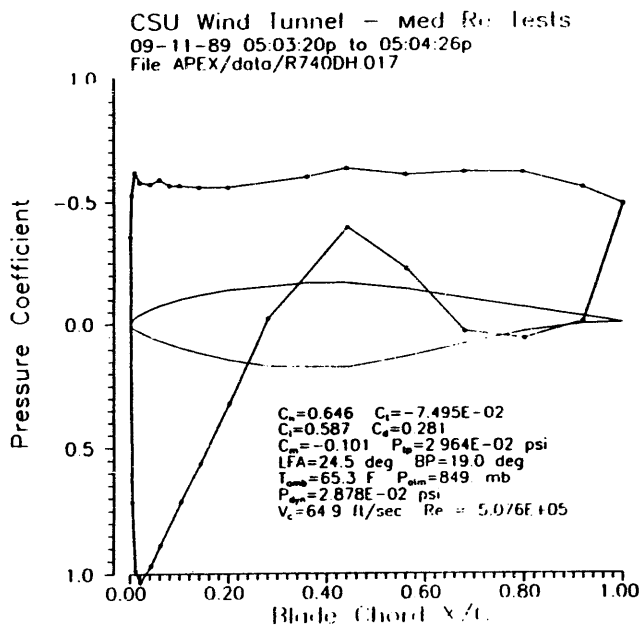
CSU Wind Tunnel – Med Re Tests
09-11-89 05:03:20p to 05:04:26p
File APEX/data/R740DH.017
Pressure Coefficient
Blade Chord X/C
C_n=0.646 C_t=-7.495E-02
C_l=0.587 C_d=0.281
C_m=-0.101 P_{tp}=2.964E-02 psi
LFA=24.5 deg BP=19.0 deg
T_{amb}=65.3 F P_{atm}=849 mb
P_{dyn}=2.878E-02 psi
V_c=64.9 ft/sec Re = 5.076E+05

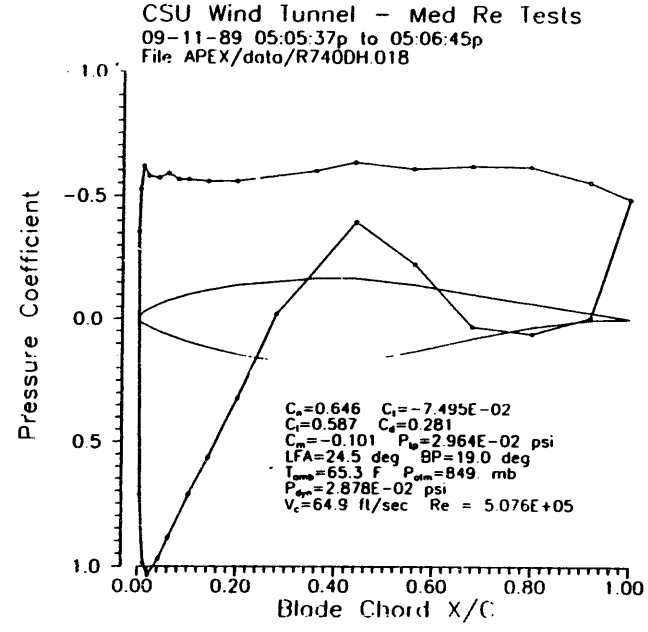
CSU Wind Tunnel – Med Re Tests
09-11-89 05:05:37p to 05:06:45p
File APEX/data/R740DH.018
Pressure Coefficient
Blade Chord X/C
C_n=0.646 C_t=-7.495E-02
C_l=0.587 C_d=0.281
C_m=-0.101 P_{tp}=2.964E-02 psi
LFA=24.5 deg BP=19.0 deg
T_{amb}=65.3 F P_{atm}=849 mb
P_{dyn}=2.878E-02 psi
V_c=64.9 ft/sec Re = 5.076E+05

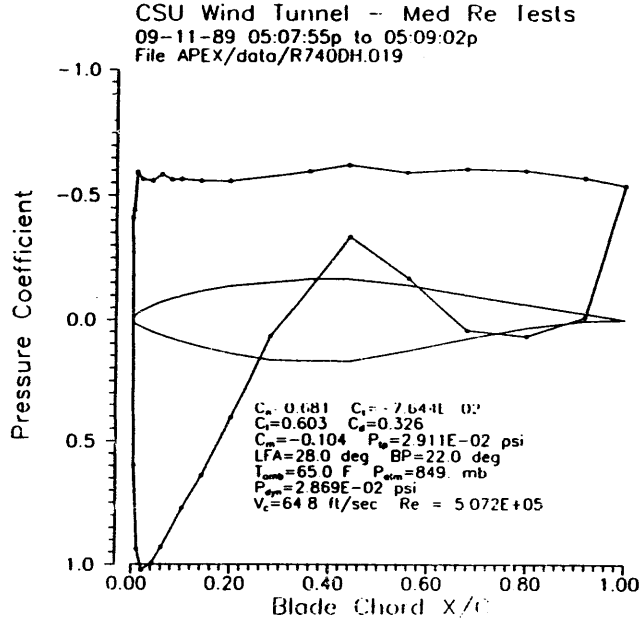
CSU Wind Tunnel – Med Re Tests
09-11-89 05:07:55p to 05:09:02p
File APEX/data/R740DH.019
Pressure Coefficient
Blade Chord X/C
C_n=0.681 C_t=-7.644E-02
C_l=0.603 C_d=0.326
C_m=-0.104 P_{tp}=2.911E-02 psi
LFA=28.0 deg BP=22.0 deg
T_{amb}=65.0 F P_{atm}=849 mb
P_{dyn}=2.869E-02 psi
V_c=64.8 ft/sec Re = 5.072E+05

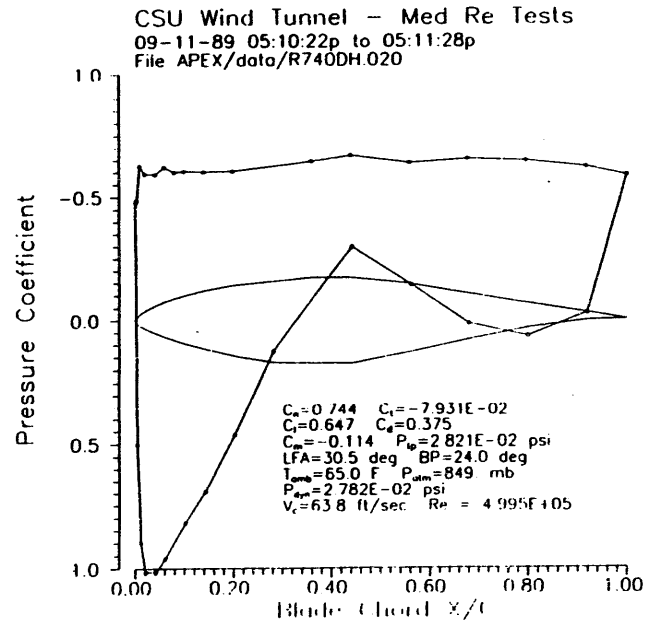
CSU Wind Tunnel – Med Re Tests
09-11-89 05:10:22p to 05:11:28p
File APEX/data/R740DH.020
Pressure Coefficient
Blade Chord X/C
C_n=0.744 C_t=-7.931E-02
C_l=0.647 C_d=0.375
C_m=-0.114 P_{tp}=2.821E-02 psi
LFA=30.5 deg BP=24.0 deg
T_{amb}=65.0 F P_{atm}=849 mb
P_{dyn}=2.782E-02 psi
V_c=63.8 ft/sec Re = 4.995E+05

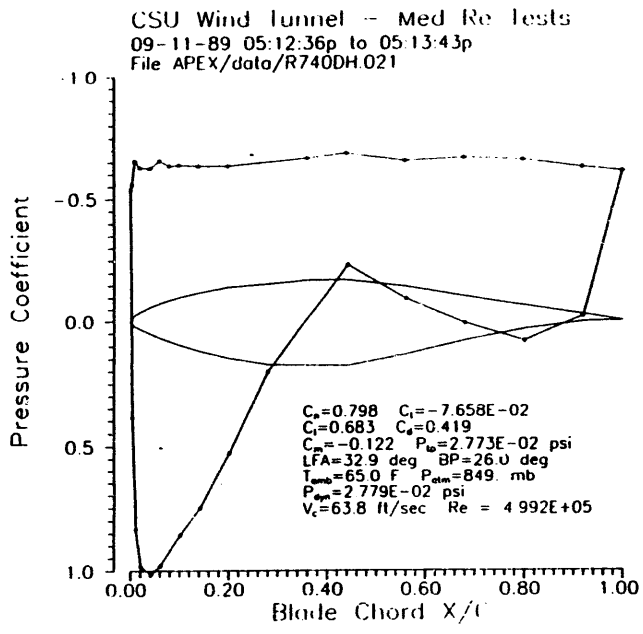
CSU Wind Tunnel - Med Re Tests
09-11-89 05:12:36p to 05:13:43p
File APEX/data/R740DH.021
Pressure Coefficient
Blade Chord X/C
-1.0
-0.5
0.0
0.5
1.0
0.00
0.20
0.40
0.60
0.80
1.00
Cn=0.798 Ct=-7.658E-02
Cl=0.683 Cd=0.419
Cm=-0.122 Ptp=2.773E-02 psi
LFA=32.9 deg BP=26.0 deg
Tamb=65.0 F Patm=849. mb
Pdyn=2.779E-02 psi
Vc=63.8 ft/sec Re = 4.992E+05

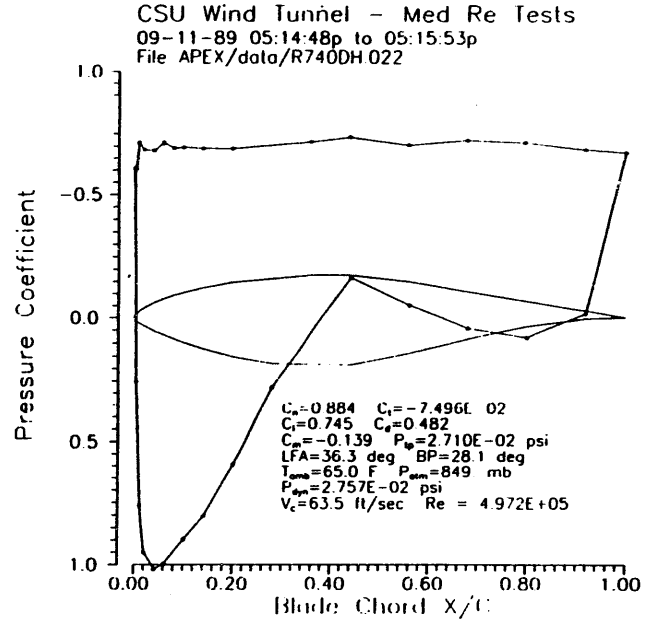
CSU Wind Tunnel - Med Re Tests
09-11-89 05:14:48p to 05:15:53p
File APEX/data/R740DH.022
Pressure Coefficient
Blade Chord X/C
-1.0
-0.5
0.0
0.5
1.0
0.00
0.20
0.40
0.60
0.80
1.00
Cn=0.884 Ct=-7.496E-02
Cl=0.745 Cd=0.482
Cm=-0.139 Ptp=2.710E-02 psi
LFA=36.3 deg BP=28.1 deg
Tamb=65.0 F Patm=849 mb
Pdyn=2.757E-02 psi
Vc=63.5 ft/sec Re = 4.972E+05

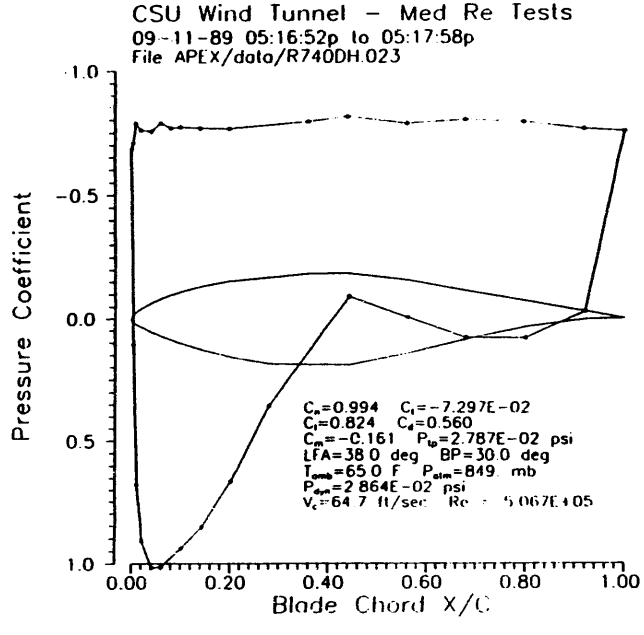
CSU Wind Tunnel - Med Re Tests
09-11-89 05:16:52p to 05:17:58p
File APEX/data/R740DH.023
Pressure Coefficient
Blade Chord X/C
-1.0
-0.5
0.0
0.5
1.0
0.00
0.20
0.40
0.60
0.80
1.00
Cn=0.994 Ct=-7.297E-02
Cl=0.824 Cd=0.560
Cm=-0.161 Ptp=2.787E-02 psi
LFA=38.0 deg BP=30.0 deg
Tamb=65.0 F Patm=849. mb
Pdyn=2.864E-02 psi
Vc=64.7 ft/sec Re = 5.067E+05

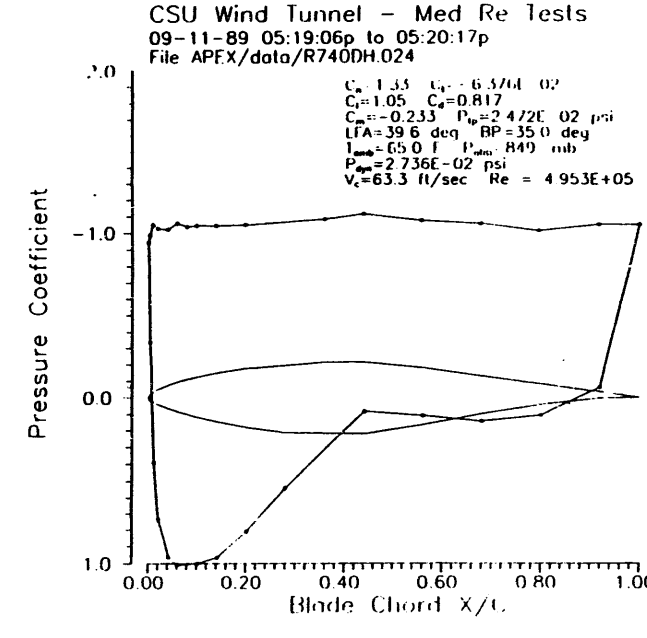
CSU Wind Tunnel - Med Re Tests
09-11-89 05:19:06p to 05:20:17p
File APEX/data/R740DH.024
Pressure Coefficient
Blade Chord X/C
-1.0
0.0
1.0
0.00
0.20
0.40
0.60
0.80
1.00
Cl=1.05 Cd=0.817
Cm=-0.233 Ptp=2.472E-02 psi
LFA=39.6 deg BP=35.0 deg
Tamb=65.0 F Patm=849 mb
Pdyn=2.736E-02 psi
Vc=63.3 ft/sec Re = 4.953E+05

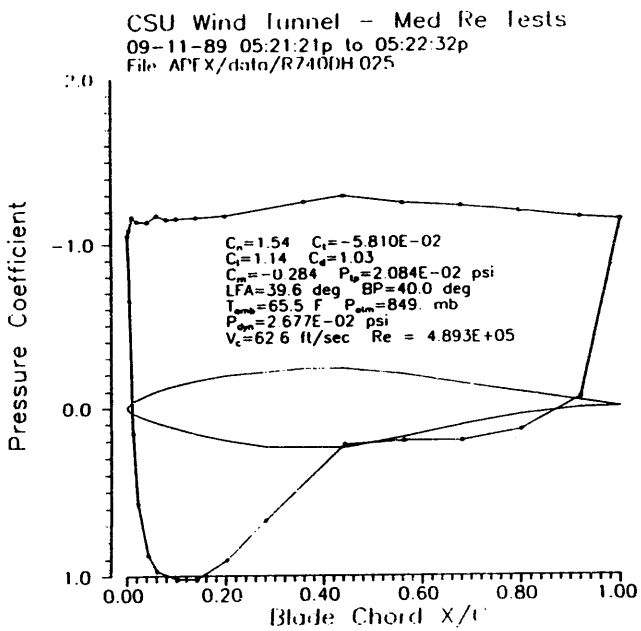
CSU Wind Tunnel - Med Re Tests
09-11-89 05:21:21p to 05:22:32p
File APEX/data/R740DH.025
C_n=1.54 C_t=-5.810E-02
C_l=1.14 C_d=1.03
C_m=-0.284 P_{tp}=2.084E-02 psi
LFA=39.6 deg BP=40.0 deg
T_{amb}=65.5 F P_{atm}=849. mb
P_{dyn}=2.677E-02 psi
V_c=62.6 ft/sec Re = 4.893E+05
Pressure Coefficient
2.0
-1.0
0.0
1.0
0.00
0.20
0.40
0.60
0.80
1.00
Blade Chord X/C

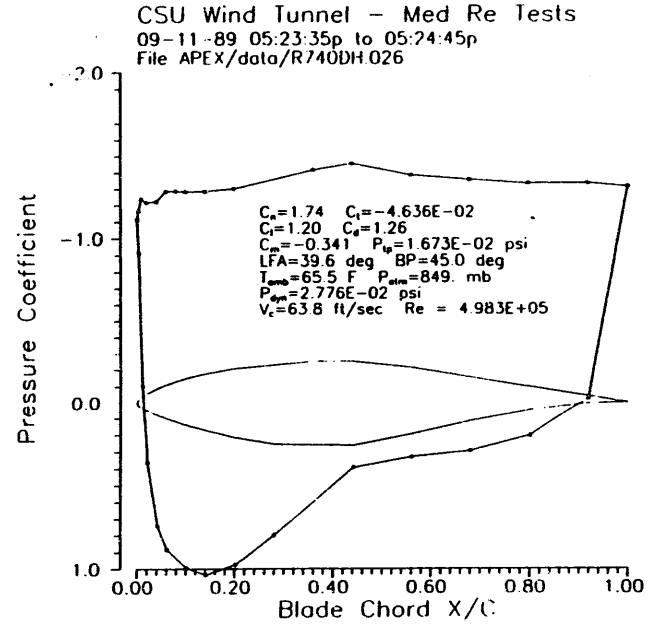
CSU Wind Tunnel - Med Re Tests
09-11-89 05:23:35p to 05:24:45p
File APEX/data/R740DH.026
C_n=1.74 C_t=-4.636E-02
C_l=1.20 C_d=1.26
C_m=-0.341 P_{tp}=1.673E-02 psi
LFA=39.6 deg BP=45.0 deg
T_{amb}=65.5 F P_{atm}=849. mb
P_{dyn}=2.776E-02 psi
V_c=63.8 ft/sec Re = 4.983E+05
Pressure Coefficient
2.0
-1.0
0.0
1.0
0.00
0.20
0.40
0.60
0.80
1.00
Blade Chord X/C

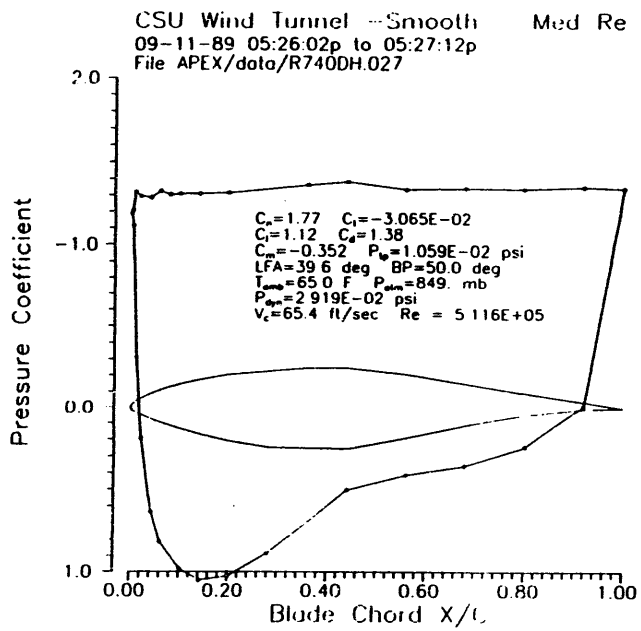
CSU Wind Tunnel -Smooth Med Re -Run 5
09-11-89 05:26:02p to 05:27:12p
File APEX/data/R740DH.027
C_n=1.77 C_t=-3.065E-02
C_l=1.12 C_d=1.38
C_m=-0.352 P_{tp}=1.059E-02 psi
LFA=39.6 deg BP=50.0 deg
T_{amb}=65.0 F P_{atm}=849. mb
P_{dyn}=2.919E-02 psi
V_c=65.4 ft/sec Re = 5.116E+05
Pressure Coefficient
2.0
-1.0
0.0
1.0
0.00
0.20
0.40
0.60
0.80
1.00
Blade Chord X/C

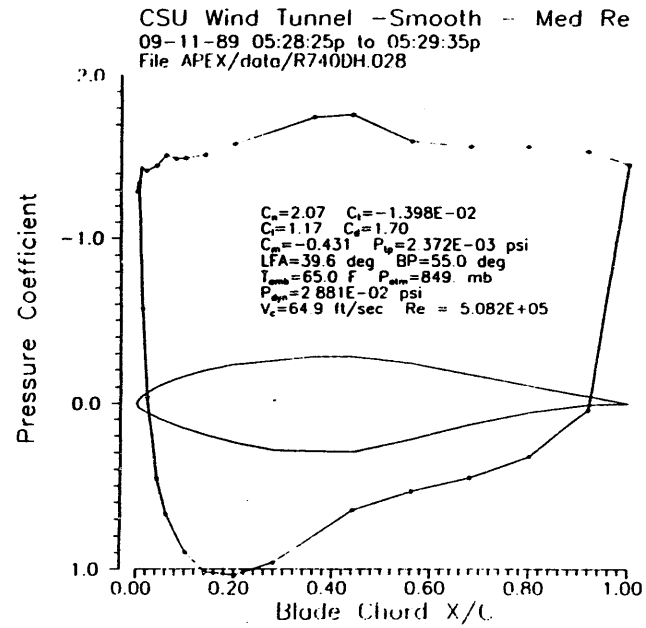
CSU Wind Tunnel -Smooth - Med Re -Run 5
09-11-89 05:28:25p to 05:29:35p
File APEX/data/R740DH.028
C_n=2.07 C_t=-1.398E-02
C_l=1.17 C_d=1.70
C_m=-0.431 P_{tp}=2.372E-03 psi
LFA=39.6 deg BP=55.0 deg
T_{amb}=65.0 F P_{atm}=849. mb
P_{dyn}=2.881E-02 psi
V_c=64.9 ft/sec Re = 5.082E+05
Pressure Coefficient
2.0
-1.0
0.0
1.0
0.00
0.20
0.40
0.60
0.80
1.00
Blade Chord X/C

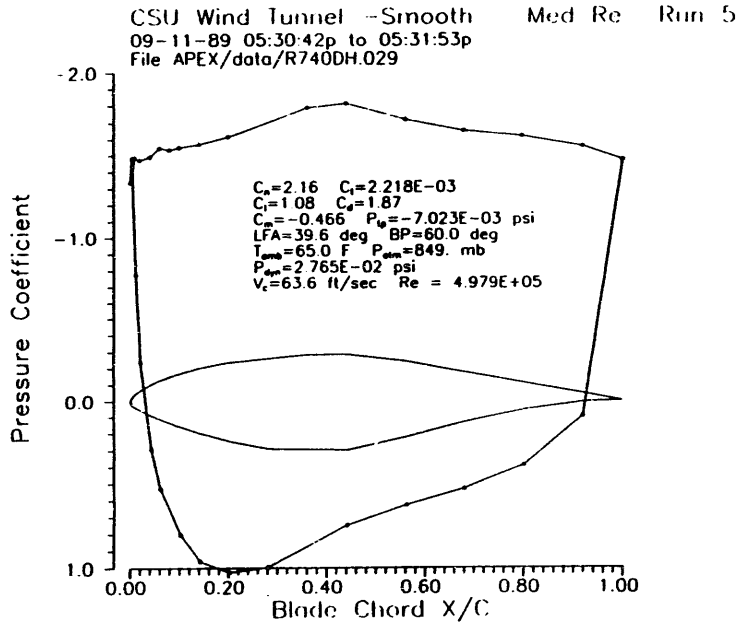
CSU Wind Tunnel -Smooth Med Re Run 5
09-11-89 05:30:42p to 05:31:53p
File APEX/data/R740DH.029
C_n=2.16 C_t=2.218E-03
C_l=1.08 C_d=1.87
C_m=-0.466 P_{tp}=-7.023E-03 psi
LFA=39.6 deg BP=60.0 deg
T_{amb}=65.0 F P_{atm}=849. mb
P_{dyn}=2.765E-02 psi
V_c=63.6 ft/sec Re = 4.979E+05
Pressure Coefficient
Blade Chord X/C

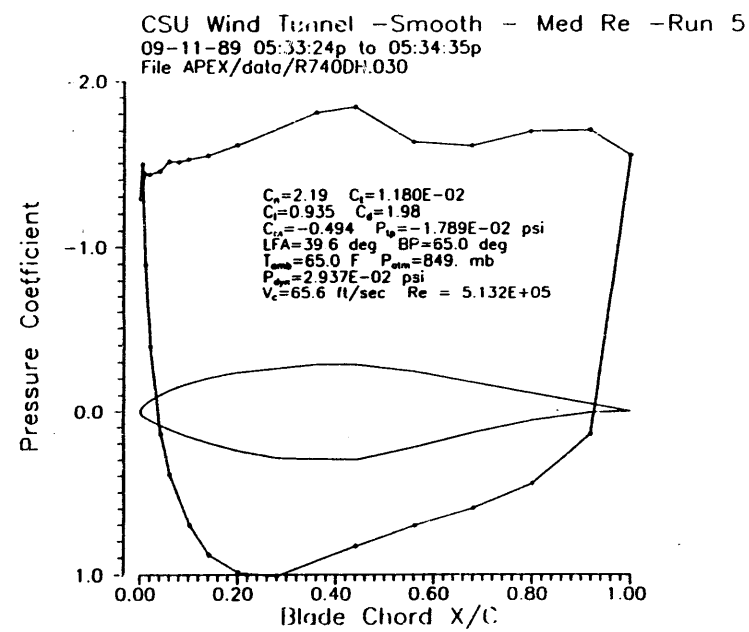
CSU Wind Tunnel -Smooth - Med Re -Run 5
09-11-89 05:33:24p to 05:34:35p
File APEX/data/R740DH.030
C_n=2.19 C_t=1.180E-02
C_l=0.935 C_d=1.98
C_m=-0.494 P_{tp}=-1.789E-02 psi
LFA=39.6 deg BP=65.0 deg
T_{amb}=65.0 F P_{atm}=849. mb
P_{dyn}=2.937E-02 psi
V_c=65.6 ft/sec Re = 5.132E+05
Pressure Coefficient
Blade Chord X/C

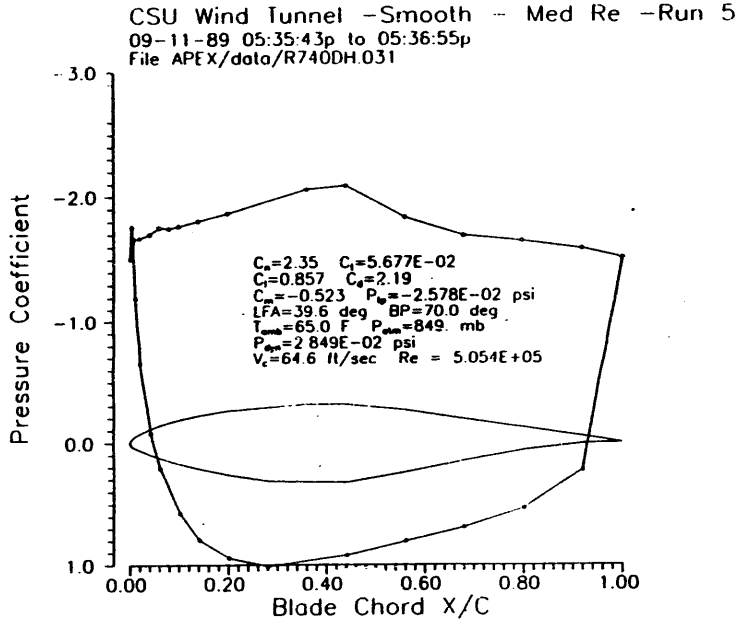
CSU Wind Tunnel -Smooth - Med Re -Run 5
09-11-89 05:35:43p to 05:36:55p
File APEX/data/R740DH.031
C_n=2.35 C_t=5.677E-02
C_l=0.857 C_d=2.19
C_m=-0.523 P_{tp}=-2.578E-02 psi
LFA=39.6 deg BP=70.0 deg
T_{amb}=65.0 F P_{atm}=849. mb
P_{dyn}=2.849E-02 psi
V_c=64.6 ft/sec Re = 5.054E+05
Pressure Coefficient
Blade Chord X/C

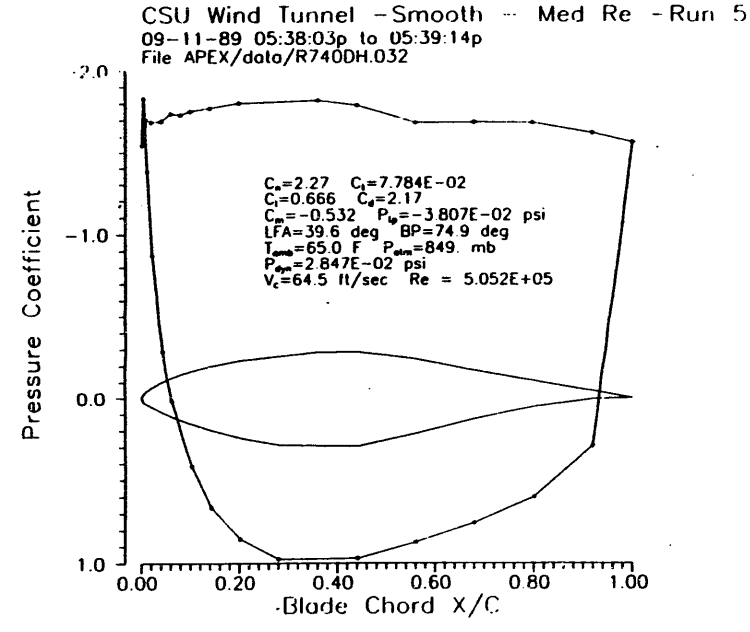
CSU Wind Tunnel -Smooth - Med Re -Run 5
09-11-89 05:38:03p to 05:39:14p
File APEX/data/R740DH.032
C_n=2.27 C_t=7.784E-02
C_l=0.666 C_d=2.17
C_m=-0.532 P_{tp}=-3.807E-02 psi
LFA=39.6 deg BP=74.9 deg
T_{amb}=65.0 F P_{atm}=849. mb
P_{dyn}=2.847E-02 psi
V_c=64.5 ft/sec Re = 5.052E+05
Pressure Coefficient
Blade Chord X/C

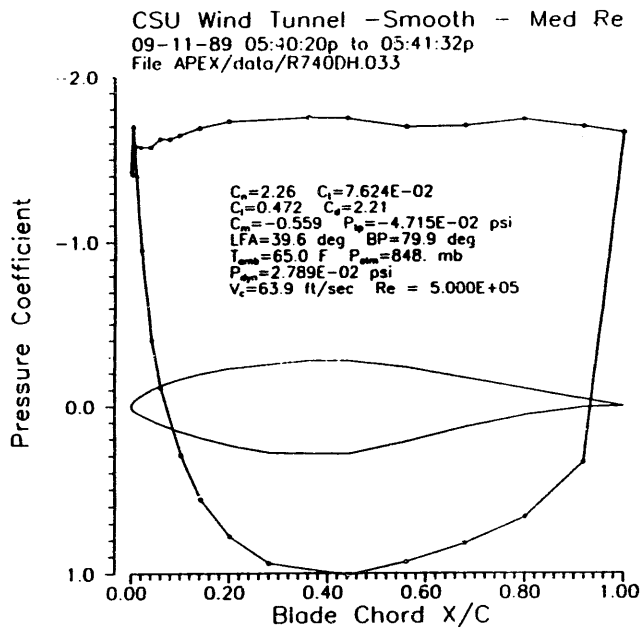
CSU Wind Tunnel -Smooth - Med Re -Run 5
09-11-89 05:40:20p to 05:41:32p
File APEX/data/R740DH.033
C_n=2.26 C_l=7.624E-02
C_l=0.472 C_d=2.21
C_m=-0.559 P_{tp}=-4.715E-02 psi
LFA=39.6 deg BP=79.9 deg
T_{amb}=65.0 F P_{atm}=848. mb
P_{dyn}=2.789E-02 psi
V_c=63.9 ft/sec Re = 5.000E+05
Pressure Coefficient
-2.0
-1.0
0.0
1.0
0.00
0.20
0.40
0.60
0.80
1.00
Blade Chord X/C

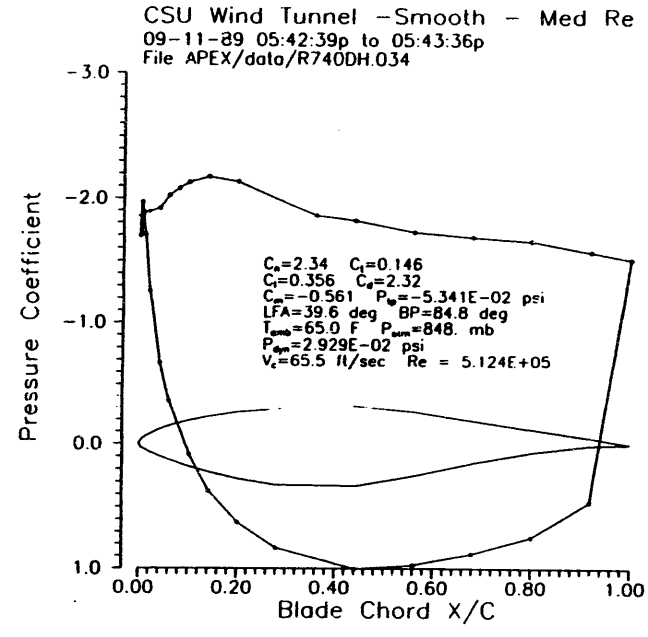
CSU Wind Tunnel -Smooth - Med Re -Run 5
09-11-89 05:42:39p to 05:43:36p
File APEX/data/R740DH.034
C_n=2.34 C_l=0.146
C_l=0.356 C_d=2.32
C_m=-0.561 P_{tp}=-5.341E-02 psi
LFA=39.6 deg BP=84.8 deg
T_{amb}=65.0 F P_{atm}=848. mb
P_{dyn}=2.929E-02 psi
V_c=65.5 ft/sec Re = 5.124E+05
Pressure Coefficient
-3.0
-2.0
-1.0
0.0
1.0
0.00
0.20
0.40
0.60
0.80
1.00
Blade Chord X/C

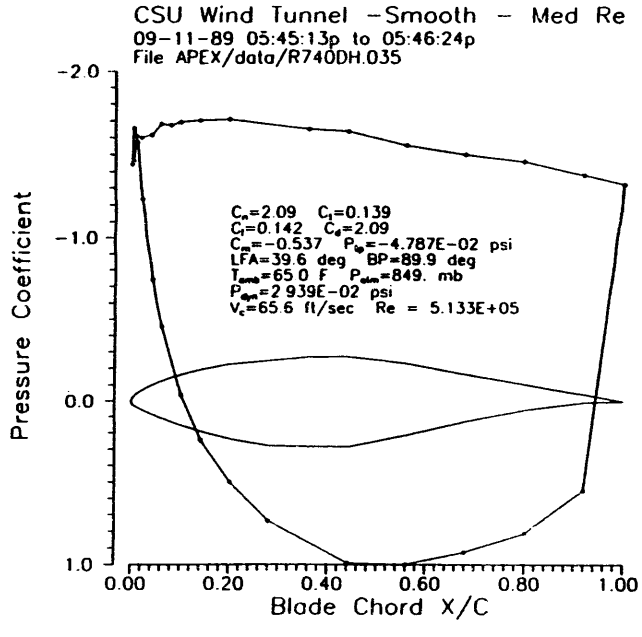
CSU Wind Tunnel -Smooth - Med Re -Run 5
09-11-89 05:45:13p to 05:46:24p
File APEX/data/R740DH.035
C_n=2.09 C_l=0.139
C_l=0.142 C_d=2.09
C_m=-0.537 P_{tp}=-4.787E-02 psi
LFA=39.6 deg BP=89.9 deg
T_{amb}=65.0 F P_{atm}=849. mb
P_{dyn}=2.939E-02 psi
V_c=65.6 ft/sec Re = 5.133E+05
Pressure Coefficient
-2.0
-1.0
0.0
1.0
0.00
0.20
0.40
0.60
0.80
1.00
Blade Chord X/C

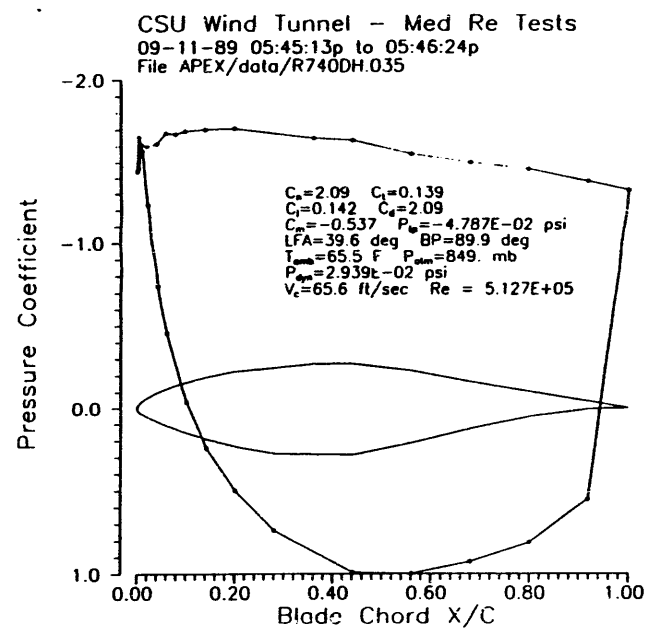
CSU Wind Tunnel - Med Re Tests
09-11-89 05:45:13p to 05:46:24p
File APEX/data/R740DH.035
C_n=2.09 C_l=0.139
C_l=0.142 C_d=2.09
C_m=-0.537 P_{tp}=-4.787E-02 psi
LFA=39.6 deg BP=89.9 deg
T_{amb}=65.5 F P_{atm}=849. mb
P_{dyn}=2.939E-02 psi
V_c=65.6 ft/sec Re = 5.127E+05
Pressure Coefficient
-2.0
-1.0
0.0
1.0
0.00
0.20
0.40
0.60
0.80
1.00
Blade Chord X/C

Appendix J

Pressure Distributions for Reynolds Number 500,000 Rough

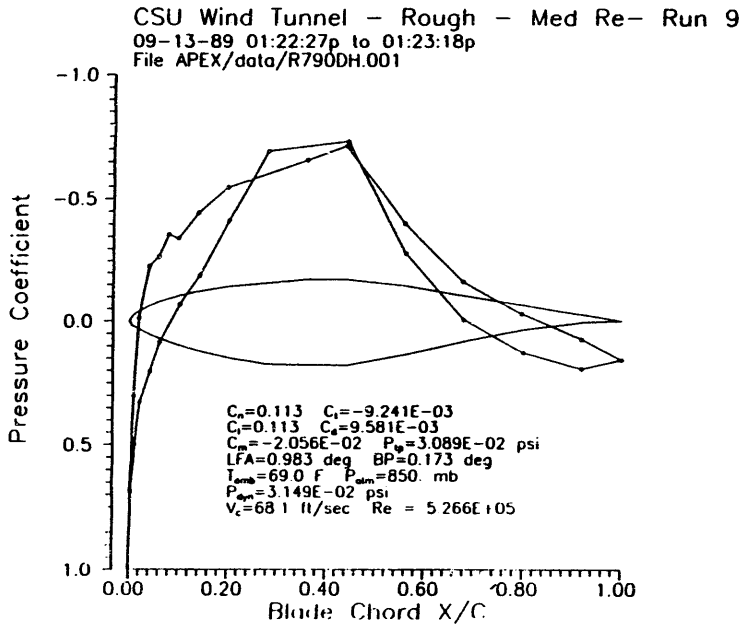
CSU Wind Tunnel – Rough – Med Re– Run 9
09-13-89 01:22:27p to 01:23:18p
File APEX/data/R790DH.001
Pressure Coefficient
Blade Chord X/C
C_n=0.113 C_t=-9.241E-03
C_l=0.113 C_d=9.581E-03
C_m=-2.056E-02 P_{tp}=3.089E-02 psi
LFA=0.983 deg BP=0.173 deg
T_{amb}=69.0 F P_{atm}=850. mb
P_{dyn}=3.149E-02 psi
V_c=68.1 ft/sec Re = 5.266E+05

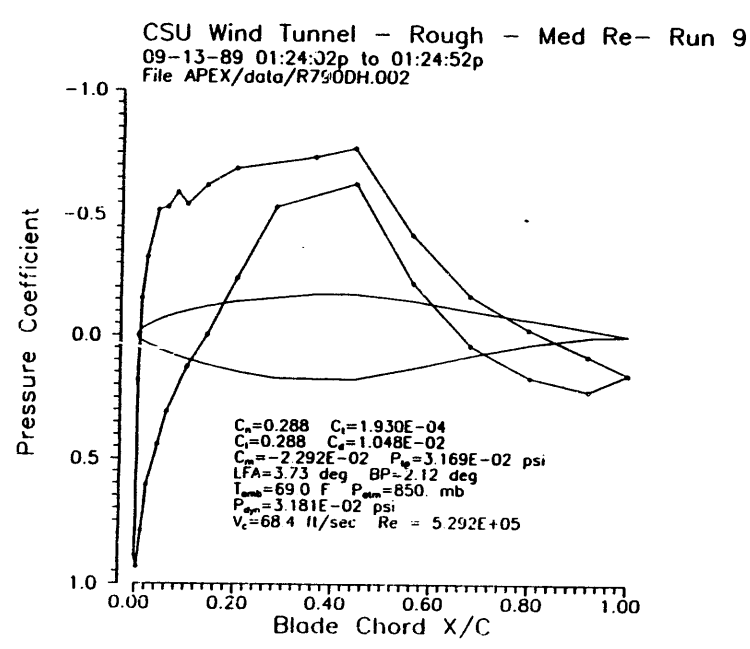
CSU Wind Tunnel – Rough – Med Re– Run 9
09-13-89 01:24:02p to 01:24:52p
File APEX/data/R790DH.002
Pressure Coefficient
Blade Chord X/C
C_n=0.288 C_t=1.930E-04
C_l=0.288 C_d=1.048E-02
C_m=-2.292E-02 P_{tp}=3.169E-02 psi
LFA=3.73 deg BP=2.12 deg
T_{amb}=69.0 F P_{atm}=850. mb
P_{dyn}=3.181E-02 psi
V_c=68.4 ft/sec Re = 5.292E+05

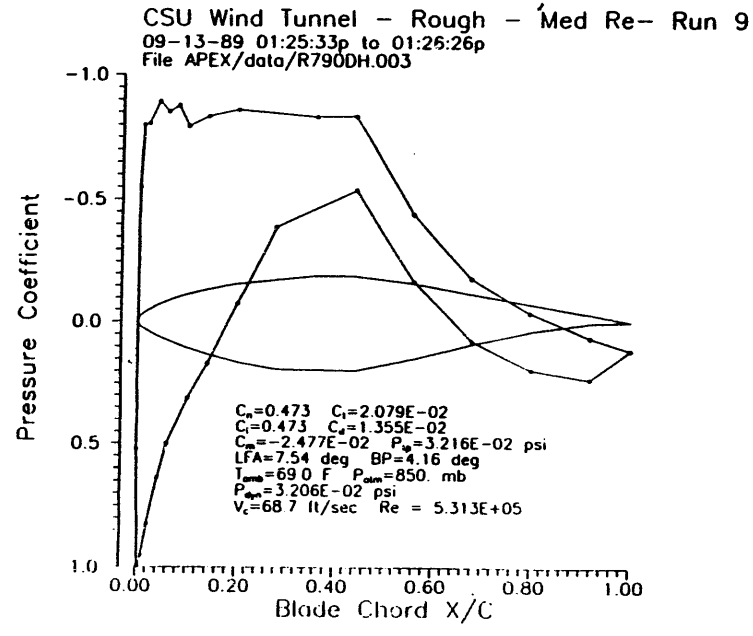
CSU Wind Tunnel – Rough – Med Re– Run 9
09-13-89 01:25:33p to 01:26:26p
File APEX/data/R790DH.003
Pressure Coefficient
Blade Chord X/C
C_n=0.473 C_t=2.079E-02
C_l=0.473 C_d=1.355E-02
C_m=-2.477E-02 P_{tp}=3.216E-02 psi
LFA=7.54 deg BP=4.16 deg
T_{amb}=69.0 F P_{atm}=850. mb
P_{dyn}=3.206E-02 psi
V_c=68.7 ft/sec Re = 5.313E+05

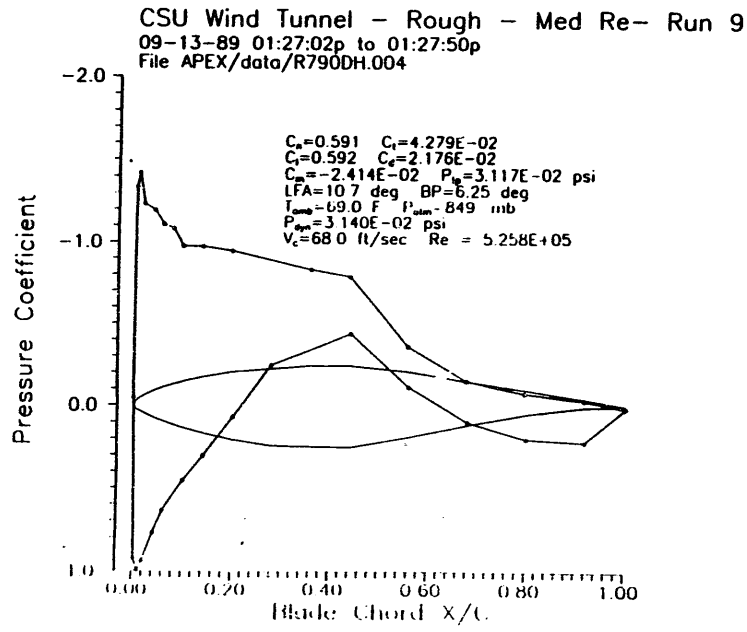
CSU Wind Tunnel – Rough – Med Re– Run 9
09-13-89 01:27:02p to 01:27:50p
File APEX/data/R790DH.004
Pressure Coefficient
Blade Chord X/C
C_n=0.591 C_t=4.279E-02
C_l=0.592 C_d=2.176E-02
C_m=-2.414E-02 P_{tp}=3.117E-02 psi
LFA=10.7 deg BP=6.25 deg
T_{amb}=69.0 F P_{atm}=849 mb
P_{dyn}=3.140E-02 psi
V_c=68.0 ft/sec Re = 5.258E+05

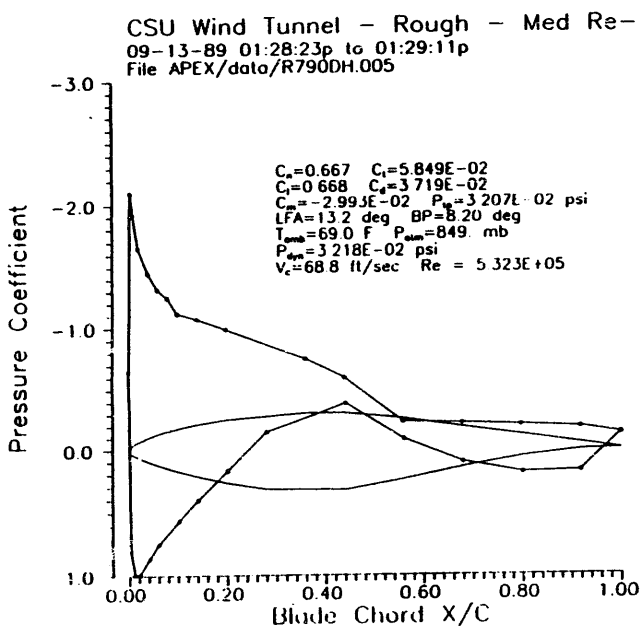
CSU Wind Tunnel – Rough – Med Re– Run 9
09–13–89 01:28:23p to 01:29:11p
File APEX/data/R790DH.005
C_a=0.667 C_t=5.849E–02
C_t=0.668 C_d=3.719E–02
C_{pb}=–2.993E–02 P_{tp}=3.207E–02 psi
LFA=13.2 deg BP=8.20 deg
T_{amb}=69.0 F P_{atm}=849. mb
P_{dyn}=3.218E–02 psi
V_c=68.8 ft/sec Re = 5.323E+05
Pressure Coefficient
Blade Chord X/C

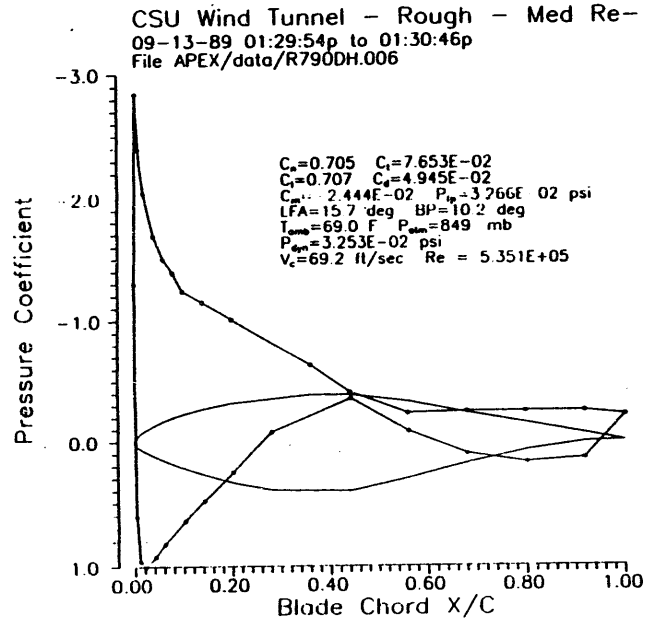
CSU Wind Tunnel – Rough – Med Re– Run 9
09–13–89 01:29:54p to 01:30:46p
File APEX/data/R790DH.006
C_a=0.705 C_t=7.653E–02
C_t=0.707 C_d=4.945E–02
C_{pb}=–2.444E–02 P_{tp}=3.266E–02 psi
LFA=15.7 deg BP=10.2 deg
T_{amb}=69.0 F P_{atm}=849. mb
P_{dyn}=3.253E–02 psi
V_c=69.2 ft/sec Re = 5.351E+05
Pressure Coefficient
Blade Chord X/C

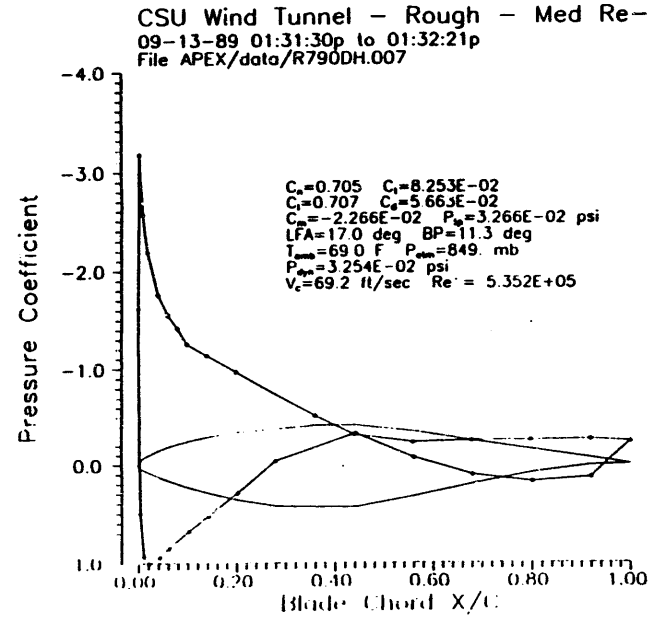
CSU Wind Tunnel – Rough – Med Re– Run 9
09–13–89 01:31:30p to 01:32:21p
File APEX/data/R790DH.007
C_a=0.705 C_t=8.253E–02
C_t=0.707 C_d=5.663E–02
C_{pb}=–2.266E–02 P_{tp}=3.266E–02 psi
LFA=17.0 deg BP=11.3 deg
T_{amb}=69.0 F P_{atm}=849. mb
P_{dyn}=3.254E–02 psi
V_c=69.2 ft/sec Re = 5.352E+05
Pressure Coefficient
Blade Chord X/C

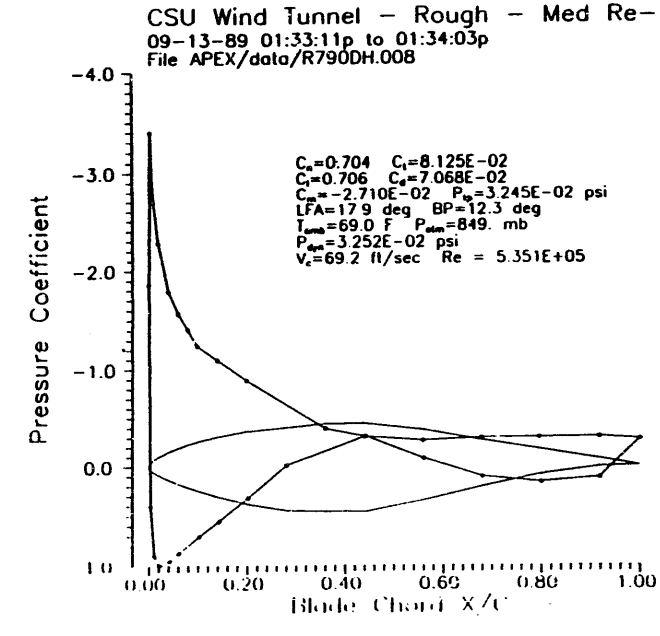
CSU Wind Tunnel – Rough – Med Re– Run 9
09–13–89 01:33:11p to 01:34:03p
File APEX/data/R790DH.008
C_a=0.704 C_t=8.125E–02
C_t=0.706 C_d=7.068E–02
C_{pb}=–2.710E–02 P_{tp}=3.245E–02 psi
LFA=17.9 deg BP=12.3 deg
T_{amb}=69.0 F P_{atm}=849. mb
P_{dyn}=3.252E–02 psi
V_c=69.2 ft/sec Re = 5.351E+05
Pressure Coefficient
Blade Chord X/C

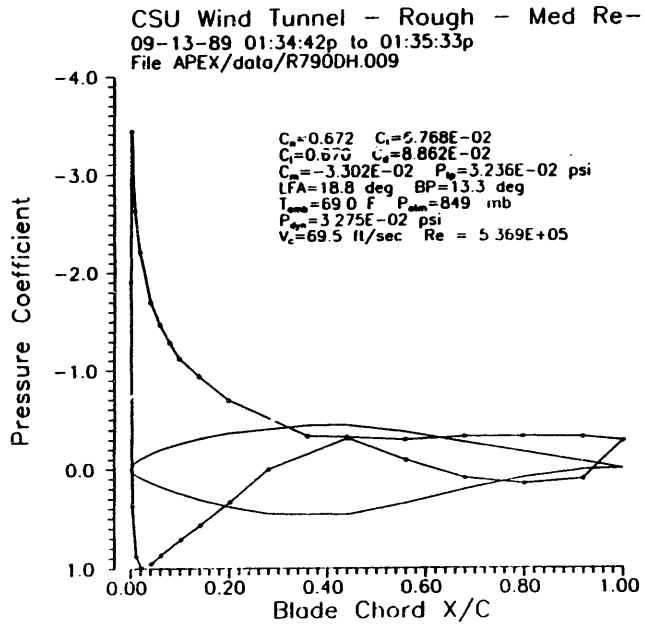
CSU Wind Tunnel – Rough – Med Re– Run 9
09-13-89 01:34:42p to 01:35:33p
File APEX/data/R790DH.009
C_n=0.672 C_t=5.768E-02
C_l=0.670 C_d=8.862E-02
C_m=-3.302E-02 P_{tip}=3.236E-02 psi
LFA=18.8 deg BP=13.3 deg
T_{amb}=69.0 F P_{atm}=849. mb
P_{dyn}=3.275E-02 psi
V_c=69.5 ft/sec Re = 5.369E+05
Pressure Coefficient
-4.0
-3.0
-2.0
-1.0
0.0
1.0
0.00
0.20
0.40
0.60
0.80
1.00
Blade Chord X/C

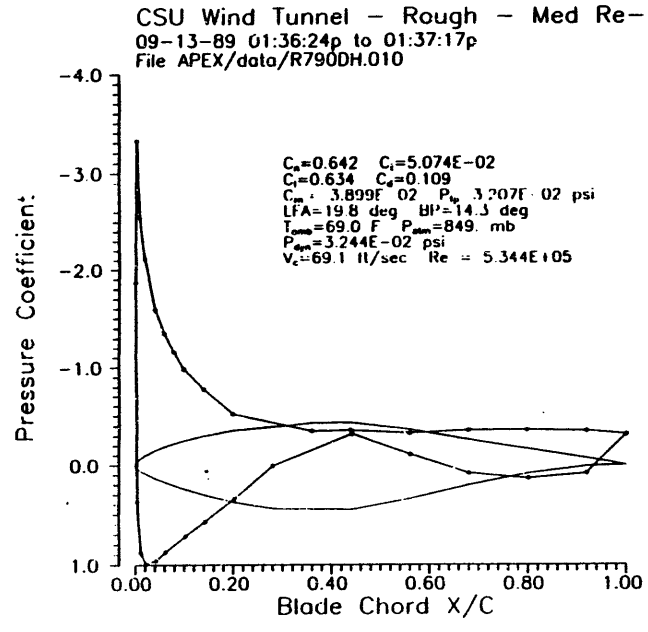
CSU Wind Tunnel – Rough – Med Re– Run 9
09-13-89 01:36:24p to 01:37:17p
File APEX/data/R790DH.010
C_n=0.642 C_t=5.074E-02
C_l=0.634 C_d=0.109
C_m=-3.899E-02 P_{tip}=3.207E-02 psi
LFA=19.8 deg BP=14.3 deg
T_{amb}=69.0 F P_{atm}=849. mb
P_{dyn}=3.244E-02 psi
V_c=69.1 ft/sec Re = 5.344E+05
Pressure Coefficient
-4.0
-3.0
-2.0
-1.0
0.0
1.0
0.00
0.20
0.40
0.60
0.80
1.00
Blade Chord X/C

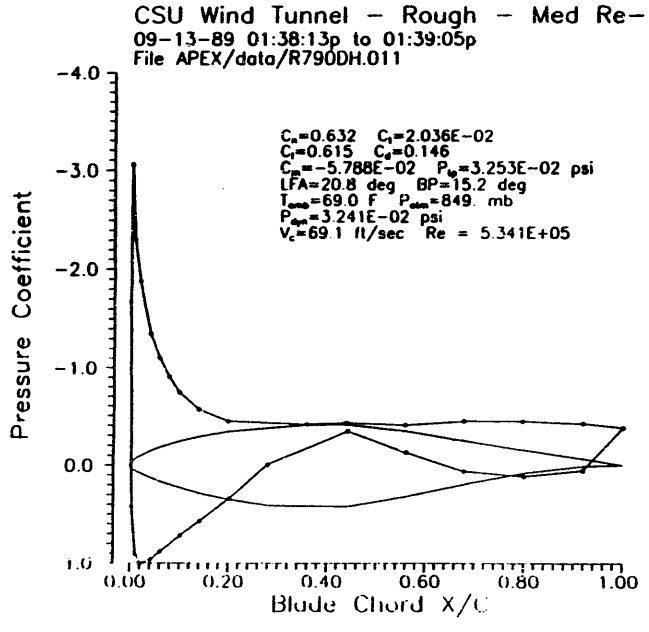
CSU Wind Tunnel – Rough – Med Re– Run 9
09-13-89 01:38:13p to 01:39:05p
File APEX/data/R790DH.011
C_n=0.632 C_t=2.036E-02
C_l=0.615 C_d=0.146
C_m=-5.788E-02 P_{tip}=3.253E-02 psi
LFA=20.8 deg BP=15.2 deg
T_{amb}=69.0 F P_{atm}=849. mb
P_{dyn}=3.241E-02 psi
V_c=69.1 ft/sec Re = 5.341E+05
Pressure Coefficient
-4.0
-3.0
-2.0
-1.0
0.0
1.0
0.00
0.20
0.40
0.60
0.80
1.00
Blade Chord X/C

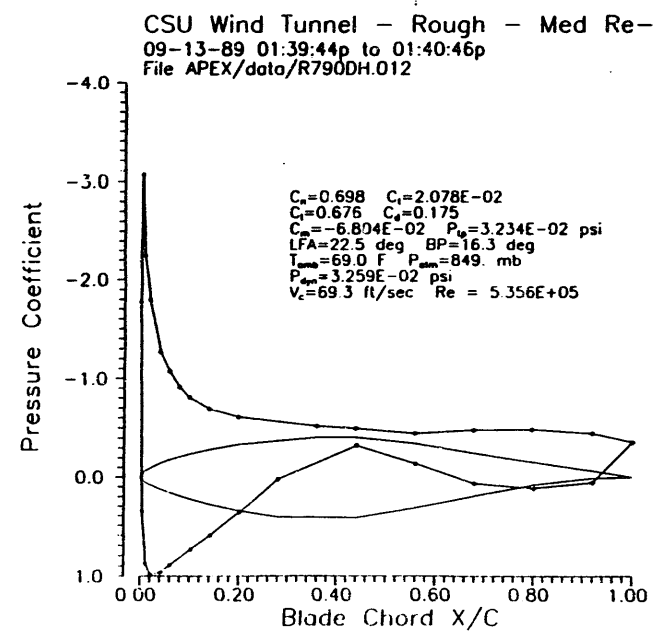
CSU Wind Tunnel – Rough – Med Re– Run 9
09-13-89 01:39:44p to 01:40:46p
File APEX/data/R790DH.012
C_n=0.698 C_t=2.078E-02
C_l=0.676 C_d=0.175
C_m=-6.804E-02 P_{tip}=3.234E-02 psi
LFA=22.5 deg BP=16.3 deg
T_{amb}=69.0 F P_{atm}=849. mb
P_{dyn}=3.259E-02 psi
V_c=69.3 ft/sec Re = 5.356E+05
Pressure Coefficient
-4.0
-3.0
-2.0
-1.0
0.0
1.0
0.00
0.20
0.40
0.60
0.80
1.00
Blade Chord X/C

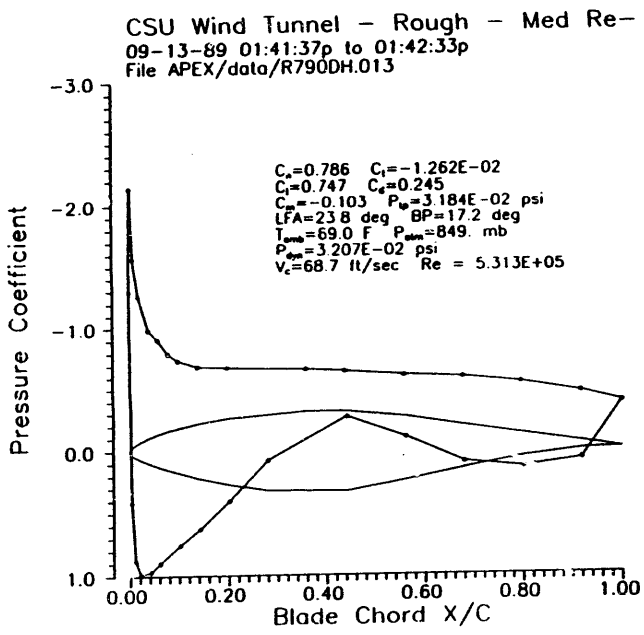
CSU Wind Tunnel – Rough – Med Re– Run 9
09-13-89 01:41:37p to 01:42:33p
File APEX/data/R790DH.013
C_n=0.786 C_t=-1.262E-02
C_l=0.747 C_d=0.245
C_{cp}=-0.103 P_{tp}=3.184E-02 psi
LFA=23.8 deg BP=17.2 deg
T_{amb}=69.0 F P_{atm}=849. mb
P_{dyn}=3.207E-02 psi
V_c=68.7 ft/sec Re = 5.313E+05
Pressure Coefficient
-3.0
-2.0
-1.0
0.0
1.0
0.00
0.20
0.40
0.60
0.80
1.00
Blade Chord X/C

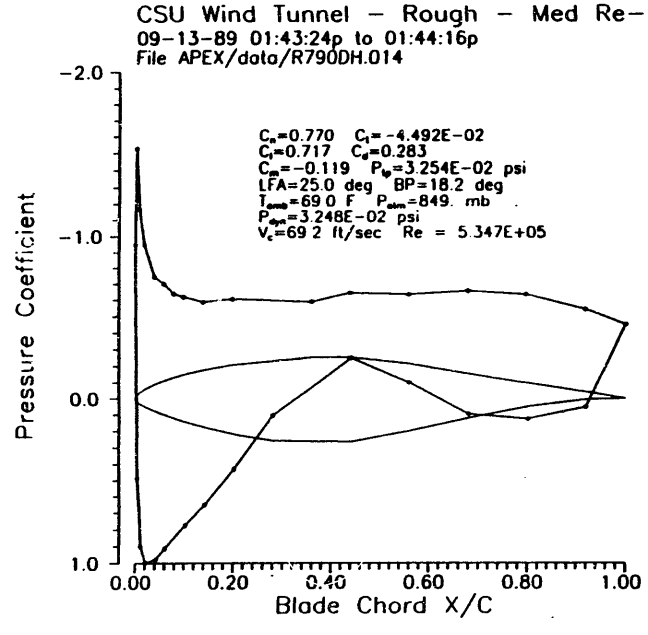
CSU Wind Tunnel – Rough – Med Re– Run 9
09-13-89 01:43:24p to 01:44:16p
File APEX/data/R790DH.014
C_n=0.770 C_t=-4.492E-02
C_l=0.717 C_d=0.283
C_{cp}=-0.119 P_{tp}=3.254E-02 psi
LFA=25.0 deg BP=18.2 deg
T_{amb}=69.0 F P_{atm}=849. mb
P_{dyn}=3.248E-02 psi
V_c=69.2 ft/sec Re = 5.347E+05
Pressure Coefficient
-2.0
-1.0
0.0
1.0
0.00
0.20
0.40
0.60
0.80
1.00
Blade Chord X/C

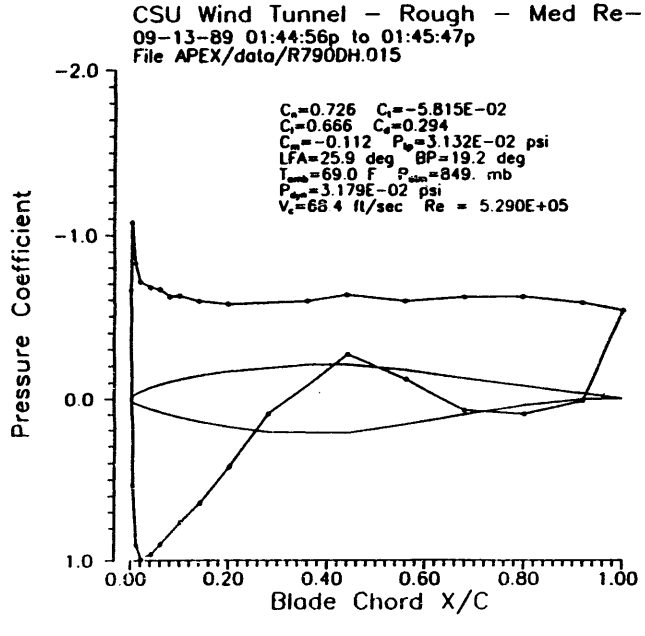
CSU Wind Tunnel – Rough – Med Re– Run 9
09-13-89 01:44:56p to 01:45:47p
File APEX/data/R790DH.015
C_n=0.726 C_t=-5.815E-02
C_l=0.666 C_d=0.294
C_{cp}=-0.112 P_{tp}=3.132E-02 psi
LFA=25.9 deg BP=19.2 deg
T_{amb}=69.0 F P_{atm}=849. mb
P_{dyn}=3.179E-02 psi
V_c=68.4 ft/sec Re = 5.290E+05
Pressure Coefficient
-2.0
-1.0
0.0
1.0
0.00
0.20
0.40
0.60
0.80
1.00
Blade Chord X/C

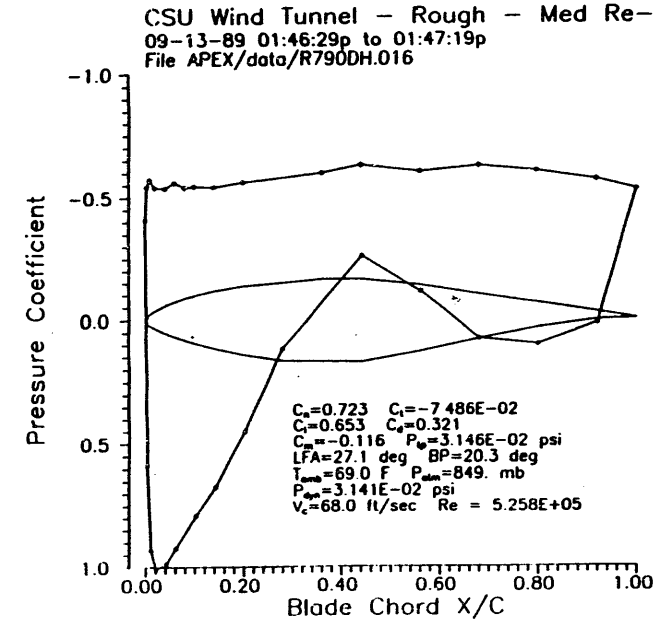
CSU Wind Tunnel – Rough – Med Re– Run 9
09-13-89 01:46:29p to 01:47:19p
File APEX/data/R790DH.016
C_n=0.723 C_t=-7.486E-02
C_l=0.653 C_d=0.321
C_{cp}=-0.116 P_{tp}=3.146E-02 psi
LFA=27.1 deg BP=20.3 deg
T_{amb}=69.0 F P_{atm}=849. mb
P_{dyn}=3.141E-02 psi
V_c=68.0 ft/sec Re = 5.258E+05
Pressure Coefficient
-1.0
-0.5
0.0
0.5
1.0
0.00
0.20
0.40
0.60
0.80
1.00
Blade Chord X/C

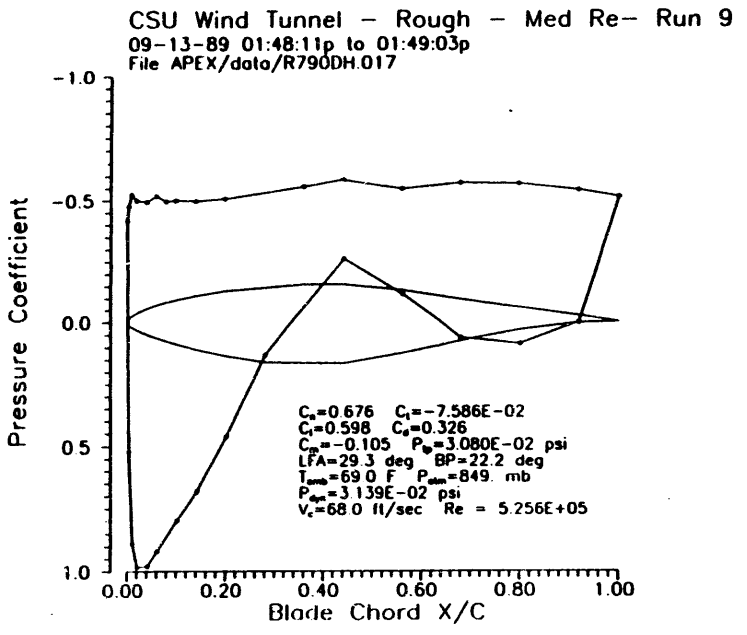
CSU Wind Tunnel – Rough – Med Re– Run 9
09-13-89 01:48:11p to 01:49:03p
File APEX/data/R790DH.017
Pressure Coefficient
-1.0
-0.5
0.0
0.5
1.0
0.00
0.20
0.40
0.60
0.80
1.00
Blade Chord X/C
C_n=0.676 C_t=-7.586E-02
C_l=0.598 C_d=0.326
C_m=-0.105 P_{tp}=3.080E-02 psi
LFA=29.3 deg BP=22.2 deg
T_{amb}=69.0 F P_{atm}=849. mb
P_{dyn}=3.139E-02 psi
V_c=68.0 ft/sec Re = 5.256E+05

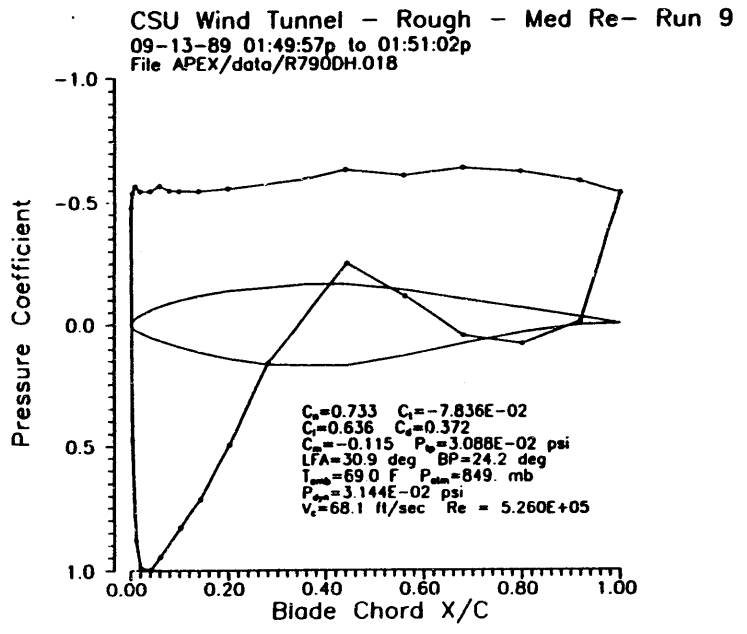
CSU Wind Tunnel – Rough – Med Re– Run 9
09-13-89 01:49:57p to 01:51:02p
File APEX/data/R790DH.018
Pressure Coefficient
-1.0
-0.5
0.0
0.5
1.0
0.00
0.20
0.40
0.60
0.80
1.00
Blade Chord X/C
C_n=0.733 C_t=-7.836E-02
C_l=0.636 C_d=0.372
C_m=-0.115 P_{tp}=3.088E-02 psi
LFA=30.9 deg BP=24.2 deg
T_{amb}=69.0 F P_{atm}=849. mb
P_{dyn}=3.144E-02 psi
V_c=68.1 ft/sec Re = 5.260E+05

Appendix K

Pressure Distributions for Reynolds Number 300,000 Smooth

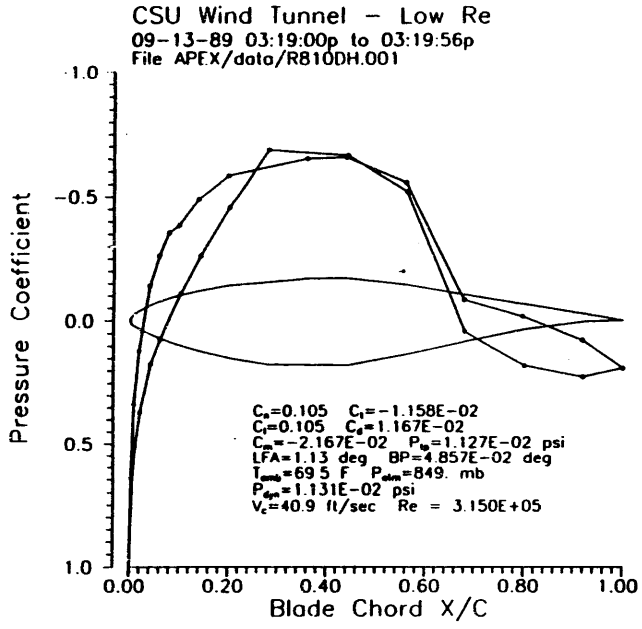
CSU Wind Tunnel - Low Re
09-13-89 03:19:00p to 03:19:56p
File APEX/data/R810DH.001
Pressure Coefficient
Blade Chord X/C
C_n=0.105 C_t=-1.158E-02
C_l=0.105 C_d=1.167E-02
C_m=-2.167E-02 P_{tp}=1.127E-02 psi
LFA=1.13 deg BP=4.857E-02 deg
T_{amb}=69.5 F P_{atm}=849. mb
P_{dyn}=1.131E-02 psi
V_c=40.9 ft/sec Re = 3.150E+05

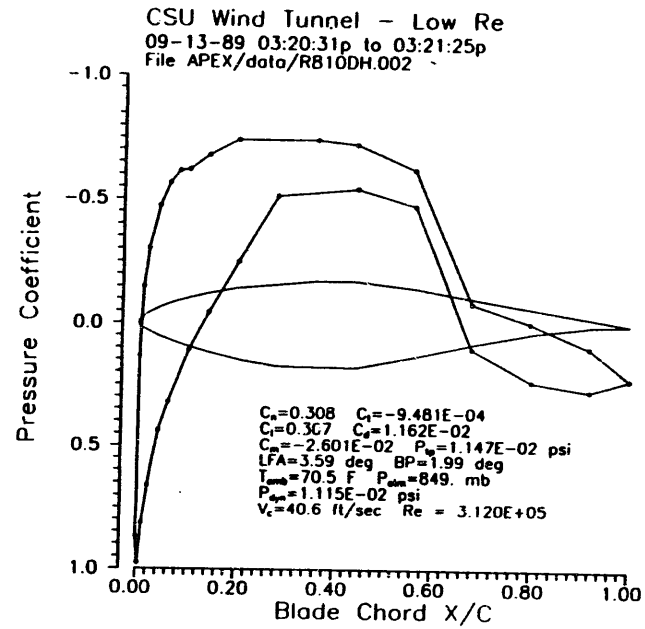
CSU Wind Tunnel - Low Re
09-13-89 03:20:31p to 03:21:25p
File APEX/data/R810DH.002
Pressure Coefficient
Blade Chord X/C
C_n=0.308 C_t=-9.481E-04
C_l=0.307 C_d=1.162E-02
C_m=-2.601E-02 P_{tp}=1.147E-02 psi
LFA=3.59 deg BP=1.99 deg
T_{amb}=70.5 F P_{atm}=849. mb
P_{dyn}=1.115E-02 psi
V_c=40.6 ft/sec Re = 3.120E+05

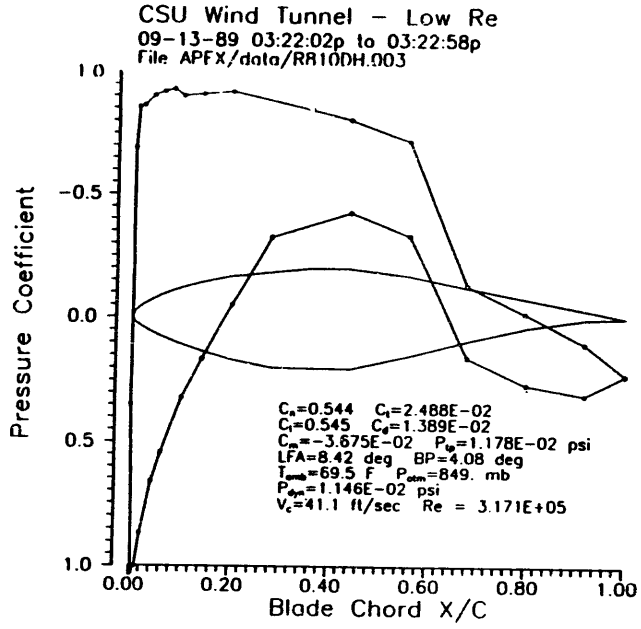
CSU Wind Tunnel - Low Re
09-13-89 03:22:02p to 03:22:58p
File APEX/data/R810DH.003
Pressure Coefficient
Blade Chord X/C
C_n=0.544 C_t=2.488E-02
C_l=0.545 C_d=1.389E-02
C_m=-3.675E-02 P_{tp}=1.178E-02 psi
LFA=8.42 deg BP=4.08 deg
T_{amb}=69.5 F P_{atm}=849. mb
P_{dyn}=1.146E-02 psi
V_c=41.1 ft/sec Re = 3.171E+05

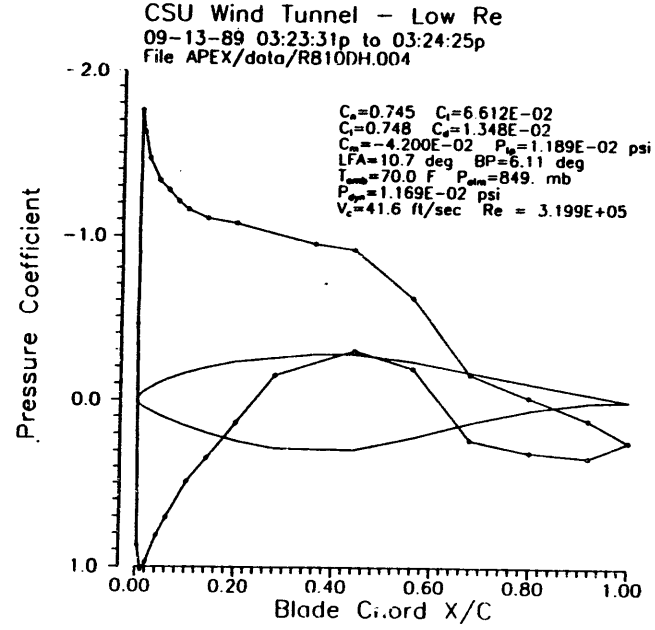
CSU Wind Tunnel - Low Re
09-13-89 03:23:31p to 03:24:25p
File APEX/data/R810DH.004
Pressure Coefficient
Blade Chord X/C
C_n=0.745 C_t=6.612E-02
C_l=0.748 C_d=1.348E-02
C_m=-4.200E-02 P_{tp}=1.189E-02 psi
LFA=10.7 deg BP=6.11 deg
T_{amb}=70.0 F P_{atm}=849. mb
P_{dyn}=1.169E-02 psi
V_c=41.6 ft/sec Re = 3.199E+05

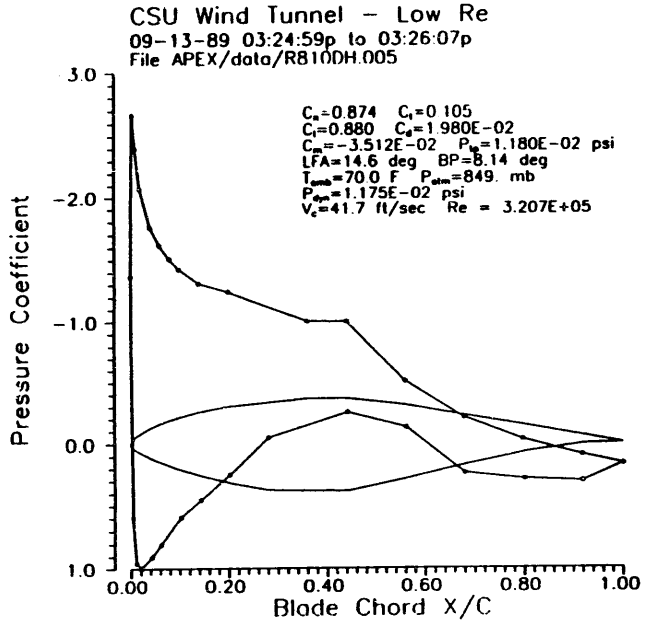
CSU Wind Tunnel – Low Re
09-13-89 03:24:59p to 03:26:07p
File APEX/data/R810DH.005
C_n=0.874 C_t=0.105
C_l=0.880 C_d=1.980E-02
C_m=-3.512E-02 P_{tp}=1.180E-02 psi
LFA=14.6 deg BP=8.14 deg
T_{amb}=70.0 F P_{atm}=849. mb
P_{dyn}=1.175E-02 psi
V_c=41.7 ft/sec Re = 3.207E+05
Pressure Coefficient
3.0
-2.0
-1.0
0.0
1.0
0.00
0.20
0.40
0.60
0.80
1.00
Blade Chord X/C

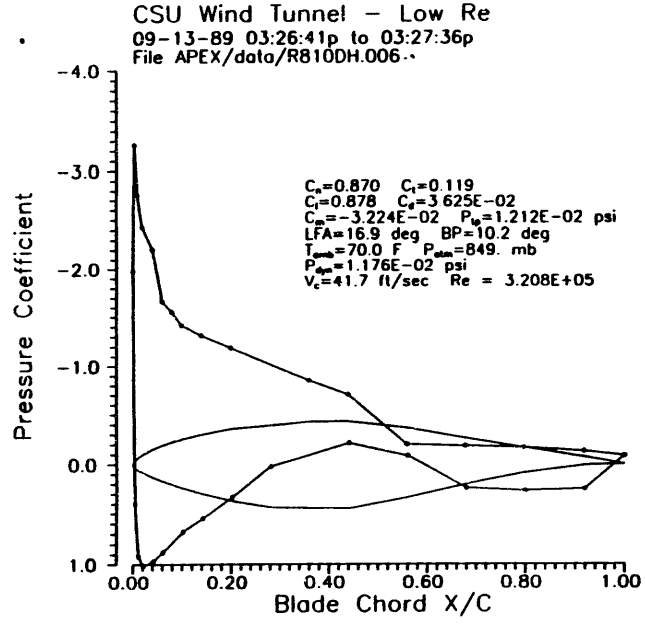
CSU Wind Tunnel – Low Re
09-13-89 03:26:41p to 03:27:36p
File APEX/data/R810DH.006
C_n=0.870 C_t=0.119
C_l=0.878 C_d=3.625E-02
C_m=-3.224E-02 P_{tp}=1.212E-02 psi
LFA=16.9 deg BP=10.2 deg
T_{amb}=70.0 F P_{atm}=849. mb
P_{dyn}=1.176E-02 psi
V_c=41.7 ft/sec Re = 3.208E+05
Pressure Coefficient
-4.0
-3.0
-2.0
-1.0
0.0
1.0
0.00
0.20
0.40
0.60
0.80
1.00
Blade Chord X/C

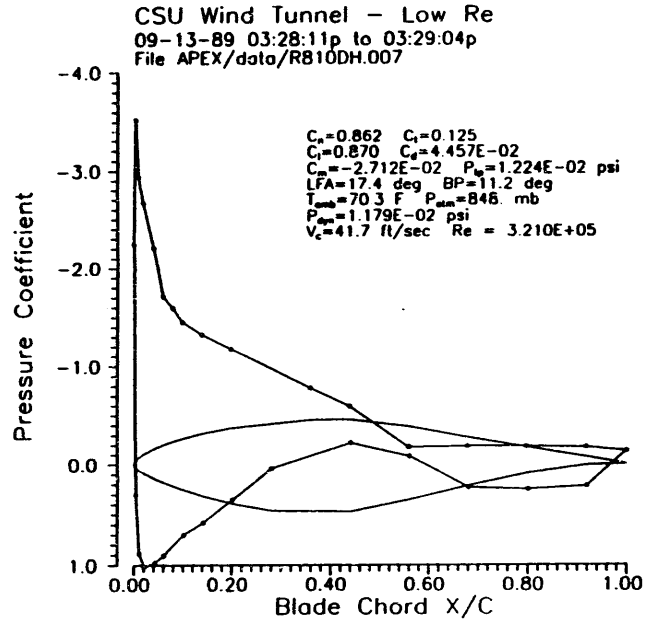
CSU Wind Tunnel – Low Re
09-13-89 03:28:11p to 03:29:04p
File APEX/data/R810DH.007
C_n=0.862 C_t=0.125
C_l=0.870 C_d=4.457E-02
C_m=-2.712E-02 P_{tp}=1.224E-02 psi
LFA=17.4 deg BP=11.2 deg
T_{amb}=70.3 F P_{atm}=848. mb
P_{dyn}=1.179E-02 psi
V_c=41.7 ft/sec Re = 3.210E+05
Pressure Coefficient
-4.0
-3.0
-2.0
-1.0
0.0
1.0
0.00
0.20
0.40
0.60
0.80
1.00
Blade Chord X/C

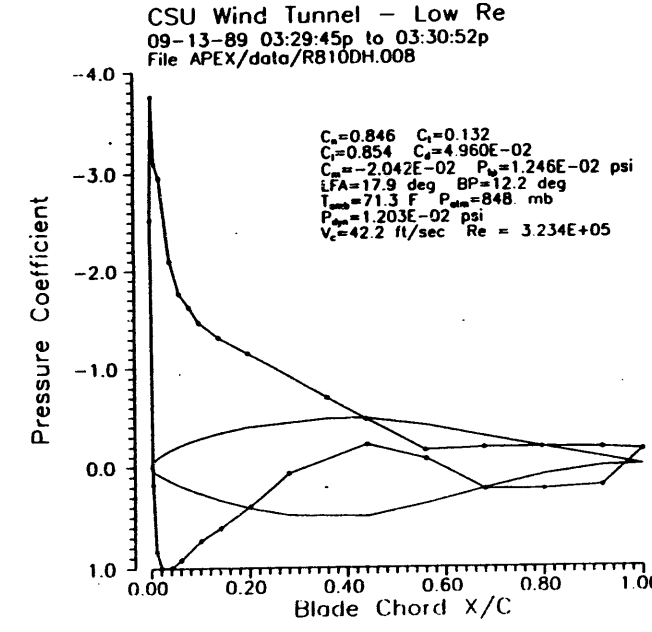
CSU Wind Tunnel – Low Re
09-13-89 03:29:45p to 03:30:52p
File APEX/data/R810DH.008
C_n=0.846 C_t=0.132
C_l=0.854 C_d=4.960E-02
C_m=-2.042E-02 P_{tp}=1.246E-02 psi
LFA=17.9 deg BP=12.2 deg
T_{amb}=71.3 F P_{atm}=848. mb
P_{dyn}=1.203E-02 psi
V_c=42.2 ft/sec Re = 3.234E+05
Pressure Coefficient
-4.0
-3.0
-2.0
-1.0
0.0
1.0
0.00
0.20
0.40
0.60
0.80
1.00
Blade Chord X/C

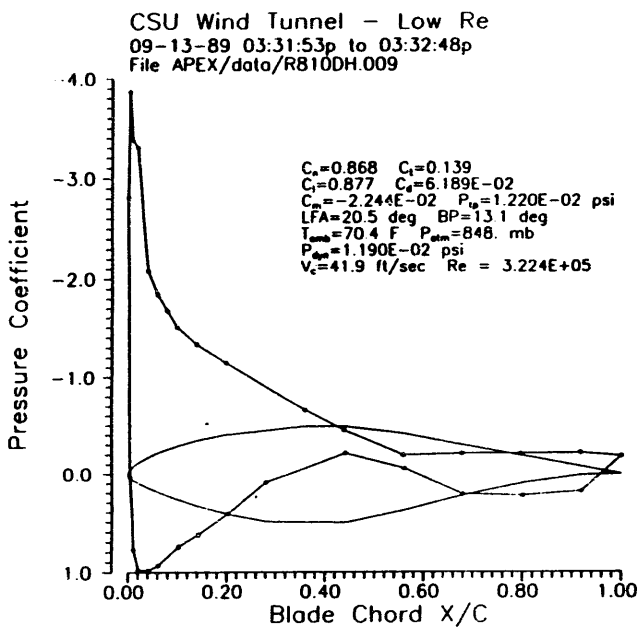
CSU Wind Tunnel - Low Re
09-13-89 03:31:53p to 03:32:48p
File APEX/data/R810DH.009
C_n=0.868 C_l=0.139
C_m=0.877 C_d=6.189E-02
C_{cp}=-2.244E-02 P_{tg}=1.220E-02 psi
LFA=20.5 deg BP=13.1 deg
T_{amb}=70.4 F P_{atm}=848. mb
P_{dyn}=1.190E-02 psi
V_c=41.9 ft/sec Re = 3.224E+05
Pressure Coefficient
-4.0
-3.0
-2.0
-1.0
0.0
1.0
0.00
0.20
0.40
0.60
0.80
1.00
Blade Chord X/C

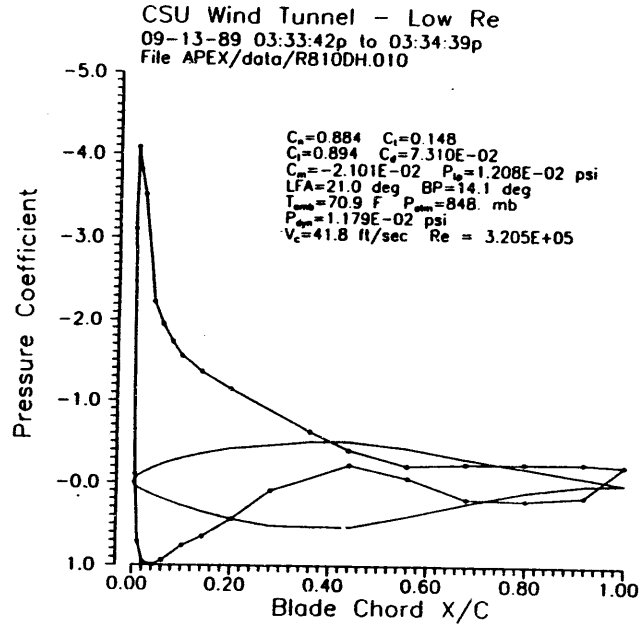
CSU Wind Tunnel - Low Re
09-13-89 03:33:42p to 03:34:39p
File APEX/data/R810DH.010
C_n=0.884 C_l=0.148
C_m=0.894 C_d=7.310E-02
C_{cp}=-2.101E-02 P_{tg}=1.208E-02 psi
LFA=21.0 deg BP=14.1 deg
T_{amb}=70.9 F P_{atm}=848. mb
P_{dyn}=1.179E-02 psi
V_c=41.8 ft/sec Re = 3.205E+05
Pressure Coefficient
-5.0
-4.0
-3.0
-2.0
-1.0
-0.0
1.0
0.00
0.20
0.40
0.60
0.80
1.00
Blade Chord X/C

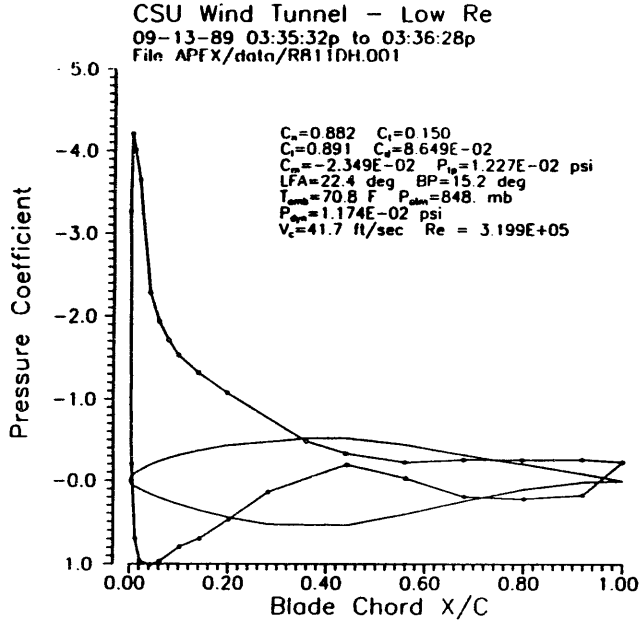
CSU Wind Tunnel - Low Re
09-13-89 03:35:32p to 03:36:28p
File APEX/data/R811DH.001
C_n=0.882 C_l=0.150
C_m=0.891 C_d=8.649E-02
C_{cp}=-2.349E-02 P_{tg}=1.227E-02 psi
LFA=22.4 deg BP=15.2 deg
T_{amb}=70.8 F P_{atm}=848. mb
P_{dyn}=1.174E-02 psi
V_c=41.7 ft/sec Re = 3.199E+05
Pressure Coefficient
-5.0
-4.0
-3.0
-2.0
-1.0
-0.0
1.0
0.00
0.20
0.40
0.60
0.80
1.00
Blade Chord X/C

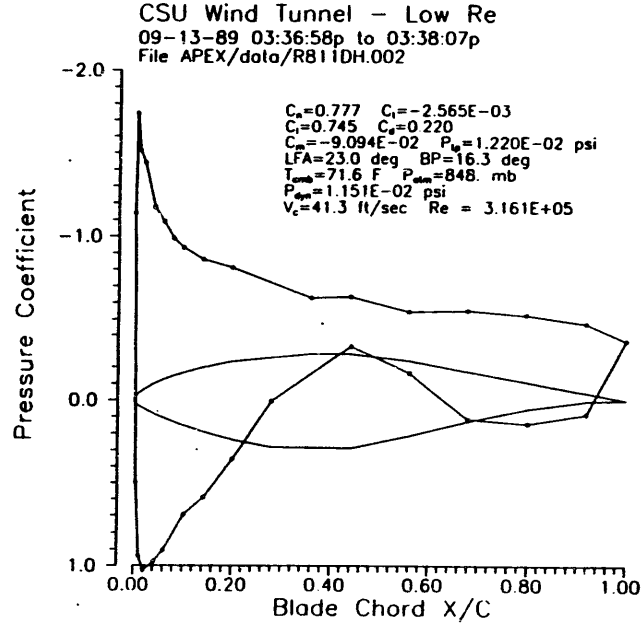
CSU Wind Tunnel - Low Re
09-13-89 03:36:58p to 03:38:07p
File APEX/data/R811DH.002
C_n=0.777 C_l=-2.565E-03
C_m=0.745 C_d=0.220
C_{cp}=-9.094E-02 P_{tg}=1.220E-02 psi
LFA=23.0 deg BP=16.3 deg
T_{amb}=71.6 F P_{atm}=848. mb
P_{dyn}=1.151E-02 psi
V_c=41.3 ft/sec Re = 3.161E+05
Pressure Coefficient
-2.0
-1.0
0.0
1.0
0.00
0.20
0.40
0.60
0.80
1.00
Blade Chord X/C

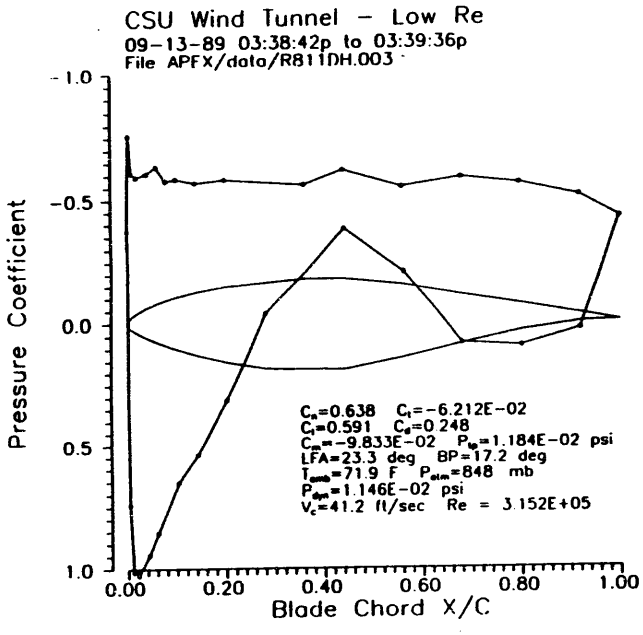
CSU Wind Tunnel – Low Re
09-13-89 03:38:42p to 03:39:36p
File APEX/data/R811DH.003
Pressure Coefficient
Blade Chord X/C
C_n=0.638 C_t=-6.212E-02
C_l=0.591 C_d=0.248
C_m=-9.833E-02 P_{tp}=1.184E-02 psi
LFA=23.3 deg BP=17.2 deg
T_{amb}=71.9 F P_{atm}=848 mb
P_{dyn}=1.146E-02 psi
V_c=41.2 ft/sec Re = 3.152E+05

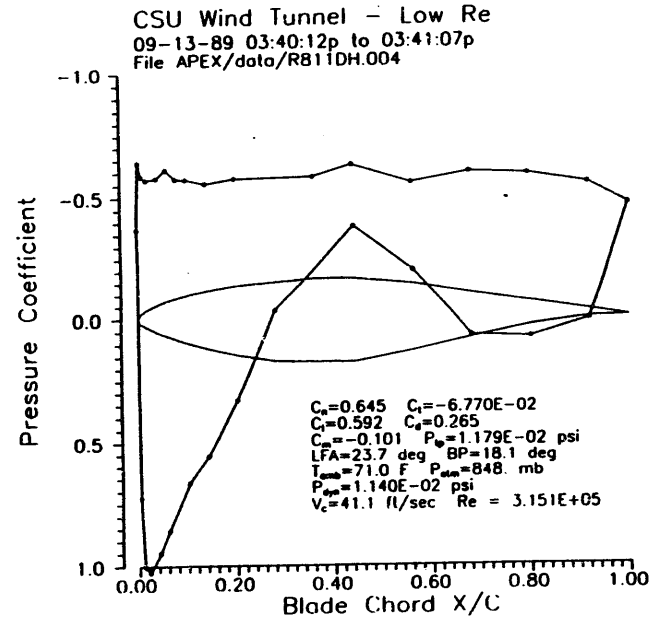
CSU Wind Tunnel – Low Re
09-13-89 03:40:12p to 03:41:07p
File APEX/data/R811DH.004
Pressure Coefficient
Blade Chord X/C
C_n=0.645 C_t=-6.770E-02
C_l=0.592 C_d=0.265
C_m=-0.101 P_{tp}=1.179E-02 psi
LFA=23.7 deg BP=18.1 deg
T_{amb}=71.0 F P_{atm}=848. mb
P_{dyn}=1.140E-02 psi
V_c=41.1 ft/sec Re = 3.151E+05

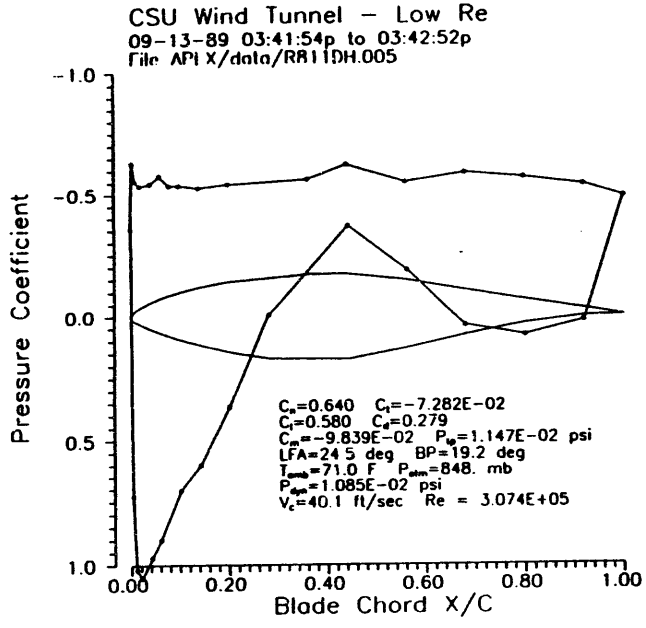
CSU Wind Tunnel – Low Re
09-13-89 03:41:54p to 03:42:52p
File APEX/data/R811DH.005
Pressure Coefficient
Blade Chord X/C
C_n=0.640 C_t=-7.282E-02
C_l=0.580 C_d=0.279
C_m=-9.839E-02 P_{tp}=1.147E-02 psi
LFA=24.5 deg BP=19.2 deg
T_{amb}=71.0 F P_{atm}=848. mb
P_{dyn}=1.085E-02 psi
V_c=40.1 ft/sec Re = 3.074E+05

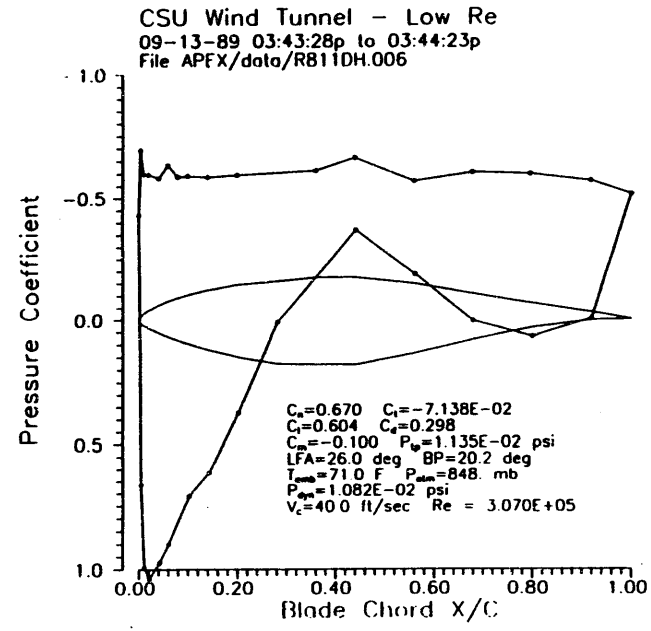
CSU Wind Tunnel – Low Re
09-13-89 03:43:28p to 03:44:23p
File APEX/data/R811DH.006
Pressure Coefficient
Blade Chord X/C
C_n=0.670 C_t=-7.138E-02
C_l=0.604 C_d=0.298
C_m=-0.100 P_{tp}=1.135E-02 psi
LFA=26.0 deg BP=20.2 deg
T_{amb}=71.0 F P_{atm}=848. mb
P_{dyn}=1.082E-02 psi
V_c=40.0 ft/sec Re = 3.070E+05

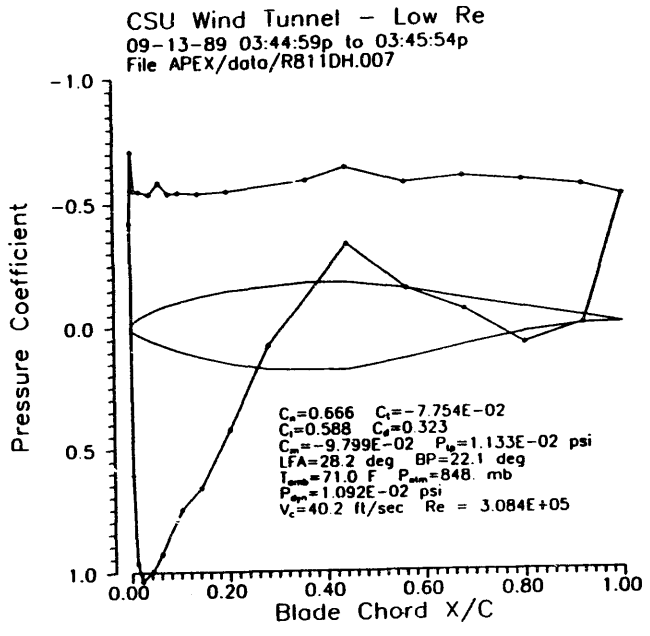
CSU Wind Tunnel – Low Re
09-13-89 03:44:59p to 03:45:54p
File APEX/data/R811DH.007
Pressure Coefficient
Blade Chord X/C
C_n=0.666 C_t=-7.754E-02
C_l=0.588 C_d=0.323
C_m=-9.799E-02 P_{tp}=1.133E-02 psi
LFA=28.2 deg BP=22.1 deg
T_{amb}=71.0 F P_{atm}=848. mb
P_{dyn}=1.092E-02 psi
V_c=40.2 ft/sec Re = 3.084E+05

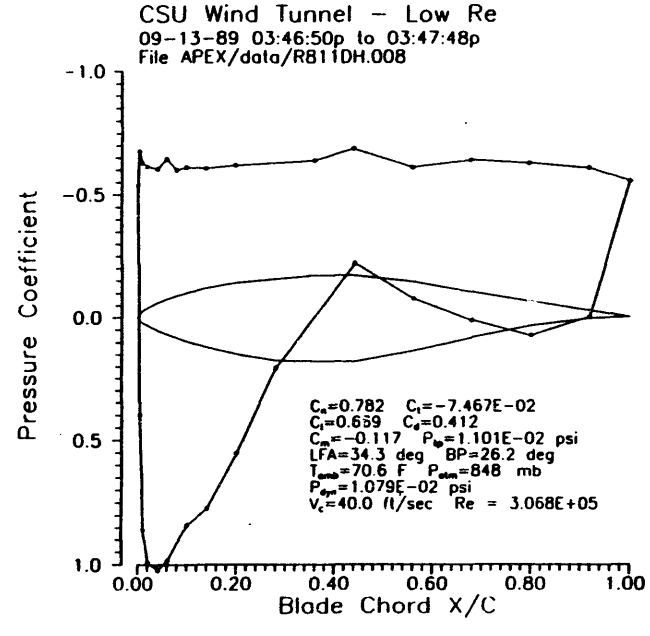
CSU Wind Tunnel – Low Re
09-13-89 03:46:50p to 03:47:48p
File APEX/data/R811DH.008
Pressure Coefficient
Blade Chord X/C
C_n=0.782 C_t=-7.467E-02
C_l=0.659 C_d=0.412
C_m=-0.117 P_{tp}=1.101E-02 psi
LFA=34.3 deg BP=26.2 deg
T_{amb}=70.6 F P_{atm}=848 mb
P_{dyn}=1.079E-02 psi
V_c=40.0 ft/sec Re = 3.068E+05

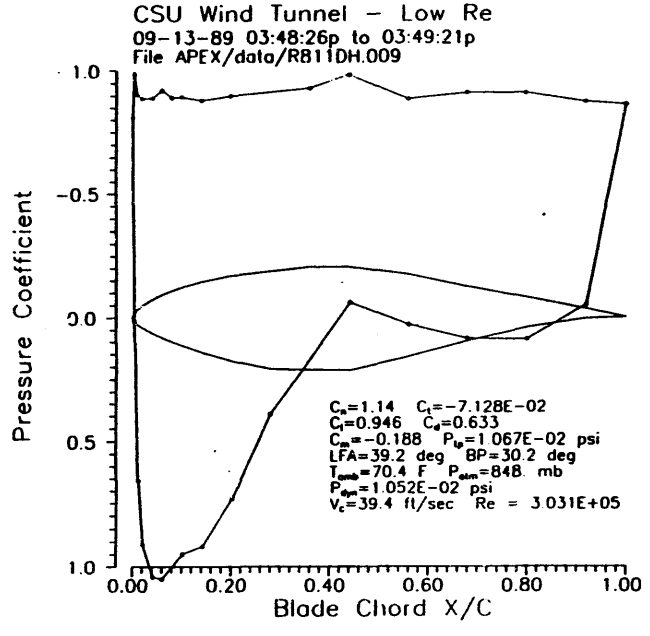
CSU Wind Tunnel – Low Re
09-13-89 03:48:26p to 03:49:21p
File APEX/data/R811DH.009
Pressure Coefficient
Blade Chord X/C
C_n=1.14 C_t=-7.128E-02
C_l=0.946 C_d=0.633
C_m=-0.188 P_{tp}=1.067E-02 psi
LFA=39.2 deg BP=30.2 deg
T_{amb}=70.4 F P_{atm}=848. mb
P_{dyn}=1.052E-02 psi
V_c=39.4 ft/sec Re = 3.031E+05

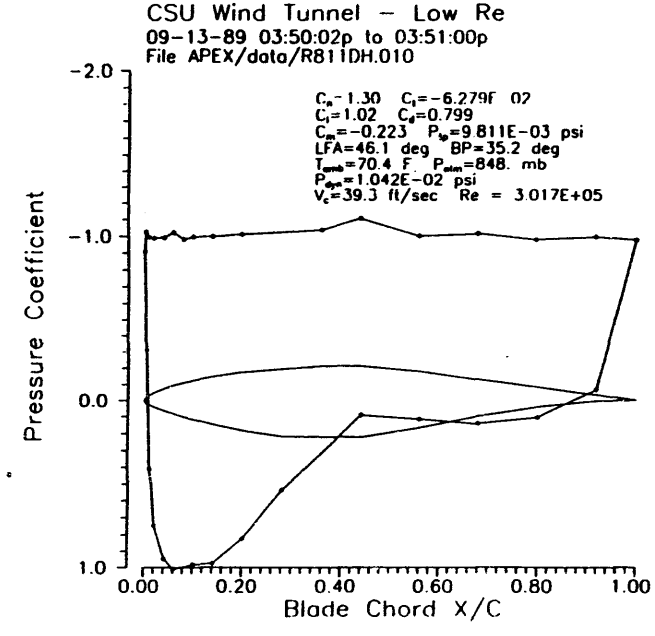
CSU Wind Tunnel – Low Re
09-13-89 03:50:02p to 03:51:00p
File APEX/data/R811DH.010
Pressure Coefficient
Blade Chord X/C
C_n=1.30 C_t=-6.279E-02
C_l=1.02 C_d=0.799
C_m=-0.223 P_{tp}=9.811E-03 psi
LFA=46.1 deg BP=35.2 deg
T_{amb}=70.4 F P_{atm}=848. mb
P_{dyn}=1.042E-02 psi
V_c=39.3 ft/sec Re = 3.017E+05

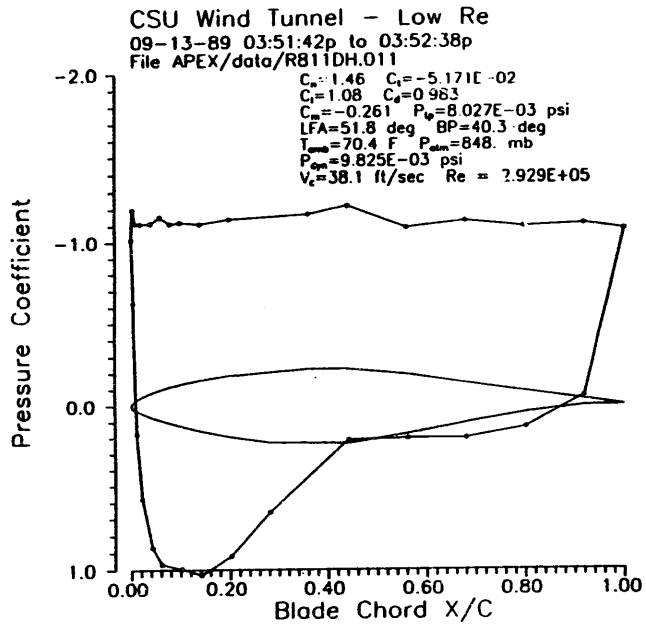
CSU Wind Tunnel - Low Re
09-13-89 03:51:42p to 03:52:38p
File APEX/data/R811DH.011
C_n=1.46 C_t=-5.171E-02
C_l=1.08 C_d=0.983
C_m=-0.261 P_{tp}=8.027E-03 psi
LFA=51.8 deg BP=40.3 deg
T_{amb}=70.4 F P_{atm}=848. mb
P_{dyn}=9.825E-03 psi
V_c=38.1 ft/sec Re = 2.929E+05
Pressure Coefficient
-2.0
-1.0
0.0
1.0
0.00
0.20
0.40
0.60
0.80
1.00
Blade Chord X/C

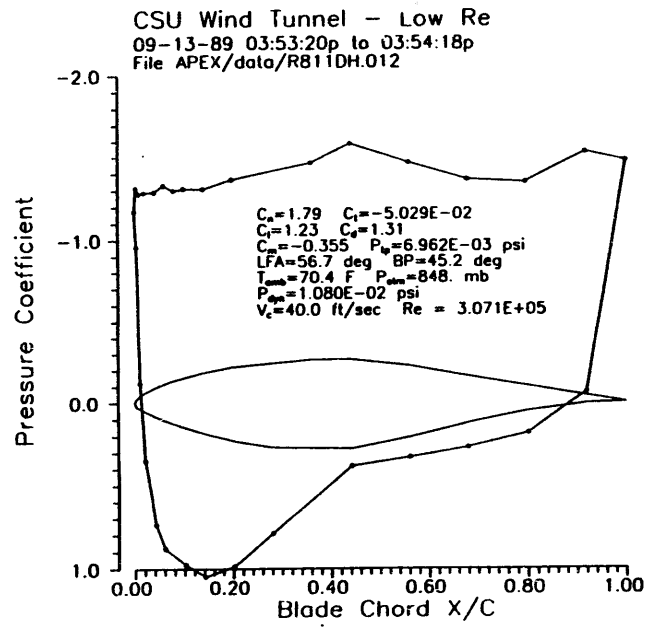
CSU Wind Tunnel - Low Re
09-13-89 03:53:20p to 03:54:18p
File APEX/data/R811DH.012
C_n=1.79 C_t=-5.029E-02
C_l=1.23 C_d=1.31
C_m=-0.355 P_{tp}=6.962E-03 psi
LFA=56.7 deg BP=45.2 deg
T_{amb}=70.4 F P_{atm}=848. mb
P_{dyn}=1.080E-02 psi
V_c=40.0 ft/sec Re = 3.071E+05
Pressure Coefficient
-2.0
-1.0
0.0
1.0
0.00
0.20
0.40
0.60
0.80
1.00
Blade Chord X/C

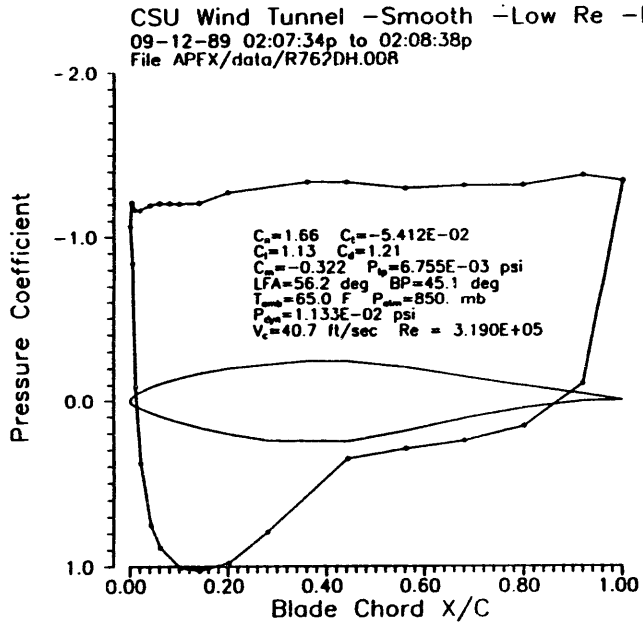
CSU Wind Tunnel -Smooth -Low Re -Run 7
09-12-89 02:07:34p to 02:08:38p
File APEX/data/R762DH.008
C_n=1.66 C_t=-5.412E-02
C_l=1.13 C_d=1.21
C_m=-0.322 P_{tp}=6.755E-03 psi
LFA=56.2 deg BP=45.1 deg
T_{amb}=65.0 F P_{atm}=850. mb
P_{dyn}=1.133E-02 psi
V_c=40.7 ft/sec Re = 3.190E+05
Pressure Coefficient
-2.0
-1.0
0.0
1.0
0.00
0.20
0.40
0.60
0.80
1.00
Blade Chord X/C

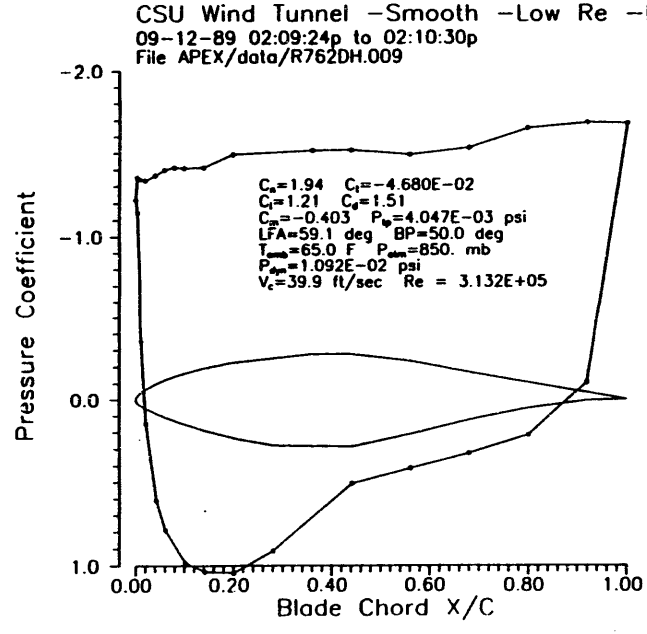
CSU Wind Tunnel -Smooth -Low Re -Run 7
09-12-89 02:09:24p to 02:10:30p
File APEX/data/R762DH.009
C_n=1.94 C_t=-4.680E-02
C_l=1.21 C_d=1.51
C_m=-0.403 P_{tp}=4.047E-03 psi
LFA=59.1 deg BP=50.0 deg
T_{amb}=65.0 F P_{atm}=850. mb
P_{dyn}=1.092E-02 psi
V_c=39.9 ft/sec Re = 3.132E+05
Pressure Coefficient
-2.0
-1.0
0.0
1.0
0.00
0.20
0.40
0.60
0.80
1.00
Blade Chord X/C

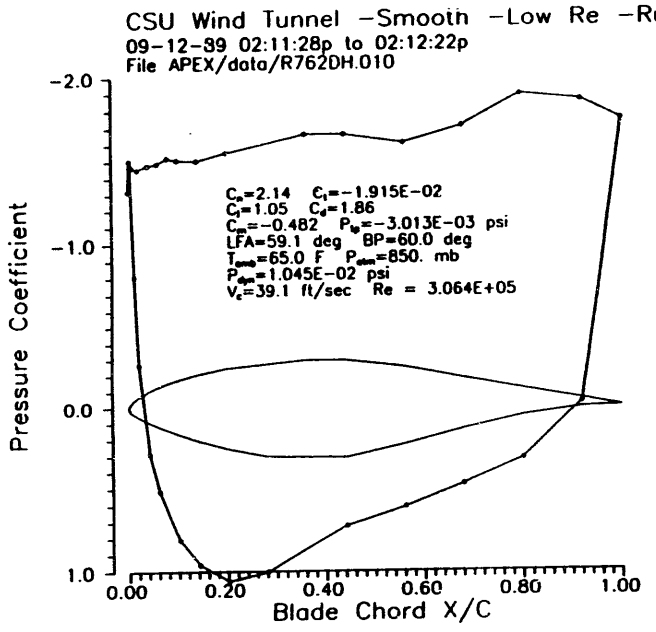
CSU Wind Tunnel -Smooth -Low Re -Run 7
09-12-89 02:11:28p to 02:12:22p
File APEX/data/R762DH.010
C_n=2.14 C_t=-1.915E-02
C_l=1.05 C_d=1.86
C_m=-0.482 P_{tp}=-3.013E-03 psi
LFA=59.1 deg BP=60.0 deg
T_{amb}=65.0 F P_{atm}=850. mb
P_{dyn}=1.045E-02 psi
V_c=39.1 ft/sec Re = 3.064E+05
Pressure Coefficient
-2.0
-1.0
0.0
1.0
0.00
0.20
0.40
0.60
0.80
1.00
Blade Chord X/C

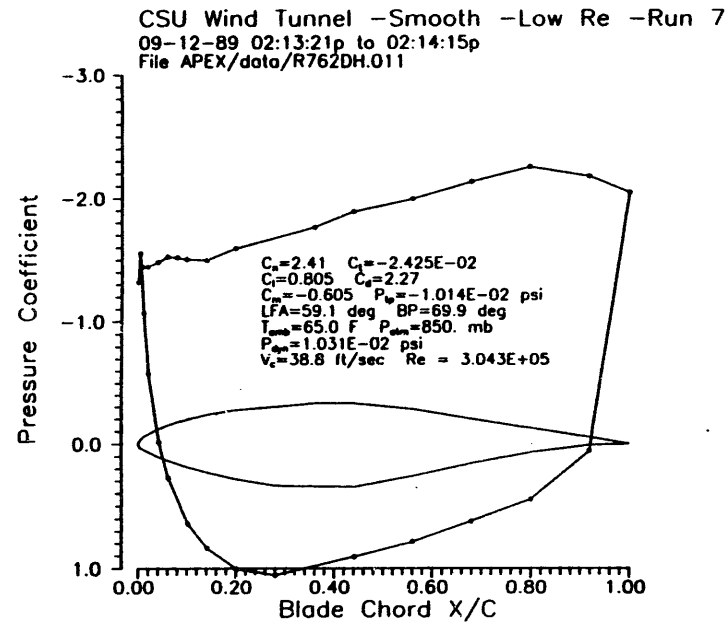
CSU Wind Tunnel -Smooth -Low Re -Run 7
09-12-89 02:13:21p to 02:14:15p
File APEX/data/R762DH.011
C_n=2.41 C_t=-2.425E-02
C_l=0.805 C_d=2.27
C_m=-0.605 P_{tp}=-1.014E-02 psi
LFA=59.1 deg BP=69.9 deg
T_{amb}=65.0 F P_{atm}=850. mb
P_{dyn}=1.031E-02 psi
V_c=38.8 ft/sec Re = 3.043E+05
Pressure Coefficient
-3.0
-2.0
-1.0
0.0
1.0
0.00
0.20
0.40
0.60
0.80
1.00
Blade Chord X/C

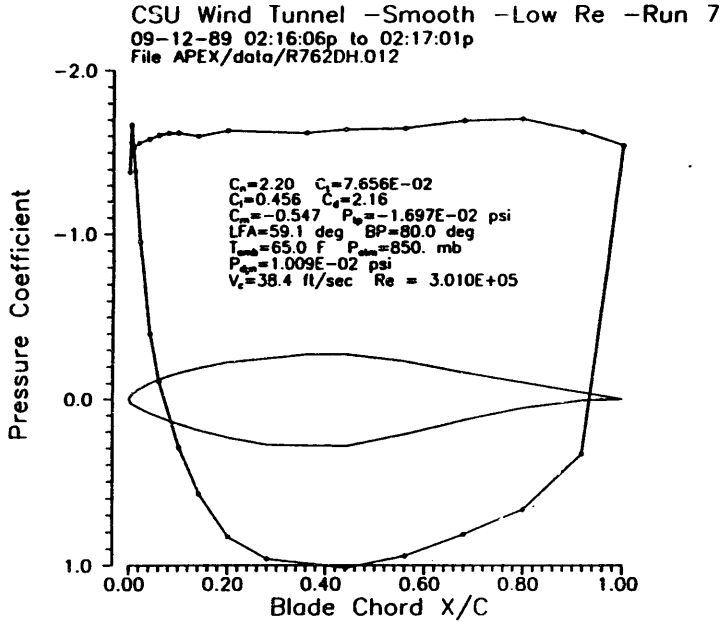
CSU Wind Tunnel -Smooth -Low Re -Run 7
09-12-89 02:16:06p to 02:17:01p
File APEX/data/R762DH.012
C_n=2.20 C_t=7.656E-02
C_l=0.456 C_d=2.16
C_m=-0.547 P_{tp}=-1.697E-02 psi
LFA=59.1 deg BP=80.0 deg
T_{amb}=65.0 F P_{atm}=850. mb
P_{dyn}=1.009E-02 psi
V_c=38.4 ft/sec Re = 3.010E+05
Pressure Coefficient
-2.0
-1.0
0.0
1.0
0.00
0.20
0.40
0.60
0.80
1.00
Blade Chord X/C

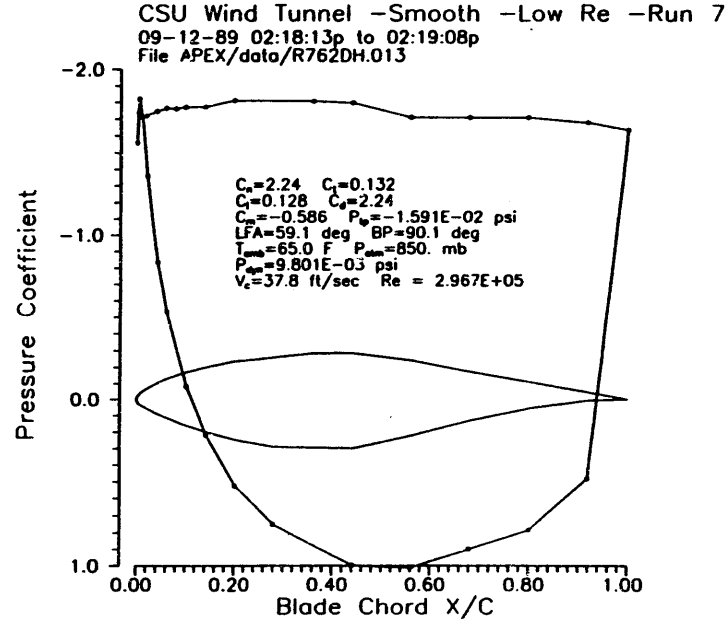
CSU Wind Tunnel -Smooth -Low Re -Run 7
09-12-89 02:18:13p to 02:19:08p
File APEX/data/R762DH.013
C_n=2.24 C_t=0.132
C_l=0.128 C_d=2.24
C_m=-0.586 P_{tp}=-1.591E-02 psi
LFA=59.1 deg BP=90.1 deg
T_{amb}=65.0 F P_{atm}=850. mb
P_{dyn}=9.801E-03 psi
V_c=37.8 ft/sec Re = 2.967E+05
Pressure Coefficient
-2.0
-1.0
0.0
1.0
0.00
0.20
0.40
0.60
0.80
1.00
Blade Chord X/C

Appendix L

Pressure Distributions for Reynolds Number 300,000 Rough

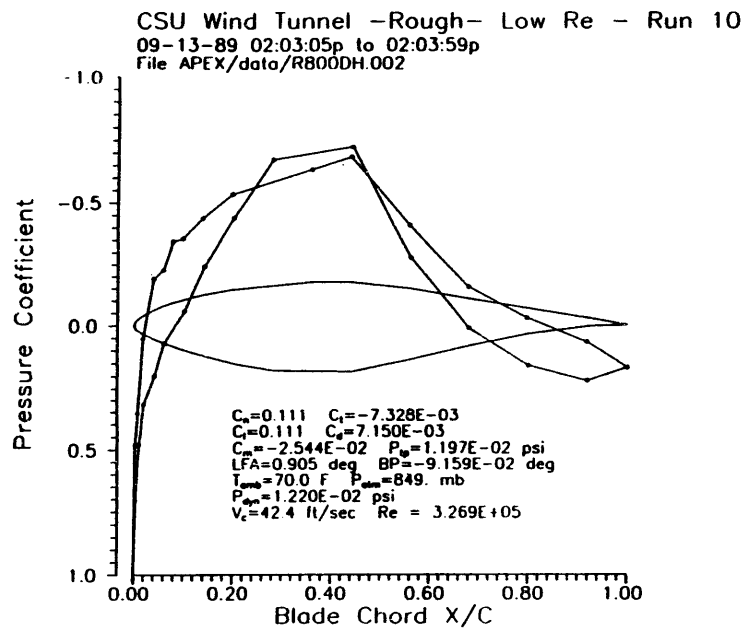
CSU Wind Tunnel -Rough- Low Re - Run 10
09-13-89 02:03:05p to 02:03:59p
File APEX/data/R800DH.002
Pressure Coefficient
Blade Chord X/C
-1.0
-0.5
0.0
0.5
1.0
0.00
0.20
0.40
0.60
0.80
1.00
C_n=0.111 C_t=-7.328E-03
C_l=0.111 C_d=7.150E-03
C_m=-2.544E-02 P_{tp}=1.197E-02 psi
LFA=0.905 deg BP=-9.159E-02 deg
T_{amb}=70.0 F P_{atm}=849. mb
P_{dyn}=1.220E-02 psi
V_c=42.4 ft/sec Re = 3.269E+05

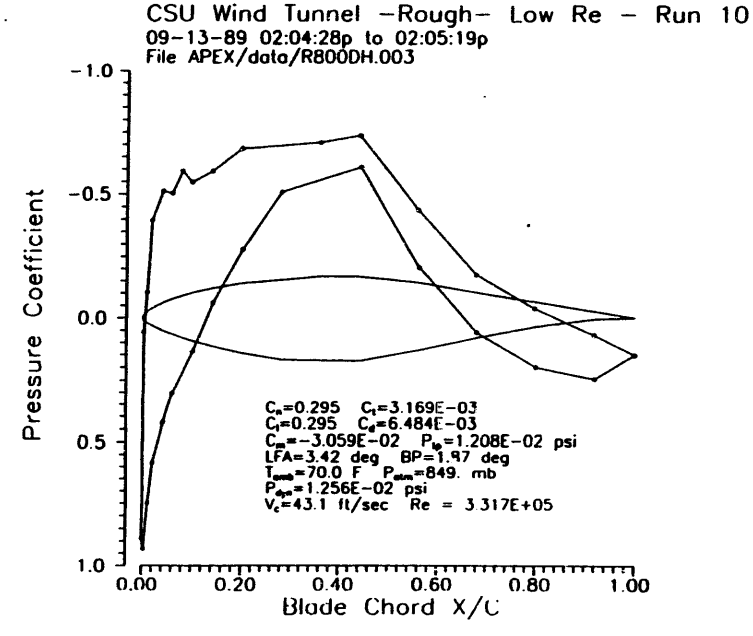
CSU Wind Tunnel -Rough- Low Re - Run 10
09-13-89 02:04:28p to 02:05:19p
File APEX/data/R800DH.003
Pressure Coefficient
Blade Chord X/C
-1.0
-0.5
0.0
0.5
1.0
0.00
0.20
0.40
0.60
0.80
1.00
C_n=0.295 C_t=3.169E-03
C_l=0.295 C_d=6.484E-03
C_m=-3.059E-02 P_{tp}=1.208E-02 psi
LFA=3.42 deg BP=1.97 deg
T_{amb}=70.0 F P_{atm}=849. mb
P_{dyn}=1.256E-02 psi
V_c=43.1 ft/sec Re = 3.317E+05

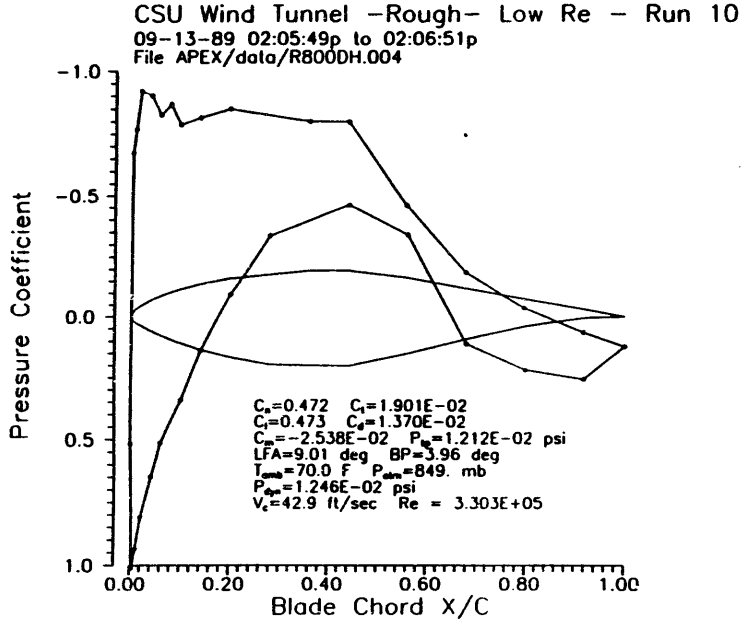
CSU Wind Tunnel -Rough- Low Re - Run 10
09-13-89 02:05:49p to 02:06:51p
File APEX/data/R800DH.004
Pressure Coefficient
Blade Chord X/C
-1.0
-0.5
0.0
0.5
1.0
0.00
0.20
0.40
0.60
0.80
1.00
C_n=0.472 C_t=1.901E-02
C_l=0.473 C_d=1.370E-02
C_m=-2.538E-02 P_{tp}=1.212E-02 psi
LFA=9.01 deg BP=3.96 deg
T_{amb}=70.0 F P_{atm}=849. mb
P_{dyn}=1.246E-02 psi
V_c=42.9 ft/sec Re = 3.303E+05

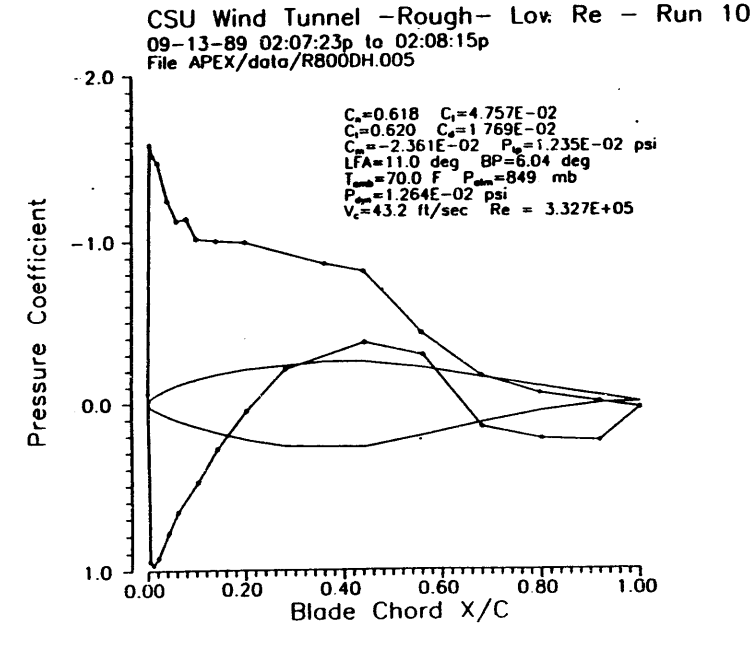
CSU Wind Tunnel -Rough- Low Re - Run 10
09-13-89 02:07:23p to 02:08:15p
File APEX/data/R800DH.005
Pressure Coefficient
Blade Chord X/C
-2.0
-1.0
0.0
1.0
0.00
0.20
0.40
0.60
0.80
1.00
C_n=0.618 C_t=4.757E-02
C_l=0.620 C_d=1.769E-02
C_m=-2.361E-02 P_{tp}=1.235E-02 psi
LFA=11.0 deg BP=6.04 deg
T_{amb}=70.0 F P_{atm}=849 mb
P_{dyn}=1.264E-02 psi
V_c=43.2 ft/sec Re = 3.327E+05

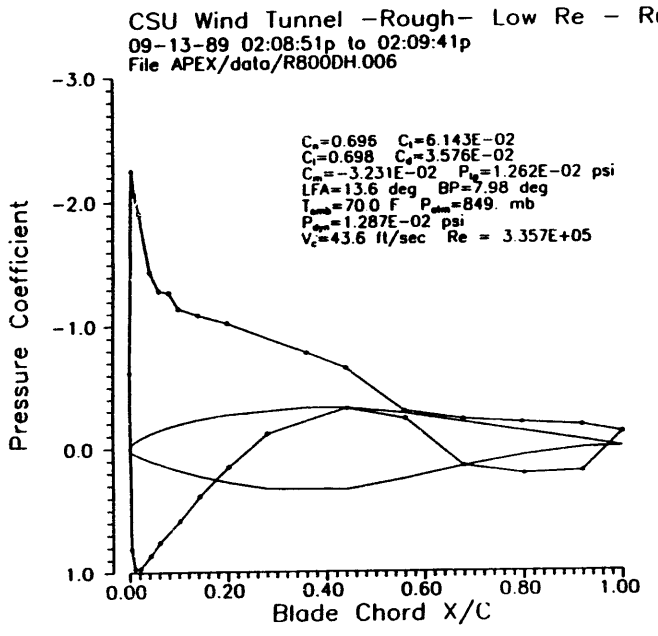
CSU Wind Tunnel -Rough- Low Re - Run 10
09-13-89 02:08:51p to 02:09:41p
File APEX/data/R800DH.006
C_n=0.696 C_t=6.143E-02
C_l=0.698 C_d=3.576E-02
C_m=-3.231E-02 P_{tip}=1.262E-02 psi
LFA=13.6 deg BP=7.98 deg
T_{amb}=70.0 F P_{atm}=849. mb
P_{dyn}=1.287E-02 psi
V_c=43.6 ft/sec Re = 3.357E+05
Pressure Coefficient
Blade Chord X/C

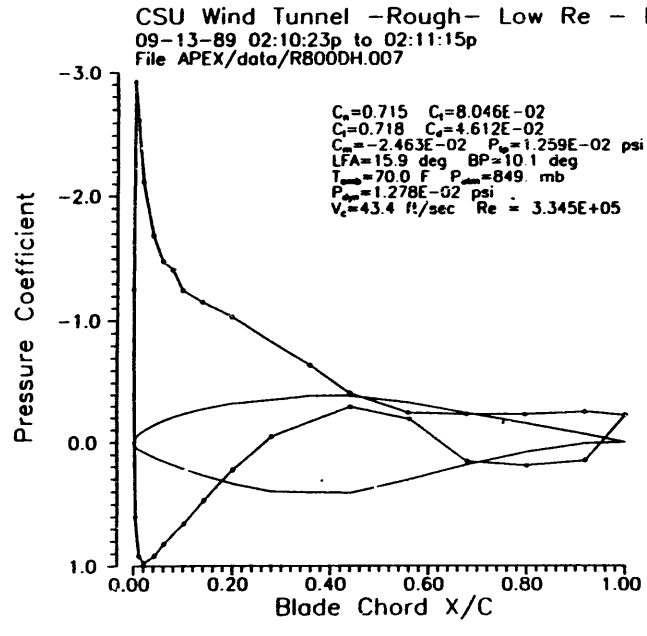
CSU Wind Tunnel -Rough- Low Re - Run 10
09-13-89 02:10:23p to 02:11:15p
File APEX/data/R800DH.007
C_n=0.715 C_t=8.046E-02
C_l=0.718 C_d=4.612E-02
C_m=-2.463E-02 P_{tip}=1.259E-02 psi
LFA=15.9 deg BP=10.1 deg
T_{amb}=70.0 F P_{atm}=849. mb
P_{dyn}=1.278E-02 psi
V_c=43.4 ft/sec Re = 3.345E+05
Pressure Coefficient
Blade Chord X/C

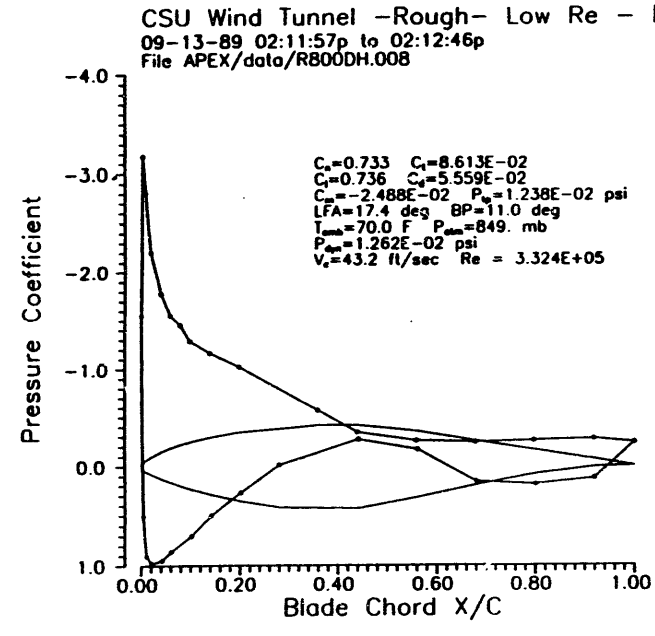
CSU Wind Tunnel -Rough- Low Re - Run 10
09-13-89 02:11:57p to 02:12:46p
File APEX/data/R800DH.008
C_n=0.733 C_t=8.613E-02
C_l=0.736 C_d=5.559E-02
C_m=-2.488E-02 P_{tip}=1.238E-02 psi
LFA=17.4 deg BP=11.0 deg
T_{amb}=70.0 F P_{atm}=849. mb
P_{dyn}=1.262E-02 psi
V_c=43.2 ft/sec Re = 3.324E+05
Pressure Coefficient
Blade Chord X/C

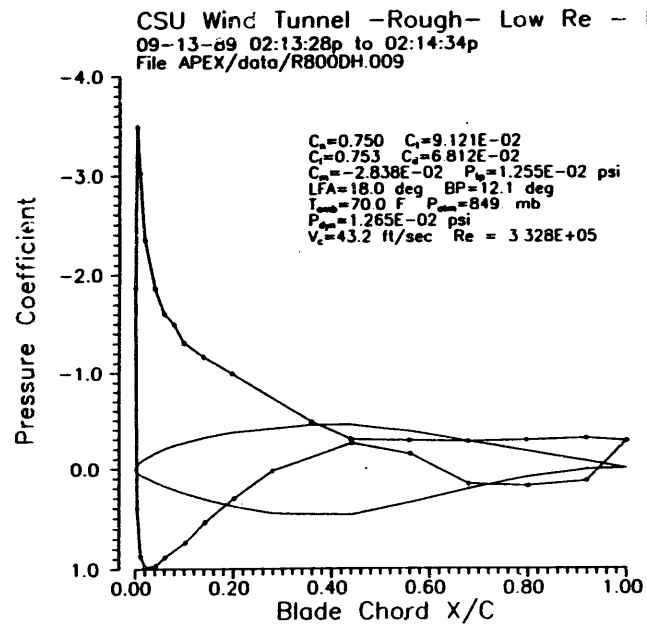
CSU Wind Tunnel -Rough- Low Re - Run 10
09-13-89 02:13:28p to 02:14:34p
File APEX/data/R800DH.009
C_n=0.750 C_t=9.121E-02
C_l=0.753 C_d=6.812E-02
C_m=-2.838E-02 P_{tip}=1.255E-02 psi
LFA=18.0 deg BP=12.1 deg
T_{amb}=70.0 F P_{atm}=849. mb
P_{dyn}=1.265E-02 psi
V_c=43.2 ft/sec Re = 3.328E+05
Pressure Coefficient
Blade Chord X/C

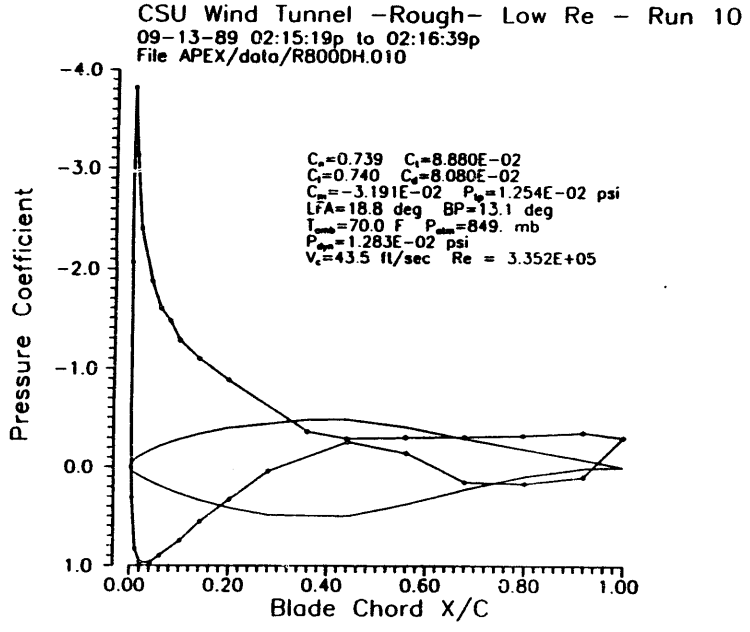
CSU Wind Tunnel -Rough- Low Re - Run 10
09-13-89 02:15:19p to 02:16:39p
File APEX/data/R800DH.010
C_n=0.739 C_t=8.880E-02
C_l=0.740 C_d=8.080E-02
C_m=-3.191E-02 P_{tp}=1.254E-02 psi
LFA=18.8 deg BP=13.1 deg
T_{amb}=70.0 F P_{atm}=849. mb
P_{dyn}=1.283E-02 psi
V_c=43.5 ft/sec Re = 3.352E+05
Pressure Coefficient
-4.0
-3.0
-2.0
-1.0
0.0
1.0
0.00
0.20
0.40
0.60
0.80
1.00
Blade Chord X/C

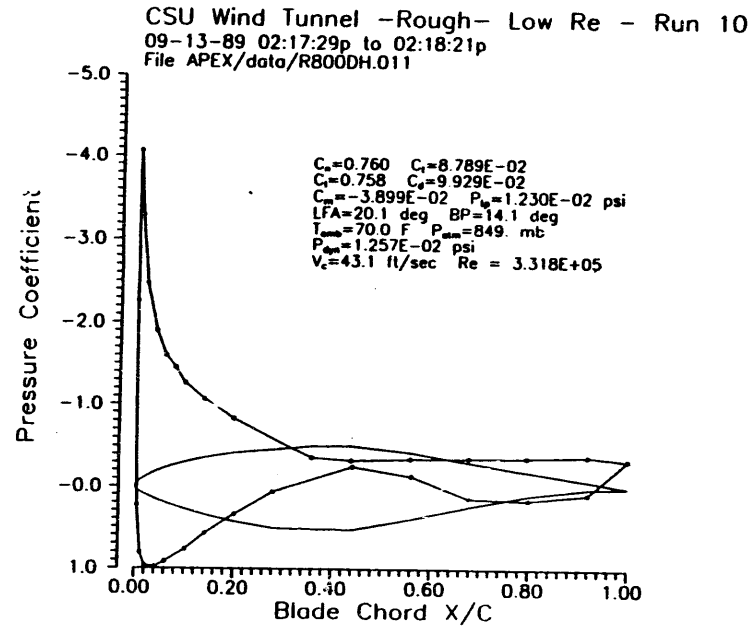
CSU Wind Tunnel -Rough- Low Re - Run 10
09-13-89 02:17:29p to 02:18:21p
File APEX/data/R800DH.011
C_n=0.760 C_t=8.789E-02
C_l=0.758 C_d=9.929E-02
C_m=-3.899E-02 P_{tp}=1.230E-02 psi
LFA=20.1 deg BP=14.1 deg
T_{amb}=70.0 F P_{atm}=849. mb
P_{dyn}=1.257E-02 psi
V_c=43.1 ft/sec Re = 3.318E+05
Pressure Coefficient
-5.0
-4.0
-3.0
-2.0
-1.0
-0.0
1.0
0.00
0.20
0.40
0.60
0.80
1.00
Blade Chord X/C

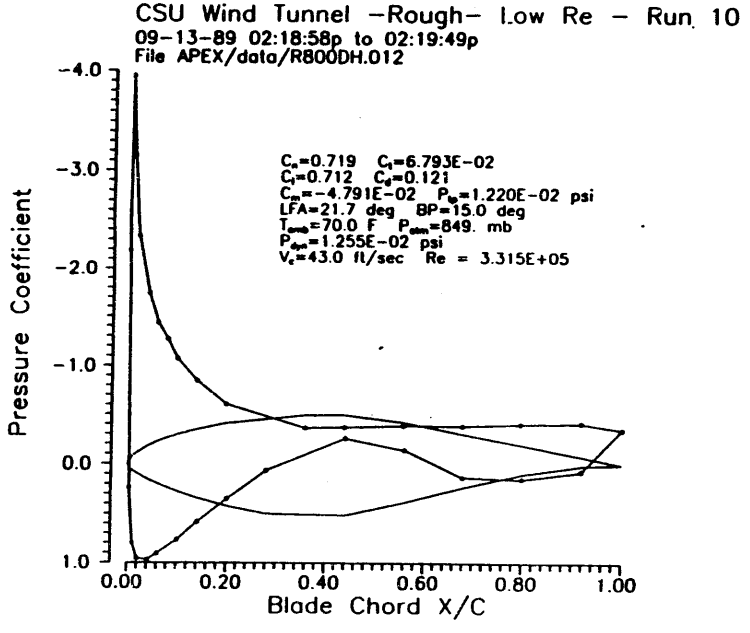
CSU Wind Tunnel -Rough- Low Re - Run 10
09-13-89 02:18:58p to 02:19:49p
File APEX/data/R800DH.012
C_n=0.719 C_t=6.793E-02
C_l=0.712 C_d=0.121
C_m=-4.791E-02 P_{tp}=1.220E-02 psi
LFA=21.7 deg BP=15.0 deg
T_{amb}=70.0 F P_{atm}=849. mb
P_{dyn}=1.255E-02 psi
V_c=43.0 ft/sec Re = 3.315E+05
Pressure Coefficient
-4.0
-3.0
-2.0
-1.0
0.0
1.0
0.00
0.20
0.40
0.60
0.80
1.00
Blade Chord X/C

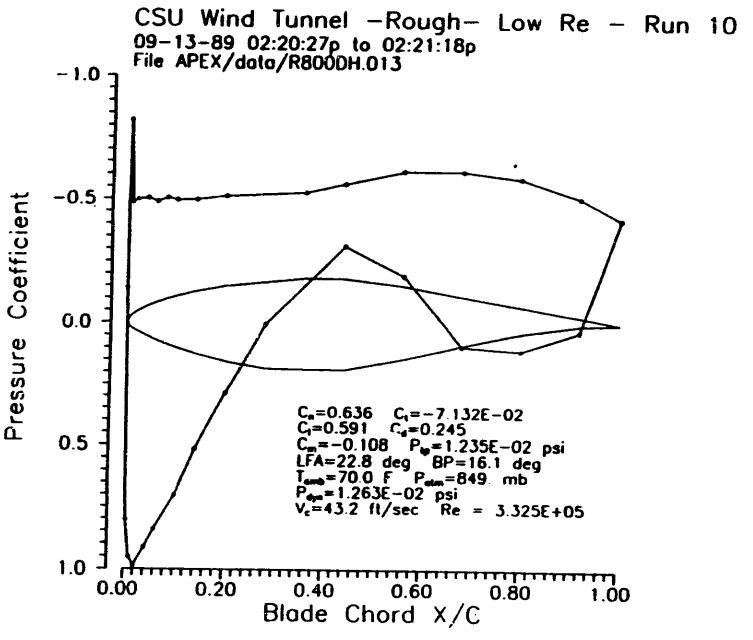
CSU Wind Tunnel -Rough- Low Re - Run 10
09-13-89 02:20:27p to 02:21:18p
File APEX/data/R800DH.013
C_n=0.636 C_t=-7.132E-02
C_l=0.591 C_d=0.245
C_m=-0.108 P_{tp}=1.235E-02 psi
LFA=22.8 deg BP=16.1 deg
T_{amb}=70.0 F P_{atm}=849. mb
P_{dyn}=1.263E-02 psi
V_c=43.2 ft/sec Re = 3.325E+05
Pressure Coefficient
-1.0
-0.5
0.0
0.5
1.0
0.00
0.20
0.40
0.60
0.80
1.00
Blade Chord X/C

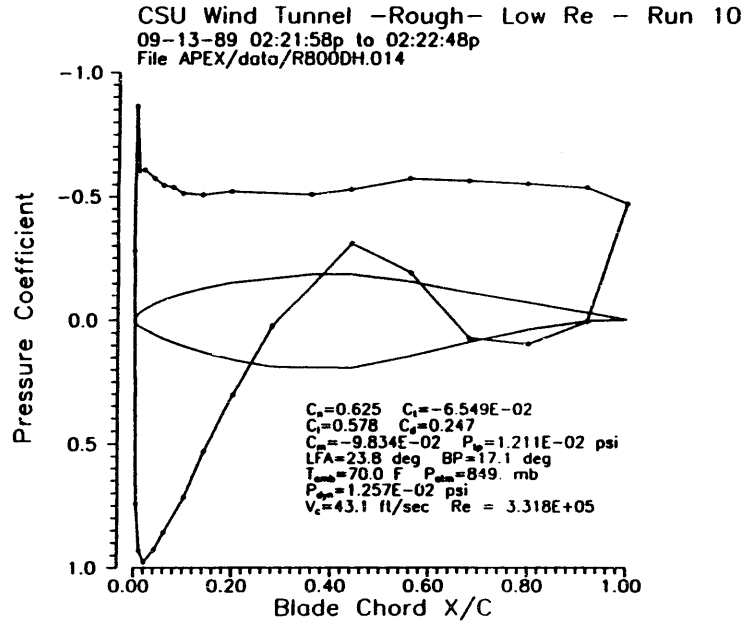
CSU Wind Tunnel -Rough- Low Re - Run 10
09-13-89 02:21:58p to 02:22:48p
File APEX/data/R800DH.014
Pressure Coefficient
Blade Chord X/C
-1.0
-0.5
0.0
0.5
1.0
0.00
0.20
0.40
0.60
0.80
1.00
C_n=0.625 C_t=-6.549E-02
C_l=0.578 C_d=0.247
C_m=-9.834E-02 P_{tp}=1.211E-02 psi
LFA=23.8 deg BP=17.1 deg
T_{amb}=70.0 F P_{atm}=849. mb
P_{dyn}=1.257E-02 psi
V_e=43.1 ft/sec Re = 3.318E+05

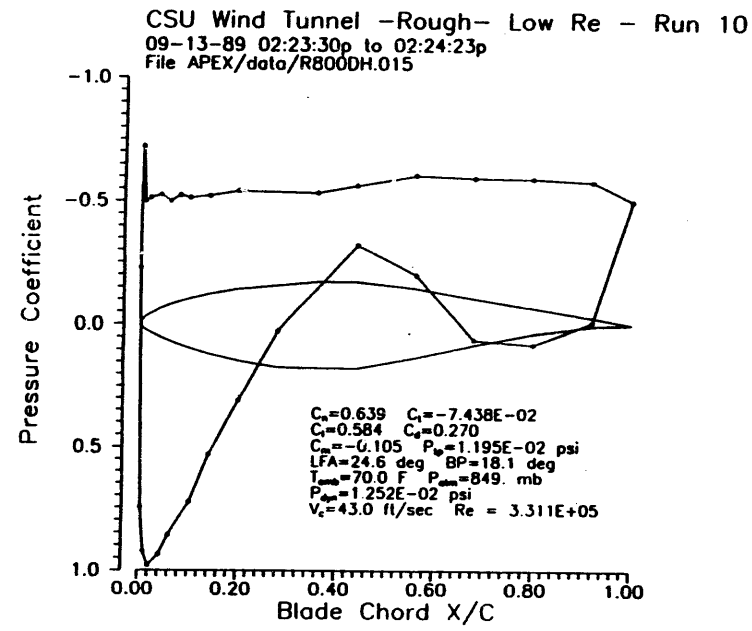
CSU Wind Tunnel -Rough- Low Re - Run 10
09-13-89 02:23:30p to 02:24:23p
File APEX/data/R800DH.015
Pressure Coefficient
Blade Chord X/C
-1.0
-0.5
0.0
0.5
1.0
0.00
0.20
0.40
0.60
0.80
1.00
C_n=0.639 C_t=-7.438E-02
C_l=0.584 C_d=0.270
C_m=-0.105 P_{tp}=1.195E-02 psi
LFA=24.6 deg BP=18.1 deg
T_{amb}=70.0 F P_{atm}=849. mb
P_{dyn}=1.252E-02 psi
V_e=43.0 ft/sec Re = 3.311E+05

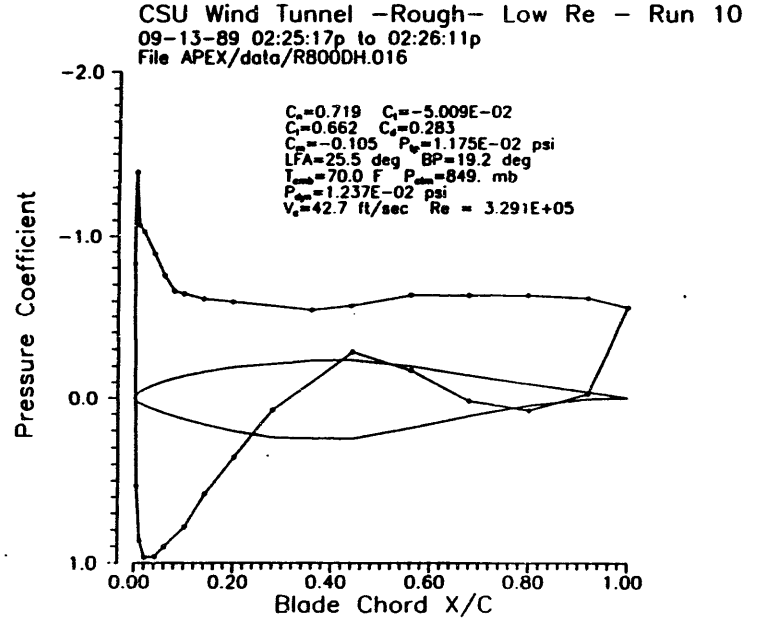
CSU Wind Tunnel -Rough- Low Re - Run 10
09-13-89 02:25:17p to 02:26:11p
File APEX/data/R800DH.016
Pressure Coefficient
Blade Chord X/C
-2.0
-1.0
0.0
1.0
0.00
0.20
0.40
0.60
0.80
1.00
C_n=0.719 C_t=-5.009E-02
C_l=0.662 C_d=0.283
C_m=-0.105 P_{tp}=1.175E-02 psi
LFA=25.5 deg BP=19.2 deg
T_{amb}=70.0 F P_{atm}=849. mb
P_{dyn}=1.237E-02 psi
V_e=42.7 ft/sec Re = 3.291E+05

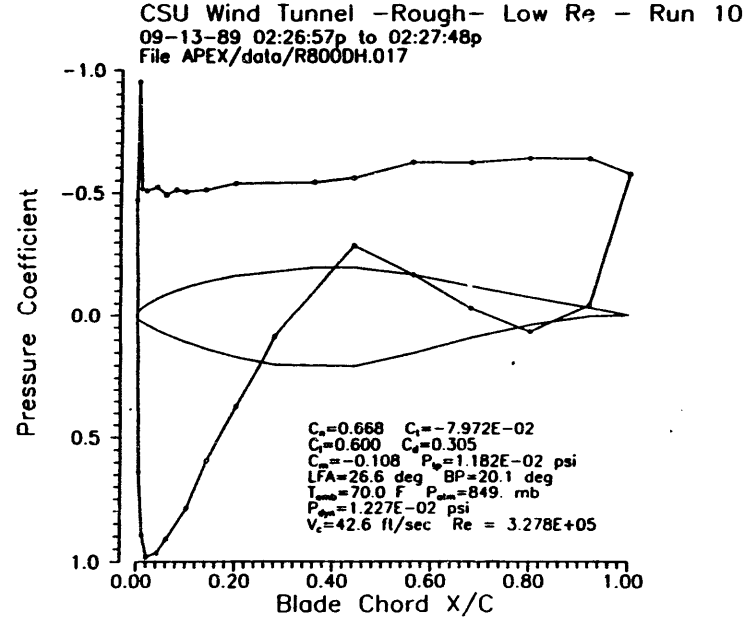
CSU Wind Tunnel -Rough- Low Re - Run 10
09-13-89 02:26:57p to 02:27:48p
File APEX/data/R800DH.017
Pressure Coefficient
Blade Chord X/C
-1.0
-0.5
0.0
0.5
1.0
0.00
0.20
0.40
0.60
0.80
1.00
C_n=0.668 C_t=-7.972E-02
C_l=0.600 C_d=0.305
C_m=-0.108 P_{tp}=1.182E-02 psi
LFA=26.6 deg BP=20.1 deg
T_{amb}=70.0 F P_{atm}=849. mb
P_{dyn}=1.227E-02 psi
V_e=42.6 ft/sec Re = 3.278E+05

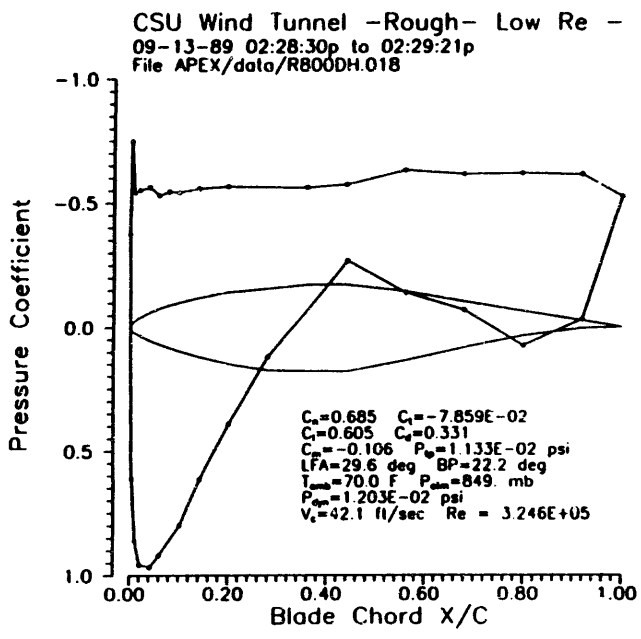
CSU Wind Tunnel -Rough- Low Re - Run 10
09-13-89 02:28:30p to 02:29:21p
File APEX/data/R800DH.018
Pressure Coefficient
-1.0
-0.5
0.0
0.5
1.0
0.00
0.20
0.40
0.60
0.80
1.00
Blade Chord X/C
C_n=0.685 C_t=-7.859E-02
C_l=0.605 C_d=0.331
C_m=-0.106 P_{tp}=1.133E-02 psi
LFA=29.6 deg BP=22.2 deg
T_{amb}=70.0 F P_{atm}=849. mb
P_{dyn}=1.203E-02 psi
V_t=42.1 ft/sec Re = 3.246E+05

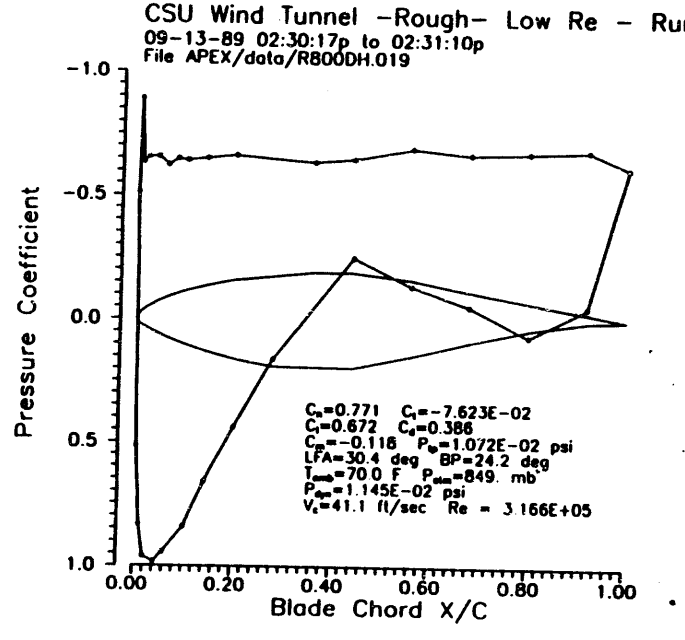
CSU Wind Tunnel -Rough- Low Re - Run 10
09-13-89 02:30:17p to 02:31:10p
File APEX/data/R800DH.019
Pressure Coefficient
-1.0
-0.5
0.0
0.5
1.0
0.00
0.20
0.40
0.60
0.80
1.00
Blade Chord X/C
C_n=0.771 C_t=-7.623E-02
C_l=0.672 C_d=0.386
C_m=-0.118 P_{tp}=1.072E-02 psi
LFA=30.4 deg BP=24.2 deg
T_{amb}=70.0 F P_{atm}=849. mb
P_{dyn}=1.145E-02 psi
V_t=41.1 ft/sec Re = 3.166E+05

Document Control Page	1. NREL Report No. NREL/TP-257-4655	2. NTIS Accession No. DE93000012	3. Recipient's Accession No.

4. Title and Subtitle

Combined Experiment Phase I—Final Report

5. Publication Date
October 1992

6.

7. Author(s)
C.P. Butterfield, W.P. Musial, D.A. Simms

8. Performing Organization Rept. No.
NREL/TP-257-4655

9. Performing Organization Name and Address

National Renewable Energy Laboratory
1617 Cole Blvd.
Golden, CO 80401

10. Project/Task/Work Unit No.
WE21.8101

11. Contract (C) or Grant (G) No.

(C)

(G)

12. Sponsoring Organization Name and Address

National Renewable Energy Laboratory
1617 Cole Blvd.
Golden, CO 80401

13. Type of Report & Period Covered
Technical Report

14.

15. Supplementary Notes

16. Abstract (Limit: 200 words)

How does wind tunnel airfoil data differ from the airfoil performance on an operating horizontal axis wind turbine (HAWT)? The National Renewable Energy laboratory has been conducting a comprehensive test program focused on answering this question and understanding the basic fluid mechanics of rotating HAWT stall aerodynamics. The basic approach was to instrument a wind turbine rotor, using an airfoil that was well documented by wind funnel tests, and measure operating pressure distributions on the rotating blade. Based on the integrated values of the pressure data, airfoil performance coefficients were obtained, and comparisons were made between the rotating data and the wind tunnel data. Care was taken to minimize the aerodynamic and geometric differences between the rotating and the wind tunnel models

This is the first of two reports describing the Combined Experiment Program and its results. This Phase I report covers background information such as test setup and instrumentation. It also includes wind tunnel test results and roughness testing.

17. Document Analysis

a. Descriptors
wind turbines; wind turbine experimental rotor dynamics; wind turbine aerodynamic pressure measurements

b. Identifiers/Open-Ended Terms

c. UC Categories
261

18. Availability Statement
National Technical Information Service
U.S. Department of Commerce
5285 Port Royal Road
Springfield, VA 22161

19. No. of Pages
222

20. Price
A10

Form No. 0069E (6-30-87)

END

DATE FILMED

2/5/93